FIB

Behaviour of Rice Husk Ash in Self-Compacting High Performance Concrete

Ha Thanh Le

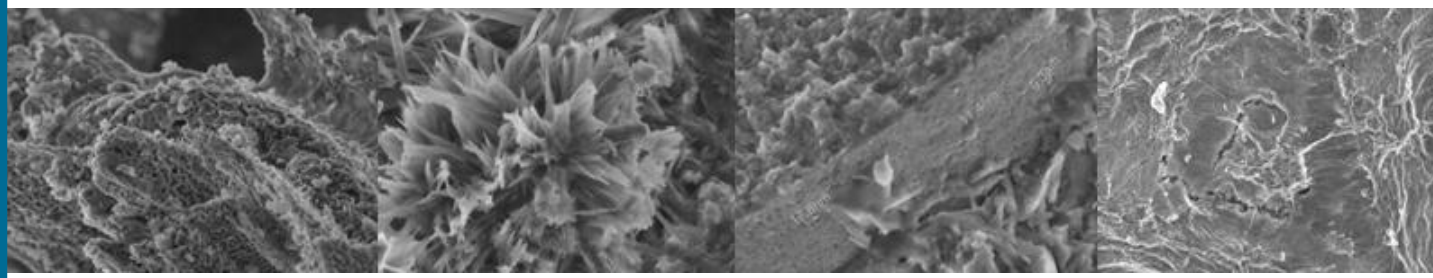

Professur Werkstoffe des Bauens

Bauhaus-Universität Weimar

Verhalten von Reisschalenasche in Selbstverdichtendem Hochleistungsbeton

Dissertation

zur Erlangung des akademischen Grades
Doktor-Ingenieur (Dr.-Ing.)

an der Fakultät Bauingenieurwesen
der Bauhaus-Universität Weimar

vorgelegt von

Ha Thanh Le

aus Vietnam

Gutachter:

Prof. Dr.-Ing. Horst-Michael Ludwig (Weimar)

Prof. Dr.-Ing. habil. Nguyen, Viet Tue (Graz)

Prof. Dr.-Ing. Frank Dehn (Leipzig)

Die öffentliche Disputation der Arbeit fand am 03.2.2015 in Weimar statt.

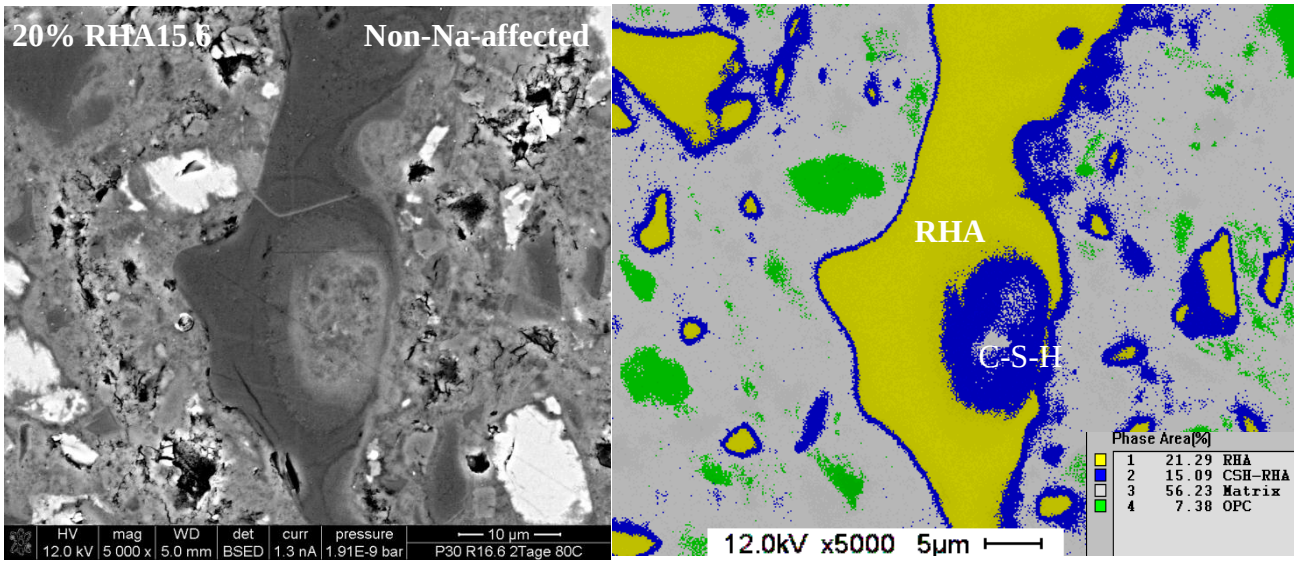

BSE-SEM (left) and EDX-phase mapping (right) images of hydrated RHA particles in non-Na-affected matrix area in paste sample at w/b of 0.30 after 1 day in mould, 1 day in water at 80 °C and 2 days in 1 M NaOH at 80 °C

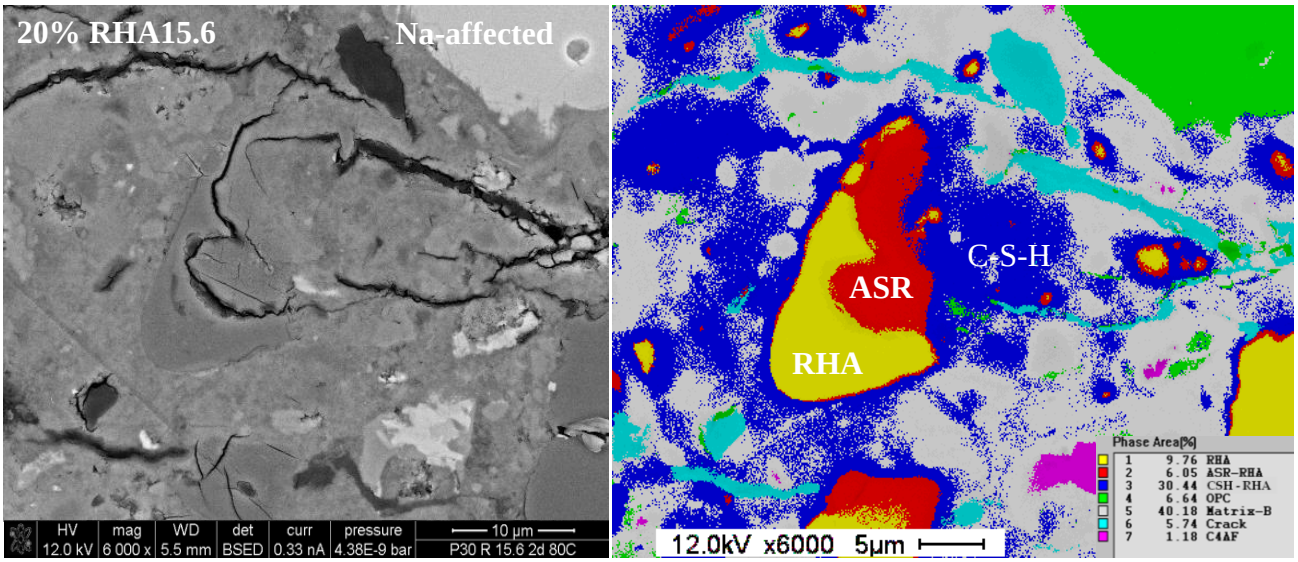

BSE-SEM (left) and EDX-phase mapping (right) images of hydrated RHA particles in Na-affected matrix area in paste sample at w/b of 0.30 after 1 day in mould, 1 day in water at 80 °C and 2 days in 1 M NaOH at 80 °C

Herausgeber:
Bauhaus-Universität Weimar
F.A. Finger-Institut für Baustoffkunde
Professur Verkstoffe des Bauens
Direktor: Prof. Dr.-Ing. Horst-Michael Ludwig
ISBN 978-3-00-048928-0

... theory

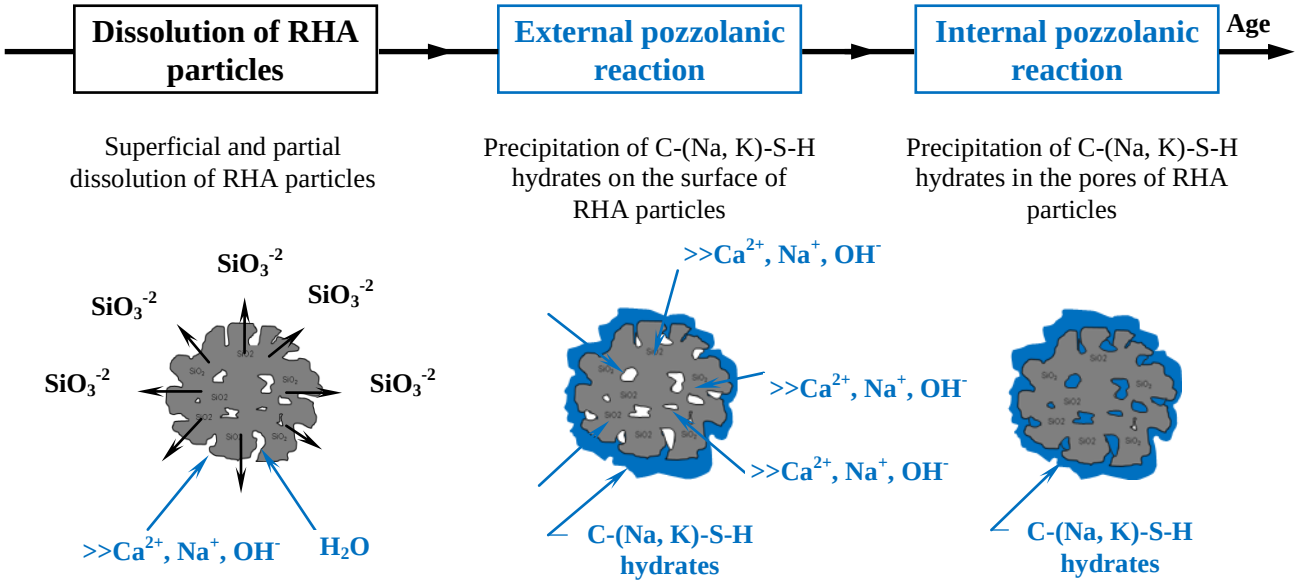

Schematic representation of the mechanism for successive pozzolanic reactions of RHA particles

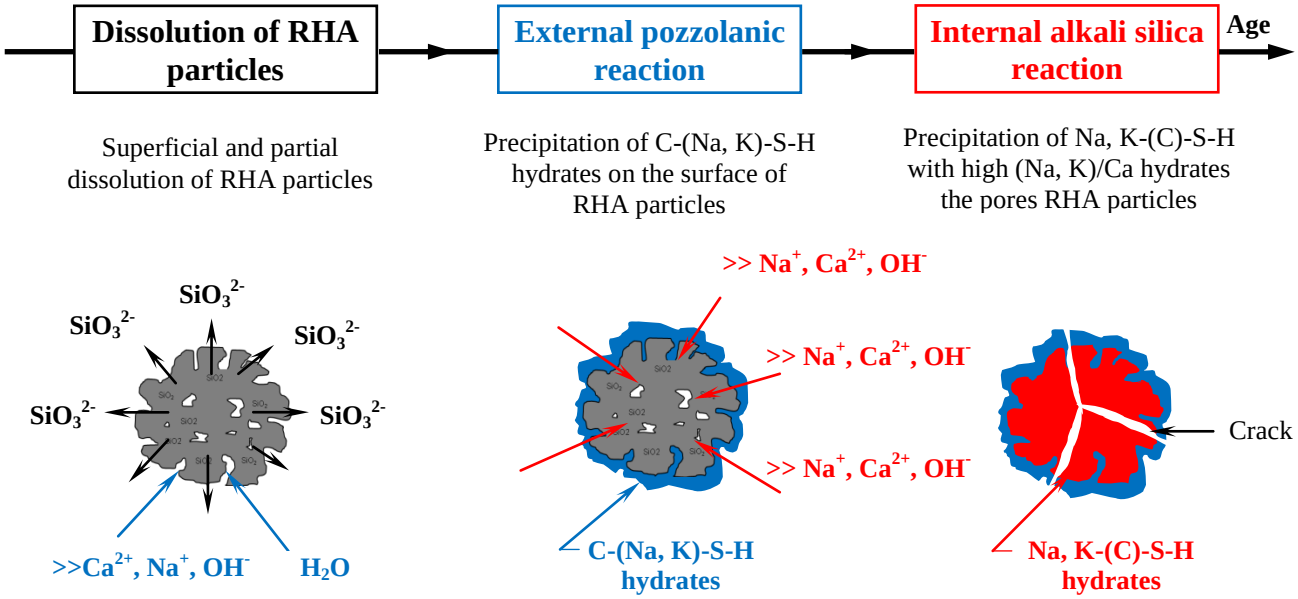

Schematic representation of the mechanism for successive pozzolanic and alkali silica reactions of RHA particles

Every medal has two sides…

… So is life.

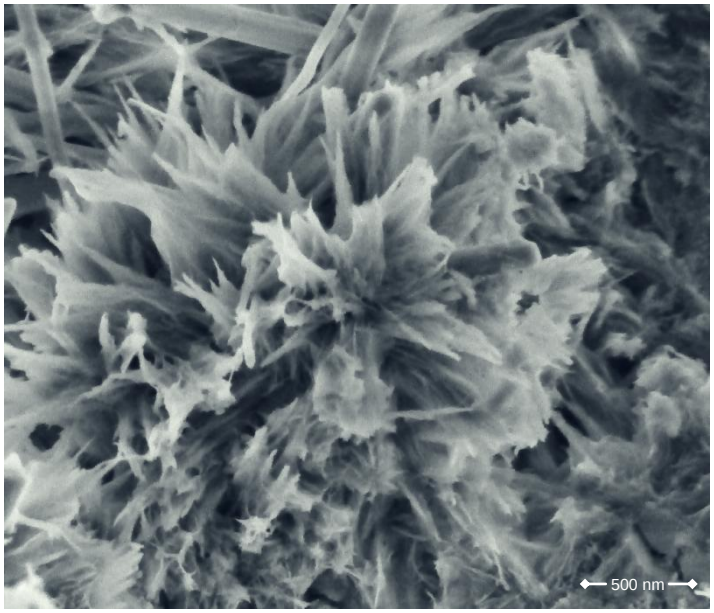

- Tobermorite-like C-S-H: Roses in Concrete -

... for my parents

Acknowledgements

The author would like to express thanks to Ministry of Education and Training of Vietnam, F.A. Finger-Institute for Building Materials Science (FIB) and German Academic Exchange Service (DAAD) for financial support.

I would like to express my greatest gratitude to my supervisor, Prof. Dr.-Ing. Horst-Michael Ludwig for his useful advice and encouragement throughout my PhD study.

I would like to express my sincerest acknowledgement to Dr.-Ing. Karten Siewert and Dipl.-Ing. Matthias Müller in my research group 'Beton' for their patience, encouragement, helpful discussion and their thorough understanding that has helped me balance my private and professional life.

I would like to thank Dr. rer. nat. Bernd Möser, Dr.-Ing.habil. Frank Bellmann, Dr.-Ing. Colin Giebson, Dipl.-Ing. Thomas Sowoidnich and Dr. rer. nat. Holger Kletti for their advice and discussions.

I am also most grateful to electron microscopic analysis and cement chemistry group for their technical assistance and discussion during my PhD study.

I gratefully acknowledge all of the staff at FIB, especially to Dipl.-Ing. Dirk Ehrhardt, Dr. rer. nat. Christiane Rößler, Dr.-Ing. Alexander Flohr, Dipl-Ing. Andreas Giese, Dipl.-Ing. Dennys Dressel, Dipl.-Ing. Simone Peters, Dipl.-Ing. Văn Viết Thiên Ân, Dipl.-Ing. (FH) Christian Matthes and Dipl.-Ing. (FH) Peisker Birgit for their technical assistance and discussion.

My thanks also go to Prof. Dr.-Ing. Bùi Văn Bội, Dr.-Ing. Bùi Danh Đại, Prof. Dr.-Ing. Phạm Duy Hữu, Prof. Dr.-Ing. Ngô Đăng Quang, and to all my colleagues, especially Mr. Mai Đình Lộc at the Institute of Construction Engineering, University of Transport and communications, Vietnam, for all their support and encouragement. A special thank to my friend, M. Eng. Nguyễn Ngọc Lân who has helped me to produce rice husk ash in Vietnam.

Finally, I express my deepest gratitude to my parents, my sister, my brother, my sister in-law, my brother in-law, my nieces and my nephew. Their love, unwavering support and encouragement help me to overcome all challenges to accomplish my PhD study.

Weimar, 05.05.2014 Lê Thanh Hà

Table of Contents

List of Abbreviations

ASR	Alkali silica reaction
BET	Brunauer-Emmett-Teller
BJH	Barrett-Joyner-Hanlenda
BSE	Backscattered electron
CH	Calcium hydroxide
C-S-H	Calcium silicate hydrates
C-(Na, K)-S-H	Calcium-alkali-silicate hydrates
Na, K-(C)-S-H	Alkali-calcium-silicate hydrates
DTA-TG	Thermal analysis
EDX	Energy-dispersive X-ray spectroscopy
FA	Fly ash
GGBFS	Ground granulated blast-furnace slag
HPC	High performance concrete
L.O.I	Loss on ignition
LSP	Limestone powder
MIP	Mercury intrusion porosimetry
MPS	Mean particle size
NanoSEM	Ultra high resolution scanning electron microscopy
QXRD	Quantitative X-ray diffraction
RHA	Rice husk ash
RPC	Reactive powder concrete
SCC	Self-compacting concrete
SCHPC	Self-compacting high performance concrete
SCM	Supplementary cementitious material
SEM	Scanning electron microscopy
SF	Silica fume
SP	Superplasticizer
SSA	Specific surface area
SSD	Superplasticizer saturation dosage
TVC	Traditional vibrated concrete
ITZ	Interface transition zone
UHPC	Ultra-high performance concrete
VMA	Viscosity modifying agent
w/b	Water to binder ratio
w/c	Water to cement ratio

Summary

Self-compacting high performance concrete (SCHPC) can be defined as the new generation of self-compacting concrete (SCC). SCHPC possesses the adequate self-compactability of SCC and the high strength and good durability of high performance concrete (HPC). In order to fulfill these requirements, a high volume of Portland cement, extensive dosage of chemical admixtures (superplasticizer - SP and viscosity modifying admixture - VMA) and expensive reactive supplementary cementitious materials (SCM), e.g. silica fume (SF), are used. SCHPC therefore is very expensive and has an adverse ecobalance. Normally, cement is partially replaced by cheaper SCMs (fly ash, limestone powder, etc.). The performance of SCHPC with these SCMs is not comparable to that of SCHPC with SF. SF is expensive due to the limited availability, especially in developing countries. The use of less-expensive rice husk ash, an agricultural waste material, as a total substitute for SF as a partial cement replacement, improves the sustainability of SCHPC. It can also help reduce environmental pollution from the disposal of rice husk and increase the benefit of rice cultivation.

Under the controlled combustion of rice husk, RHA can be produced. RHA has a very high amorphous silica content, comparable with SF. The pore structure is a very important property of the material. Due to water adsorption, the incorporation of RHA decreases flowability, and increases viscosity and thus the segregation resistance of concrete. These properties are all required for fresh SCHPC. The hydration of Portland cement blended with SCM is very complex because the hydraulic reactions of Portland cement and SCM take place simultaneously and might interact with each other. RHA differs from other SCMs, mainly in its porous structure and its high alkali content. Consequently, the mechanism for the hydration of Portland cement blended with RHA may be different from the SF and more complicated. Most pozzolanic reactive SCMs, e.g. SF, fly ash, etc., can reduce the damage of ASR, because of the conversion of calcium into additional C-S-H phases, the refinement of the cement matrix and the alkali absorption of the pozzolanic low Ca/Si C-S-H phases. The effect of RHA on alkali-silica reaction (ASR) is largely unknown and should be fully investigated in the work.

The main objective of the present thesis study is to investigate the characteristics of the RHA and then its behaviour in SCHPC with respects to rheological properties, hydration and microstructure development and ASR, in comparison with SF.

The summary of the findings, contributions, and the main conclusions in the present thesis study are given following:

- The RHA in this study is a macro-mesoporous amorphous siliceous material with a very high content of amorphous silica (comparable with SF). The pore size distribution is the most important parameter of RHA. This parameter affects pore volume, specific surface area (SSA), and thus the water demand and the pozzolanic reactivity of RHA. SSA of the RHA derives from the internal surface in the pores and the external surface on the surface of the particles. During grinding, most of the macropores collapse, decreasing the internal SSA of RHA, but increasing the external SSA of RHA.

- C-S-H-phases as pozzolanic reaction products can be observed on the porous surface of RHA particles and SF particles after 4 hours of hydration in the $Ca(OH)_2$ - pozzolana suspension. Pozzolanic reactivity in terms of $Ca(OH)_2$ - consumption of the SF is higher than that of RHA. The pozzolanic reactivity of coarse RHA is higher than that of the fine one possibly due to the higher adsorption of calcium ions into the pores of the RHA particles. That induces an internal pozzolanic reaction.
- A new method for proportioning SCHPC was developed on the basis of the basic requirements for ordinary concrete according to DIN EN 206-1 and DIN 1045-2. SP demand for SCHPC is closely related to SP saturation dosage of mortar formulated from SCHPC. The pozzolanic reactivity indices of the SCMs were used to predict the expected compressive strength. The pozzolanic reactivity index of RHA is 1, the same as that of SF.
- The incorporation of RHA decreases mini-slump flow, and increases the SP adsorption, the SP saturation dosage, yield stress and plastic viscosity of mortar. The increase in plastic viscosity is considerably higher than the decrease in mini-slump flow of mortar. This effect of RHA is much stronger than that of SF, especially when the coarser RHA and the higher content of RHA are used.
- Fresh mortar formulated from SCHPC is a shear-thickening material. The shear-thickening degree decreases over time. The incorporation of RHA/SF decreases the shear-thickening degree. The increase in RHA/SF content reduces the degree of shear-thickening. The effect of SF is much stronger than that of RHA.
- The incorporation of RHA/SF increases the degree of cement hydration in mortar. Effect of SF is stronger than RHA at early age and vice versa. The coarse RHA is more effective than the fine one at late ages. The process of cement hydration in the RHA/SF blended cement paste can be explained by nucleation site effect due to the large SSA and internal water curing effect due to water in pore structure in the case of RHA.
- The incorporation of RHA/SF changes the hydration process of the clinker minerals, i.e. C_3S, C_2S. The hydration degree of C_3S in the RHA/SF blended cement matrix is higher than in the reference sample. The incorporation of RHA/SF increases the C_3S hydration rate from 3 to 14 days. The degree of C_3S and C_2S hydration in the RHA blended cement paste is higher than that in the SF blended cement paste. From 28 to 91 days, the degree of cement hydration in the coarse RHA (22.6 µm) blended cement paste increased mainly due to the increase in C_2S hydration
- The variation in mean particle size (MPS) of RHA, resulting in the variation of pore structure, results in the variation in pozzolanic reactivity and the effect of pozzolanic reaction on the pore refinement of the cement matrix. External pozzolanic reaction of RHA contributes to the pore refinement in the cement matrix, whereas the internal pozzolanic reaction partially or completely contributes to the consolidation of pores inside RHA particles by its products. The fine RHA (5.7 µm) is more effective in pore refinement in the cement matrix than the coarse RHA (22.6 µm) due to its higher external pozzolanic reactivity. Pozzolanic reactivity and dispersion of SF particles are significantly better than

those of RHA. This results in the lower capillary porosity and the better refinement of pore structure in the cement matrix.

- SF is significantly more effective than RHA in mitigating ASR in mortar containing reactive greywacke aggregate. The increase in MPS of RHA increases the expansion of mortar bars containing reactive greywacke aggregate and non-reactive basalt aggregate due to ASR. The incorporation of fine RHA decreases the expansion of mortar bars containing reactive greywacke aggregate due to ASR.
- RHA has paradoxical effect on ASR in cement paste formulated from SCHPC in presence of the high alkali concentration. RHA constitutes rather than mitigates ASR deterioration. RHA particles indeed act as micro-reactive aggregates and react with alkali hydroxide to generate the expansive ASR products even when particle size of RHA is in the range of 5.7-22.6 μm. Increasing the particle size of RHA and temperature increases the alkali silica reactivity of RHA.
- In presence of the high alkali concentration, the pozzolanic and alkali silica reactions of RHA take place successively from the exterior to the interior of RHA particles. The mechanism for the successive reactions of RHA is proposed. The pozzolanic reaction takes place outside the particles forming the pozzolanic hydrate rim, which acts as a semi-permeable membrane tightly packing the RHA particles. The alkalis react with silica in pores of the RHA particles, producing ASR gels that react with Ca ions, adsorb water in the pores of the RHA particles and expand.
- The oxide composition of C-S-H as pozzolanic products of RHA containing an amount of sodium and potassium: C-(Na, K)-S-H. The ASR products of RHA contain an amount of calcium: Na, K-(C)-S-H. Where the Ca/Si ratio and (Na+K)/Si of pozzolanic reaction products are much higher and lower than those of ASR products respectively.

Zusammenfassung (German summary)

Selbstverdichtender Hochleistungsbeton (engl.: Self-Compacting High Performance Concrete-SCHPC) kann als eine neue Generation von selbstverdichtendem Beton (SCC) definiert werden. SCHPC hat die Verarbeitbarkeit des SCCs, d.h. eine hohe Fließfähigkeit sowie eine gute Sedimentationsstabilität, sowie hohe Druckfestigkeit und gute Dauerhaftigkeit des Hochleistungsbetons (HPC). Um diese Eigenschaften von SCHPC erzielen zu können, müssen bislang hohe Zementgehalte, umfangreiche Dosierung von chemischen Zusatzmitteln (Stabilisierer und Fließmittel) und kostenintensive puzzolanische Betonzusatzstoffe (z. B. Silikastaub) verwendet werden. Nachteilig bei dieser Art der SCHPC-Zusammensetzung sind die damit verbundenen hohen Kosten und der hohe CO_2-Fußabdruck entsprechender Materialien. Besonders kostentreibend ist der Einsatz von teurem Silikastaub, welcher allerdings in modernen SCHPC-Rezepturen eine zentrale funktionale Rolle spielt (Festigkeit, Dauerhaftigkeit etc.) und durch preiswertere Stoffe (Kalksteinmehl, Quarzmehl u.a.) nicht gleichwertig zu ersetzen ist. Insbesondere in Entwicklungsländern ist Silikastaub darüber hinaus kaum in entsprechender Qualität verfügbar. Die Substitution von Silikastaub durch preiswerte Reisschalenasche (RHA), einem landwirtschaftlichen Abfallmaterial, würde nicht nur die Ökobilanz von SCHPC verbessern, sondern auch die Umweltbelastung, die durch die Entsorgung von Reisschalen entsteht, reduzieren. Bei der kontrollierten Verbrennung von Reisschalen entsteht RHA. RHA hat einen sehr hohen amorphen Kieselsäuregehalt, vergleichbar mit dem von Silikastaub. Die ausgeprägte Porenstruktur stellt eine sehr wichtige Eigenschaft des Materials dar. Aufgrund der dadurch hervorgerufenen starken Wasserabsorption verringert die Zugabe von RHA die Fließfähigkeit, erhöht aber auch die Viskosität und damit die Sedimentationsstabilität des Betons. Diese Eigenschaften sind für die Verarbeitung von SCHPC essentiell. Die Hydratation von Portlandzement mit Kompositmaterialien wie Silikastaub oder RHA ist sehr komplex, weil die Reaktionen von Portland-Zement und die der Kompositmaterialien sich überlagern und miteinander interagieren. Im Vergleich zu den meisten anderen puzzolanisch reagierenden Kompositmaterialien (auch Silikastaub) weist RHA eine offene Porenstruktur und einen höheren Alkaligehalt auf. Folglich unterscheidet sich der Mechanismus der Hydratation von Portlandzement mit RHA von der Hydratation von Portlandzement mit Silikastaub. Die meisten puzzolanisch reagierenden Kompositmaterialien (Silikastaub, calcinierte Tone, Steinkohlenflugasche) können eine schädigende Alkali-Kieselsäure-Reaktion reduzieren, da über die Umwandlung von Calciumhydroxid in zusätzliche C-S-H-Phasen das Gefüge verdichtet wird und die Alkaliaufnahmefähigkeit der C-S-H-Phasen durch verringerte Ca/Si-Verhältnisse erhöht wird. Die Auswirkung von RHA auf die AKR ist weitgehend unbekannt und soll in der Arbeit umfassend untersucht werden.

Das Hauptziel der vorliegenden Arbeit ist es, die verfügbaren RHA umfangreich zu charakterisieren. Im weiteren Schritt werden die Eigenschaften von SCHPC mit RHA im Hinblick auf Rheologie, Hydratation und Mikrostrukturentwicklung sowie Alkali-Kieselsäure-Reaktion (AKR) untersucht und mit der Leistungsfähigkeit konventioneller SCHPCs auf Basis von Silikastaub verglichen.

Die Zusammenfassung der Ergebnisse, Beiträge, und die wichtigsten Schlussfolgerungen in der vorliegenden Arbeit sind folgt festgelegt:

- In der vorliegenden Arbeit wurde gezeigt, dass RHA ein makro-mesoporöses, amorphes, silikatisches Material mit einem sehr hohen Gehalt an amorpher Kieselsäure (vergleichbar mit dem von Silikastaub) ist. Die Porengrößenverteilung ist der wichtigste Parameter von RHA. Dieser Parameter beeinflusst direkt das Porenvolumen und die spezifische Oberfläche (engl.: specific surface area- SSA). Auch der Wasseranspruch und selbst die puzzolanische Reaktivität hängen von diesem Parameter ab. Dabei wird die SSA von RHA sowohl von der inneren (innerhalb der Partikel) wie auch von der äußeren Oberfläche (Partikeloberfläche) bestimmt. Beim Mahlen werden die meisten Makroporen aufgebrochen und die innere SSA von RHA nimmt ab. Gleichzeitig nimmt die äußere SSA von RHA zu.
- Die C-S-H-Phasen als puzzolanische Reaktionsprodukte auf der porösen Oberfläche der RHA- und Silikastaub-Partikel können erstmals nach 4 Stunden Hydratationszeit in der $Ca(OH)_2$-Puzzolan-Suspension beobachtet werden. Die puzzolanische Reaktivität die mit Hilfe des $Ca(OH)_2$-Verbrauchs bestimmt wurde, ist bei Einsatz von Silikastaub höher als bei RHA. Dabei ist die puzzolanische Reaktivität von RHA stark von der zur Verfügung stehenden Oberfläche abhängig, d.h. grobe RHA weist eine höhere Reaktivität als feine RHA auf. Dies ist möglicherweise auf die höhere Absorption von Ca-ionen in die Poren (innere Porosität) der groben RHA Partikel zurückzuführen, was eine interne puzzolanische Reaktion induziert.
- Eine neue Methode zur Proportionierung von SCHPC wurde auf der Basis von DIN EN 206-1 und DIN 1045-2 entwickelt. Der Fließmittel-Anspruch für die Selbstverdichtbarkeit von SCHPC ist eng mit der Fließmittel-Sättigungsdosierung von SCHPC-Mörteln verbunden. Die puzzolanische Reaktivität der eingesetzten Kompositmaterialien wurde verwendet, um die erwartete Druckfestigkeit vorherzusagen. Der Puzzolanische-Reaktivitäts-Index von RHA liegt bei 1,0 und ist vergleichbar mit dem von Silikastaub.
- Die Zugabe von RHA verringert das Setzfließmaß. Hingegen werden die Fließmittel-Adsorption, die Fließmittel-Sättigungsdosis, die Fließsgrenze und die plastische Viskosität des Mörtels erhöht. Die Auswirkung von RHA auf die o.g. Parameter ist viel stärker als dies bei Silikastaub der Fall ist, insbesondere wenn gröbere RHA Partikel mit höherer innerer Porosität zum Einsatz kommen.
- Im Hinblick auf die rheologischen Eigenschaften wirken Frischmörtel aus SCHPC im Vergleich zu anderen Mörteln scherverdickend. Die Zugabe von RHA bzw. Silikastaub verringert den scherverdickenden Effekt. Dabei ist die Wirkung von Silikastaub wesentlich stärker als die von RHA.
- Die Zugabe von RHA bzw. Silikastaub erhöht den Hydratationsgrad von Zement im Vergleich zu Systemen ohne diese Kompositmaterialien signifikant. Silikastaub wirkt sich dabei insbesondere auf die Reaktion im frühen Stadium aus, während RHA eher die Spätreaktion beeinflusst. Innerhalb der Gruppe der RHA ist eine gröbere Partikelfraktion bezüglich der Hydratationsgraderhöhung effektiver als eine feinere. Die Hydratationsbeeinflussung in RHA- bzw. Silkastaub-Zementpasten kann durch eine heterogene Keimbildung aufgrund der großen SSA der Kompositmaterialien und/ oder durch im ausgeprägten Porensystem intern gespeichertes Wasser, welches für die Nachbehandlung des Betons zur Verfügung steht, erklärt werden.

- Die Zugabe von RHA bzw. Silikastaub ändert den Hydratationsprozess der Klinkerminerale, d.h. von C_3S und C_2S. Der Hydratationsgrad von C_3S in der mit RHA/Silikastaub versetzten Probe ist größer als derjenige in der Referenzprobe. Durch Zugabe von RHA/Silikastaub wird die Hydratationsrate von C_3S zwischen 3 und 14 Tagen erhöht. Im Vergleich zur Silikastaub enthaltenden Probe ist der Hydratationsgrad von C_3S und C_2S größer in Anwesenheit von RHA. Zwischen 28 und 91 Tagen wird der Hydratationsgrad des Zements hauptsächlich durch den erhöhten Hydratationsgrad von C_2S bei Anwesenheit von groben RHA (22,6 µm) hervorgerufen.
- Eine Änderung der mittleren Korngröße der RHA (engl.: Mean particle size - MPS) bewirkt eine Änderung der puzzolanischen Reaktivität. Dabei laufen bei der hochporösen RHA puzzolanische Reaktionen sowohl im Inneren des Korns wie auch auf der Kornoberfläche ab. Die externe puzzolanische Reaktion von RHA verfeinert die Porenstruktur der Zementsteinmatrix, während die interne puzzolanische Reaktion teilweise oder vollständig die Poren innerhalb der RHA-Partikel mit Reaktionsprodukten ausfüllt. Zur Verfeinerung der Porenstruktur in der Zementsteinmatrix ist die feine RHA (5,7 µm)viel effektiver als die grobe RHA (22,6 µm). Die puzzolanische Reaktivität von Silikastaub-Partikeln ist im Vergleich zur RHA deutlich höher. Dies führt bei entsprechenden Mörteln zu einer niedrigeren Kapillarporosität in der Zementsteinmatrix.
- Silikastaub mindert eine schädigende Alkali-Kieselsäure-Reaktion in Mörteln mit reaktiver Grauwacke als Gesteinskörnung deutlich effektiver als RHA. Bei RHA ist die Wirkung bezüglich einer AKR-Minderung stark von der mittleren Korngröße der Aschen abhängig. Grobe RHA mit hohem MPS führen zu einer erhöhten Expansion bei Mörteln mit reaktiver Grauwacke. Hingegen kann feine RHA eine Expansion dauerhaft verhindern.
- Es konnte der Nachweis erbracht werden, dass RHA-Partikel bezüglich einer AKR als mikroreaktive Aggregate wirken, die mit Alkalilauge reagieren und expansive AKR-Produkte bilden. Dabei führen gröbere Partikel zu stärkeren Expansionen, während feinere Partikel zu keinen nennenswerten Dehnungen führen und sogar dehnungsmindernd wirken.
- In Anwesenheit hoher Alkalikonzentrationen laufen die puzzolanische und die Alkali-Kieselsäure-Reaktion von RHA nacheinander ab. Die Reaktion verläuft dabei von außen nach innen. Die puzzolanische Reaktion beginnt am äußeren Rand des Korns unter Bildung von puzzolanischen Hydratationsprodukten, die bezüglich der AKR als semipermeable Membran wirken. Im zweiten Schritt reagieren die Alkalien mit der Kieselsäure in den Poren der RHA-Partikel und produzieren dabei AKR-Gele. Das AKR-Gel reagiert mit Calcium-Ionen und absorbiert Wasser aus den Poren der RHA-Partikel. Als Folge kommt es zum Aufbau eines Quelldrucks, der zur Expansion des Gesamtsystems und zur Rissbildung führt.
- Die chemische Zusammensetzung der C-S-H-Phasen aus der puzzolanischen Reaktion von RHA zeigt neben den Hauptoxiden auch Natrium und Kalium als Komponenten. Daher wird postuliert, dass es sich um C-(Na, K)-S-H-Phasen handelt. Die AKR-Gele aus der Reaktion der Alkalien mit RHA weisen eine ähnliche Zusammensetzung mit allerdings niedrigerem Ca/Si-Verhältnis und höherem (Na+K)/Si-Verhältnis auf.

1. Introduction

1.1. Background to the research

Important trends in research and development of construction materials are the improvement of properties, the enhancement of service life and environmental sustainability. These trends lead to the development of a new generation of self-compacting concrete (SCC), which is known as self-compacting high performance concrete (SCHPC). SCHPC possesses adequate self-compactability, namely filling ability, passing ability and segregation resistance of SCC, and high strength and good durability of high performance concrete (HPC) [1]. Segregation resistance of SCHPC is controlled using viscosity modifying agents (VMA) or high amounts of powder or a combination of both [2]. At the same time, reactive supplementary cementitious materials (SCM) are utilized to fulfil the high strength and durability requirements of HPC [1, 3].

One of the main disadvantages of SCHPC is its high cost due to the extensive use of chemical admixtures, such as superplasticizer (SP) and viscosity modifying admixtures (VMA); the use of a high volume of Portland cement and expensive supplementary cementitious materials, i.e. silica fume (SF). High cement content usually introduces high hydration heat, high autogenous shrinkage and high cost. Moreover, the consumption of natural resources and carbon dioxide emissions associated with cement production can cause serious environmental impacts [4]. One solution to reducing the cost of SCHPC is the use of less-expensive SCMs as a substitute for SF as a partial cement replacement. Rice husk ash (RHA), with its high amorphous silica content, is a very good replacement for SF with regard to compressive strength and durability of concrete [1, 5-9]. Apart from a function as a SCM, RHA has been used to improve viscosity and hence segregation resistance of SCHPC [1, 10].

RHA is the residue of completely incinerated rice husk under proper conditions. Rice husk, the outer covering of a rice kernel, is an agricultural waste from the milling process of paddy. Rice husk is abundant in many rice cultivating countries, e.g. Vietnam, India and China. Each ton of paddy rice can produce approximately 200 kg of rice husk, which on combustion produces about 40 kg of ash [6]. According to ''Rice market monitor'' report [11], the global rice paddy production in 2011 was about 723 million tons, which produces approximately 145 million tons of rice husks. Normally, rice husk from paddy rice mills is disposed directly into the environment or sometimes is dumped or burnt in open piles on the fields. This results in serious environmental pollution, especially when it is disintegrated in wet conditions.

Therefore, using less-expensive and locally available RHA produced from rice husk to modify viscosity of concrete, to replace SF totally as a partial cement replacement brings benefits to the economy, the technical properties of concrete and the environment. Up to now, to the author's knowledge, no comprehensive research has been implemented to investigate the pore structure of RHA in detail and the effect of the pore structure and chemical composition of RHA on properties of fresh and hardened SCHPC and its durability.

As mentioned above, RHA is a prospective SCM for SCHPC due to technical properties, the economy of concrete as well as the environmental protection. To accomplish knowledge on RHA applied in concrete, the following points should be considered:

1) RHA is classified as a highly reactive pozzolan. It possesses a very high silica content similar to that of SF [5]. The significant difference between them is that SF is a dense material, whereas RHA is a porous material [5, 12]. Pore structure of this material plays a very important role in cementitious materials. With the given amorphous silica content, the change of this characteristic results in a different specific surface area and therefore a different pozzolanic reactivity and different water adsorption of RHA [13]. These parameters dramatically influence properties of fresh and hardened RHA modified cementitious materials. The pore structure and other characteristics of RHA should therefore be paid attention to in full detail.

2) RHA absorbs a large amount of mixing water into its pores when added to the concrete mixture. That results in a lower water-cement ratio (w/c) of bulk cement paste and hence lower workability of the concrete. Therefore, in order to obtain an acceptable workability, it is necessary either to use a higher amount of mixing water or to introduce SP into the concrete mixture. From the opposite point of view, however, the reduction in w/c of the bulk cement paste due to the absorbing capacity of RHA increases plastic viscosity, eliminates bleeding and improves segregation resistance of concrete mixture. It should be borne in mind that requirements for fresh SCHPC are not only workability, i.e. filling ability and passing ability, but also segregation resistance. Theoretically, a compromise between good workability and adequate segregation of concrete can be made by adjusting pore parameters of RHA particles at a given w/c ratio. This effect of RHA on rheological properties of fresh SCHPC has not yet been thoroughly investigated.

3) The state of art on mechanism for hydration of cement blended with SCMs such as SF, fly ash (FA), ground granulated blast-furnace slag (GGBFS), etc., is still not fully understood. It can be said that the hydration of the binder is very complex and depends on the chemical composition, the fineness, and the amount of reactive phases of SCM and the composition of the interacting solution. As summarized by Lothenbach [14], the inclusion of SCM with Portland cement results in a more complicated system because the hydraulic reactions of the Portland cement and SCM take place simultaneously and might interact with each other. It is proposed that the addition of SCM to Portland cement contributes extra space for the hydration products of clinker phases due to the higher water to cement ratio at the same water-binder (cement +SCM) ratio and extra nucleation sites for the precipitation of hydrated phases due to the higher fineness of SCM in terms of finer SCM compared to cement. Moreover, the pozzolanic reaction of SCM, e.g. rich-silica SCM, occurs parallel with hydraulic reaction of cement. The pozzolanic reaction of SF, a typical rich-silica SCM, occurs for months with 20-80 % reacted content. The reaction forms low Ca/Si C-S-H ''tobermorite-like'' compared to high Ca/Si C-S-H ''jennite-like'' from the hydration of Portland cement. The low Ca/Si C-S-H takes up aluminum and/or alkalis. As mentioned above, RHA has a similar amorphous silica content to SF, but the alkali content of RHA, with about 3 wt.%, is significantly higher than that of SF [5, 6, 13, 15]. Additionally, in comparison with other SCMs, i.e. SF, RHA particles have a highly porous structure. Consequently, the mechanism for the hydration of Portland cement blended with RHA may be different from that for SF and more complicated, and the products

from RHA pozzolanic reaction may be formed with higher incorporated alkalis. To date, this aspect has not yet been clearly understood.

4) Pore structure is a very important physical property of RHA that influences the properties of fresh, hardened concrete and the durability of RHA containing concrete as well. A variation in mean particle size (MPS) of RHA results in a variation in the pore structure in RHA particles [6, 13, 16], i.e. pore size distribution, leading to different plastic viscosity and air void content, as well as the hydration degree of cement blended with RHA in SCHPC. Moreover, RHA particles with a porous structure themselves might be weak points dispersed in very dense matrix, especially when the coarse ones are used. These factors dramatically influence the development of compressive strength of the concrete at various water-binder (w/b) ratios. A question should be raised as to which MPS is most suitable to achieve the best compressive strength and adequate self-compactability of SCHPC at a given w/b ratio.

5) It is well documented that alkali-silica reaction (ASR) is a deleterious reaction caused by a reactive aggregate and cement paste pore solution. The reaction between alkali hydroxides in concrete pore solution and amorphous or poorly crystalline silica phases in aggregates or SCMs forms alkali silica gel which absorbs water and expands [17-20]. Blending Portland cement with one or more pozzolanic materials, such as silica fume (SF), metakaolin, low-calcium fly ash (FA), and slag [17, 19-22] is strongly attributed to the most effective solution to reducing expansion caused by ASR. It has been noted that large agglomerated SF particles act as reactive aggregates rather than as pozzolanic materials and contribute to ASR [18, 23]. RHA possesses very high silica content similar to that of silica fume (SF). However, the significant differences between them are that RHA particles are porous and much larger than ones of SF. Furthermore, alkali content, i.e. Na_2O and K_2O of RHA is much higher than that of SF [6, 13, 16]. RHA particles themselves can provide sufficient conditions, i.e. humidity from the water absorbed in its pores, alkali, and reactive silica, in mortar and concrete with saturated calcium hydroxide solution to prompt ASR. RHA with enough coarse particle size may actually act as alkali silica reactive aggregates, thereby accelerating ASR rather than mitigating it. This provides motivation for investigating the alkali silica reactivity of RHA, especially in the environment of SCHPC with a high amount of cement then a high probability of high alkali content.

1.2. Objectives of this thesis

The objective of this research is to analyze the characteristics of RHA and investigate the behaviour of RHA in SCHPC, compared to SF. The following aspects are investigated in this research:

- Pore structure and other characteristics of RHA are paid attention to in full detail. Based on those its effect on properties of SCHPC can be explained.
- An attempt is made to propose a mix-design method to produce SCHPC incorporating various SCMs with adequate self-compactability and compressive strength as high as possible, i.e. 90-130 MPa, particularly in the presence of RHA.
- The effect of RHA in combination with or without other SCMs, such as LSP, FA on self-compactability, i.e. filling ability, passing ability, viscosity then segregation resistance and compressive strength of SCHPC is investigated.

- The effect of porous RHA on rheological properties and the resulting self-compacting properties of SCHPC is taken into account in detail.
- The effect of RHA in terms of pore structure, namely pore volume, pore size distribution, and chemical composition on the hydration and microstructure development as well as the pozzolanic hydrates formed in cement matrix, and the resulting compressive strength of mortar and SCHPC is accounted for.
- The alkali silica reactivity of RHA is considered. RHA with enough coarse particle size may actually act as micro-alkali silica reactive aggregates, thereby accelerating ASR reaction rather than mitigating it.

1.3. Outline of this thesis

The content of this thesis consists of the study of key characteristics of RHA and their effect on the rheological properties, self-compactability, hydration and microstructure development, compressive strength, and durability of mortar and SCHPC as summarized in Fig. 1.1.

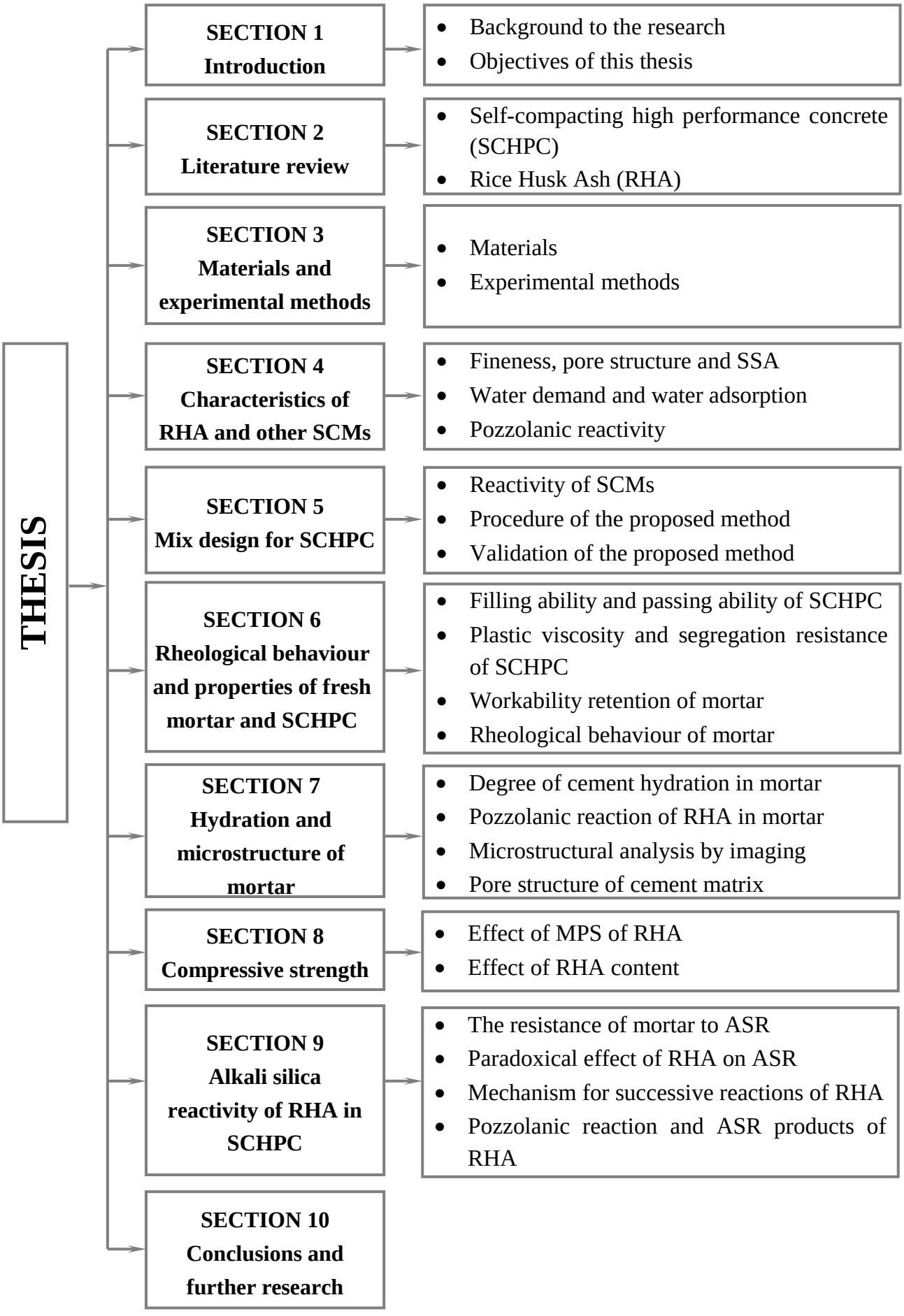

Fig. 1.1 Outline of this thesis

2. Literature Review on Self–compacting High Performance Concrete and Rice Husk Ash

2.1. General

In this section, the main aspects of SCHPC, such as the definition, constituent materials, performance criteria, mixture design method, self-compactability, mechanical properties, and durability are briefly described. A part from the primary knowledge on SCHPC, the production, the characteristics of RHA and the use of RHA in mortar and concrete are also reviewed in the second main part.

2.2. Self–compacting high performance concrete

2.2.1. Definition

SCHPC is considered a special type of concrete, which is defined on the basis of the concepts of SCC and HPC. As a result, SCHPC possesses the adequate self-compactability (filling ability, passing ability and segregation resistance) of SCC and the high strength and good durability of HPC [1]. In comparison with other coarse aggregate concretes, a SCPHC is an optimized-advantage concrete in terms of workability, compressive strength, durability and improvement in the environment and working conditions [1, 24].

The high performance of SCHPC compared to that of ordinary concrete mainly originates from the exceptional mixture proportions and material components. A part from the basic materials used for ordinary concrete, a high amount of SP, SCMs, and/or without a viscosity modifying admixture (VMA) are permanently employed in SCHPC. Compared to traditional vibrated concrete (TVC), SCHPC has a considerably higher binder (SCM and cement) content, a greater fine aggregate content and a less quantity of coarse aggregate, and a lower water-binder (w/b) ratio of 0.20-0.40 [1, 25-28]. In Fig. 2.1, typical volume proportions of SCC, compared to those of Reactive Powder Concrete (RPC), HPC and Ultra High Performance Concrete (UHPC), are illustrated respectively.

Self-compactability of SCHPC can be obtained by compromise between flowing ability (filling and passing ability) and segregation resistance. These two properties are also interrelated; the optimal flowing ability can only be reached from the optimal segregation resistance or vice versa. On the one hand, optimal flowing ability can be achieved by the use of SP, a decreased coarse aggregate content, and a high amount of binder at a low w/b ratio. Optimal segregation resistance can be attained by a decreased coarse aggregate content and an increased binder content at a low w/b ratio or by the use of VMA. Additionally, a reduced coarse aggregate size is beneficial to both optimal flowing ability and segregation resistance[1, 26, 28]. Safiuddin suggested the basic principles of SCHPC adapted from Okamura [28] as displayed in Fig. 2.2.

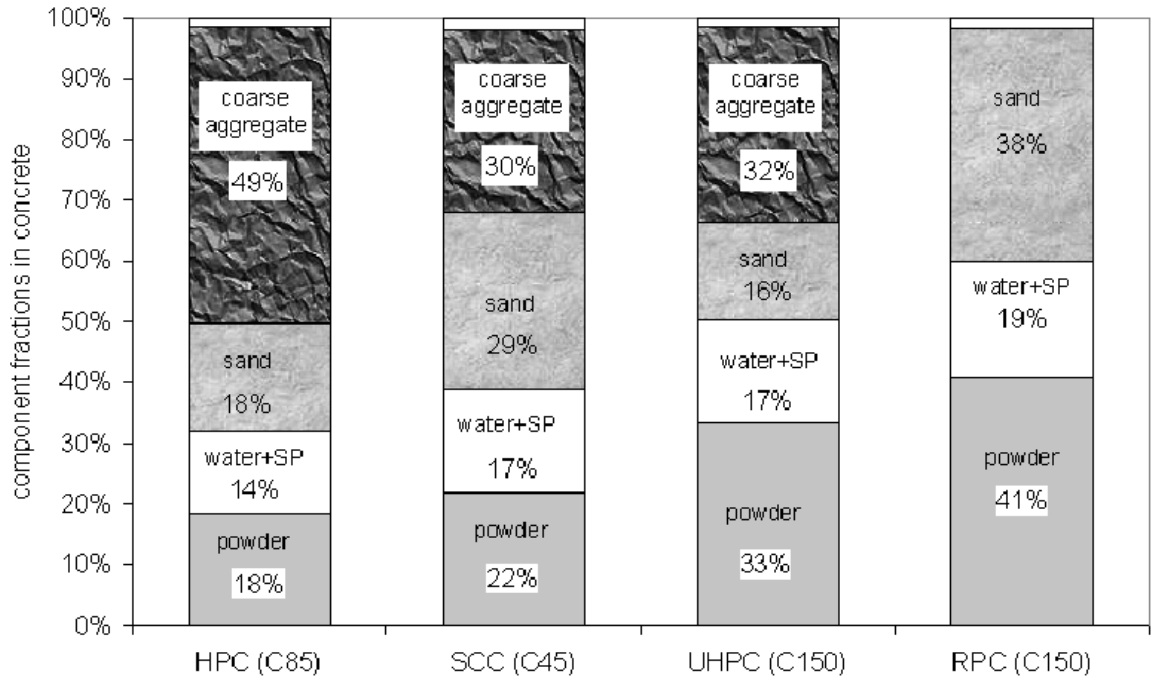

Fig. 2.1 Component volume fractions in HPC, SCC and UHPC [29]

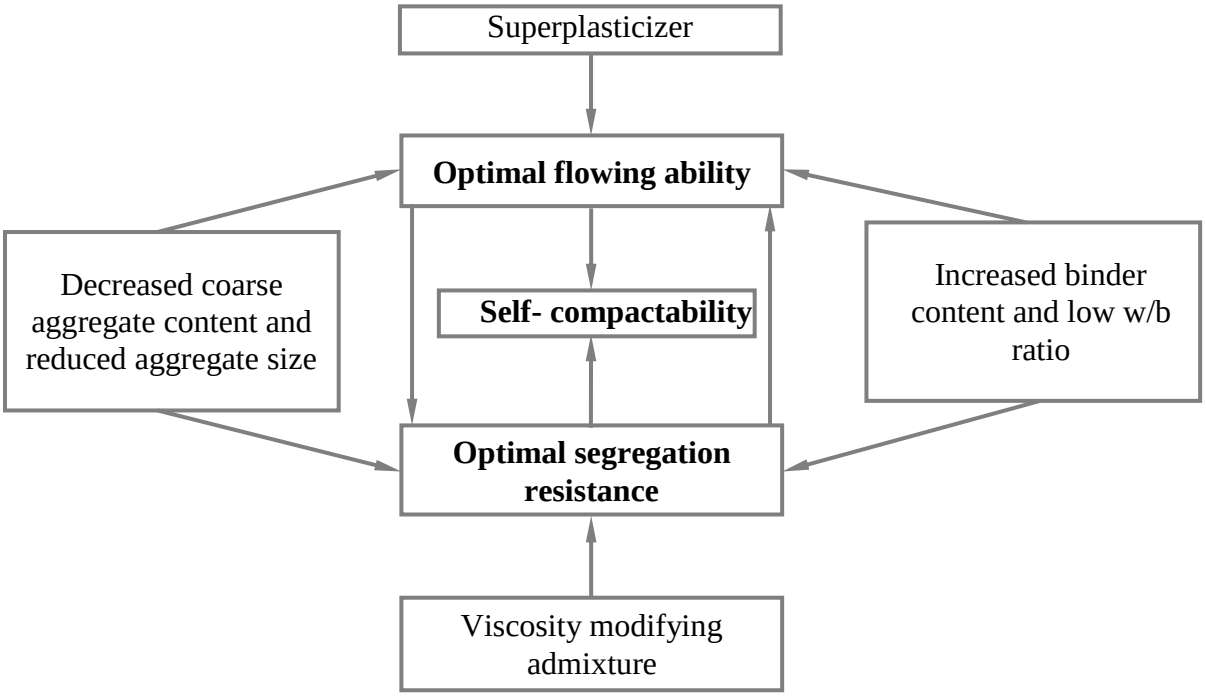

Fig. 2.2 Basic principles of SCHPC [1]

Similar to SCC, SCHPC may be categorized into three types: the powder type, viscosity agent type and the combination type [1, 2]:

- The powder type: Self-compactability is provided by the large amount of binder (cement and SCM) and the limited coarse aggregate content, along with SP at the low w/b ratio. The large amount of binder which normally ranges from 550 to 650 kg/m^3 and the low w/b ratio induce plastic viscosity and hence segregation resistance, whereas flowing ability is provided by SP [26].

- Viscosity agent type: This type of SCHPC is characterised by the lower amount of binder (350-450 kg/m^3) and the presence of VMA. The plastic viscosity and thus the segregation resistance are controlled by VMA, whereas SP provides flowing ability [28].
- The combination type: Both the binder content between 450 and 550 kg/m^3 and VMA are used. The self-compactability can be achieved by the increased binder amount, VMA, and SP at the low w/b ratio [30].

2.2.2. Constituent materials for SCHPC

A high amount of SP, SCMs, and/or without VMA are permanently employed in SCHPC besides the basic materials used for TVC, namely Portland cement, mixing water, fine and coarse aggregate. As a general rule, the constituent materials that conform to the standards and specification for ordinary concrete can be used to produce SCHPC. However, SCHPC mixes are more sensitive to variation in material properties than ordinary concrete [24].

Portland cement

Portland cement is mostly used to produce SCHPC. The cement is blended with SCMs to improve the flowing ability of fresh SCHPC [28]. Portland cement is the main factor influencing the density of cement paste and thus the segregation resistance of SCHPC [1]. During hydrating, Portland cement refines the microstructure and binds other components together, resulting in durability and compressive strength of concrete [31, 32].

Supplementary cementing materials

In respect of mixture proportions, SCHPC is distinguished from ordinary concrete mainly due to the higher content of binder or powder (cement and SCMs). Using SCMs as a partial replacement for cement can decrease the cement content in concrete which helps to reduce the cost of SCC/SCHPC as well as limit the negative effects of heat of cement hydration, particularly reducing the risk of cracking from thermal strains. Furthermore, SCMs contribute to a larger volume of paste in concrete which is one key factor in achieving great workability. The cement paste (binder paste in general) coats and separates the particles of aggregate, forming a ''lubricating'' layer, which reduces the friction between them and facilitates their movement and arrangement [24]. At least one or more SCMs are usually incorporated with Portland cement to produce SCHPC. Over 25 % ternary binders (cement and two SCMs) and about 5 % quaternary binders (cement and three SCMs) have been used [33]. All kinds of SCMs, i.e. nearly inert, pozzolanic and latent hydraulic have been applied. Each kind of SCM has different effects on properties of both fresh and hardened concrete.

Limestone powder: Limestone powder (LSP) is largely used in SCC. The addition of LSP results in an increase in the yield stress but does not affect the plastic viscosity and the fluidity of the concrete for a given w/c ratio [34-36]. However, when LSP is used beyond the critical content, the addition of LSP dramatically increases plastic viscosity depending on w/c ratio. LSP is considered a nearly inert SCM. LSP does not or only slightly take part in the hydration of cement, and does not contribute compressive strength of SCC [37, 38]. On the other hand, the addition of fine LSP can enhance the rate of cement hydration [39, 40] and strength development, as well as improve the deformability and stability of fresh SCC [40]. It is

attributed that finely ground LSP offers nucleation sites for the hydration products of cement and possible chemical reactions involving cement hydrates and $CaCO_3$.

Fly ash: Fly ash (FA) is commonly used to produce SCC. The addition of FA to concrete increases the workability and long-term compressive strength. Concrete containing FA needs less SP to obtain a similar mini-slump flow compared with concrete containing only cement as binder, due to its spherical particles and lower water demand compared to cement [41-45]. The use of FA as a partial replacement of cement can significantly improve rheological properties of flowing concrete and SCC [35, 46]. Furthermore, inclusion of FA also results in higher VMA demand.

Silica fume: Silica fume (SF) is an industrial by-product of the production of silicon and ferro-silicon alloys. SF is a main ingredient of HPC due to its exceptional properties, i.e. ultra-fine and spherical particles and very high amorphous silica content of about 90 wt.%. However this product is very expensive [13, 35, 47, 48]. The addition of SF in SCC increases yield stress and viscosity and thus significantly reduces slump flow, segregation and bleeding due to its high fineness [35, 36, 49, 50]. Incorporating SF in concrete results in an increase in compressive strength, modulus of elasticity, and flexural strength, and improves durability even at early ages compared to other SCMs [35, 50].

Rice husk ash: Rice husk ash (RHA) is the residue of incinerating rice husk under controlled temperature conditions. Rice husk is an agricultural waste from the milling process of paddy rice in developing countries. Similar to SF, RHA possesses a high content of amorphous silica and large specific surface area. RHA is a good replacement for SF with respect to compressive strength and durability of concrete. The significant difference between them is that SF particles are spherical, dense and extremely fine, whereas RHA particles are angular, porous and rather coarse. The porous structure of RHA plays an important role in its behaviour in cementitious materials. With the same amorphous silica content, the change of this characteristic results in a different specific surface area and, therefore, in a different pozzolanic reactivity and a higher water adsorption of RHA. Furthermore, the alkali content, i.e. K_2O of RHA is much higher than that of SF [1, 5, 6, 13, 16]. These parameters can influence the fresh and hardened state properties and the durability of RHA-modified cementitious materials.

Chemical admixtures

It is well known that SCHPC has exceptional self-compactability compared to ordinary concrete originating from chemical admixtures such as SP and VMAs.

Superplasticizers: To meet the full self-compactability of SCHPC at a very low w/b ratio, SP is of the most importance. The flowing ability of SCHPC is originated from the SP by liquefying and dispersing effects. The liquefying effect decreases yield stress and plastic viscosity while the dispersing effect deflocculates the solid particles and frees the entrapped water, thus reducing the inter-particle friction and flow resistance. This results in the improvement of the flowing ability of concrete [1, 51, 52].

All sulfonate-based superplasticisers, namely sulfonated melamine-formaldehyde condensates, sulfonated naphthalene-formaldehyde condensates, and polycarboxylates can be used to produce SCHPC. Compared to sulfonate-based superplasticiser, polycarboxylate-based SPs are

most commonly used to produce SCHPC due to their higher dispersing effect, longer consistence retention and greater robustness, qtd. in [35, 50]. Moreover, Yamada et al. [53] and Golaszewski and Szwabowski [54] have found that polycarboxylate-based SPs can reduce greater yield stress and less plastic viscosity, especially at low w/b ratio.

In SCHPC proportioned with a very low w/b ratio, a dosage of SP near to the saturation dosage is commonly introduced in order to fulfill its self-compactibility. The adsorption behaviour and the compatibility of SP with cement and SCMs should be paid much attention to as they significantly affect self-compactability. These properties of SP depend on the type of SP, cement [53, 55, 56] and SCMs [16].

Viscosity modifying admixtures: Viscosity modifying admixtures (VMA) are also referred to as stabilizers, anti-washout admixtures, viscosity enhancing admixtures and water retaining admixtures. Normally, VMAs are used to produce SCHPC, under water concrete, pumping concrete. For SCHPC, introduction of VMA changes the rheological properties of concrete by increasing the plastic viscosity and cohesion and by causing a small increase in the yield stress. This results in a reduction in the bleeding and segregation of the concrete. Furthermore, VMA makes SCHPC less sensitive to variations in the moisture content of the aggregate; minimal effect of changes in properties of the materials; lower powder content; and better robustness against the impact of variations in the concrete constituents and in site conditions [2, 49].

Water

Water is an obligatory component of SCHPC. Water necessitates combining with SP to achieve self-compactability of SCHPC, and hydrating cement, then producing paste to bind the aggregates together [28]. As a result, water significantly influences properties of fresh and hardened concrete. Water reduces the yield stress and viscosity. Free water plays a key role influencing the filling ability and segregation resistance of SCHPC [35, 57].

Aggregate

To meet self-compactability, a lower total aggregate content, a greater ratio of fine aggregate to coarse aggregate and a smaller maximum aggregate size compared to ordinary concrete are utilized to produce SCHPC. A continuous grading of aggregates is attributed to result in a better flow ability. A wide range of aggregate sources, of aggregate types, sizes and shapes and of aggregate particle size distribution has been used to produce SCHPC properly [35, 50, 58]. In Fig. 2.3, particle size distributions of 11 aggregates considered suitable for SCHPC are shown [59]. From an

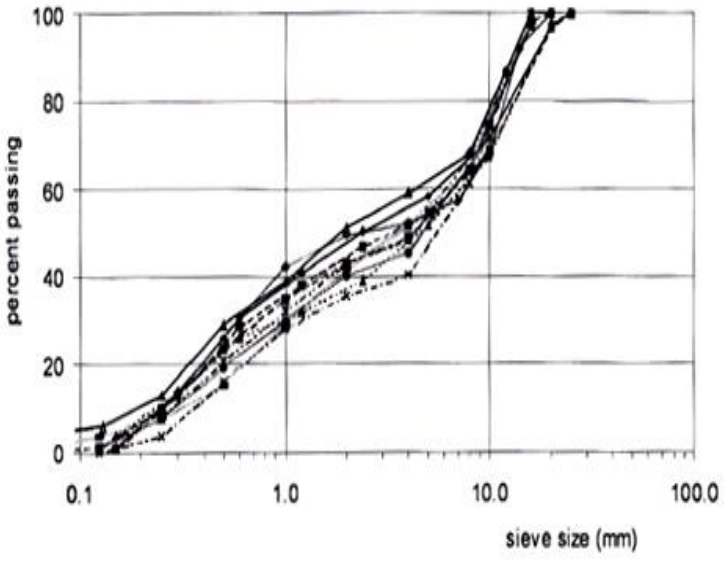

Fig. 2.3 Overall aggregate gradings for typical SCC mixes from Testing-SCC project partners

analysis of the combined grading curves for all particles, i.e. coarse aggregate, fine aggregate, SCMs and cement, Brouwers and Radix have found that the particle size distribution given by Funk and Dinger's equation (Eq 2.1) with a value for q of 0.25 is suitable for SCHPC, whereas a value for q of 0.50 which gives the Fuller curve is more suitable for ordinary concrete. Two overall grading curves of aggregate with D_{max} of 20 mm and D_{min} of 0.1 mm are provided in Fig. 2.4. It is clear that the content of fine aggregate in SCC/SCHPC is higher than that of ordinary concrete [24].

$$P(D) = \frac{D^q - D_{min}^q}{D_{max}^q - D_{min}^q} \quad (2.1)$$

Where, P(D) is the percentage of aggregate passing the sieve with D mm in size. D_{min}, D_{max} are the minimum and maximum particle sizes in the aggregate blend.

Key characteristics, such as shape, angularity, and texture; particle size distribution (including maximum aggregate size); and microfines characteristics are paid much attention to in the selection of aggregates for SCHPC [35, 50]. The differentiation between fine aggregates and coarse aggregates depends on the local availability and practice, such as 4 mm in Europe [60], 4.75mm in USA [61], 5 mm in Japan and 8 mm in Sweden, qtd in [35]. Material smaller than 0.075 mm in Japan [28] or 0.125 mm in Europe [49] is considered as powder.

Coarse aggregate

Similar to ordinary concrete, coarse aggregate plays a very important role in influencing the flowing ability, segregation resistance, and strength of SCHPC [28, 62, 63]. The shape and the particle size distribution of coarse aggregate directly affect the flow and passing ability and segregation resistance of SCHPC and its required paste content. Both rounded and angular crushed coarse aggregates have been used to produce SCHPC depending on local availability [33]. Rounded aggregates (gravel) are preferable to angular aggregates for achieving the high flowing ability of SCHPC, as less yield stress and plastic viscosity in concrete mixture can be obtained with the rounded-shape aggregates because of less inter-particle friction. Whereas angular crushed aggregates are beneficial to high strength and strong interfacial bond due to rough surface texture and interlocking characteristic [1, 60]. But greater water demand is required for the angular crushed aggregates due to their surface texture, aspect ratio, and angularity that results in higher yield stress and viscosity and hence lower flowing ability of SCHPC [63]. However, the reduction in flowing ability can be

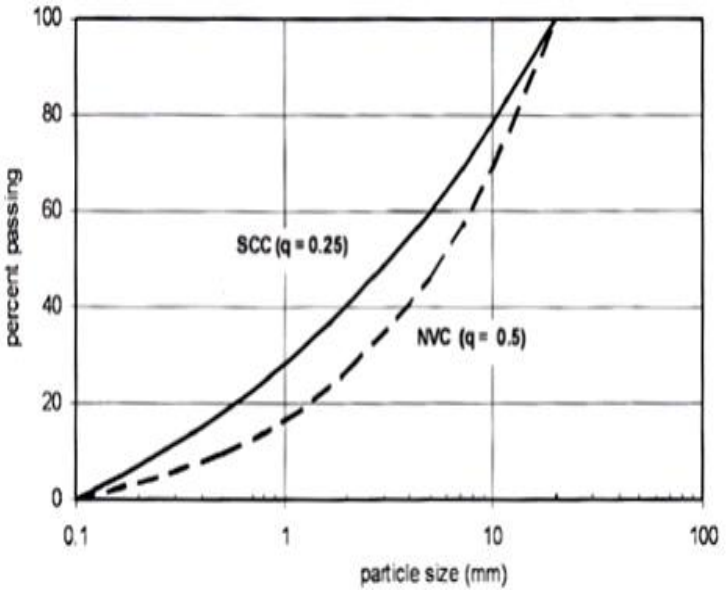

Fig. 2.4 Preferred aggregate grading curves for SCC and original concrete

compensated by the addition of SP. To fulfill both adequate self-compactability and high strength, angular crushed aggregate should be recommended.

The smaller size is conducive to achieve higher strength and to reduce segregation in fresh SCHPC [1, 64]. Generally, the normal maximum size in the range of 16-20 mm has been applied to produce SCHPC [33, 60]. Well-graded coarse aggregates are conducive to an increase in packing density which improves the flowing ability and segregation resistance in fresh concrete [32, 35]. Better packing also helps to improve hardened properties and durability because of the minimized voids and dense structure [1, 65]. Furthermore, Okamura and Ozawa have indicated that well-graded coarse aggregates can be used in higher contents in SCHPC [28].

Fine aggregate

SCHPC possesses a greater fine aggregate content than that of ordinary concrete. With an appropriate content, fine aggregates can improve the flowing ability and segregation resistance of SCHPC [1, 28, 66]. Similar to coarse aggregates, the shape and gradation of fine aggregates also influence properties of fresh and hardened SCHPC. Natural sand is usually preferable to angular crushed sand for achieving a better flowing ability. Angular fine aggregates are not conducive to the flow ability, because they can increase the plastic viscosity of mortar in SCHPC [67]. However, the angular fine aggregates which are chemically inert, sound, low absorbent, and free from deleterious substances should be selected to attain high strength and good durability of SCHPC, since the adverse effect on flow ability can be eliminated by using SP and reducing the content of fine aggregate [1]. Generally, it is documented that the paste content of SCHPC can be reduced, when fine aggregates are well-graded [49]. Hu and Wang [68] have shown that the flow of mortar is greater with the well-graded fine aggregates and hence the flowing ability of SCHPC may be improved. In addition, the packing density, and thus the hardened properties and durability of concrete can be improved with the well-graded fine aggregates [65].

2.2.3. Performance criteria for SCHPC

SCHPC is required to fulfill self-compactability criteria of SCC in the fresh state, and to achieve good hardened properties and good durability of HPC in the hardened state as well [1]. The self-compactability criteria for SCHPC, i.e. filling ability, passing ability, flow rate (viscosity) and segregation resistance are evaluated by test results. Filling ability; passing ability; viscosity; and segregation resistance are measured by slump flow; J-ring or L-box; T_{500} or V-funnel and sieve segregation tests which are regulated in standards DIN EN 12350-8; DIN EN 12350-12 or DIN EN 12350-10; DIN EN 12350-8 or DIN EN 12350-9; and DIN EN 12350-11, respectively. The requirements for the properties of fresh SCC that may be specified for SCHPC can be found in Japanese guidelines [69] or in European guidelines [49] and European standards [70]. Table 2.1 presents the requirements for the properties of fresh SCC while performance criteria for HPC are presented in Table 2.2 [1].

Table 2. 1 The requirements for the properties of fresh SCC/SCHPC according to DIN EN206-9

Slump-flow		Viscosity			Passing ability		Segregation resistance	
Class	Slump flow (mm)[a]	Class	T_{500} (sec)[b]	V-funnel (sec)	Class	J-ring step height (mm)	Class	Sieve segregation (%)
SLF1	550-650	VS1/VF1	< 2	< 9[c]	PJ1	≤10 with 12 bars	SR1	≤20
SLF2	660-750	VS2/VF2	≥ 2	9-25[d]	PJ2	≤10 with 16 bars	SR2	≤15
SLF3	760-850	-	-	-	-	-	-	-

Permissible deviation: [a] ± 50mm; [b] ± 1s; [c] ± 3s; [d] ± 5s

Table 2.2 Performance criteria for HPC/SCHPC [1]

Method	Property	Performance criteria
Air content by pressure method	Fresh air content	4 to 8 %
Axial compression on cylinders	Early-age compressive strength	> 20 MPa
	28 and 91 days compressive strength	> 40 MPa
Ultrasonic pulse velocity by PUNDIT	Physical quality or condition (packing, uniformity, etc.)	≥ 4575 m/s
Porosity by fluid displacement method	Total porosity as an indicator of strength and transport properties	7 - 15 %
Adsorption by water saturation technique	Water adsorption as an indicator of durability	3 - 6 %
True electrical resistivity by Wenner probe	Electrical resistance to corrosion	> 5 - 10 kΩ-cm
Rapid chloride ion penetration	Electrical charged passed as an indicator of corrosion resistance	< 2000 C
Normal chloride ion penetration at 6 months	Penetrated chloride value as an indicator of corrosion resistance	< 0.07 %
Durability factor after 300 cycles of freeze-thaw	Resistance to freezing and thawing	> 0.80

2.2.4. Mixture design for SCC/SCHPC

The mix design can be understood combining the constituent materials in the optimum proportions to give concrete with the requirements of fresh and hardened properties for a particular application [24]. Generally, in the mix proportioning of ordinary concrete, the required compressive strength is the primary criterion. With SCHPC, however, self-compact ability, high compressive strength, and good durability are equally taken into account in proportioning mixtures [1].

Regarding the properties of SCC/SCHPC, there exist two main mix design approaches to proportion mixtures. One approach emphasizes self-compactability, and ignores or does not give equal importance to compressive strength and durability [28, 49, 50, 60]. The other approach considers self-compactability as well as compressive strength as the targets of mix design for SCC/SCHPC. Compressive strength of SCC designed by these methods ranges mostly from 30 to 90 MPa [1, 63, 64, 71-75]. Regarding the utilization of SCM in SCHPC, several individual SCMs such as FA, RHA, SF, GGBFS, etc., are taken into consideration in mix design of SCC/SCHPC to ensure adequate self-compactability and required compressive strength [1, 63, 64, 75]. It is generally known that each SCM has its own advantages and

disadvantages. Combinations of various SCMs can exploit their advantages and increase the cement replacement level. For instance, the addition of FA in concrete can increase flowing ability, and can reduce SP dosage to reach a given flowing ability due to its spherical particles and lower water demand compared to cement [76]. Concrete containing FA has higher long-term compressive strength, however lower one at early ages than that of control concrete [41-45]. Effective cement replacement by FA is assumed to a range of 0-33 wt.% [77, 78]. RHA can be used as a VMA to increase the segregation resistance of SCHPC. An increasing RHA content decreases the slump flow, passing ability of concrete due to its pore structure and very high water demand, especially at low w/b ratios [10]. With the replacement of cement by up to 20 wt.%, RHA can increase the compressive strength of concrete at 28 days, especially at later ages due its pozzolanic effect and internal water curing effect. The effect of RHA on compressive strength can be comparable with SF [1, 6, 9]. Therefore, the combination of RHA and FA can be beneficial to self-compactability and compressive strength of SCHPC, SP and VMA dosages, and it can extend the cement replacement content. Following this philosophy, a method for proportioning SCHPC that considers the combination of various SCMs to fulfill adequate self-compactability requirements while simultaneously achieving a particular high compressive strength in range of over 90 MPa, and good durability is investigated.

2.2.5. Rheology and properties of fresh SCHPC

SCHPC needs a combination of key distinct properties, i.e. filling ability, passing ability, and segregation resistance, that must reach adequate levels to be self-compacting and remain so during transport and placing. The other fresh properties that should be considered are unit weight and air content.

Filling ability

Filling ability, so called unconfined flowability, is defined as the ability of fresh concrete to flow into and fully fill all spaces within the formwork under its self-weight [24, 49, 60]. This property is associated with two aspects: total flow capacity refers to how far a fresh SCHPC can flow; and flow rate refers to how fast a fresh SCHPC can flow. Filling ability is a compromise between flow capacity and flow rate to allow any air entrapped during the mixing and placing to escape and reach adequately compacted concrete [24]. Filling ability is basically affected by aggregate content, particle size distribution of aggregate, w/b ratio, binder content and SP dosage of concrete [28, 35, 79]. A high filling ability of SCHPC can be achieved by reducing inter-particle friction among solid particles, namely coarse aggregate, sand and powder in concrete by introducing a SP and by using a lower coarse aggregate content. Inter-particle friction can be also reduced if continuously graded materials, aggregates and powder are used [44, 79]. Too low or too high water content (w/b ratio) results in low filling ability. Increasing water content could increase filling ability due to reduction in inter-particle friction, otherwise viscosity is reduced, thus leading to segregation and bleeding. Filling ability can be improved by introduction of SP. SP decreases the inter-particle friction as mentioned above, and also maintains the flow capacity and flow rate [35].

Passing ability

Passing ability, so called confined flowability, is defined as the ability of fresh concrete to flow through confined spaces between steel reinforcing bars without segregation or blocking [24, 49,

60]. Blocking occurs when fresh concrete flows and approaches a narrow space, the different flow rate of coarse aggregate and mortar results in a locally high content of coarse aggregate. Therefore, passing ability is governed by the factors affecting filling ability such as the size, shape and content of coarse aggregate, and by the number and spacing of the reinforcing bars. Increasing the filling ability of fresh concrete and limiting the segregation of coarse aggregates are both effective in improving passing ability [1, 80].

Segregation resistance

Segregation resistance (also called stability) is defined as the ability to remain uniform both during transport and placing (dynamic stability) and after placing (static stability) [24, 49, 60]. SCHPC is susceptible to segregation because it consists of materials with different sizes and specific gravities. Segregation can occur between water and solid (bleeding) or between paste and aggregate or between mortar and coarse aggregate in both dynamic and static states [60, 81]. This phenomenon is related to the plastic viscosity and density of the cement paste. Segregation will occur if the density of the aggregate is greater than that of the cement paste and the viscosity of the paste is low [24]. Enhancement of segregation resistance can be attained by a high amount of cementing materials, a small maximum size of aggregate, a limited content of coarse aggregates, and a low w/b. The use of VMA can also improve the segregation resistance of SCHPC [2, 82]. It is reported that the high degree of filling ability in good SCHPC can mitigate the effect of non-uniform distribution of aggregate due to segregation on strength and durability, especially when the paste/ the mortar has relatively high compressive strength.

Interactions between filling ability, passing ability and segregation resistance

Filling ability, passing ability and segregation resistance are strongly interrelated, particularly in certain conditions [24]. A variation of one property will normally affect one or both of the others. For example, poor filling ability as well as poor segregation can cause insufficient passing ability, i.e. blocking. Increasing filling ability can increase risk of segregation. SCHPC is actually a compromise between filling ability and segregation resistance [35].

Consistence retention

Consistence retention, sometimes called open-time, refers to the ability of the mixture to retain the compactability during transportation and placing [24]. The properties of fresh SCHPC should be maintained until placing, usually 60-90 minutes [35, 44]. Consistence retention is mainly governed by the powder-SP interaction because of different effects of powder on the adsorption of water and admixtures [83] and the lower adsorption of SP on the hydrated phases of cement [84]. It is well documented that compared to the other SP, the polycarboxylate-type SP can be more beneficial to consistence retention [85]. Besides, the consistence retention of SCHPC can also be affected by the composition of cement and SCMs, the formation and coagulation of cement hydrates [55], the w/b ratio and the chemical structure of the SP [53, 86].

Rheology and properties of fresh concrete

Rheology is ''the branch of science dealing with deformation and flow of matter''[24]. Fresh concrete usually is considered as a multi-phase material, namely a dispersion of aggregate particles in a viscous fresh cement paste. In which cement paste is also considered as a multi-phase material made up of cement and SCMs particles (particularly in SCHPC mixtures)

suspended in water. The application of rheology in fresh concrete appears a substantial challenge, because the rheological properties of fresh concrete change over time in a non-linear manner. To analyze fresh concrete, yield stress, plastic viscosity and thixotropy are important rheological terms and the following fundamental assumptions are issued, namely fresh concrete is [24]:

- a homogeneous material of a uniform composition
- an isotropic material which has the same properties in all directions
- a continuum, with no discontinuities between any two locations within the concrete.

Two types of behaviour of fresh concrete are Newtonian and non-Newtonian presented in Fig. 2.5.

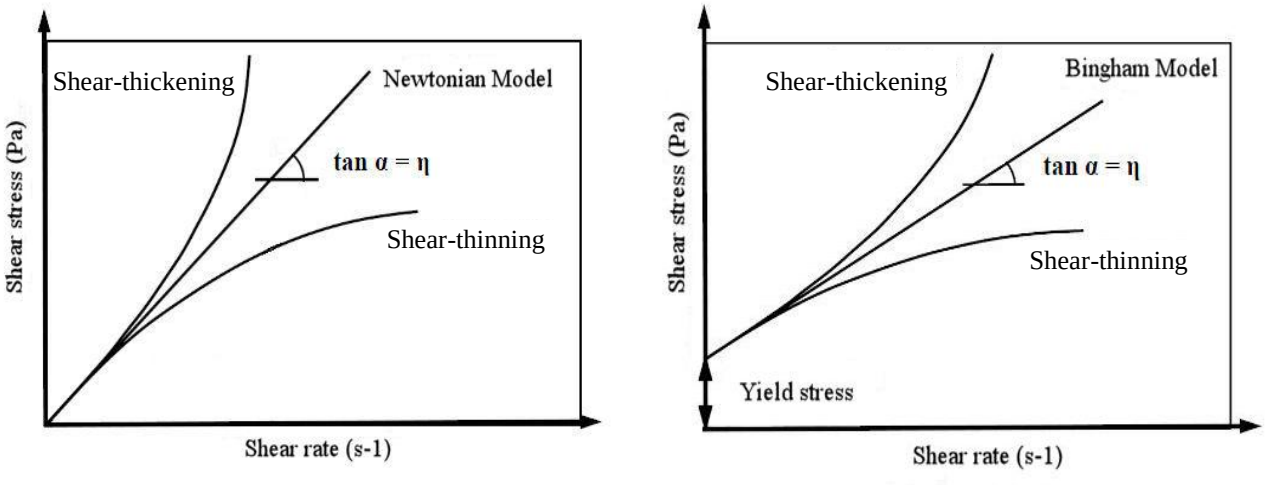

Fig. 2.5 Newtonian, Bingham and different types of non-Newtonian flow models [87]

As can be seen in Fig. 2.5, the relationship between the shear stress (τ) and shear rate (γ) of Newtonian liquids, such as water and oil, is linear. That is a straight line starting at origin [88]. This relationship can be written as:

$$\tau = \eta.\gamma \tag{2.2}$$

Where, η is the coefficient of viscosity.

The non-Newtonian fluid, which exhibit a linear relationship between shear stress and shear rate but which flows only when the shear stress exceeds a certain minimum level (Fig. 2.5). The minimum value is called the yield stress (τ_0), and the equation of the line can be written as:

$$\tau = \tau_0 + \mu.\gamma \tag{2.3}$$

Where τ_0 is the yield stress, and μ is the plastic viscosity. Eq. 2.3 represents what is known as the Bingham model. The Bingham model represents the behaviour of fresh concrete at low shear rate [24].

Although the Bingham model is more sophisticated than the Newtonian, much more complicated behaviour is very common. As seen in Fig. 2.5, the flow curve may not linear at all, and it may intersect the stress axis at zero or at a greater stress. The flow curve exhibits a rapid increase of shear stress with shear rate, which indicates a shear-thickening behaviour. It is more and more difficult to make a material whose flow curve behaviours shear-thickening flow

more quickly at high shear rates. Opposite shear-thickening behaviour, it is shear-thinning behaviour, as seen in Fig. 2.5 [88]. A material, whose flow curve behaviours shear-thickening or shear-thinning, and intersect the stress axis at zero, is called a pseudoplastic material. The behaviour of this material follows approximately exponential relationship expressed as [24]:

$$\tau = A.\gamma^n \quad (2.4)$$

Where, A is a constant related to the consistence of the fluid and n<1 (shear-thinning) or n>1 (shear-thickening). Eq. 2.4 represents what is also known as the Ostwald-de Waele model. Other various models have been proposed to describe the non-linear relationship: the Herschel-Bulkley model (Eq. 2.5) and the more alternative modified Bingham model [89-91] (Eq. 2.6).

$$\tau = \tau_0 + k.\ \gamma^n \quad (2.5)$$

$$\tau = \tau_0 + \mu.\ \gamma\ + c.\gamma^2 \quad (2.6)$$

Where k is consistency factor ($Pa.s^n$); n is flow index, n<1 (shear-thinning) or n>1 (shear-thickening); μ is plastic viscosity (Pa.s); γ is shear rate (s^{-1}) and c: second order parameter ($Pa.s^2$). The parameter c/μ corresponds to index n in Herschel-Bulkley model, and therefore describes shear thickening behaviour [91].

Thixotropy is also an important rheological term to describe fresh concrete, particularly fresh SCHPC. Thixotropy is defined as ''the ability of a material to reduce its resistance to flow (apparent viscosity) with increase flow (shear) or agitation and to regain its original stiffness when rest, the process being repeatable and reversible'' [24]. Thixotropy can be understood based on the microstructure of the fluid. Among particles there exist weak inter-particle forces which will create a network structure and result in the flocculation. When outside mechanical shear is applied, such weak inter-particle forces cannot be maintained, breaking the flocculation and causing a reduction in yield stress and viscosity. Once the fluid is, however, placed at rest, the flocculation and the microstructural network will be rebuilt due to the inter-particle forces [92]. Based on the microstructural point of view, the thixotropy of cementitious materials can be considered as the coagulation and the separation of particles when placing at rest and when shearing is applied to the cement particles respectively [93]. However, the basic physical description cannot fully explain the nature of thixotropical properties of cementitious materials, as the hydration of cement processes over time, resulting in different phases and states of cementitious materials. Thixotropy of cement paste is time-dependent due to the changes of materials from one phase to another [92]. Regarding SCHPC, after casting into the form, a structure will be rebuilt and viscosity increases. The concrete, to some extent, supports its own weight which results in low pressure on formwork and a high casting rate. Therefore, the thixotropic property improves the static stability or reduces the risk of segregation after placing [35].

In rheological terms, a combination of low yield stress and a moderate plastic viscosity are required to fulfill filling ability and segregation resistance of SCHPC [24]. The low yield stress value is necessary to improve flowing ability, while viscosity must be high enough to maintain a homogeneous system during transport and placing until the start of hardening, and to ensure proper flow rate, passing ability and segregation resistance.

In Fig. 2.6, the general effects of different constituent materials on the rheological properties of concrete in general are shown. It can be seen that the yield stress is dramatically decreased while the viscosity is not changed very much when SP is introduced. Furthermore, SP increase the viscosity at some point. In comparison with SP, both the yield stress and the viscosity are decreased by water. A large increase in water content may result in segregation in concrete. Paste is another important factor influencing the yield stress and the plastic viscosity. Increasing paste volume will result in a decrease in yield stress and an increase in viscosity and vice versa. Incorporation of FA or GGBFS leads to a decrease in the yield stress of concrete. However, GGBFS increases the viscosity while FA reduces it possibly due to the spherical particles of FA.

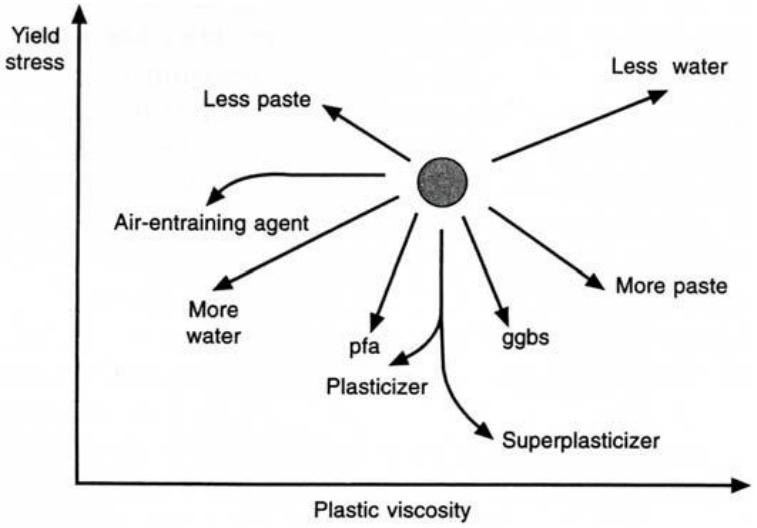

Fig. 2.6 General effects of concrete constituents on yield stress and plastic viscosity

The effects of the constituent materials above on Bingham parameters of general concrete can be similar to that of SCHPC, because SCHPC is produced by the same constituent materials. The effects of SCMs on rheological properties are more important for SCHPC due to its larger powder content. As mentioned previously, a part from FA and GGBFS, LSP, SF and RHA become more common SCMs used to produce SCHPC. The effect of RHA on Bingham parameters has not yet been studied in detail. Furthermore, a combination of various SCMs can bring synergistic effect on the rheological properties of SCHPC. The effects of SCMs on rheological properties of SCHPC are also discussed in Section 2.2.2.

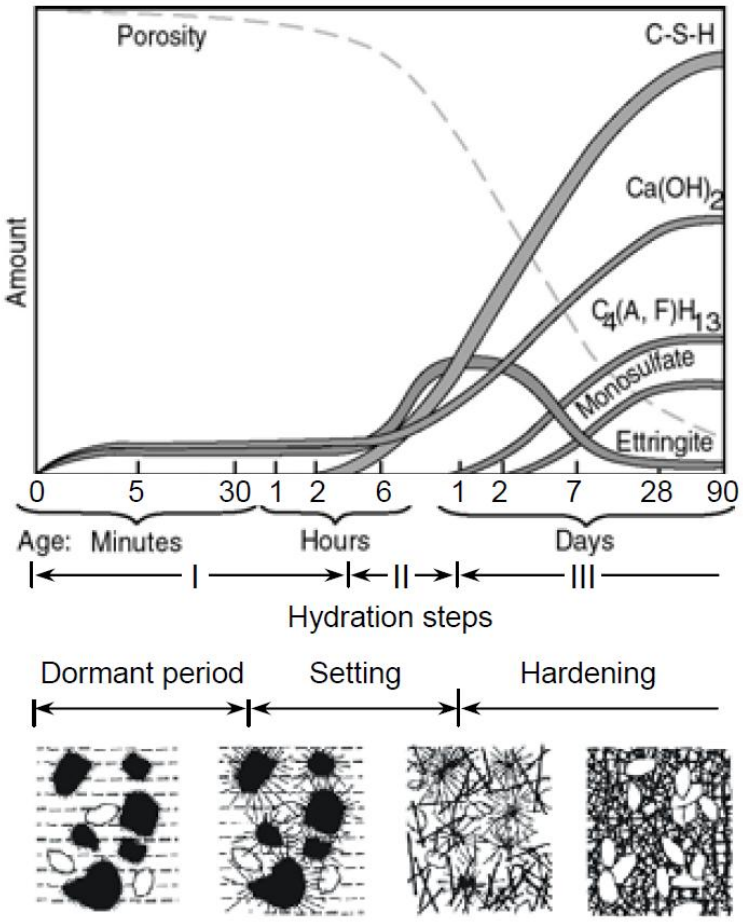

Fig. 2.7 Schematic representation of the formation of hydrate phases and the structure development during cement hydration [98]

2.2.6. Properties of hardened SCHPC

Similar to TVC, e.g. HPC, the wide variation in hardened properties of

SCHPC can be obtained. It is well documented that three main factors: the modified mixture proportions, the improved microstructure and homogeneity, and the absence of vibration can be attributed to the differences in hardened properties between TVC and SCHPC [50, 94].

Hydration and microstructure

As mentioned in Section 2.2.4, to obtain the very specific properties of SCHPC, SCMs and chemical admixtures generally constitute a significant part of the mixture proportions. That results in an important influence on the hydration and microstructure development and properties of the concrete [95-97]. The microstructure of a cementitious material mainly results from the cement hydration process. The microstructure development in pure cement paste results from the formation of hydration products and the distribution of the pore structure network. The products formed during the hydration contain calcium silicate hydrates (C-S-H), calcium hydroxide (CH), and calcium trisulfoaluminate hydrate-ettringite (AFt) as well as other minor products. The hydration process and the development of microstructure of Portland cement are diagrammatically presented in Fig. 2.7 [13, 98]. The degree of cement hydration depending on the w/c ratio is illustrated in Fig. 2.8 [13, 99], where the hydration process of each clinker phase is considerably different (Fig. 2.9) [100]. In order to meet self-compactability and very high compressive strength, the w/b ratio of SCHPC is low, from 0.25 to 0.4, as analyzed in Section 5.3 below. The maximum degree of cement hydration in SCHPC can be estimated in range of 58-70%.

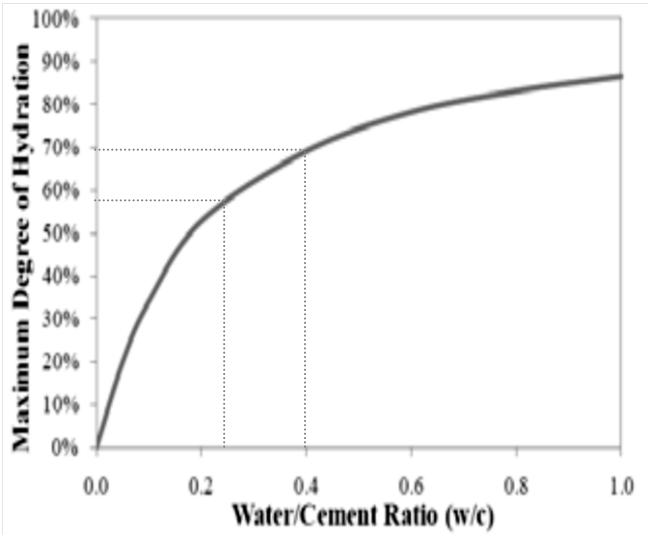

Fig. 2.8 Relation between maximum degree of cement hydration in practice and w/c ratio [13, 99]

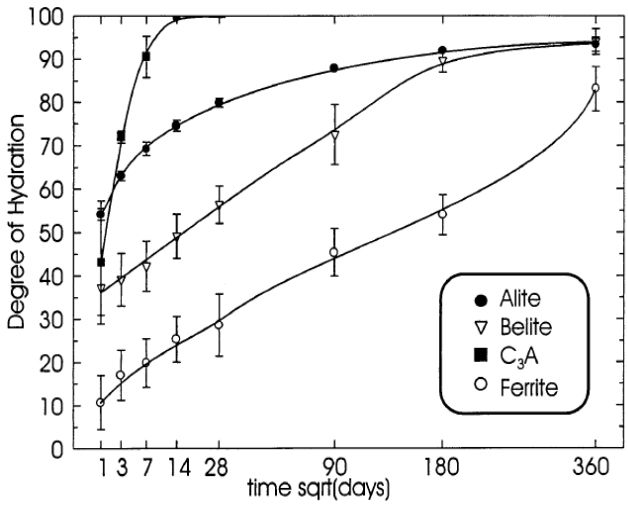

Fig. 2.9 Degree of hydration of the four principal clinker phases of Portland cement determined by QXRD, at w/c of 0.5[100]

The blending of SCMs with Portland cement influences the process and the degree of cement hydration. This results in a variation in amount and kind of hydrates formed and thus the volume, the porosity and finally the mechanical properties and the durability of the cementitious materials. The hydration mechanisms of SCMs blended cement is more complicated than that of the pure cement that is well identified [101]. Because the hydration of cement and hydraulic reaction of the SCMs take place simultaneously and also interact, they have an effect on the process and the rate of each other [14]. It is proposed that the hydration of clinker phases occur and then reaction of SCM starts later. The presence of SCMs strongly accelerates the hydration

of cement at early ages [14, 102]. Some aspects of SCMs, such as chemical composition, fineness, the amount of reactive phases, govern the kinetics of reactivity of SCMs. It is very difficult to quantify the detailed effect of these aspects on the reaction of SCMs in the blended system. The effect of SCMs on the blended cement is attributed to chemical and physical aspects. In the case of silica rich SCMs, such as SF, pozzolanic reaction is proposed to induce the formation of C-S-H with a low Ca/Si ratio, so-called ''tobermorite- like'' C-S-H. Low Ca/Si C-S-H phases can take up more aluminium in its structure than high Ca/Si ones generated from the hydration of Portland cement [103, 104]. The formation of C-A-S-H phases will lead to an increased uptake of alkalis and a decrease of dissolved calcium [105, 106]. It has been realized that even inert materials, such as LSP and quartz powder, may significantly influence the hydration of clinker phases [107, 108]. This can be so-called physical effect contributed by extra space for the cement hydrates due to the higher water to cement (clinker) ratio and by the enhanced nucleation sites for precipitation of cement hydrates.

Hardened concrete is considered as a three-phase material: aggregate, bulk cement paste and interfacial transition zone (ITZ) [1, 109]. The ITZ mainly contains a water film, a calcium hydroxide layer on the surface of aggregate, and a porous matrix layer between calcium hydroxide layer and bulk cement matrix [1, 110]. Mixture proportion of SCHPC is significantly different from that of TVC. The component of coarse aggregates is dramatically decreased, therefore the cement matrix is more important. The addition of SCMs and chemical admixture makes the structure of the cement matrix change [97]. The partial replacement of cement by SCMs enhances capillary segmentation, pore refinement and porosity reduction due to micro-filling and pozzolanic effects [1, 97]. During casting, ordinary concrete is vibrated, and the accumulation of water on the surfaces of coarse aggregate occurs. That results in the porous and weak interfacial zones between aggregates and bulk cement matrix [96]. The ITZ in SCHPC is improved due to the elimination of the compacting process. Furthermore, w/b ratio of SCHPC is as low as that of HPC, therefore, the rich microstructure of SCHPC will also be obtained due to the processes of filling in the capillary pores at reduced water content or low w/b ratio with SP [1].

Porosity

Porosity of concrete refers to the pores in bulk cement paste, ITZ and aggregates. It is one of the main factors affecting strength of concrete [32]. In most cases, the porosity of the aggregates is not important for the ultimate properties of concrete. The porosity of concrete can be classified as gel pores, capillary pores and air voids, as shown in Fig. 2.10. The spaces between the hydration products, i.e. interspacing between C-S-H sheets, are considered as gel pores. The mean distance between C-S-H sheets is mentioned smaller than 3nm [24, 32, 111]. The gel pores is assumed to be too small to affect the compressive strength and permeability of hardened paste and concrete. The gel pore volume increases with degree of cement hydration. The gel pores are normally filled with pore solution that maters in respect of creep and shrinkage.

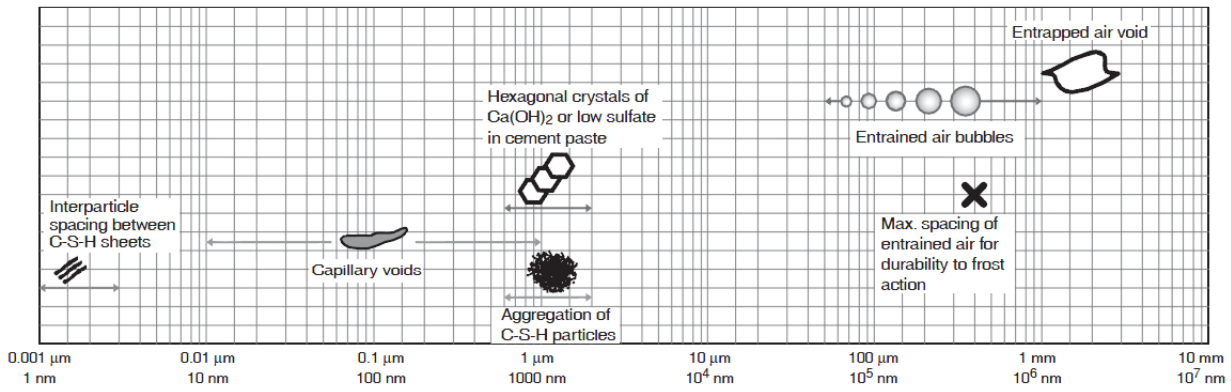

Fig. 2.10 Dimensional range of different phases in a hydrated cement paste [111]

Capillary pores are formed, because the initial volume of cement and water is larger than the volume of hydration products. They contain the capillary voids and the remaining capillary water. The volume and the dimension of these pores are governed by the cement content, w/c ratio and the hydration of cement. Capillary pores are in range from 10-50 nm in well hydrated cement paste made with a low w/c ratio. Whereas they vary from 3-50 µm for young cement paste made with a high w/c ratio. The capillary porosity considerably influences strength and permeability and hence the durability of concrete [1, 24]. Compared to TVC, the total and capillary pore volume are assumed to be low in SCHPC (7 to 15 %) due to the better refinement of pore structure in SCHPC [1, 112]. The low w/b ratio, the higher packing density resulting from good compaction, the greater degree of cement hydration because of better dispersion of cement particles in the presence of SP, and the pozzolanic and micro-filling effects of SCMs are accounted for the refined pore structure in SCHPC. In Fig. 2.11, the pore size distribution of the cement matrix in UHPC, HPC, and ordinary concrete (normal strength concrete-NC) is shown. The pore size distribution and porosity in cement matrix of SCHPC with very high compressive strength is expected to be near to those of UHPC.

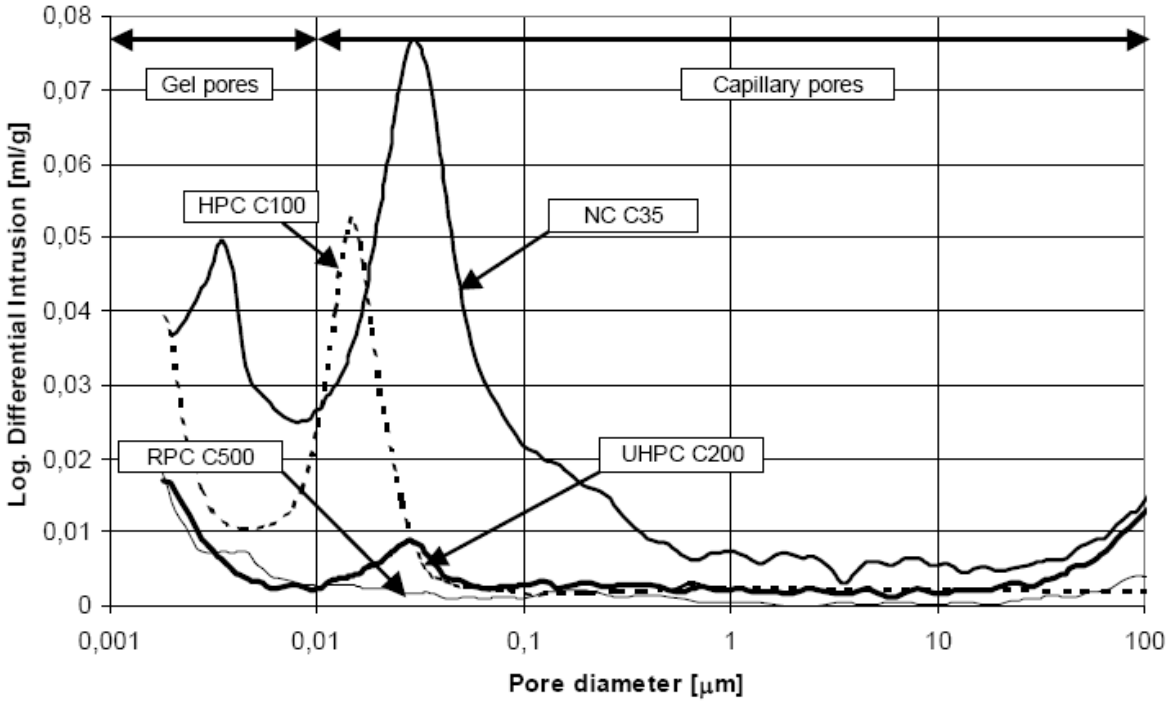

Fig. 2.11 Pore size distribution of UHPC, HPC and Normal Strength Concrete (NC)[113]

Compressive strength

The basic relationships between compressive strength of SCHPC and its mixture proportion, production, placing and curing remain the same as those for TVC. To guarantee the self-compaction, a significantly higher amount of binder (cement and SCMs) is used in SCHPC compared to TVC and, conversely, the proportion of coarse aggregate is lower in SCHPC. To some extent, the difference is inevitably reflected in the performance of the hardened SCHPC. The microstructure of SCHPC, particularly ITZ between cement matrix and aggregates, will be improved due to the addition of high amount of SCMs and the absence of vibration. This results in a good performance of hardened SCHPC with regard to strength and durability. However, the relationships between the properties of microstructure and the performance of hardened concrete remain the same as any kind of concrete, regardless of compaction or self-compaction [24]. Compressive strength of SCHPC varies from 50 to 100 MPa, depending on w/b ratio and binder composition [1, 33, 35]. In principle, basic relationships between composition of concrete, i.e. w/c ratio, and compressive strength applied to TVC can be used for SCHPC. SCHPC can be designed for a large range of compressive strength. The development rate and values of compressive strength mainly depend not only on the w/b ratio but also the amount and activity of SCMs. It is noticed that self-compaction in fresh state does not mean high performance and high strength in hardened state [24, 50]. Indeed, it is very difficult to reach very high compressive strength in hardened state while self-compacting properties are satisfied because of a very low w/b ratio used.

Flexural and tensile strength

Flexural and tensile strength is related to compressive strength. An increase in compressive strength leads to an increased flexural and tensile strength, however, the increasing rate of flexural and tensile strength is lower. The ITZ characteristics tend to be a very important factor influencing flexural and tensile strength, with a greater degree than compressive strength [50, 114]. In comparison with TVC, the flexural and tensile strength of SCHPC is typically improved, possibly due to the improved ITZ and the better microstructure of bulk cement matrix [94, 115].

2.2.7. Durability of SCHPC

In general, durability is understood as a general analysis of the service life and the performance of concrete in an aggressive environment. The deterioration of concrete can be caused by physical and chemical damage. The physical damage results from wetting/drying, freeze/thaw or heating/cooling cycles, and the chemical damage includes sulphate attack, acid attack, chloride attack and alkali-silica reaction (ASR) in which water acts as a carrier. The resistance of the cover layer to transport mechanisms of gas and liquid, e.g. permeation, adsorption and diffusion, dramatically influences durability of concrete. Therefore, oxygen permeability, water sorptivity and chloride conductivity of concrete are often tested to indicate durability performance of concrete [35, 116].

Primarily, the transport properties of concrete are influenced by the volume and pore structure of the paste, and ITZ between the paste and aggregate. Although SCHPC is proportioned with the higher paste volume, the pore structure of the bulk paste, and ITZ are improved due to the

low w/b ratio, the use of SCMs and the elimination of vibration. That results in improved durability of SCHPC compared to the TVC [50, 117].

Sulphate resistance

Portland cement concrete can be deteriorated by solutions containing sulphate ions, sodium, potassium, magnesium, and calcium sulphate in some natural or polluted ground water. The sulphate damage can lead to strength loss, expansion, spalling of surface layers and, ultimately, disintegration [97]. It has been found that Ettringite ($C_3A.3CaSO_4.32H_2O$), thaumasite ($CaCO_3.CaSO_4.CaSiO_3.15H_2O$), and gypsum ($CaSO_4.2H_2O$) are the main deterioration products of cementitious material exposed to sulphate solutions [97, 118-121]. It is reported that, in comparison with TVC, the initiation time for sulphate attack is later in SCHPC due to its denser microstructure. The incorporation of SCMs in SCHPC refines the capillary pore system and thus results in better ability to resist sulphate attack.

Freezing and thawing resistance

With denser microstructure, SCHPC can have an improved durability, including freezing and thawing resistance, in comparison with TVC. The ability of SCHPC to resist freezing and thawing cycles is mainly governed by the degree of saturation in the concrete, exposure conditions to freezing and thawing, air-void content, and tensile strength of the bulk cement paste, which is similar to TVC [97]. As is the case with TVC, SCHPC can be susceptible to damage by exposure to repetitive freeze-thaw cycles. If the air-void content in concrete is not high enough, capillary water will expand approximately 9 % during freezing, resulting in micro-cracking and loss of strength and stiffness. Furthermore, the differential deformation between aggregate and paste can occur during freezing. Because the aggregate can be contracted, the cement paste expands if sufficient air voids are not well-distributed. That results in microcraking at ITZ and a further decrease in stiffness of concrete. In general, when SCHPC is prepared with sound aggregate and proper air-void system, its resistance to freezing and thawing is fulfilled [122-124]. In order to meet the requirements of resistance to freezing and thawing, an air-void system with defined geometric structure is required to take up volume extension of the freezing water. The use of effective air-entraining agent (AEA) can ensure the stabilization of micro air voids in concrete.

Carbonation

Carbonation is of major importance for reinforced concrete. Basically, carbonation is the chemical reaction between the hydrated cement paste and CO_2 molecules penetrating into concrete, A simplified equation for the carbonation of portlandite is given below.

$$Ca(OH)_2 + CO_2 + H_2O = CaCO_3 + 2H_2O$$

Carbonates are formed by this chemical reaction, and thus OH^- ions are reduced. This results in a drop in the pH value in the pore solution. Once the pH value decreases by below 9, the steel reinforced bar will be depassive, and will be corroded in presence of water and oxygen [97]. For SCHPC with a high compressive strength, the carbonation depth measured by phenolphthalein after 6 months is very low, and nearly 0 for compressive strength of over 100 MPa [125]. The carbonation of SCHPC is governed by the diffusion velocity of CO_2 molecules through concrete and by amount of carbonable material in concrete. The diffusion velocity mainly depends on the

porosity of concrete and the amount of moisture in the pores. The diffusion velocity is higher, when the porosity is larger and filled with a lower amount of water. The pore structure of SCHPC is considerably refined due to the low w/b ratio and the addition of SCMs. On the other hand, the carbonable material is dependent on binder composition system. The carbonation depth is lower with higher content of C-S-H and $Ca(OH)_2$ in concrete [97]. With the presence of SCMs, particularly reactive ones, the higher content of C-S-H in SCHPC can be obtained. That results in a reduction in the risk of carbonation.

Alkali-silica reaction

Alkali-silica reaction (ASR) is a deleterious reaction caused by a reactive aggregate and cement paste pore solution. The reaction between alkali hydroxides in concrete pore solution and amorphous or poorly crystalline silica phases in aggregates or SCMs forms alkali silica gel which absorbs water and expands [17-20]. The higher cement content leads to a higher amount of soluble alkalis in the pore solution. This results in higher probability of ASR. Generally, cement is partially replaced by SCMs to reach the high volume of paste. The effect of SCMs on ASR is dependent on their chemical and mineralogical composition, MPS and the content used in concrete [97]. Furthermore, a higher dosage of SP and VMA used in SCHPC will increase the amount of alkali content in pore solution. Because SP and VMA contain a certain amount of alkali ions, such as sodium sulphate [97, 126, 127]. The amount of alkali content released from SP and VMA is relatively small compared to that from cement, however, the possible influence should be taken into account. It is also noted that although the microstructure of SCHPC is denser than that of TVC due to the low w/b ratio, the use of SCMs, and the lack of vibration, ASR can occur even in HPC with a dense structure [97, 128, 129].

2.3. Rice husk ash and using rice husk ash in mortar and concrete

2.3.1. General

In rice cultivating countries, rice husk is mostly attributed as an agricultural waste. Rice husk is abundant in many parts of the world, and constitutes about one fifth of about 723 million tons of rice paddy over the world in 2011, including about 40 million tons in Vietnam [11]. Normally, rice husk is not properly treated, causing serious environmental pollution. When rice husk is incinerated at properly controlled temperatures, the obtained ash consists of about 95 wt.% amorphous silica and has porous structure. RHA has a very high pozzolanic reactivity comparable with SF [6]. RHA can be used to partially replace Portland cement in concrete. The utilization of RHA as a SCM in concrete is a useful solution to the environmental problem of this waste, reduces the cement content in concrete then carbon dioxide emissions in atmosphere, and reduces the cost of concrete as well. From the environmental and economic impacts, RHA can seem to be **a sustainable SCM**.

In this section, some aspects, namely RHA production, properties of RHA, effect of RHA on workability, the hydration and microstructure development of cement paste, effect of RHA on some durability properties, and the combination of RHA with other SCMs, are presented.

2.3.2. Reactive RHA production

The quality of RHA for use as a SCM in concrete is significantly dependent on reactivity of the ash. The pozzzolanic reactivity of RHA is governed by the form of silica present, carbon

content and porous structure formed in its particles. With the same rice husk source, these physico-chemical properties of RHA vary with the temperature and the duration and environment of combustion as well as pretreatment of husk before combustion. According to Bui and Nair [6, 130], in order to obtain highly reactive ash with low carbon content and high surface area, a low firing temperature and short retention period should be used. It is suggested that the combustion with temperature below 750 ^{o}C will be sufficiently safe to produce highly reactive RHA. From one ton of paddy, about 200 kg (20 wt.%) of husk is generally yielded. After complete combustion about 50 kg of RHA (5 wt.%) is produced and the silica content in the produced ash may reach over 95 wt.%. Representatively, rice husk consists of organic matter and inorganic mineral matter. The inorganic mineral matter (about 20 wt.%) has the main component of silica whereas the organic matter contains 38% cellulose, 22 wt.% lignin, 18 wt.% pentosans and 2 wt.% other matter. During combustion, the organic matter is removed, yielding silica ash.

To obtain highly reactive RHA, some combustion methods have been suggested by some authors, namely a cyclone-type furnace produced by Mehta-Pitt in 1976, a fluidized bed system designed by Takuma, a tub-in basket type rice husk burner developed by Kapur in 1981. A brick incinerator by the Cement Research Institute of India, and a drum incinerator by the Pakistan Council of Specific and Industrial Research (PCSIR) in 1979 [6, 13, 130].

2.3.3. Properties of RHA

Fineness, pore structure, and specific surface area

After burning process, the organic matter, i.e. the cellulose-lignin matrix of the rice husk decomposes leaving behind a porous silica skeleton. The highly porous structure of the ash induces a large surface area (Fig. 2.12). The porous structure including mostly internal pores depends on the burning conditions, i.e. temperature and duration of combustion and the treatment of rice husk before burning. The pore size distribution in RHA particles determined by Barrett-Joyner-Hanlenda (BJH) contains macropores (>50 nm), mesopores (2-50 nm), and micropores (<2 nm).

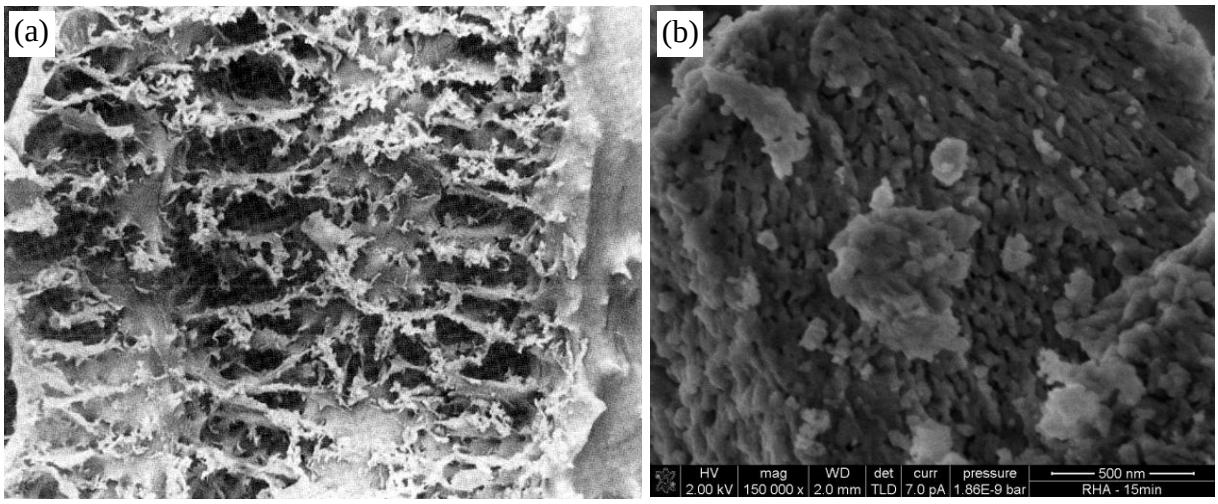

Fig. 2.12 Skeletal structure of RHA (736x) (a) [13, 131]; pore structure on surface of ground RHA particle (b) [16]

Based on the database reported in [132, 133], it can be determined that the specific surface area of the ash determined by Brunauer-Emmett-Teller (BET) method tends to increase significantly with a higher pore volume in RHA particles. Where pore volume mainly depends on pore size distribution, i.e. increases with a higher content of micropores and mesopores, and a lower content of macropores, as can be seen in Fig. 2. 13 and Fig. 2.14.

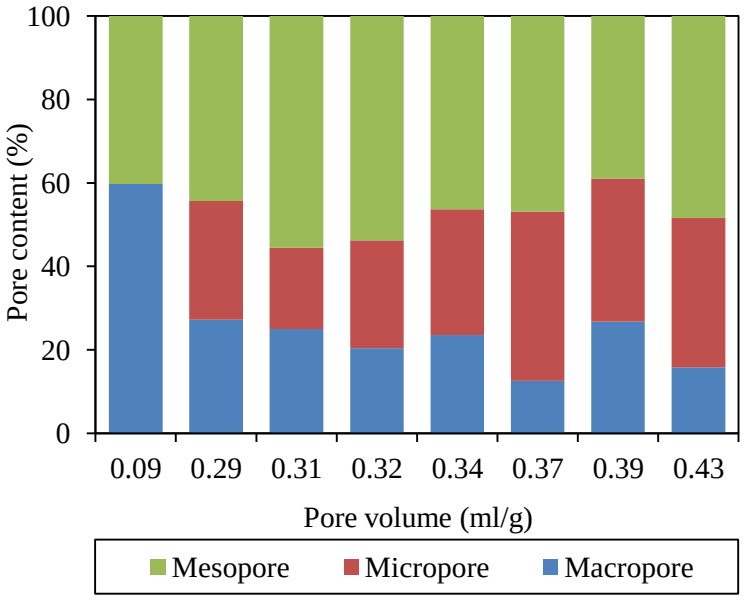

Fig. 2. 13 Pore volume vs. pore size distribution in RHA particle

Normally, the SSA of a dense material increases with higher degree of grinding or fineness. For RHA, as analysed above, BET-SSA of RHA is governed by pore size distribution in RHA particles. BET-SSA of RHA lies in range of 20 to 270 m^2/g [6] whereas this value of SF is about 18-23 m^2/g [13, 134, 135]. From the morphological aspect, it is clearly found that SF is a dense material and RHA is a porous material. The pore structure of RHA results in its extremely high surface area whereas its average particle size is still fairly coarser than that of SF. In comparison with SF having a mean particle size of 0.1-1µm [13, 134, 135], RHA with a mean particle size of 5-45 µm possesses a larger surface area, even as much as three times larger. [1, 5, 6, 13, 136-138].

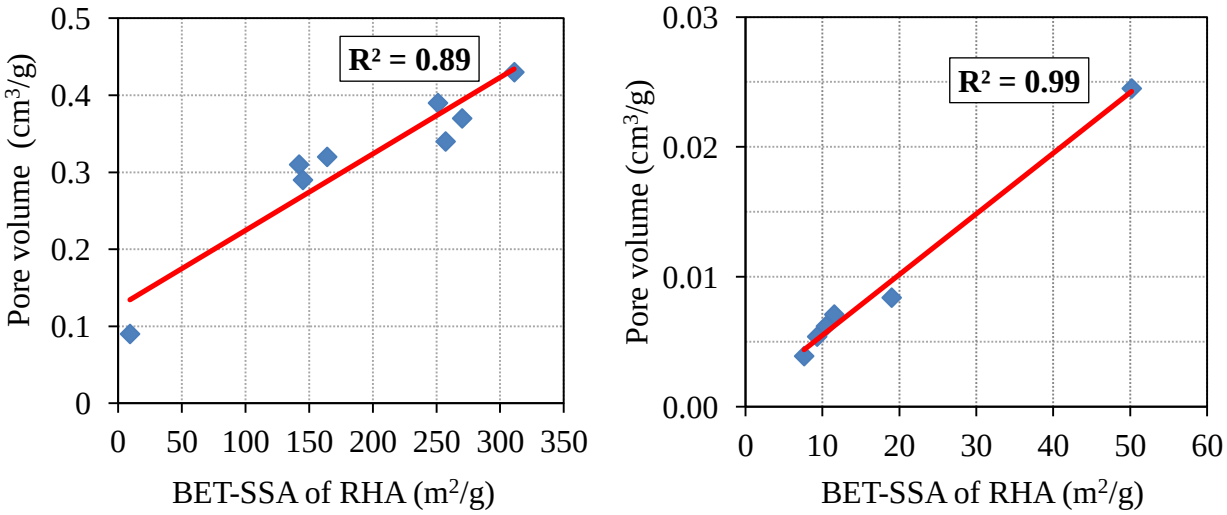

Fig. 2.14 Relation between pore volume and BET-SSA of RHA [132, 133]

Chemical and mineral compositions of RHA

Chemical analysis of RHA reveals that silica is the main component, besides a minor amount of alkali oxides and other metallic oxides. The silica content of RHA varies from 85 to 95 wt.%. The major impurities of RHA are formed by unburnt carbon and alkali oxides, in which potassium content dominates sodium content [6, 16, 38, 139]. The potassium content is in the

range of 0.72 to 3.84 wt.% [139]. The silica content of RHA is strongly dependent on the cultivating condition of the rice plant, such as geographical conditions, types of paddy, soil chemistry, climate and fertilizers, and pretreatment as well as combustion condition, as discussed previously. It should be noted that the alkali content in RHA is clearly higher than that of SF. That might result in a different behaviour of RHA in cementitious materials compared to that of SF. The chemical composition of RHA produced in various countries is given in Table 2.3.

Table 2.3 Chemical composition of RHA (wt.%) in varous countries[139]

Countries	SiO_2	Al_2O_3	Fe_2O_3	CaO	MgO	K_2O	Na_2O	SO_3	L.O.I
USA	94.50	Trace	Trace	0.25	0.23	1.10	0.78	1.13	*
Malaysia	93.10	0.21	0.21	0.41	1.59	2.31	*	*	2.36
Brazil	92.90	0.1	0.43	1.03	0.35	0.72	0.02	0.10	*
India	90.70	0.40	0.40	0.40	0.50	2.20	0.10	0.10	4.80
Canada	87.20	0.15	0.16	0.55	0.35	3.68	1.12	0.24	8.55
Vietnam	86.90	0.84	0.73	1.40	0.57	2.46	0.11	*	5.14
Iraq	86.80	0.40	0.19	1.40	0.37	3.84	1.15	1.54	3.30

*- Not reported; L.O.I- Loss On Ignition

Pozzolanic reactivity of RHA

Generally, the reactivity of a pozzolanic SCM is the extent of the chemical reaction occurring between the active components of the SCM, calcium hydroxide and water [13]. The pozzolanic reaction is considered as a dissolution-precipitation process, similar to that of C_3S. For SCMs, the process is slower because it takes more time to dissolve ions, i.e. Si ion, and reach supersaturated and equilibrium state [16]. When rice husk is burnt under properly controlled temperatures, the obtained ash is a porous siliceous amorphous material. With high silica content and large SSA, the pozzolanic reactivity of RHA can be comparable with that of SF [6, 12, 140]. In order to evaluate the reactivity of RHA, some methods have been proposed, as following: According to Mehta [141], the reactivity is evaluated by percentage of RHA dissolving in 0.5 M boiled sodium hydroxide in a period of 3 min. The reactivity measured by this method, the so-called “silica activity index”, is in the range of 50 to 85. Payá, J., et al.[142] proposed a rapid analytical method, in which the reactivity of RHA is determined by amorphous silica fraction of RHA dissolving in glycerol

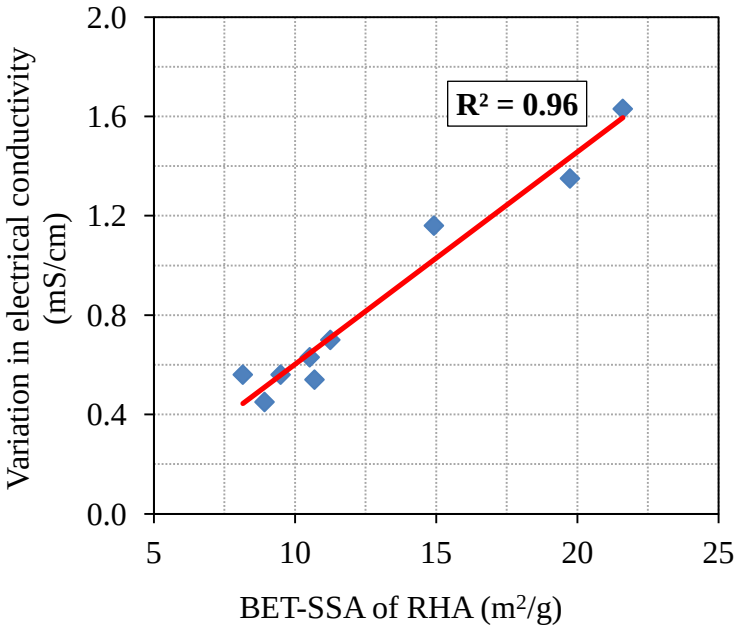

Fig. 2.15 Relation between BET-SSA of RHA and electrical conductivity

solution. More commonly, the reactivity of RHA and other pozzolan, i.e. SF, is indirectly evaluated by the reduction in the electrical conductivity of a $Ca(OH)_2$ (CH) - pozzolan suspension [143]. Originally, the reactivity of pozzolan is evaluated by the reduction in electrical conductivity of saturated CH solution at 40 °C 2 minutes after pozzolan addition. A pozzolanic material is dispersed in a calcium hydroxide saturated solution, then its active constituents will react with calcium hydroxide, resulting in a decrease in the concentration of Ca ion and hence in electrical conductivity. Experimental results have shown that amorphous silica content and BET-SSA as well as the soluble oxide content of pozzolan are the main factors influencing the electrical conductivity of CH-pozzolan suspension [144-146]. The electrical conductivity of CH-RHA suspension 2 minutes after RHA addition appears to increase with a higher SSA of RHA, as displayed in Fig. 2.15. Nguyen [13] and Van [16] have used this method to evaluate the reactivity of RHA. The results show that after 2 minutes the electrical conductivity of CH-RHA suspension still continues to decrease sharply by about 600 minutes and 360 minutes, respectively. The reduction in electrical conductivity can be due to the adsorption of Ca ion on the surface of RHA particles (so called ‘‘external surface’’) and into pores of RHA particles (so called ‘‘internal surface’’), and then pozzolanic reaction. Furthermore, the electrical conductivity is a function not only of the concentration of Ca ion but also of other cations, i.e. Na, K ion and, etc., dissolved from the RHA and SF [16]. Therefore, in order to evaluate more accurately the reactivity of RHA or SF, the electrical conductivity value of CH-pozzolan suspension subtracting the value of water-pozzolan suspension should be determined by the time the electrical conductivity reach constant. Where the reduction of electrical conductivity reflects the reduction in Ca ion due to pozzolanic reaction.

Besides, the pozzolanic reactivity of RHA and SF can also be examined by determination of CH content in hardened cement paste by thermal or XRD analysis [146-148] or by determination of compressive strength of mortar containing RHA or SF at the constant w/b and heat treatment [12], the so-called ‘‘accelerated pozzolanic strength reactivity index’’ [149]. Pozzolanic reaction is one of the main factors influencing CH content in cement paste, and compressive strength of mortar. The addition of SCMs, including inert or pozzolanic, results in an increase in the degree of cement hydration due to extra space for the cement hydrates caused by a higher water to cement (clinker) ratio and by the enhanced nucleation sites for precipitation of cement hydrates. It is more complicated that RHA is a porous material. RHA can absorb a certain amount of mixing water into its pores, therefore the w/c of bulk cement paste will be lower, particularly at very low w/b ratio. At later ages, the absorbed water can be released to maintain the hydration of cement [16, 148]. So it can be said that the CH content in the blended cement paste and the compressive strength of the blended cement mortar or concrete depends not only on the pozzolanic reactivity but also the physical properties of RHA, i.e. MPS, pore size distribution, and then SSA. Consequently, it is very difficult to evaluate accurately the pozzolanic reactivity of RHA by means of CH content consumption and compressive strength. It is more difficult to compare the reactivity of RHA to that of SF by means of CH content consumption and compressive strength. The high BET-SSA of RHA results from the high porosity meanwhile its particle size is much larger (about 25-50 times) than that of SF [5, 13, 16]. That may result in a difference in the pozzolanic reaction process between RHA and SF [16]. And the effect of pozzolanic activity of RHA on hydration and microstructure of the

blended cement paste may be different from that of SF. The effect of RHA on hydration and then microstructure of cement paste and resulting compressive strength will be analysed in more detail in the next section.

2.3.4. Effect of RHA on properties of mortar and concrete

Water demand and workability

The addition of RHA increases the water demand of the blended cement paste and concrete [150-153]. With 20 wt.% cement replacement by RHA, decreasing MPS of RHA from 31.3 to 11.5 μm (increasing SSA from 27.4 to 30.4 m^2/g, respectively) increases the water demand or the SP dosage to reach the given workability (the given slump of 210-220 mm) [152]. An increase in a partial cement replacement by RHA results in a higher water demand or a higher SP dosage to maintain certain workability [6, 137, 153, 154]. The similar effect of RHA content on the workability of UHPC is obtained [13, 16], however the SP dosage needed for a given workability is reduced proportionally with the decrease of MPS of RHA from 15.5 to 3.6 μm [9]. The contradictory effect of MPS of RHA on workability might be due to the differences in pore size distribution, and then SSA of RHA, and in type of concrete. Therefore, the effect of pore structure of RHA on workability of concrete proportioned with various w/b ratios is needed to investigate in detail.

Microstructure and hydration

Regarding physical properties, RHA is different from the other SCMs, such as LSP, FA, SF. etc. due to its pore structure. RHA may have similar and different effects on the hydration of cement and microstructure of the blended cement paste compared to the other SCMs, especially SF. It is found that at w/b ratio of 1.0, the hydration heat of the 30 wt.% RHA blended paste is higher than that of the control paste (100% cement), during 12 h hydration. And after 3 days, the sample containing 10 wt.% RHA has higher content of CH than the sample containing 10 wt.% quartz powder. This indicates that the addition of RHA stimulates the hydration of cement at early age, and hence more heat and more CH in the RHA-blended cement paste are produced [155]. On the contrary, Nguyen et al. showed that at w/b ratio of 0.18, the degree of cement hydration in the 20 wt.% RHA-blended cement paste in UHPC is lower than that of the control sample after 1 and 3 days by analysis of backscattered electron images and the CH content, respectively [148]. However, the degree of cement hydration in the RHA blended cement paste appears to be higher than in the control sample and the SF-blended paste at late ages. It is ascribed to the internal water curing effect of RHA [16, 147, 148]. RHA may absorb a certain amount of mixing water in its pores. At late ages, the humidity in the blended cement paste decreases, the absorbed water will be released and hence keep the hydration of cement continuous. It is obvious that the addition of RHA may increase or decrease the degree of cement hydration at early ages, and change the process of cement hydration. It might depend on the amount of water interacted between the pore structure of RHA particles and the bulk cement paste. Or from the other point of view, the pore structure of RHA plays a very important role in hydration mechanisms of cement blended with RHA, because it governs the SSA influencing nucleation site effect and the amount of water interacted with the bulk cement paste. Hence, the effect of pore structure of RHA on the degree and the process of cement hydration is one of the main objectives of the present PhD study.

Regarding the pozzolanic reactivity of RHA in the blended cement paste, the degree and process of RHA pozzolanic reaction, and its effect on microstructure development, i.e. pore refinement, of the blended cement paste are still not clear. It is generally known that the addition of SCMs will refine the pore structure of cement matrix by the pozzolanic reaction products, and extra cement hydration products due to the higher cement hydration ascribed to the physical effects. As it is reported that the effect of RHA on acceleration of cement hydration in the blended cement paste is stronger than that of SF [13, 147, 148, 155]. Furthermore, RHA has a higher content of alkali oxides resulting in a higher pH value in the blended cement paste, a much larger SSA-BET, and a similar silica content compared to SF. So the reactivity of RHA can be comparable with or higher than that of SF in the blended cement paste. That may result in a higher amount of hydration products in the RHA blended cement paste compared to that in SF blended cement paste. However, the pore refinement in RHA blended cement paste appears much less than in SF-blended cement paste [13, 16, 147, 148]. It is very important to note that although MPS of RHA is much bigger than that of SF, BET-SSA of RHA is similar or much larger than that of SF [5, 13, 16]. The BET-SSA results from the pore structure inside RHA particles (internal SSA) and the specific surface on surface of RHA particles (external SSA). That may result in the difference between the process of pozzolanic reaction of RHA and the effect of RHA on the pore refinement in the blended cement paste and those of SF. This point will also be clarified in the present PhD study.

Compressive strength

Compressive strength mainly results from the hydration and microstructure development of cement paste. As analyzed above, addition of RHA will accelerate cement hydration and refine the pore structure of blended cement matrix due to the pozzolanic reaction products and extra hydration cement products. That results in an increase in the compressive strength of RHA-blended cement mortar and concrete. The published literature shows that increasing RHA content up to 30 wt.% can increase the compressive strength of mortar and concrete [1, 6, 9, 16, 137, 151, 153, 155-157]. In the range of 0-20 wt.%, the higher level of cement replacement by RHA, the higher the compressive strength at ages later than 3 days [1, 6, 153]. It can be found that compressive strength of concrete containing RHA still develops considerably at late ages, i.e. after 28 days.

The effect of MPS of RHA on compressive strength is shown to depend on the w/b ratio of mortar and concrete. At very w/b ratio of 0.18, compressive strength of UHPC tends to increase with decreasing MPS of RHA regardless of ages [9]. Whereas the 7-day compressive strength of mortar proportioned with the w/b ratio of about 0.50 reaches the maximum value at optimum MPS of RHA toward the coarse size [12]. It can be found that the pore structure characteristics of RHA, i.e. pore size distribution, pore volume, and then SSA, is governed by fineness of RHA particles. The variation in MPS will result in the variation in water adsorption into RHA particles. The amount of absorbed water may influence differentially the cement hydration and the resulting compressive strength of concrete at various w/b ratios. The effect of MPS on compressive strength of SCHPC at various low w/b ratios will be investigated, in consideration into pore structure characteristics in this PhD study.

Comparing the effect of RHA on compressive strength with that of SF has been investigated. The results show that in some cases, the concrete containing RHA has higher compressive strength than the concrete containing SF. The comparison will also be conducted in SCHPC in this PhD study.

It is very important to note that for SCHPC proportioned with a low w/b ratio, self-compacting properties have to be fulfilled first, followed by the properties of hardened concrete, such as compressive strength. The addition of porous RHA will lead to increase plastic viscosity, and decrease filling and passing abilities of mixture. In order to fulfill adequate self-compacting properties and reach very high compressive strength, MPS and content of RHA admixed in SCHPC might be different from that in TVC. Therefore, effect of MPS and content of RHA on rheological properties and compressive strength of SCHPC simultaneously, particularly at a very low w/b ratio, will be taken into account in the present PhD study.

Durability

The presence of RHA decreases the total porosity, increasing the electrical resistivity and the Ultrasonic pulse velocity of concretes [1, 8]. This indicates the improvement in pore structure and hence better durability of concretes. Incorporation of RHA also improves the water adsorption and the resistance to chloride penetration and sulphate attack [5, 137, 153, 156, 158-161]. The carbonation of RHA-modified concrete is improved as well [160, 162].

Regarding ASR in RHA admixed cementitious materials, Hasparyk et al. [163] reported that after 28 days in NaOH 1M at 80 °C, the expansion of mortar bars prepared in accordance with ASTM C1260 decreases with higher RHA content replacing cement in the range of 0-15 wt.%. Where the reactive aggregates used are quartzite and basalt, and MPS of RHA is 4 µm. The 14-day expansion of specimens containing 12 or 15 wt.% RHA is lower than the prescribed limit of 0.10 %. It is observed that the expansion of specimens admixed SF or RHA increase rapidly from 14 to 28 days. The improvement of ASR resistance of RHA-modified mixtures containing reactive aggregate is also concluded by Mehta et al. [5]. The ASTM C1260 standard was also applied to evaluate the effectiveness of RHA on ASR resistance in study of Rodriguez de Sensate, G.[7]. The results showed that with MPS of 8 µm, the amorphous RHA is more effective than the partially crystalline RHA in ASR resistance, with respect of expansion of mortar bars after 14 days of immersion. Increasing content of both types of RHA decreases the 14-day expansion. It is observed that the specimens containing 20 wt.% amorphous RHA passes the expansion criterion, and the specimens containing 30 wt.% partially crystalline RHA are just at the prescribed limit at 14 days of immersion. Whereas the experimental results of Ramezanianpor et al.[164] revealed that RHA tends to be beneficial to control ASR of reactive aggregates in the range of 7-10 wt.% cement replacement. And surprisingly, increasing the amount of RHA leads to an increase in the expansion.

The resistance of RHA-modified UHPC (without reactive aggregate) to ASR has been evaluated [16]. After 14 days even 28 days of immersion in NaOH 1M at 80 ^{o}C, the expansion of 40x40x160 mm^3 sized samples containing RHA with MPS of 7.41 µm is larger than that of sample containing SF, but still far below the threshold of the ASR test according to ASTM C1260-01 and the German standard [165]. However, from the pictures (Fig. 2.16), it can be

observed that visible cracks appear on the surface, particularly at the edges of samples. That indicates ASR may occur in very dense matrix of UHPC in the presence of RHA.

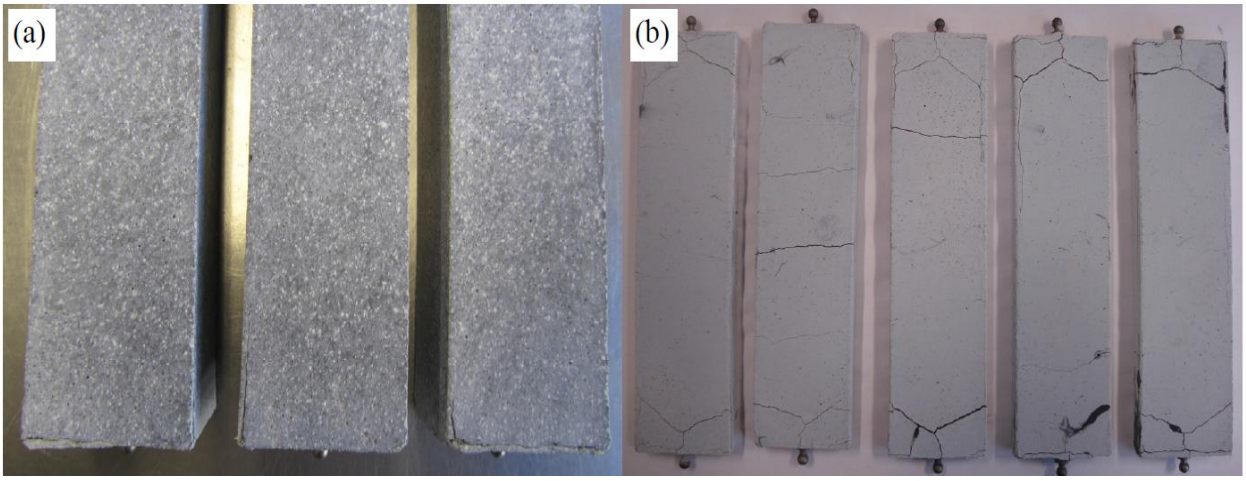

Fig. 2.16 Cracking along the edges of 40x40x160 mm^3(a) and on the surface 10x40x160 mm^3(b) sized UHPC samples containing RHA [16]

Due to the higher amount of cement, a higher amount of soluble alkali content can be present in the pore solution in SCHPC. That results in higher probability of ASR. Furthermore, ASR can occur even in HPC with a dense structure [97, 128, 129] and may occur in UHPC with very dense matrix in presence of RHA. Hence, the resistance of SCHPC to ASR, and the effect of RHA on resistance of SCHPC to ASR will be considered in detail in this PhD study.

2.3.5. The use of RHA in SCHPC

RHA has been used as a SCM to produce SCHPC at various w/b ratios of 0.30, 0.35, 0.40 and 0.50. The RHA content used is in the range of 0-30 wt.% [1]. The investigation was conducted on SCHPC as well as paste, and mortar formulated from SCHPC. The results of this study reveal that the increase in RHA content increases flow time of the pastes, particularly at the lower w/b ratio. The slump flow of the mortars decreases with the higher RHA content and the lower w/b ratio. Slump flow of both paste and mortar increases with higher SP dosages, however the excessive SP dosages are not effective in the flowing ability due to the segregation problem in the form of bleeding [1, 166]. Similar to the pastes, the flow time of SCHPC increases with the higher RHA content, and the lower w/b ratio. It is explained that the higher cement replacement by RHA increases volume and surface area of the binder and hence results in higher plastic viscosity of paste, and paste in concrete. Where the effect of the reduction in aggregate volume and increase in paste volume seem to be less significant. The slump flow ranges from 600 to 770 mm, where slump flow with or without J-ring increases considerably with the lower w/b ratio and the greater RHA content. This is ascribed to the increased paste volume and decreased aggregate content of concrete with the lower w/b ratio and higher RHA content. Cement replacement by RHA in weight leads to an increase in paste volume due to the lower density of RHA, and the resulting slump flow increases. The characteristics of RHA, i.e. pore structure, is not really taken into account as a main factor influencing the flowing ability of SCHPC.

In another study [10], the addition of 25 and 50 wt.% RHA to the mixture proportion of SCC leads to a decrease in the w/b ratio from 0.40 to 0.38 and to 0.36, respectively. As the amount of

RHA increases, the V-funnel time increases, and the slump flow decreases with the same dosage of SP. Herein, it is unclear whether the increased V-funnel time, and the decreased slump flow is due to the reduced w/b ratio or the higher RHA content. Furthermore, RHA has been used to replace sand in producing SCC [167], as well as to combine with FA and GGBFS to produce SCC [168]. In order to meet a certain slump flow, increasing RHA content increases SP dosage or water demand. The addition of RHA induces longer flow time, indicating higher viscosity [167, 168].

With regard to the properties of hardened SCHPC containing RHA, in the range of 0-20 wt.%, the higher RHA content, the higher compressive strength of SCHPC, particularly at the late ages [1, 169]. The maximum compressive strength of SCHPC containing RHA is approximately 100 MPa after 56 days at w/b of 0.30 [1] and after 180 days at w/b of 0.35 [169]. Increasing RHA content increases the ultrasonic pulse velocity and true electrical resistivity and decrease the water adsorption and total porosity of SCHPC. This indicates good durability of SCHPC containing RHA [1].

The addition of RHA to SCHPC mixtures influences the properties of fresh concrete by physical aspect, and the properties of hardened concrete by both physical and chemical aspects. In case of SCHPC, the physical properties, i.e. MPS and pore structure, of RHA will dramatically influence the rheological properties of paste, and then resulting self-compacting properties of SCHPC. Therefore, the characteristics of RHA, particularly pore structure, should be considered first and then the rheological properties of SCHPC can be explained. The effect of pore structure on rheological properties and resulting properties of fresh SCHPC will be investigated in detail in the present PhD study.

Compared to TVC, the self-compacting properties of SCHPC must be fulfilled first, and then high compressive strength and good durability. In order to reach very high compressive strength, w/b ratio is very low. Fulfilling adequate filling ability of SCHPC at very low w/b ratio is a challenge, particularly in the presence of RHA. The problem is also taken into account in this PhD study.

Besides pozzolanic reaction (chemical aspect), pore structure of RHA (physical aspect) is of importance in hydration and microstructure of the blended cement paste and resulting compressive strength and durability of concrete. The effect will be more pronounced at a very low w/b ratio. Consequently, the hydration and microstructure of RHA blended cement paste in SCHPC is one of main points in this PhD study.

3. Materials and Experimental methods

3.1. Materials

Ordinary Portland cement (CEM I 52.5 R conforming to DIN EN 197-1), undensified SF, RHA, FA, LSP, natural sand with a maximum size of 2 mm, and crushed basalt stone (2-5 mm, 5-8 mm, 8-11 mm, 11-16 mm) were used in this study. RHA was used in this study with six different MPSs of 5.7, 6.5, 7.7, 12.0, 15.6, and 22.6 µm. The characteristics of these types of RHA will be analyzed in the next section. X-Ray patterns of RHA, SF and FA are shown in Fig. 3.1. The RHA sample has a large amount of amorphous material, i.e. 96.7 wt.% amorphous, 2.3 wt.% quartz and 0.7 wt.% Calcite, similar to the SF sample (98.8 wt.% amorphous, < 1 wt.% quartz and 1 wt.% Calcite), and larger than FA sample (73.5 wt.% amorphous, 8.9 wt.% quartz , < 1 wt.% Calcite, 16.0 wt.% Mullite, and 1.0 wt.% Hematite). This indicates that RHA is an amorphous siliceous material similar to SF, and more reactive than FA, whereas LSP is considered as an inert material. It has a main content of Calcite (80.1 wt.%), and other minerals (Quartz, Dolomite, Muscovite, etc.). The chemical composition and the physical properties of cement, RHA and other SCMs are summarized in Table 3.1 and Table 3.2 respectively. Fig. 3.2 shows the Scanning Electron Microscopic (SEM) images of pore structure on surfaces and morphology of the finely ground RHA, SF, LSP and FA. The particles of RHA are angular and still have porous structure after grinding. Particle size distributions of RHA5.7 (the number indicates MPS of RHA), cement, and other SCMs used in this study are displayed in Fig. 3.3.

Table 3.1 Chemical composition (wt.%) of cement and SCMs

Materials	SiO_2	Al_2O_3	Fe_2O_3	CaO	MgO	SO_3	Na_2O	K_2O	L.O.I
Cement	19.4	5.3	2.5	61.2	1.2	3.2	0.07	0.61	4.9
RHA	87.0	0.8	0.4	1.2	0.6	0.4	0.4	2.63	3.7
SF	96.6	0.7	0.2	0.3	0.4	0.1	0.16	0.65	0.9
FA	56.6	25.8	6.4	2.5	1.3	0.6	0.62	2.08	2.9
LSP	10.9	4.2	1.3	46.8	1.2	0.6	0.3	1.02	34.0

L.O.I-Loss On Ignition

Table 3.2 Physical properties of material used in this study

Parameters	Cement	RHA	SF	FA	LSP	Sand	Basalt
Density (g/cm^3)	3.09	2.27	2.26	2.27	2.74	2.65	3.05
Mean particle size (µm)	7.07	5.70	0.35	16.39	7.88	-	-
n- The RRSB slope	0.509	0.653	1.302	0.498	0.539	0.79	0.49
x'- The location parameter of RRSB (µm)	11.34	8.37	0.41	28.51	11.01	483.6	6421.8
BET-SSA [Blain] (m^2/g)	[0.595]	25.21	18.09	2.14	6.88	-	-
Water adsorption (wt.%)	-	-	-	-	-	0.08	0.8
Moisture content (wt.%)	-	-	-	-	-	0.0	0.2

RRSB-Rosin, Rammler, Sperling and Bennett

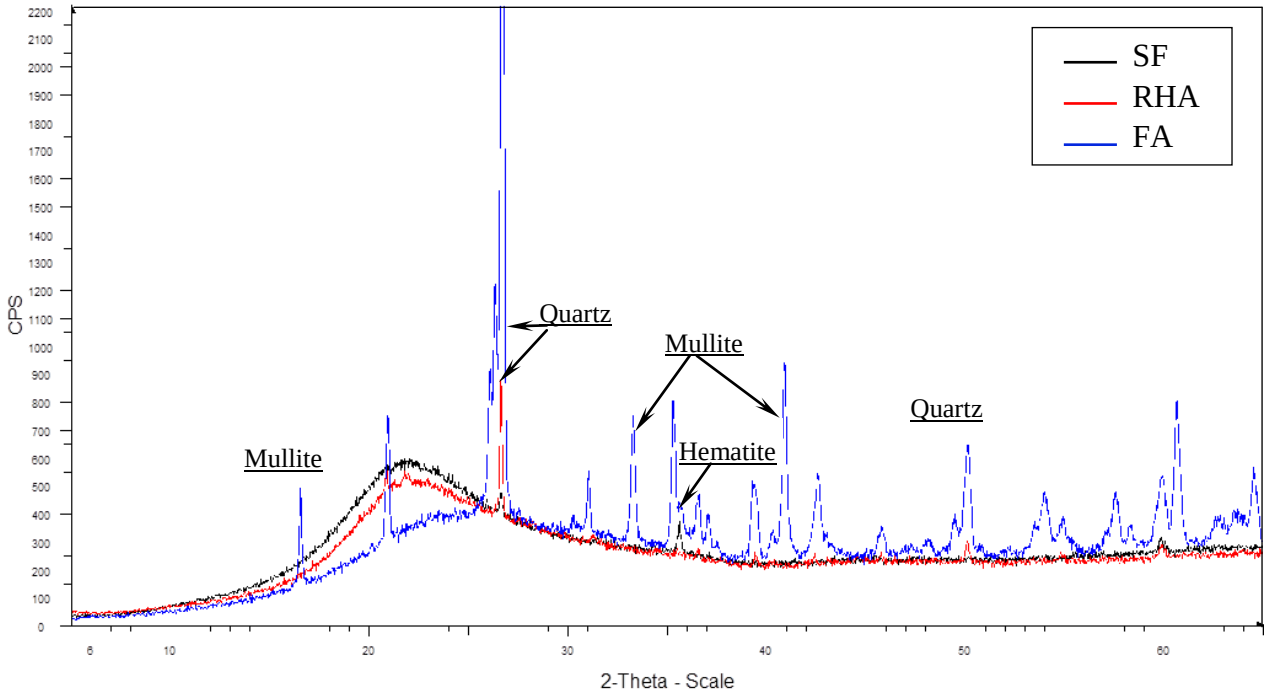

Fig. 3.1 XRD patterns of RHA and SF

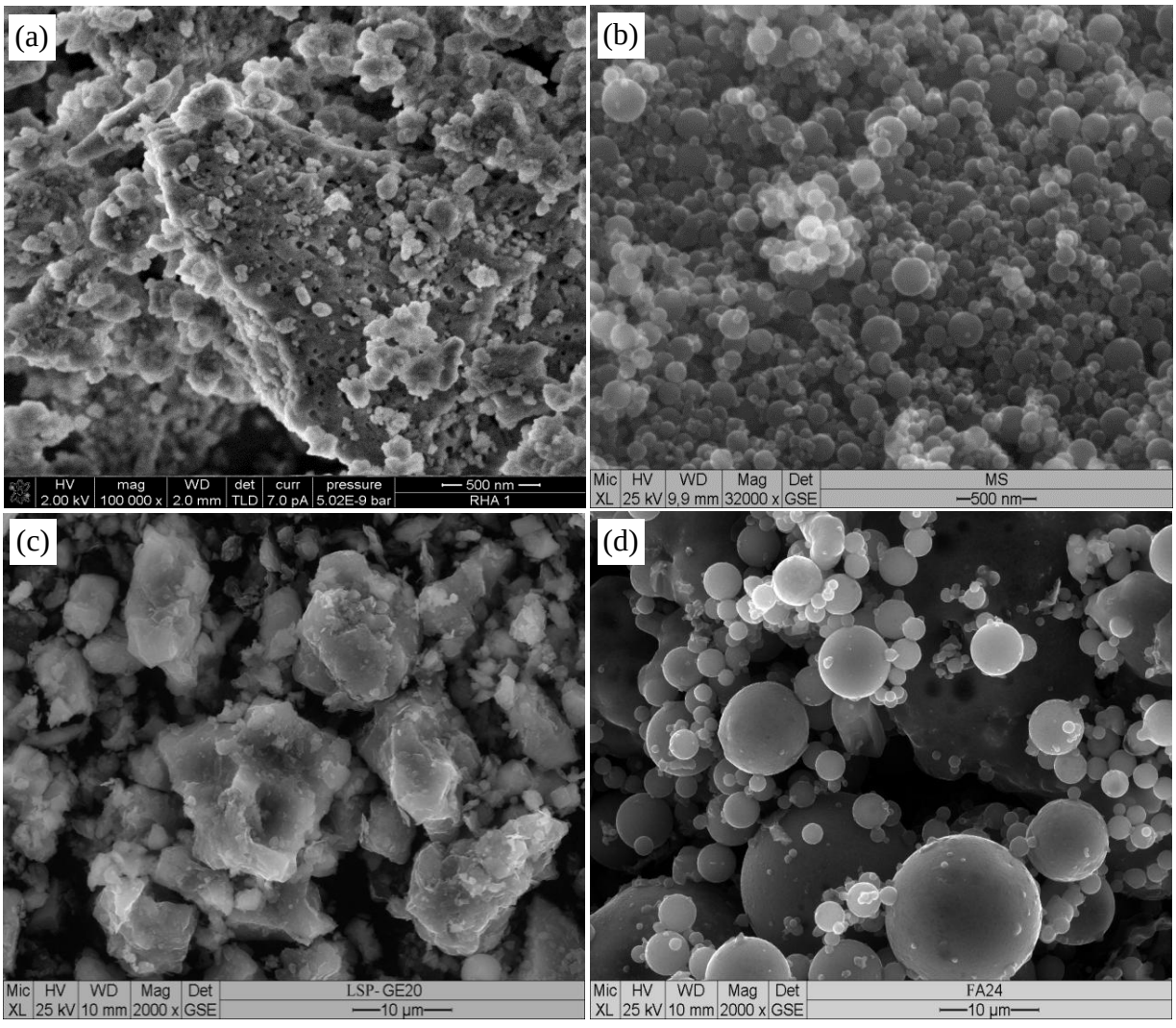

Fig. 3.2 SEM images of finely ground RHA(a); SF (b); LSP (c); FA (d)

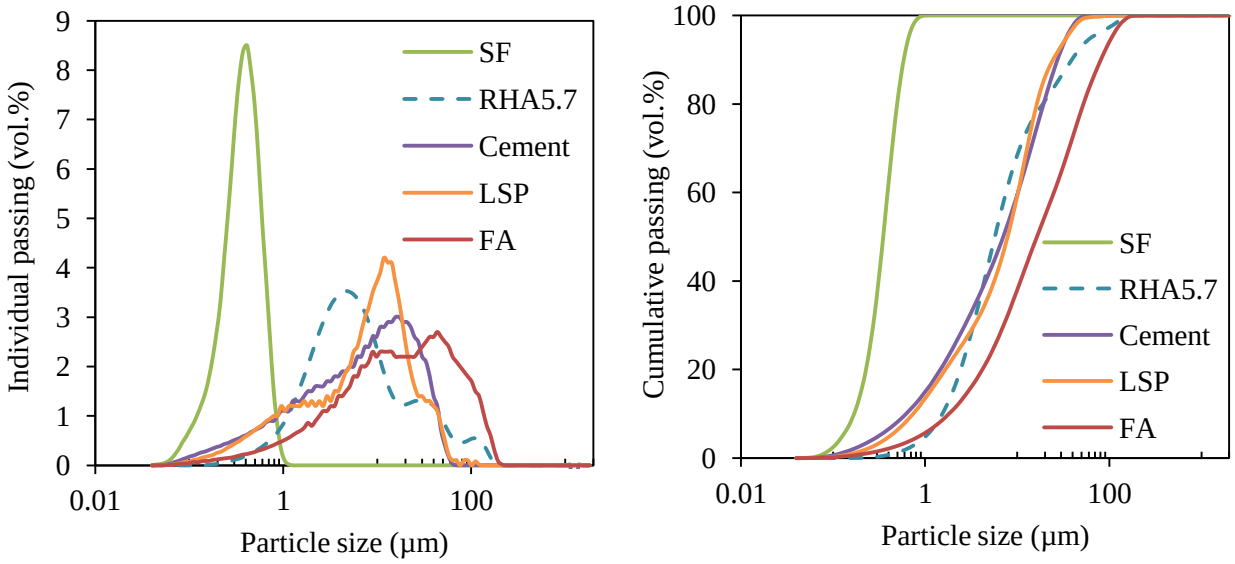

Fig. 3.3 Particle size distribution of cement and SCMs

The mineral composition calculated by the quantitative X-ray diffraction (QXRD) phase analysis (Rietveld) and compressive strength of Portland cement are displayed in Table 3. 3. A polycarboxylate-based SP with density of 1.08 g/cm^3 and 40 wt.% solid content was used in this study.

Table 3. 3 Mineral composition and compressive strength of cement

Mineral composition (wt.%)				Compressive strength (MPa)		
C_3S	C_2S	C_3A	C_4AF	2 days	7 days	28 days
50.1	17.8	9.8	7.6	36.2	56.6	65.4

In addition, in order to investigate ASR in mortar formulated from SCHPC. The natural sand was replaced by reactive greywacke and non-reactive basalt aggregates with maximum particle size of 4 mm. The greywacke was composed of 50.6 Quartz, 9.9 Alkalifieldspar, 26.9 Plagioclase, 4.3 Biotite, 3.2 Chlorite, 3.5 Muscovite, 0.9 Pyrite and 0.7 other minerals (Rutile, Titanite, and Hematite), in wt.%. Whereas the composition of basalt was: 39.1 Augite, 38.8 Plagioclase, 12.5 Olivine, 3.0 Magnetites, 2.5 Hornblende, 2.1 Nepheline, 1.0 Chlorite, and 1.0 other minerals (Biotite and Analcime), in wt.%. Densities of greywacke and basalt are 2.73 and 3.03 g/cm^3 respectively.

3.2. Experimental methods

3.2.1. Characteristics of RHA and other SCMs

Pore structure, specific surface area and fineness

To analyze the characteristics, RHA was ground in a ball mill for different periods of time, i.e. 15, 30 … 540 minutes. Laser diffraction (LS 230, Beckman Coulter) was used to determine mean particle sizes (MPS) of RHA and other SCMs. BET-SSA of RHA and other SCMs was determined by the Brunauer-Emmett-Teller method (ASAP 2000, Micromeritics). And, the Barrett-Joyner-Hanlenda (BJH) method (SA 3100, Beckman Coulter) was used to measure pore volume and pore size in RHA particles. BET and BJH methods are employed by the nitrogen

adsorption and desorption techniques. More detail about these methods can be found elsewhere [170, 171]. Additionally, the pore structure and morphology of RHA particles were analyzed by an ultra high resolution scanning electron microscope (Nova NanoSEM 230).

Water demand and water adsorption

The water demand of RHA, other SCMs, and cement was determined in accordance with the Puntke method [172]. A certain amount of powder was filled into a proper cup with the flat bottom. Water was sprayed gradually and then the powder and water were kneaded thoroughly. After that the cup with wet powder was shaken with a certain frequency. The desired saturation point was reached when the surface of wet powder was levelled and brilliant. A mirror-smooth surface indicated water surplus.

To determine the water adsorption capacity of RHA and other SCMs, 5.0 g of each SCM were exposed to 97.5 % relative humidity at 20 °C until constant weight. The weight of the samples was determined before and after drying at 110 °C [16]. Saturated K_2SO_4 solution was used to create the 97.5 % RH condition at 20 °C [173].

Pozzolanic reactivity

The pozzolanic reactivity of reactive SCMs, i.e. RHA with different MPS, SF and FA, was indirectly measured by the reduction in the electrical conductivity of the saturated CH solution before and after the addition of pozzolan. 5.0 g pozzolan were added into 200 ml saturated calcium hydroxide solution at 40 ^{o}C. The electrical conductivity was recorded by a dual conductivity meter (S47 SevenMulti, Mettler Toledo) up to 900 min of hydration. The CH-pozzolan suspensions have liquid to solid ratio (l/s) of 40. During measurement, the suspensions were stirred at velocity of 350 rpm, and maintained at 40 ^{o}C by thermostatic bath (heating and cooling). The procedure of this test method is proposed by Luxan et al. [143]. As analyzed above, to minimize the effect of water soluble components in pozzolans, i.e. Na, K ion, on the electrical conductivity of CH-pozzolan suspensions, the reduction in the electrical conductivity value of CH-pozzolan suspension subtracting the value of water-pozzolan suspension was used to evaluate the pozzolanic reactivity of pozzolans.

Additionally, the hydration of residues obtained from filtering the CH-pozzolan suspensions were stopped by isopropanol and then dried at 35 ^{o}C until constant weight. Reaction products and microstructure of the residues of the CH-pozzolan suspensions after 4 and 24 hours of hydration was qualitatively compared by scanning electron microscopy.

3.2.2. Properties of paste, mortar and SCHPC

Properties of fresh paste, mortar and SCHPC

To examine whether the mixture proportions designed by the proposed method could meet the self-compactability and compressive strength requirements, the following test methods were carried out.

Slump flow test: In accordance with DIN EN 12350-8, this test method was carried out to measure filling ability and flow rate T_{500} that indicates plastic viscosity of fresh concrete (Fig. 3.4a and c).

J-ring test: In accordance with DIN-EN12350-12, this test method was used to assess filling ability and passing ability of fresh concrete through reinforcement (Fig. 3.4 b and d).

V-funnel test: In accordance with DIN-EN12350-9, this test method was carried out to measure the flow time through the V-funnel. The plastic viscosity of fresh concrete can be evaluated based on the V-funnel flow time, and the arching effect of aggregate can be detected as well.

Sieve segregation test: This test method was carried out in accordance with DIN-EN12350-11. The test aims at investigating the resistance of SCHPC to segregation by measuring the portion of the fresh SCHPC sample passing through a 5 mm sieve. If the SCHPC has poor resistance to segregation, the paste or mortar can easily pass the sieve. Therefore, the sieved portion indicates whether the SCHPC is stable or not.

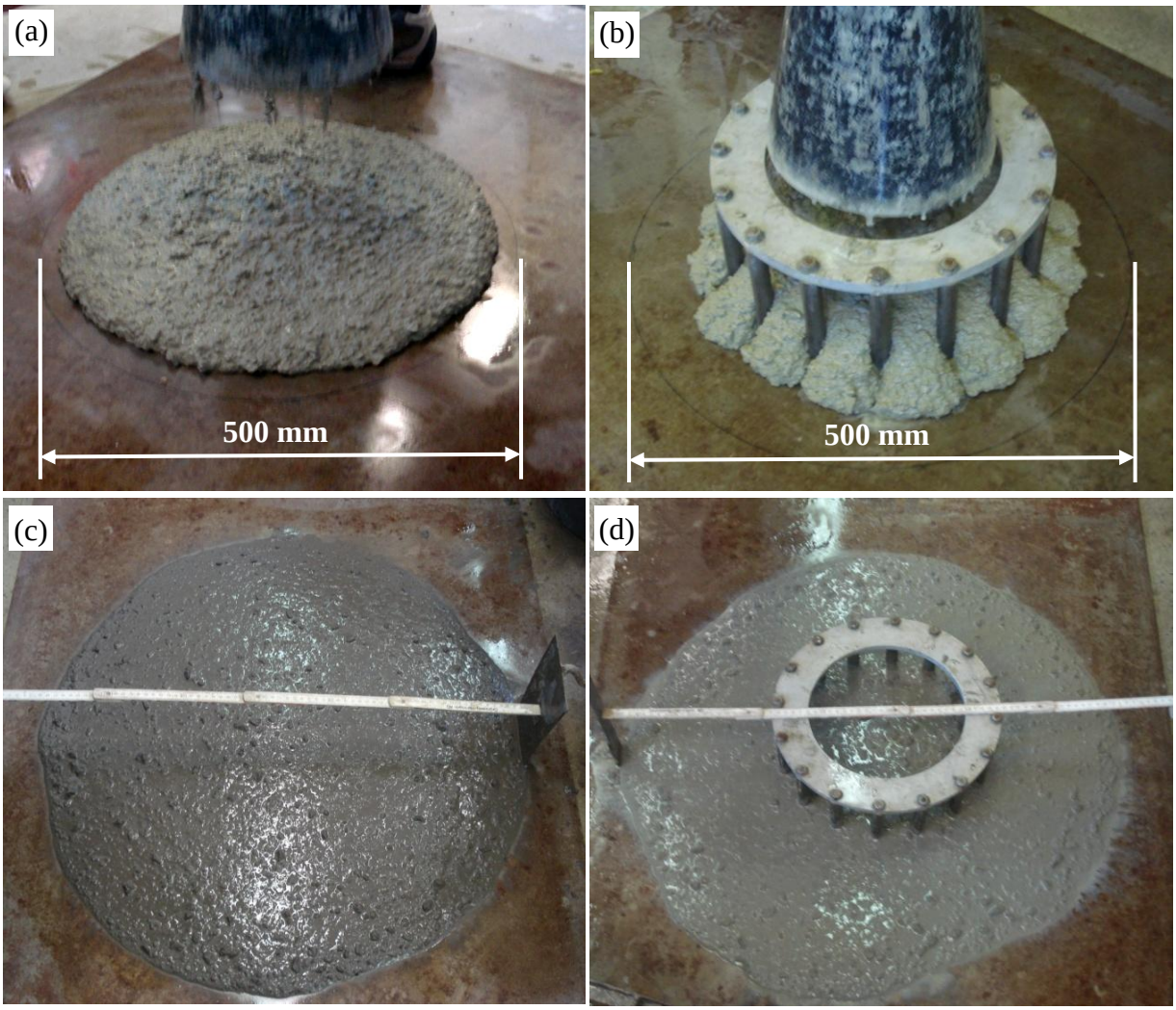

Fig. 3.4 Slump flow test with mixture containing RHA (a, c) and J-ring test (b, d) with referent mixture

Rheological properties of mortar were measured by a Viskomat NT with a basket probe (Schleibinger, Germany), as can be seen in Fig. 3.5. The measurements were started 15, 30 and 60 min after water addition. During the measurement, temperature of the samples was kept constant at 20 °C by a water bath. In order to eliminate the effects due to thixotropy, the measurement was started at maximum rotational velocity of 12 rpm for 80 seconds, and then the velocity decreased in 14 steps of 20 seconds each. Immediately after measurement, a maximum velocity and about 70 % of the maximal velocity were applied again to detect segregation and/or thixotropy [91, 174, 175], as shown in Fig. 3.6. If segregation occurs, the torque at these points is significantly higher than former values due to blocking.

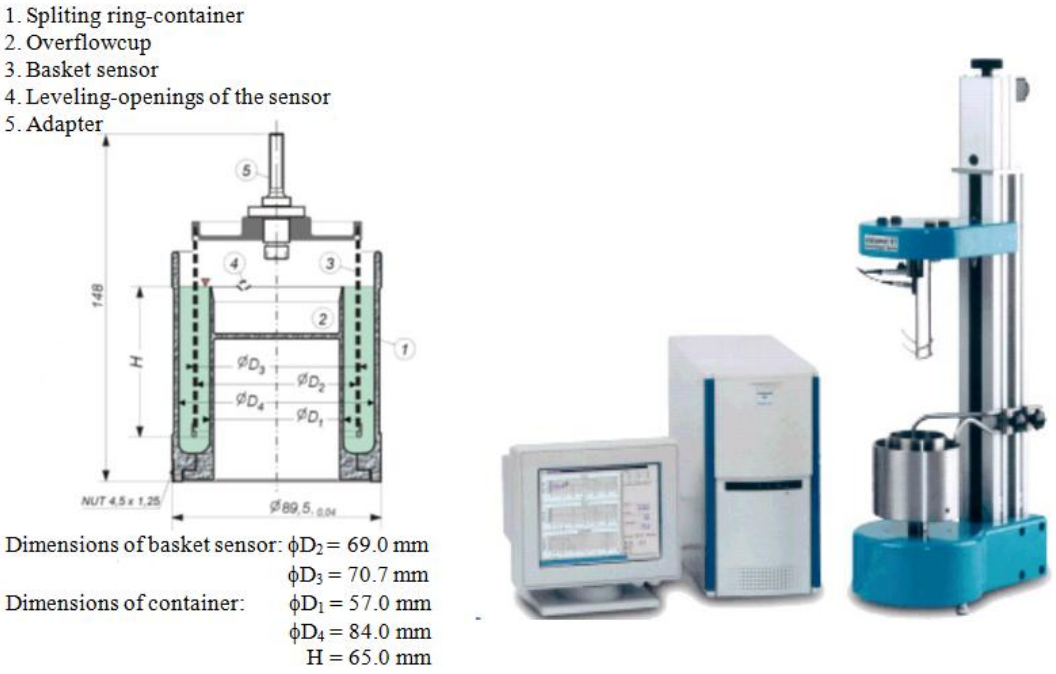

Fig. 3.5 Basket probe and Viskomat NT with mortar paddle produced by Schleibinger

The calibration proposed by Vogel [175, 176] was applied to calculate shear stress (τ) and shear rate (γ) from torque (T) and rotational velocity (N) respectively, as presented in Eq. 3.1 and Eq. 3.2.

$$\tau = 0.958 * T, (Pa) \quad (3.1)$$

$$\gamma = 0.584 * N, (s^{-1}) \quad (3.2)$$

The limitation of the use of the basket probe is described by the critical shear rate (γ_{crit}). The critical rate is calculated from the yield stress and viscosity, as following:

$$\gamma_{crit} = 0.196 * \frac{\tau_0}{\eta}, (s^{-1}) \quad (3.3)$$

The values of shear rate lower the critical shear rate will not be used to determine the yield stress [175, 176]. Flow curves obtained from all tests expressed linearity with shear rates lower than 0.58 1/s (1rpm) and non-linearity with the higher ones. Therefore, yield stress and plastic viscosity were calculated in accordance with the Bingham model with shear rates below 0.58 1/s. Excellent linear regression ($R^2 \geq 0.99$) was considered. To evaluate shear-thickening behaviour, the modified Bingham model was applied with the higher shear rates.

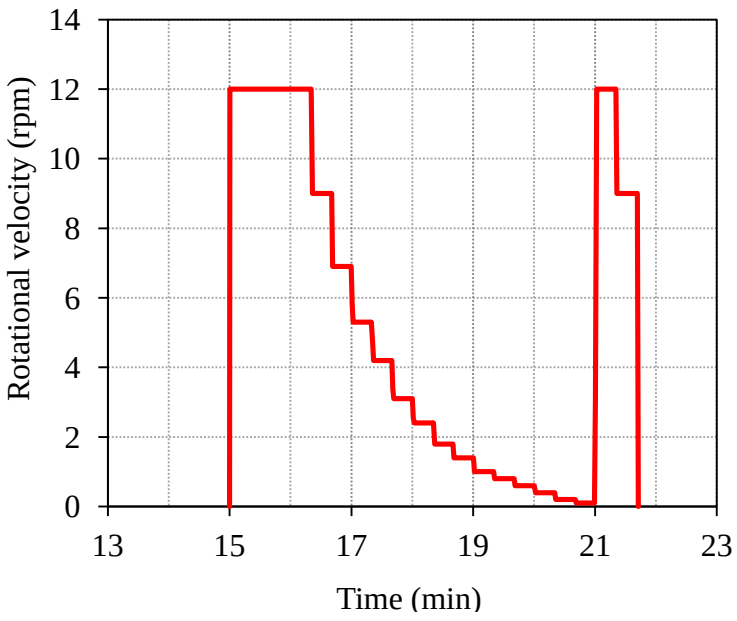

Fig. 3.6 Protocol to reach the steady flow curve

This model is presented in Eq. 2.6. The parameter c/μ corresponds to index n in Herschel-Bulkley model, therefore describes shear-thickening behaviour [91].

Slump flow and flow time of fresh mortar were determined by using mini-cone slump flow, mini-V-funnel time tests respectively, described in EFNARC [60]. Flow rate of mortar was also evaluated by T_{250} time which is spread time for a diameter of 250 mm, corresponding to T_{500} time measured in SCC [60, 136], as shown in Fig. 3.7. Superplasticizer saturation dosage (SSD) of mortar was determined by testing the mini-cone slump flow. The SSD is defined as the SP dosage beyond which slump flow does not increase significantly.

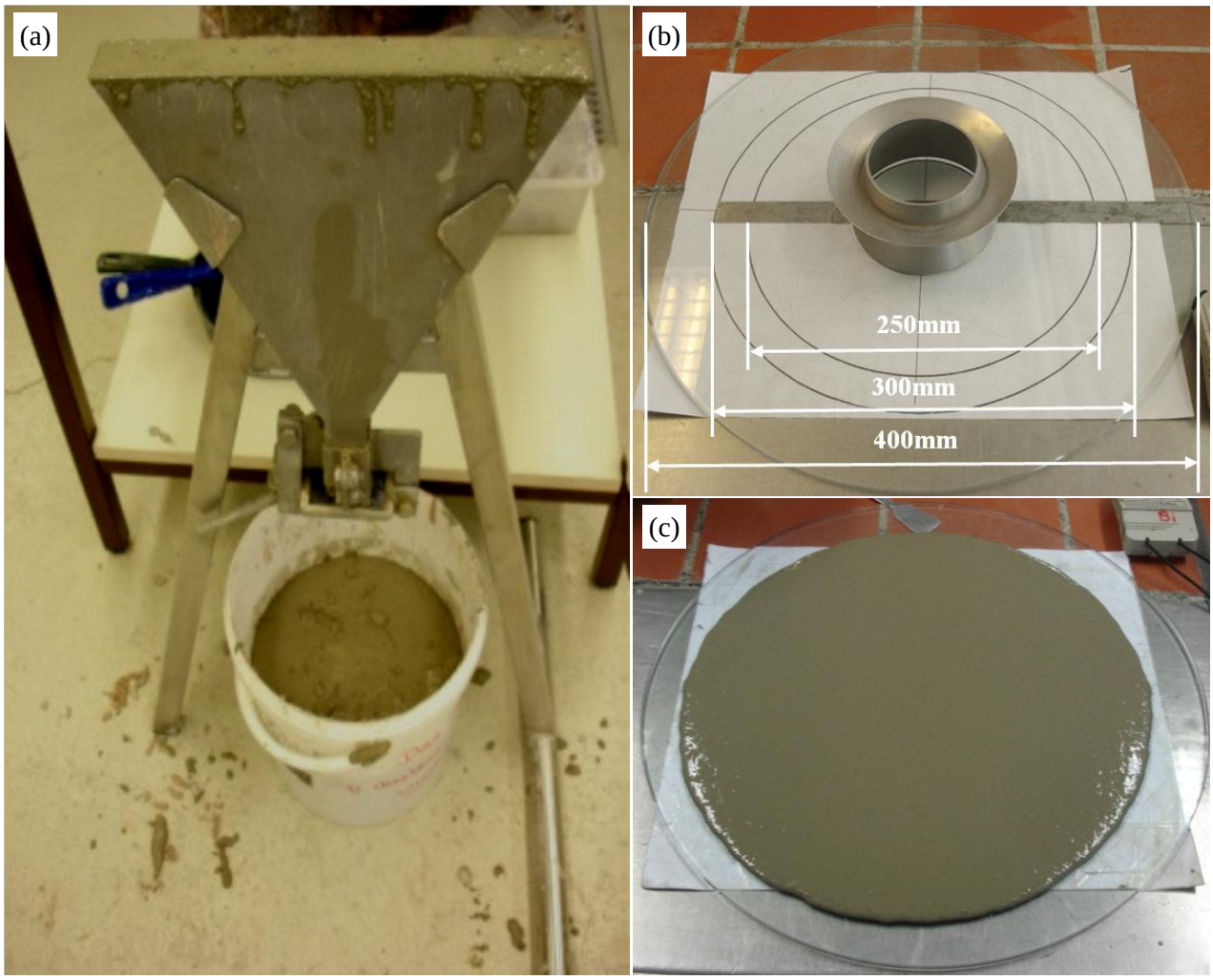

Fig. 3.7 Mini-V-funnel test (a)[177]; Mini-cone slump flow and flow rate-T_{250} test (b,c)

Paste formulated from mortar was used to determine SP adsorption after 15 minutes on cement and SCM particles. Approximately 10 ml of pore solution obtained from the paste by means of centrifugation was filtered (0.20 μm filter) and stabilized by adding 5M HNO_3 acid. Total organic carbon content (TOC) of these pore solutions were determined by using a Multi EA 4 000/Analytik Jena. The content of SP absorbed on binder (cement and SCM) was calculated from the TOC content of the corresponding SP-water suspension. The TOC content of the pore solution filtered from paste without SP was taken into account.

Compressive strength

Cubic specimens of 150x150x150 mm^3 for compressive strength of SCHPC were cast without vibration and compaction. After 1 day, the specimens were demoulded, stored in water at 20±2

^{o}C for 6 further days, and then cured in controlled room at 20±2 ^{o}C and 65±5 % relative humidity until testing at 3, 7, 28, and 56 days according to DIN-EN12390-2. Compressive strength of concrete was determined under DIN-EN12390-3. Three specimens of each mixture were tested and the average values were reported.

Mortar specimens having dimensions of 40 x 40 x 160 mm^3 were cast without vibration and compaction, and were cured in moulds at temperature of 20 ^{o}C and 95 % relative humidity for 1 day. After demoulding the specimens were stored in water at 20 ^{o}C until testing at 3, 7, 28, 91 days. Compressive strength was tested according to DIN EN 196-1. Six specimens of each mixture were tested and the average values were reported.

Hydration and microstructure

Microstructure of mortar samples was examined by an ultra high resolution scanning electron microscope (SEM) (Nova NanoSEM 230, FEI) (Fig. 3.8a). The working distance was 5.5 mm and an acceleration voltage of 15 kV was used. With SEM, the Backscattered electron images obtained can provide two-dimensional information of the microstructure, i.e., phases and phase distribution. In Fig. 3.8b, a typical BSE image of the hardened Portland cement paste and its grey level histogram are shown. It can be observed that the main phases in the microstructure of cement, namely pore, hydration products, and anhydrous cement, appear with sharply different grey levels, depending on their densities. Anhydrous cement particles and the CH appear bright and light grey, while other hydration products, i.e., C-S-H are various shades of darker grey. The pores, which are filled by epoxy having low average atomic number, appear uniformly black [13]. In this study, BSE imaging was conducted on the polished epoxy-impregnated specimens to investigate microstructure and quantify anhydrous cement of the cement paste in the mortar samples. The BSE images were captured with dimension of 1024×943 pixels and with a magnification of 500x. At least 12-15 images were captured to ensure acceptable representation of each sample [148, 178-180]. Samples were tested at ages of 28 and 91 days. Based on stereological principles, it is assumed that with sufficient sampling, area fractions in two-dimensional cross sections in BSE images can be equal to three-dimensional volume fractions of Portland cement. The degree of cement hydration can be calculated from the volume of unhydrated cement [181, 182].

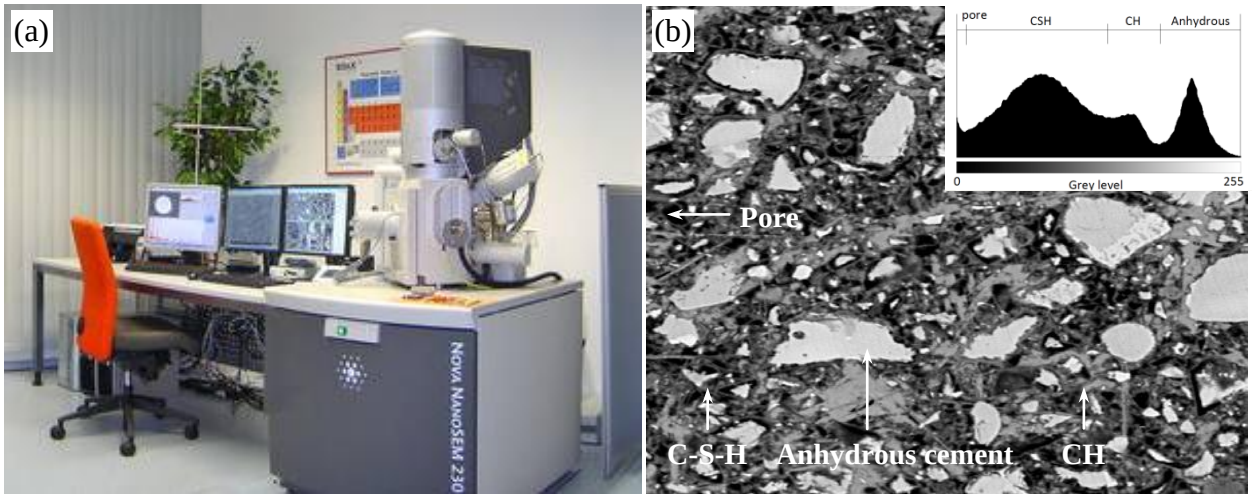

Fig. 3.8 Nova NanoSEM 230, FEI (a); A typical BSE image of the Portland cement paste and its grey level histogram (b) [13]

In order to determine the thickness of ITZ between sand surface and the blended cement matrix, images with a magnification of 4000s were captured. A total number of 12 images were captured for each sample in this study. The thickness was determined by the variation in the grey level. For each image, 20 frames with a length of about 20 µm were arranged along the surface of sand particles (Fig. 3.9). The grey levels of these frames were obtained by using software Scandium. The average value of all grey level of all frames of all images was used to estimate the ITZ [13].

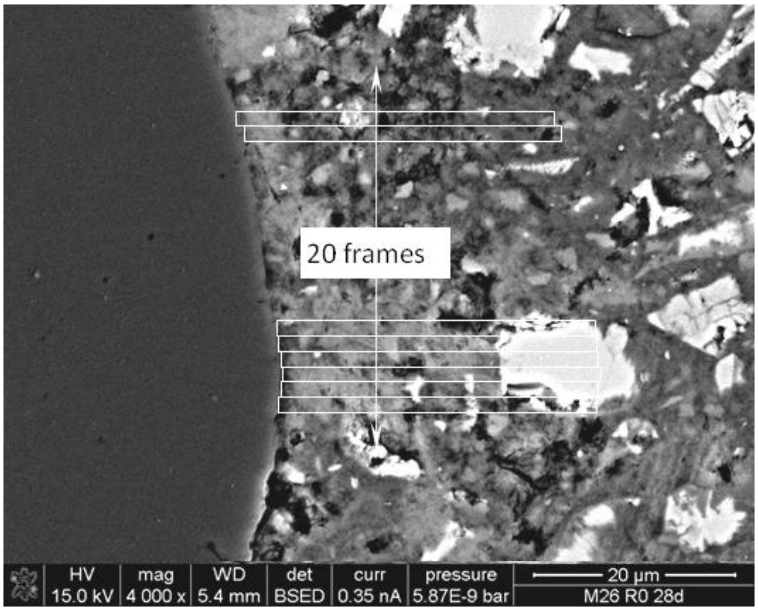

Fig. 3.9 determination of ITZ by analysing grey level

Additionally, energy dispersive X-ray spectroscopy (EDX) in combination with BSE imaging was carried out on polished sections of mortar to investigate the distribution of calcium, alkali, silicon and RHA/ SF particles in the blended paste matrix of mortar. EDX was also used to quantify chemical composition of C-S-H phases formed by pozzolanic reaction.

EDX, considered a non-destructive analytical technique, is a qualitative and quantitative X-ray microanalytical technique used in conjunction with SEM that provides information on the chemical composition of a sample for elements with atomic number. An electron beam is focused on the sample in a SEM. The electrons from the primary beam penetrate and interact with the atoms in the sample, resulting in the emission of X-rays. The X-rays are captured and analyzed by an Energy Dispersive detector which shows the signal as a spectrum of intensity (number of X-rays or X-ray count rate) versus X-ray energy. The elements can be identified by the energies of the characteristic X-rays, while the concentrations of the elements are quantified by the intensities of the characteristic X-ray peaks, as can be seen in Fig. 3.10. The spatial resolution of SEM-EDS analysis depends on the size of the interaction volume, which is governed by the accelerating voltage and the mean atomic number of the sample. For

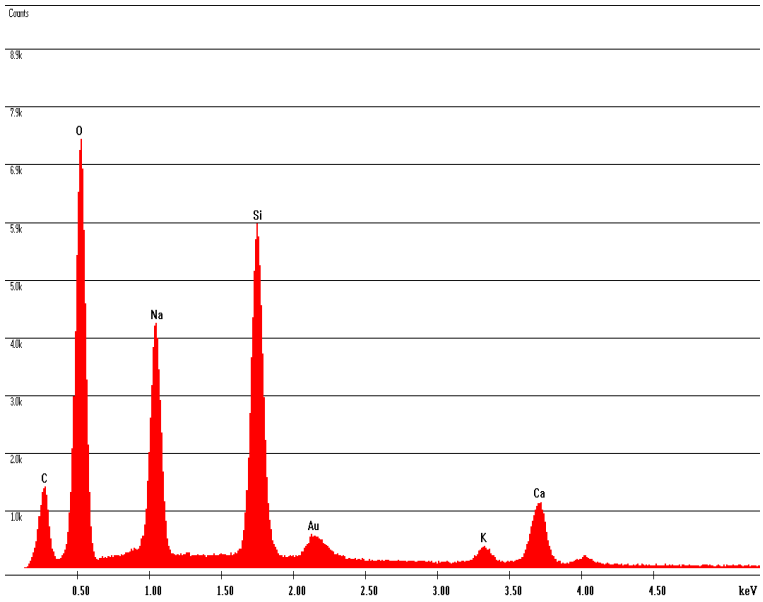

Fig. 3.10 X-rays spectra for ASR products formed inside a RHA particle

SEM-EDS, spatial resolution and depth resolution is about a few microns [183, 184].

The total porosity and pore size distribution of mortar samples were determined by Mercury intrusion porosimetry (MIP-Micromeritics, Autopore IV 9500) with the pressure up to 210 MPa. The sample pieces of 3-5 mm were collected and immersed in isopropanol for 1 day to stop hydration and then dried at 40 °C until constant weight. The weight of each sample was about 10 g. Based on the consumption of mercury during the intrusion process and the respective pressure, the total porosity and the pore size radius distribution in the range from 3nm to 220 μm in the samples was determined. The samples were measured at 3, 28 and 91 days.

The calcium hydroxide (CH) content of binder pastes was determined from the results of thermal analysis (DTA/TG). In which the second-derivative differential thermal (DTA) curve was used to detect the onset of weight loss [185, 186]. The thermal analyses were conducted on SDT Q600, TA instruments, with a heating rate of 10 ^{o}K/min up to 1000 ^{o}C in nitrogen atmosphere with nitrogen flow of 100 ml/min. For the thermal analysis, hydration of the sample pieces were stopped by isopropanol addition and dried at 40 ^{o}C until constant weight, as mentioned above. Sample powder with size less than 63 μm obtained after grinding was used for thermal analysis. Samples were tested at ages of 3, 28, and 91 days.

The X-ray diffractometry (XRD) (D5000, Bruker) was applied to study the hydration process of Portland cement and Portland cement blended with RHA or SF in mortar over the time (Fig. 3.11). As described above, the sample pieces were collected and stopped by isopropanol, and then ground to a particle size of < 45 μm for XRD. The XRD patterns of mortar samples were recorded at the measurement range between 4-70° 2θ. The quantitative X-ray diffraction (QXRD) phase analysis (Rietveld) was carried out on mortar samples without and with 20 wt.% zincite as the internal standard (TOPAS 4.2, Bruker AXS, Germany) to determine clinker minerals and other minerals in the blended cement paste of mortar samples over time.

Fig. 3.11 X-ray diffractometer Siemens D5000

Alkali Silica Reaction

The accelerated mortar bar method according to ASTM C 1260 or the German Alkali Guidelines [165, 187] was applied to evaluate the effect of RHA on ASR in mortar formulated from SCHPC in comparison with that of SF. Mortar bars having dimension of 40x40x160 mm^3 were cast without vibration. Three bars were produced for each mixture. After 1 day at 20 ^{o}C in a moist room, the mortar bars were demoulded and stored in water containers at 80 ^{o}C for a further period of 1 day. Thereafter, the mortar bars were immersed in NaOH 1M or in water at

80 ^{o}C with volume of solution to mortar ratio of 4 and expansions were measured after 5, 9, 14, 28 and 56 days.

Furthermore, the testing procedure for mortar bars mentioned above was applied to evaluate alkali silica reactivity of RHA in paste formulated from SCHPC. Paste bars having dimension of 10x10x60 mm^3 were cast without vibration. Three bars were produced for each mixture. After 1 day at 20 ^{o}C in a moist room, the paste bars were demoulded and stored in water containers at 20, 40 and 80 ^{o}C for a further period of 1 day. Thereafter, the paste bars were immersed in NaOH 1M at 20, 40 and 80 ^{o}C with volume of solution to paste ratio of 4. The visual inspection was conducted to observe visible cracks on the surface of paste bars over time.

The paste sample after 2 days of immersion in NaOH at 80 ^{o}C was immersed in isopropanol to stop hydration and then dried at 35 °C until constant weight. To obtain an overview of ASR damage and location of ASR gels, environmental scanning electron microscope (ESEM) and an ultra high resolution scanning electron microscope (Nova NanoSEM 230, FEI) were applied. The working distance was about 5.5 mm, and an acceleration voltage of 12 kV was used. With NanoSEM test, the dried samples were epoxy-impregnated, then cut and polished. Backscattered electron (BSE) imaging in combination with EDX mapping was carried out on polished sections of paste samples to investigate the distribution of sodium, silicon, and RHA particles. The morphology and chemical composition of C-S-H phases and alkali silica gel were characterized by BSE imaging in combination with EDX mapping on polished sections of paste/ mortar samples.

Additionally, in order to evaluate the alkali silica reactivity of RHA, RHA was mixed with $Ca(OH)_2$ powder and NaOH 1 M, then stored at 20 and 80 ^{o}C. The products generated by the reaction were characterized by SEM images in combination with EDX as well.

Mixing and casting

All SCHPC mixtures were prepared in a Pemat ZK30 mixer with total mixing time of 13 minutes. The mixing procedure was shown in Fig. 3.12.

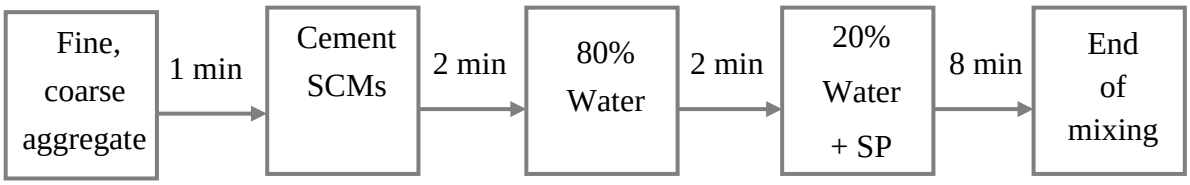

Fig. 3.12 Mixing procedure for SCHPC

All mortar mixtures were prepared in a Hobart mixer (5 litters) at 140 rpm with total mixing time of 9 minutes (for 0.26-w/b mixtures) and 6 minutes (for 0.30 and 0.34-w/b mixtures). The mixing procedure was shown in Fig. 3.13.

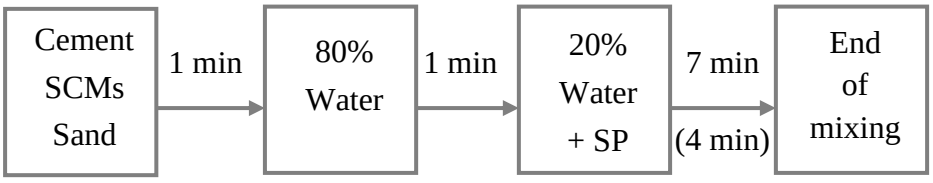

Fig. 3.13 Mixing procedure for mortar

For ASR tests, Teflon was used to prepare specimen moulds to prevent the inhibition of the penetration of water and NaOH into specimens. For all tests, samples were cast without vibration and compaction, and were cured in moulds at 20 ^{o}C and 95 % relative humidity for one day.

4. Characteristics of RHA and other SCMs

4.1. Production of reactive Rice Husk Ash

In this thesis study, rice husk was burnt in a simple incinerator prototype in Vietnam which was designed following the principle of the atmospheric bubbling fluidized bed [188, 189]. The capacity of this incinerator is about $1m^3$ of rice husk, and very suitable for a laboratory scale. After about 12 hour-combustion duration, about 20-25 kg of ash was obtained. During the burning process, the husks burn themselves once without control. The dimensions and structure of the incinerator prototype can be seen in Fig. 4.1. The burning process was started with fire at the bottom using a small amount of waste paper. Then after about 4-6 hours the highest temperature of 780 ^oC was obtained. The carbon unburnt content of the ashes was recorded to vary between 2 and 5 wt.%.

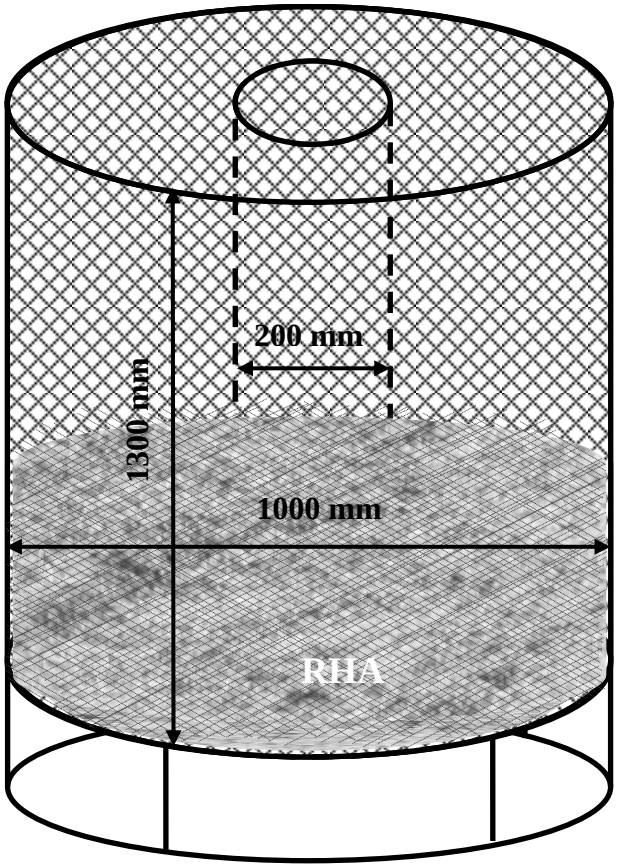

Fig. 4.1 The incinerator prototype used to burn rice husk (dimensions in mm)

4.2. Fineness, pore structure and specific surface area

To analyze characteristics of RHA, the ash obtained after combustion was ground in a ball mill with diameter of 620 mm, length of 300 mm and rotation speed of 29.6 rpm for different periods of time, i.e. 15, 30 … 540 min. In order to grind 5 kg RHA, 70 kg steel balls, i.e. 6 kg of 38.6 mm, 23.1 kg of 29.6 mm, 15.4 kg of 24.6 mm and 25.5 kg of 20.4 mm, were added into the mill in each batch. The effect of the grinding time on fineness, pore structure and SSA is summarized in Table 4.1. Generally, increasing grinding time decreased MPS of RHA, pore volume and average pore size in RHA particles. Meanwhile BET-SSA of RHA slightly

increased with grinding time regardless of lower pore volume (Fig. 4.2). Previous investigations also show an increase in the BET-SSA of RHA sample during an intermediate grinding period [6, 13, 144]. It is obvious that MPS of RHA declines over grinding time, dramatically in first period of 90 min. The MPS of unground RHA is 86.2 µm, after 15, 30, 45, and 90 min MPSs are 22.6, 15.6, 12.0 and 7.7 µm, respectively. Over the course of grinding time from 90 to 540 min, a slight decrease in MPS of RHA was obtained.

Table 4.1 Effect of grinding time on MPS, pore structure and BET-SSA of RHA

Grinding time (min)	0	15	30	45	90	240	540
MPS (µm)	86.2	22.6	15.6	12.0	7.7	6.5	5.7
n- The RRSB slope	0.590	0.707	0.663	0.674	0.707	0.631	0.653
x'- The location parameter of RRSB (µm)	116.3	32.3	22.9	17.4	10.6	10.2	8.4
Mean pore size (nm)	125.48	78.72	67.00	53.52	58.77	46.81	31.85
Pore volume (ml/g)	0.3970	0.1169	0.1224	0.1030	0.1059	0.0981	0.0799
BET-SSA (m^2/g)	20.09	22.02	22.36	22.94	23.05	25.11	25.21

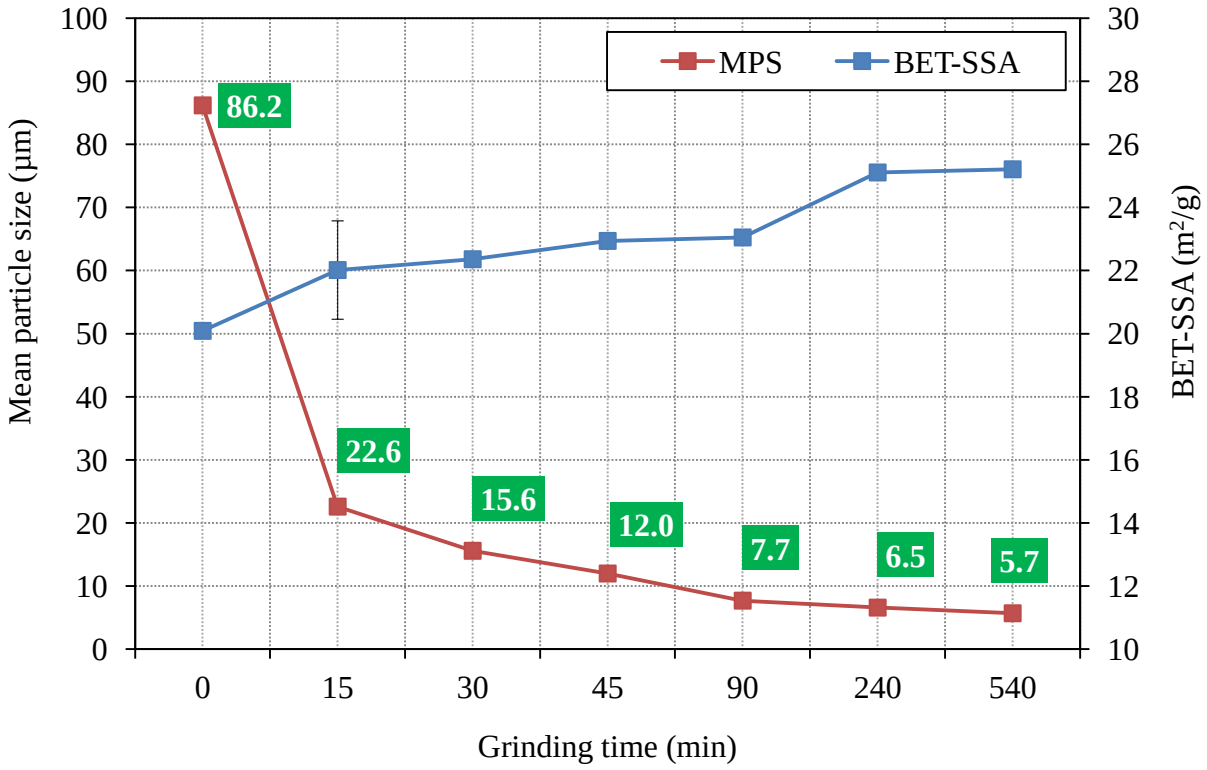

Fig. 4.2 Effect of the grinding time on MPS and BET-SSA of RHA

The particle size distribution of RHA at different grinding periods is illustrated by SEM imaging in Fig. 4.3 and laser diffraction analysis in Fig. 4.4. Together with the decrease in MPS, the morphology of RHA particles seem to be more spherical, as seen in Fig. 4.3.

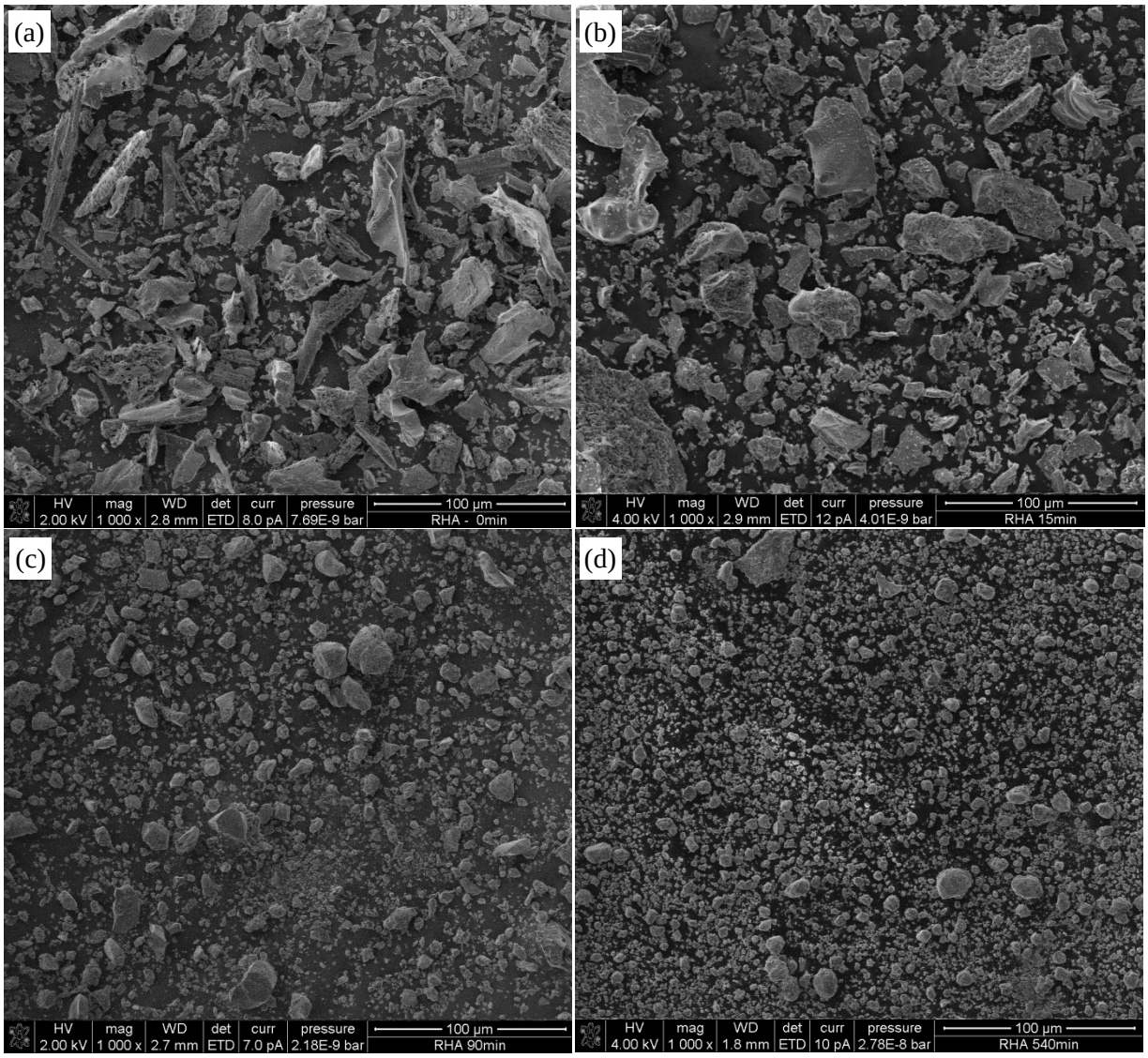

Fig. 4.3 Particle size distribution of RHA at different grinding periods by SEM imaging: unground (a), 15 min (b), 90 min (c), and 540 min (d)

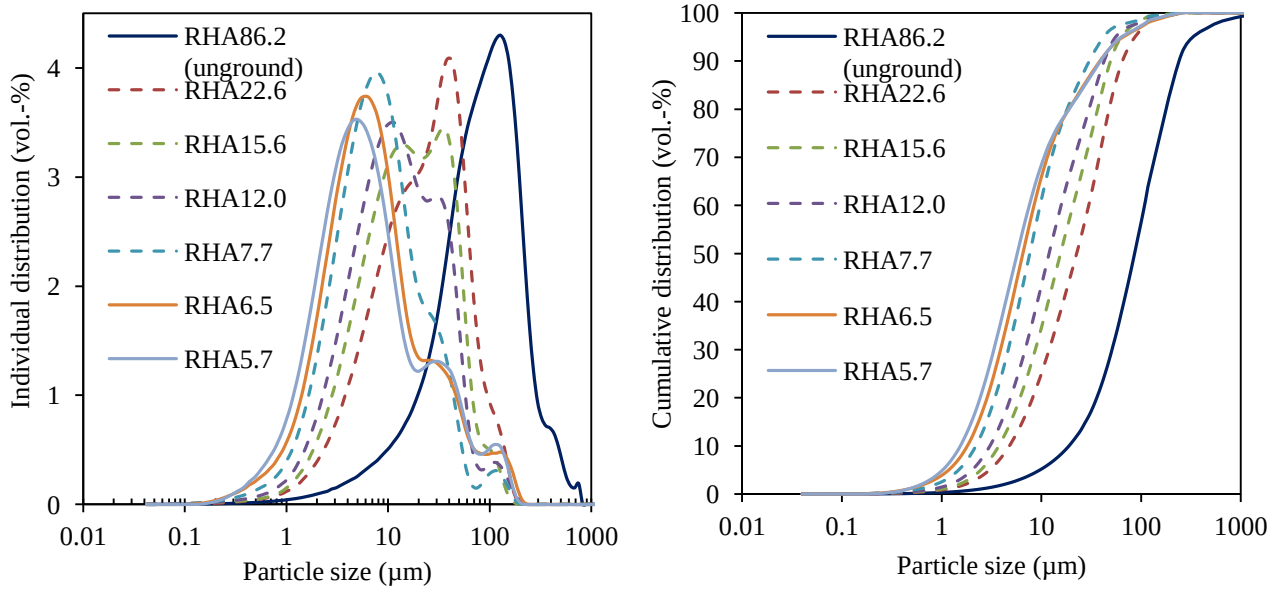

Fig. 4.4 Particle size distribution of RHA at different grinding periods by laser diffraction analysis

The pore size distribution of RHA particles at different grinding periods is shown in Fig. 4.5 and Fig. 4.6 by BJH analysis and SEM imaging respectively. It can be obtained that the RHA is a porous material including mostly macropores (>50 nm) and mesopores (2-50 nm). It appears that only most macro pores collapsed during grinding time (Fig. 4.5). Increasing grinding time increased the macro pores collapsed, and hence resulted in the lower total pore volume in RHA particles (Fig. 4.7) and the smaller average pore size (Table 4.1).

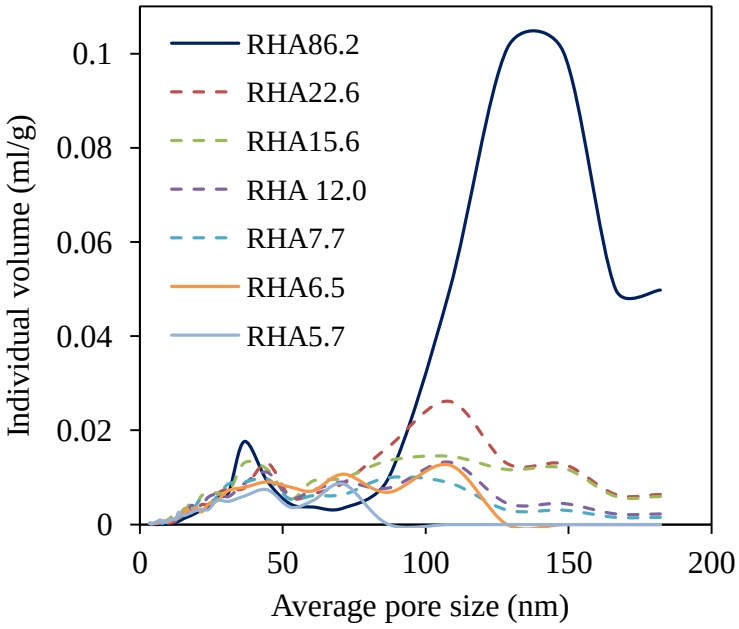

Fig. 4.5 Pore size distribution in RHA particles at different grinding periods by BJH analysis

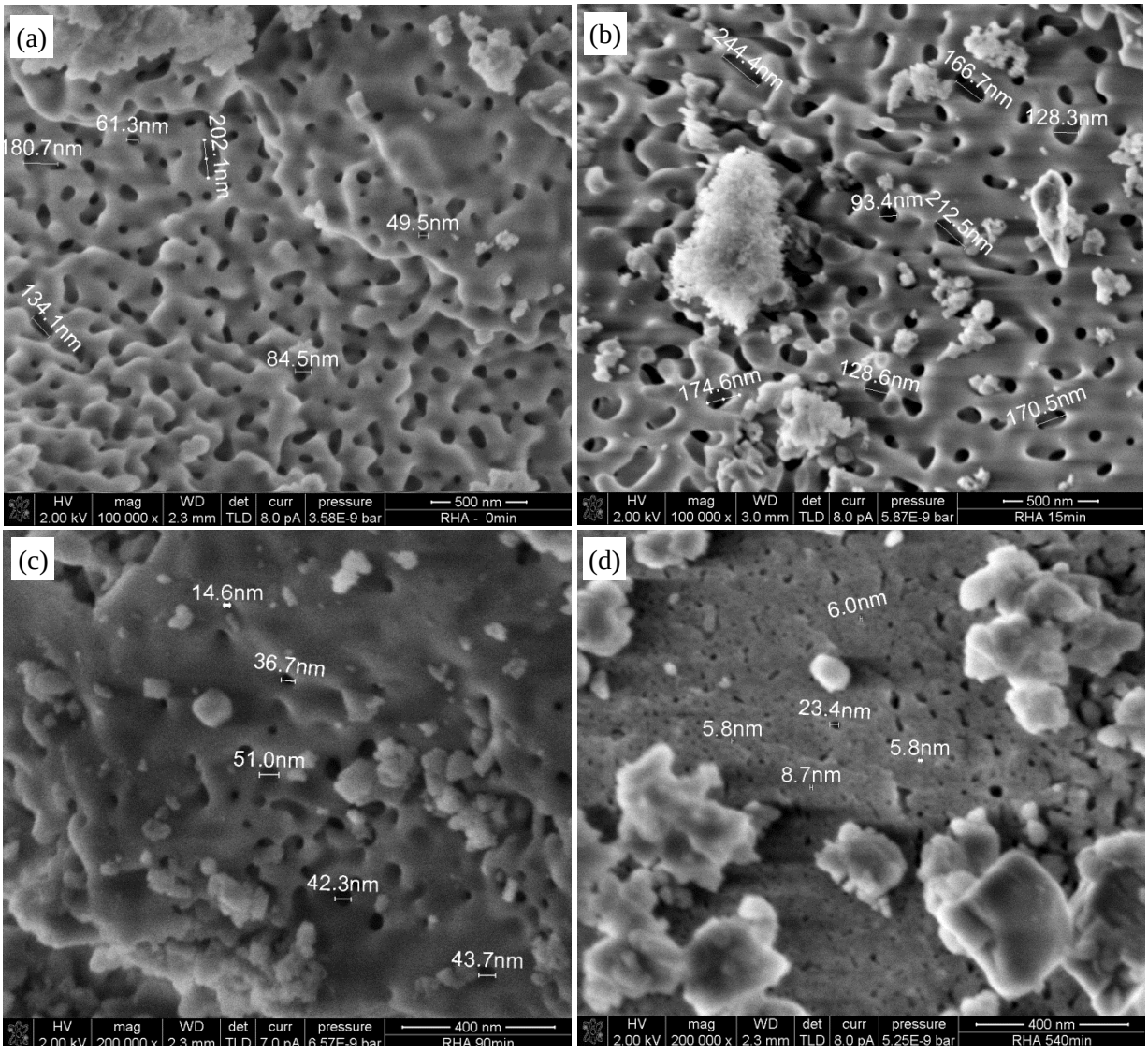

Fig. 4.6 Pore size distribution in RHA particles at different grinding periods by SEM imaging: unground (a), 15 min (b), 90 min (c), and 540 min (d)

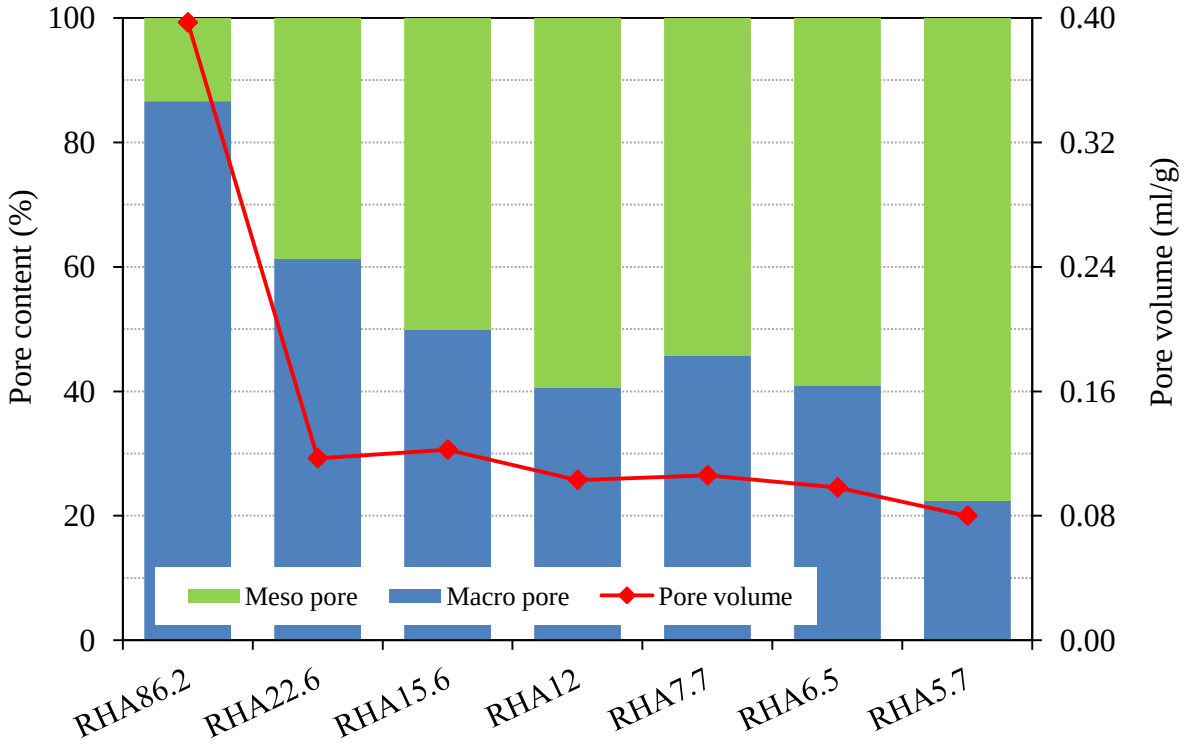

Fig. 4.7 Macro-meso pore content and pore volume of RHA with different particle sizes

In Fig. 4.8, the surfaces of the RHA particles after 15 min and 30 min of grinding are shown. It is found that there exist two types of surface of RHA particles, porous surface and dense surface (lower side of Fig. 4.8a and upper left corner of Fig. 4.8b). The dense surface was formed and covered the pore structure, while new porous surfaces might be formed after grinding.

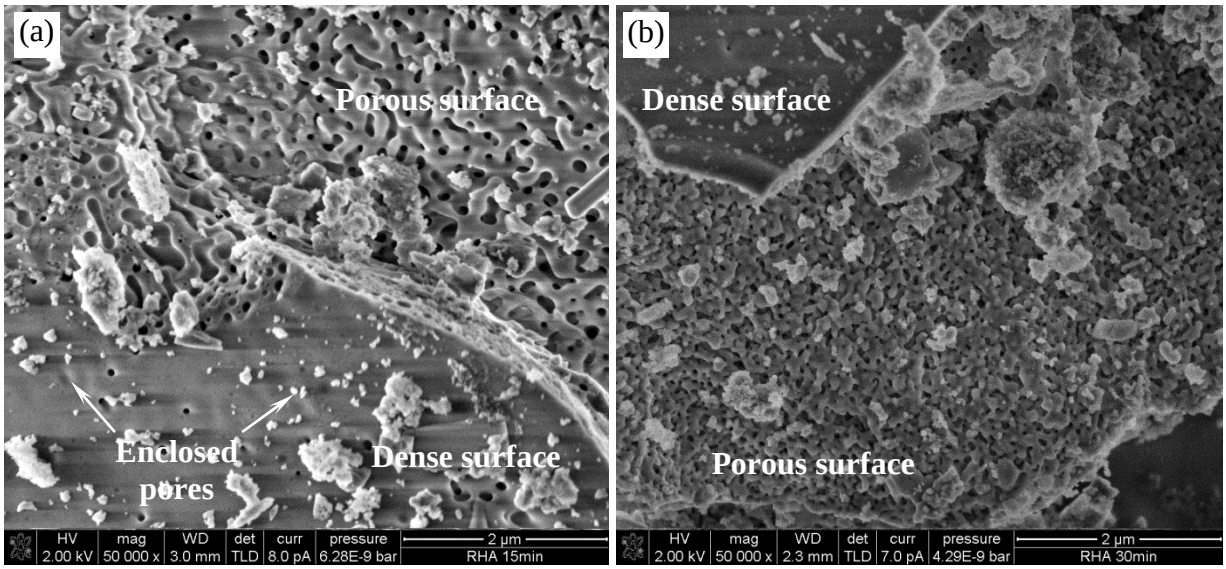

Fig. 4.8 Existence of dense and porous surfaces of ground RHA particles

4.3. Water demand and water adsorption

Water demand of cement and SCMs determined by the Puntke method is displayed in Fig. 4.9. The water demand of RHA was considerably larger than that of cement and other SCMs, depending on MPS of RHA. The higher water demand was obtained with coarser MPS of RHA. This result is closely associated with pore volume of RHA mentioned above. With large BET-SSA, water demand of SF is similar to that of RHA 5.7, and much higher than that of cement

and FA. Whereas water adsorption of RHA increased with the finer MPS of RHA or larger SSA of RHA, and was much higher than those of SF and FA respectively (Fig. 4.10).

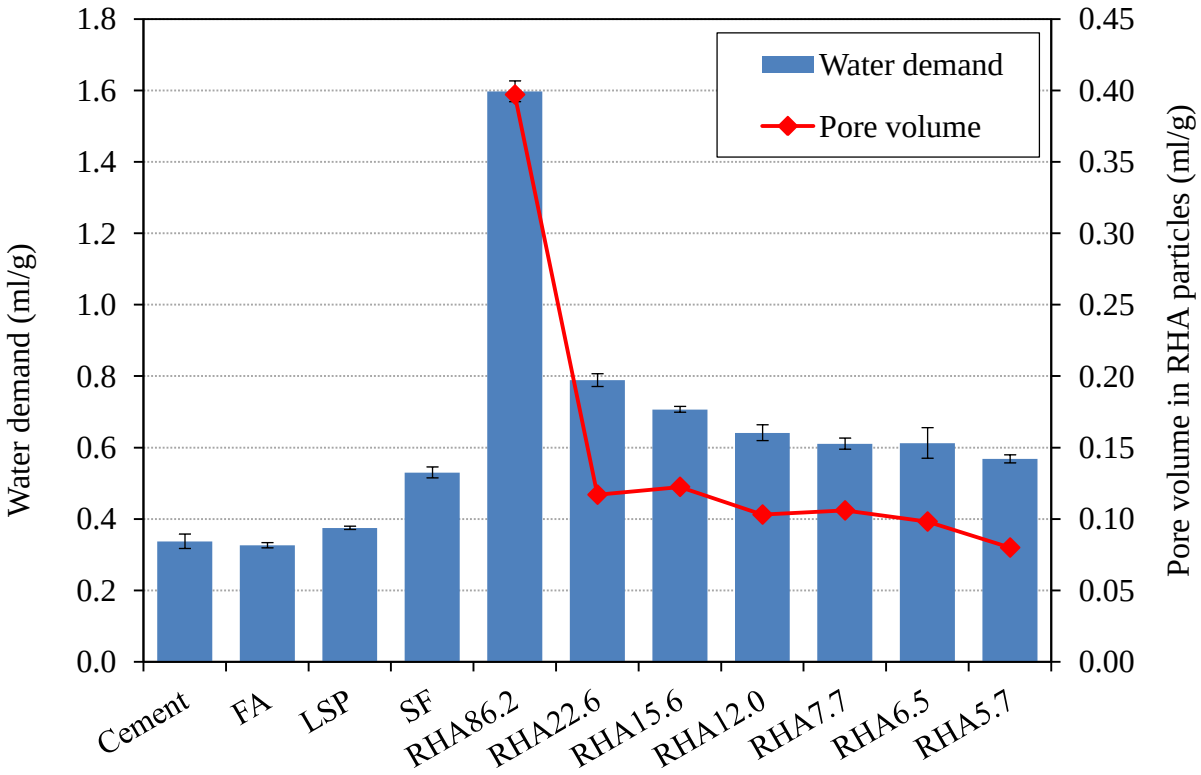

Fig. 4.9 Water demand of cement, RHA and other SCMs determined by the Puntke method

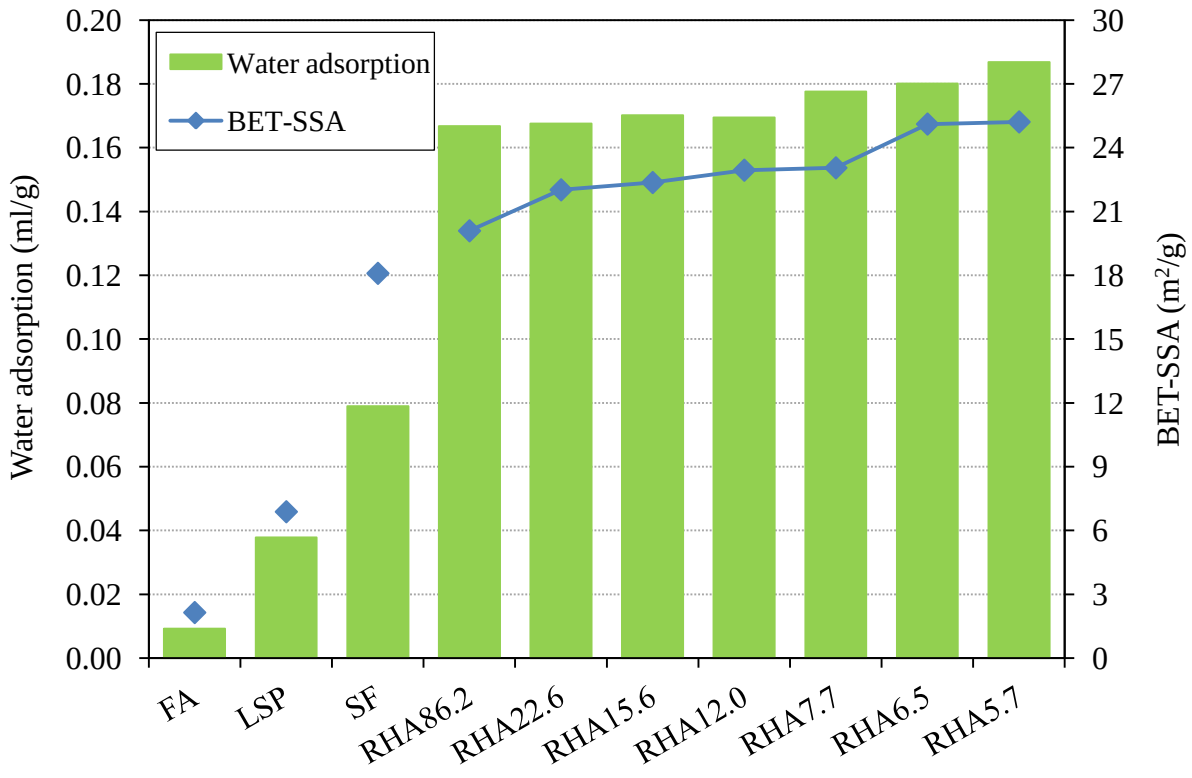

Fig. 4.10 Water adsorption of RHA and and other SCMs

4.4. Pozzolanic reactivity

Fig. 4.11 shows the electrical conductivity curves of the suspensions containing RHA5.7, RHA22.6, SF, and FA. The variation in electrical conductivity depended on MPS of RHA. This indicates that the hydration extent and the process of pozzolanic reaction of RHA were influenced by its MPS. In the first period of 263 min, the electrical conductivity values of the CH-RHA5.7 suspension were lower than that of the CH-RHA22.6 suspension. In the last period (from 263 to 900 min), the effect was considerably changed. That means pozzolanic reactivity of RHA in early period was greater with the fine RHA5.7, however total reactivity of RHA was higher with the coarse RHA22.6. It is also observed that during the initial period of 120 min, the electrical conductivity values of the CH-RHA5.7 suspension were lower than those of the CH-SF suspension. Thereafter, the situation was reversed (Fig. 4.11). About 10 min after decreasing, the electrical conductivity values of CH-FA suspension kept constant. These values of CH-FA suspension were significantly higher than those of CH-RHA and CH-SF suspensions. This indicates that the pozzolanic reactivity of FA is significantly lower than those of RHA and SF.

The electrical conductivity curves of water-pozzolan suspension are illustrated in Fig. 4.12. The electrical conductivity values of water-

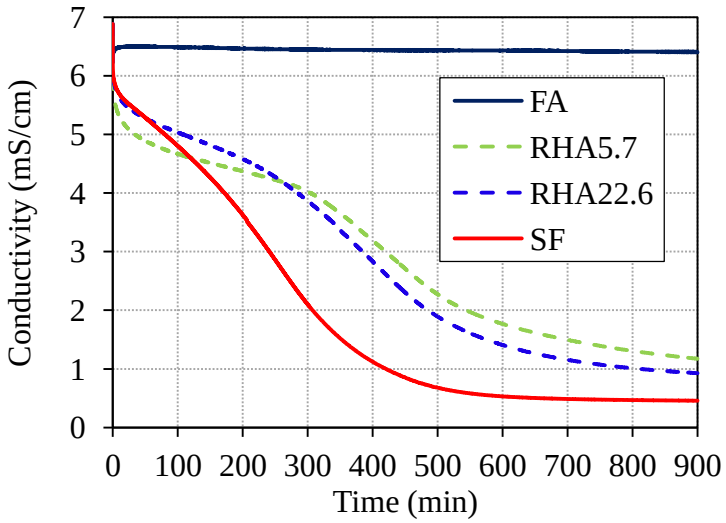

Fig. 4.11 Electrical conductivity over time of CH-pozzolan suspensions at 40 °C

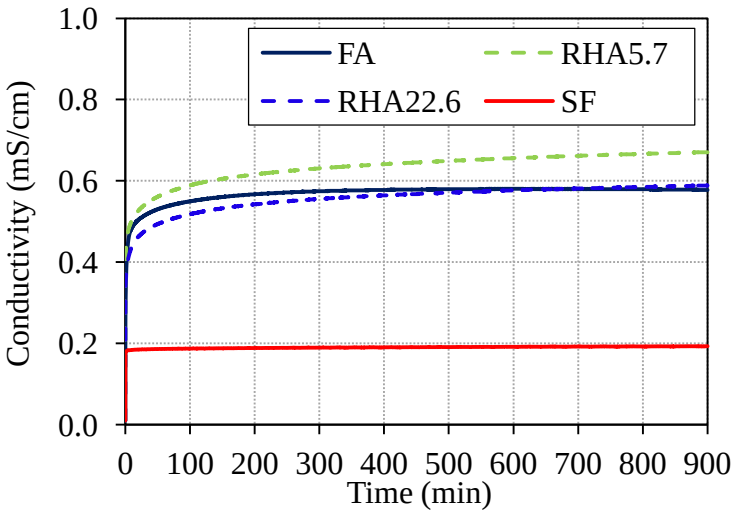

Fig. 4.12 Electrical conductivity over time of water-pozzolan suspensions at 40 °C

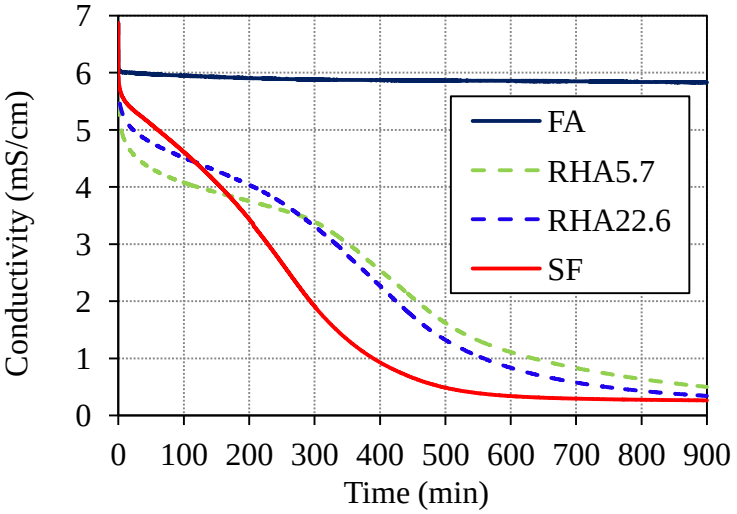

Fig. 4.13 Corrected electrical conductivity over time of CH-pozzolan suspensions at 40 °C

pozzolan suspension increased over time and were much less than those of CH-pozzolan suspension. The electrical conductivity considerably increased in the first period of 100 min for water-FA suspension, 130 min for water-RHA suspension and 1 min for water-SF suspension. The increase in the electrical conductivity indicates the dissolubility of components of pozzolan. Clearly, dissolved components of RHA and FA were much higher than that of SF and depended on MPS of RHA. The difference in BET-SSA and alkali content might be the main reason for that phenomenon. In order to evaluate the reduction in the electrical conductivity due to pozzolanic reaction, i.e. the reduction in Ca ions, more correctly, the electrical conductivity values in water-pozzolan suspension were subtracted from the ones in CH-pozzolan suspension. The obtained values are presented in Fig. 4.13. It can be seen that the shape and the slopes of all corrected curves were similar to those of the electrical conductivity curves in CH-pozzolan suspension (Fig. 4.11). That indicates the dissolved components of pozzolan strongly affected electrical conductivity in CH-pozzolan suspension only in the initial period of time after pozzolan addition.

The hydrated RHA22.6, RHA5.7, and SF particles and the pozzolanic reaction products formed on their surfaces after 4h and 24h in CH-RHA/SF suspensions are shown in Fig. 4.14, Fig. 4.15, Fig. 4.16, Fig. 4.17 and Fig. 4.18. The pozzolanic reaction products, described as foil-like C-S-H phases, were formed after 4h. The similar results are also observed in other study [16]. The C-S-H phases were only formed on the porous surface of RHA particles (Fig. 4.14 and Fig. 4.15). From 4h to 24h, it is clearly observed the qualitative increase in the amount of C-S-H phases (Fig. 4.15, Fig. 4.16, Fig. 4.17 and Fig. 4.18). This is closely related to the reduction in electrical conductivity, i.e. the reduction in Ca ion in CH-RHA/SF suspension, as shown in Fig. 4.11. In the case of FA, although the electrical conductivity decreased (Fig. 4.11), no C-S-H phases were observed on surface of FA particles after 4 h and 24 h. The reduction in the electrical conductivity of CH-FA suspension might be mainly due to the crystallization of portlandite and the Ca ion-adsorption of FA particles (Fig. 4.19).

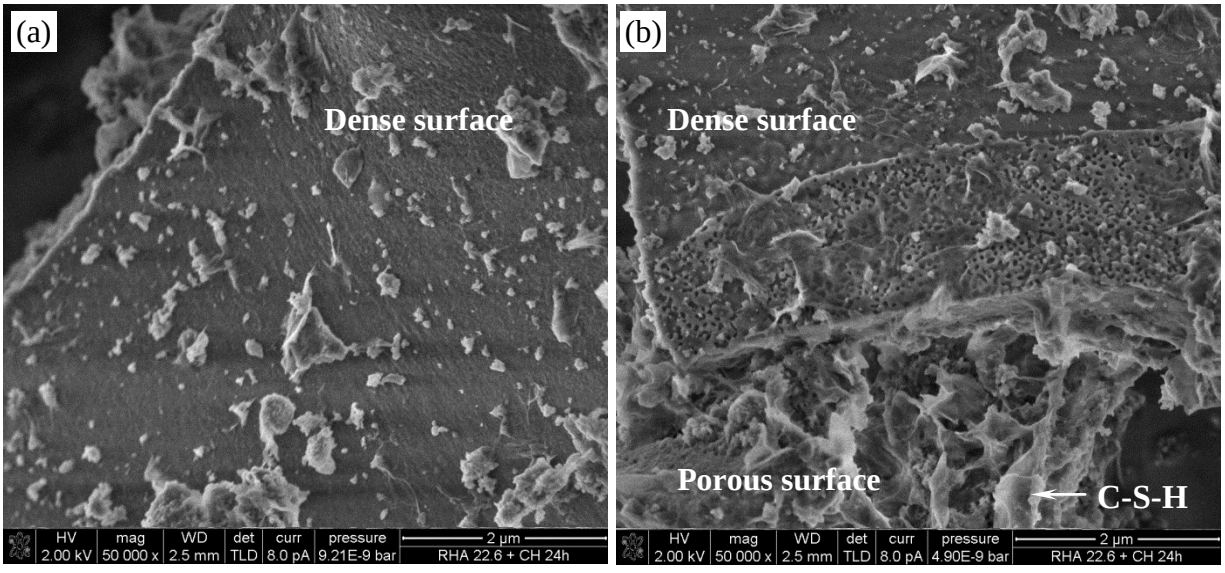

Fig. 4.14 Hydrated dense surface without foil-like-CSH phase (a), and hydrated porous surface with foil-like-CSH phase (b)

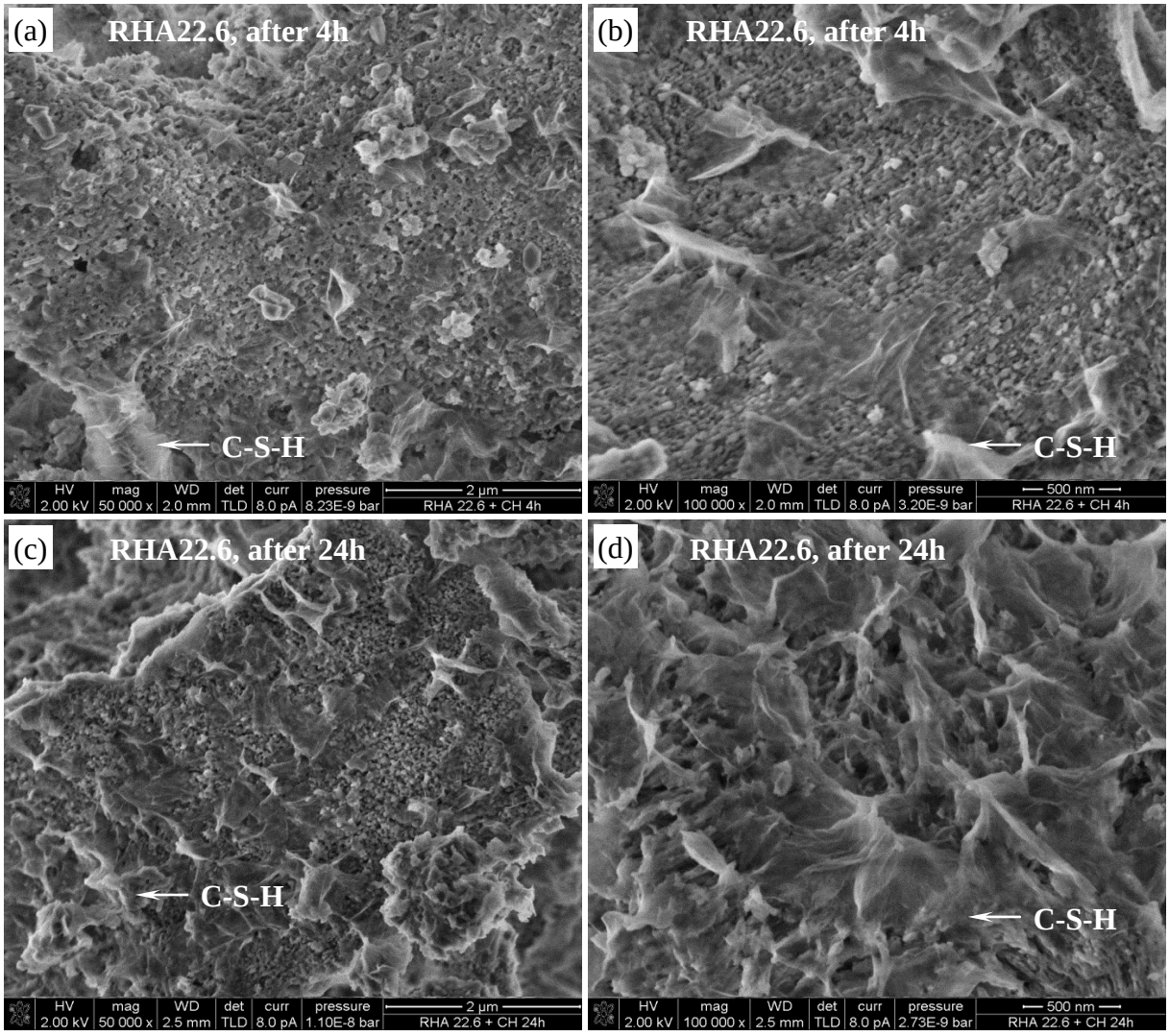

Fig. 4.15 SEM images of the hydrated RHA22.6 in CH solution (l/s = 40 at 40°C) after: 4h (a, b) and 24h (c, d) showing foil-like C-S-H phases on the porous surface of RHA particles.

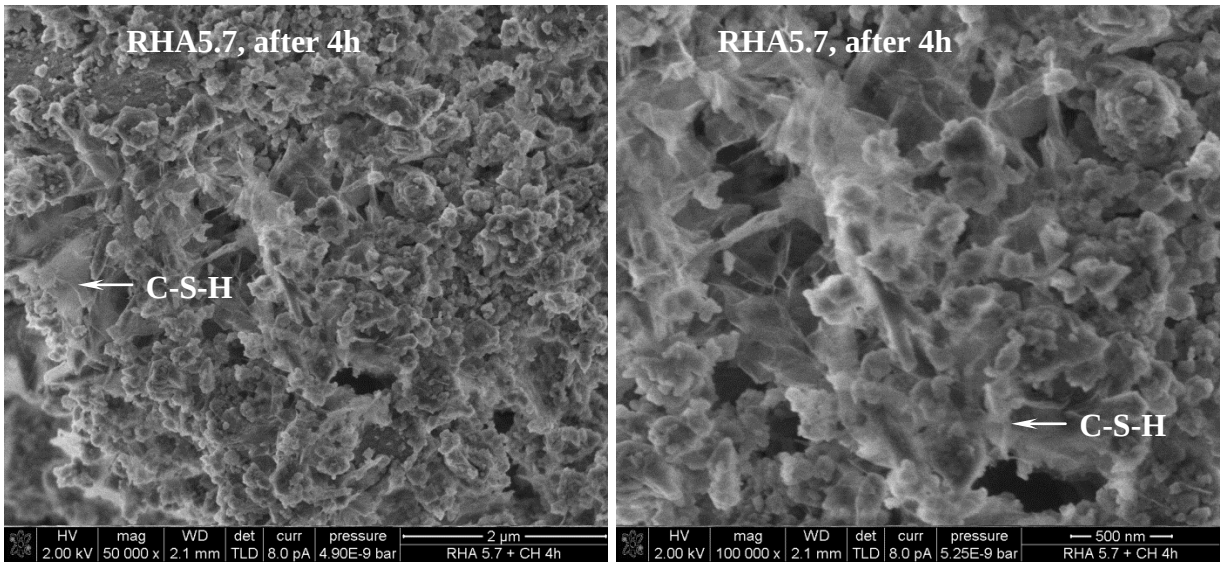

Fig. 4.16 SEM images of the hydrated RHA5.7 in CH solution (l/s = 40 at 40°C) after 4h showing foil-like C-S-H phases formed and connected the small RHA particles.

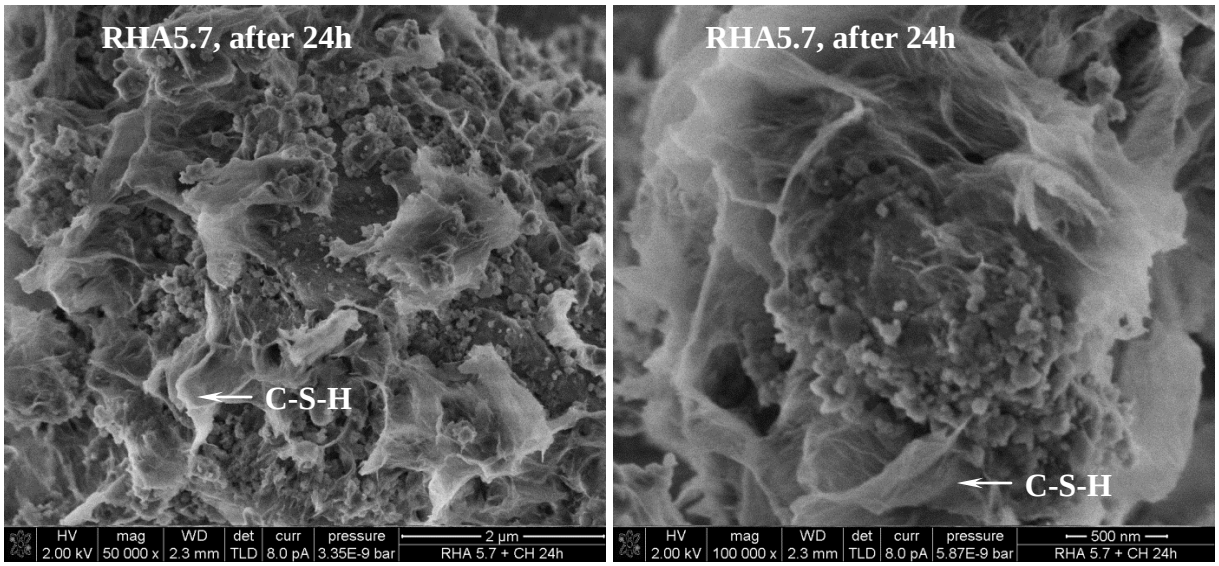

Fig. 4.17 SEM images of the hydrated RHA5.7 in CH solution (l/s = 40 at 40°C) after 24h showing foil-like C-S-H phases formed and connected the small RHA particles.

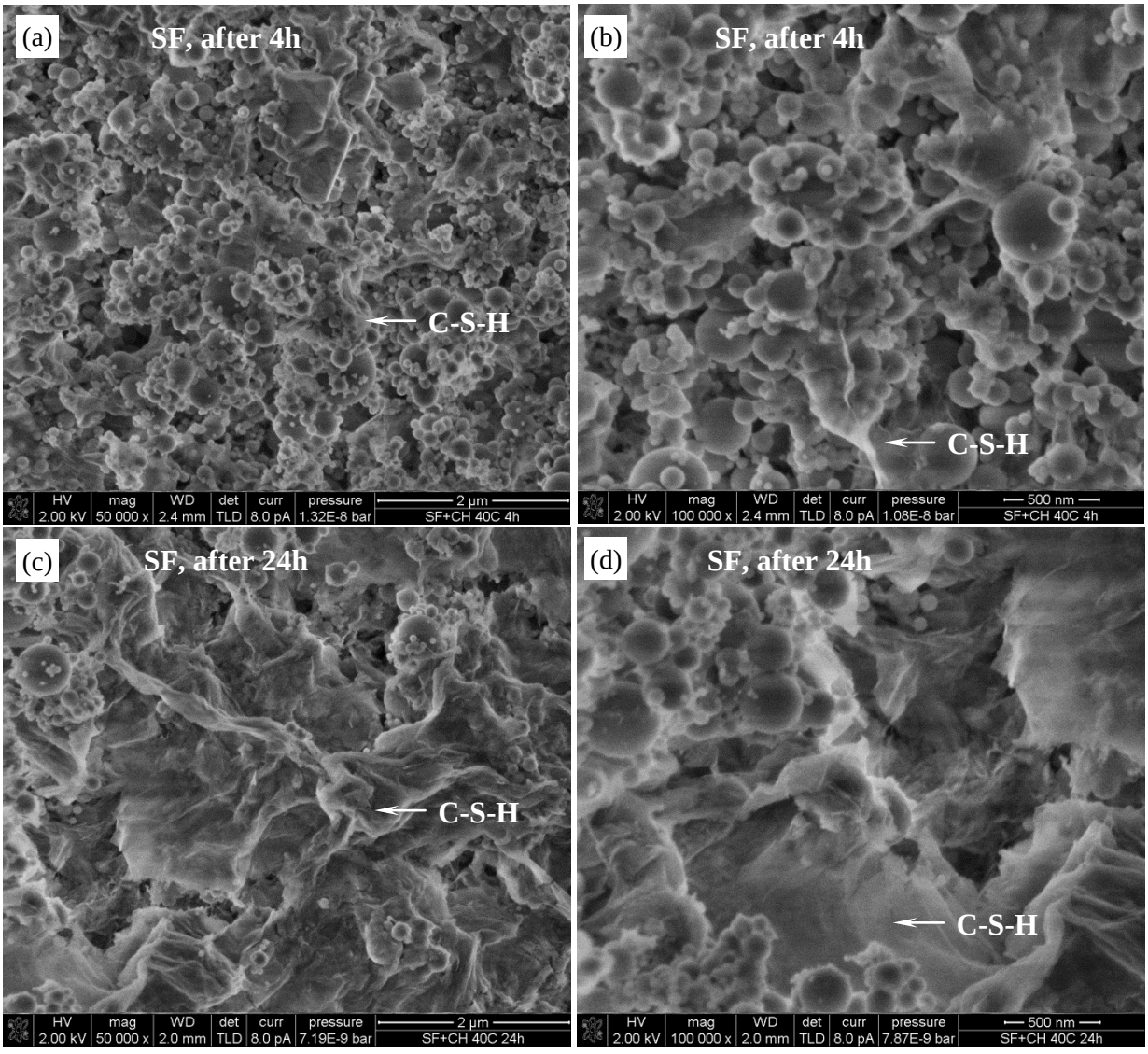

Fig. 4.18 SEM images of the hydrated SF in CH solution (l/s = 40 at 40°C) after: 4h (a, b) and 24h (c, d) showing foil-like C-S-H phases formed and connected the spherical SF particles.

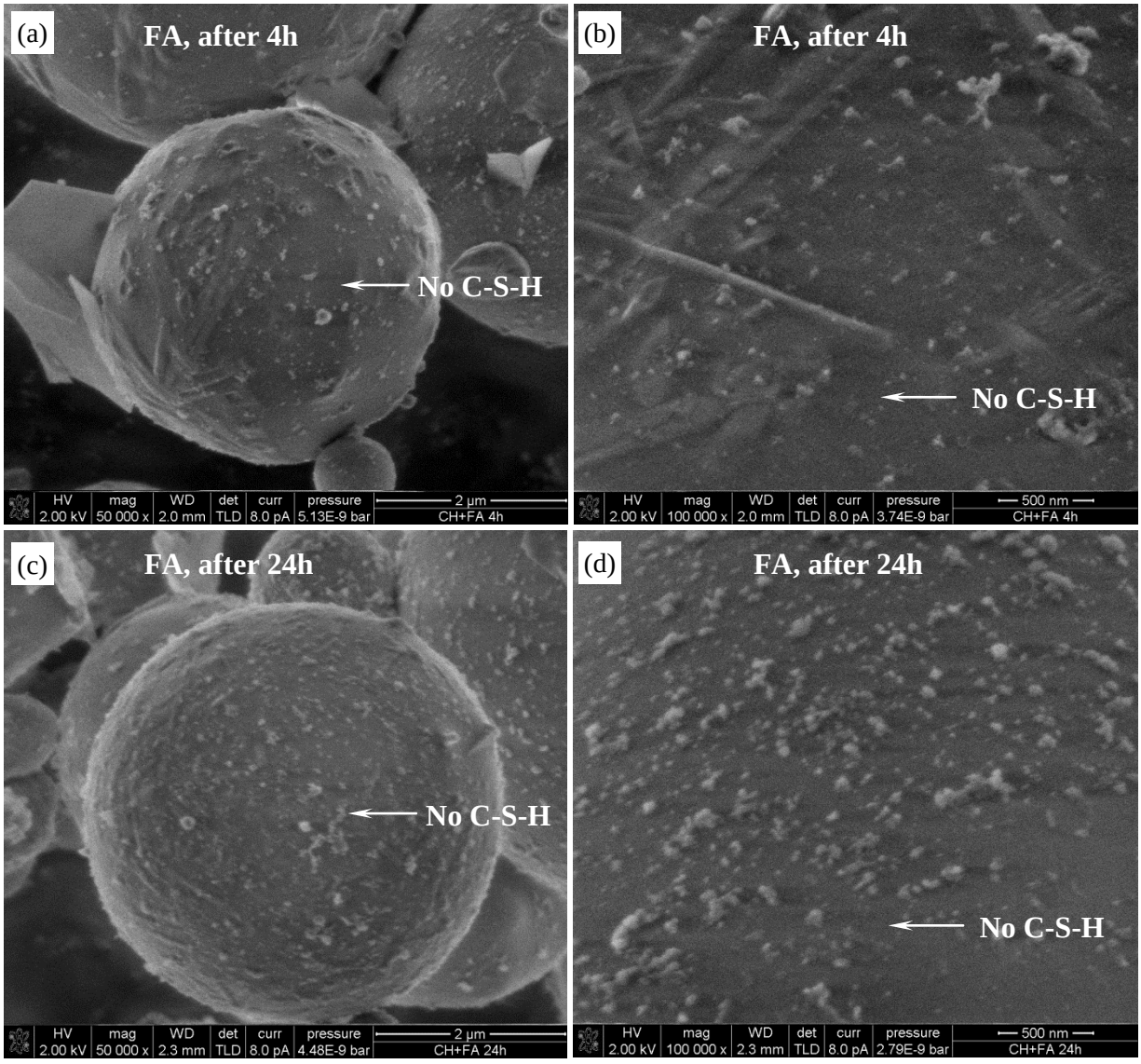

Fig. 4.19 SEM images of the hydrated FA in CH solution (l/s = 40 at 40°C) after: 4h (a, b) and 24h (c, d) showing no C-S-H phases formed on surface of FA particles.

The reduction in the electrical conductivity of the CH-pozzolan suspension 2 and 90 min after pozzolan addition is shown in Fig. 4.20. In this test, FA, SF and RHA with different MPS were used. Obviously, from 0 to 2 min, the higher the SSA of pozzolan, the greater the decrease in electrical conductivity of the CH-pozzolan suspension, possibly due to the higher adsorption of Ca ions, associated with the results of water adsorption (Fig. 4.10). The highest value of electrical conductivity in CH-RHA suspension after 2 min is 1.23 mS/cm, higher than those in CH-SF and CH-FA suspensions. In accordance with the criteria proposed by Luxan [143], the reactivity of RHA is higher than those of SF. However, the reduction in the electrical conductivity in CH-SF suspension passed that in CH-RHA after 900 min. This indicates that the higher content of Ca ions was consumed by SF after long time of hydration.

For RHA, the opposite effect of MPS on the reduction in electrical conductivity after 900 min was observed. Namely, the coarser RHA had the stronger effect on the reduction in the electrical conductivity. The coarser RHA has larger pore volume inside its particles, and hence the higher CH adsorption into the pores over time might be the main reason for the greater reduction in the electrical conductivity.

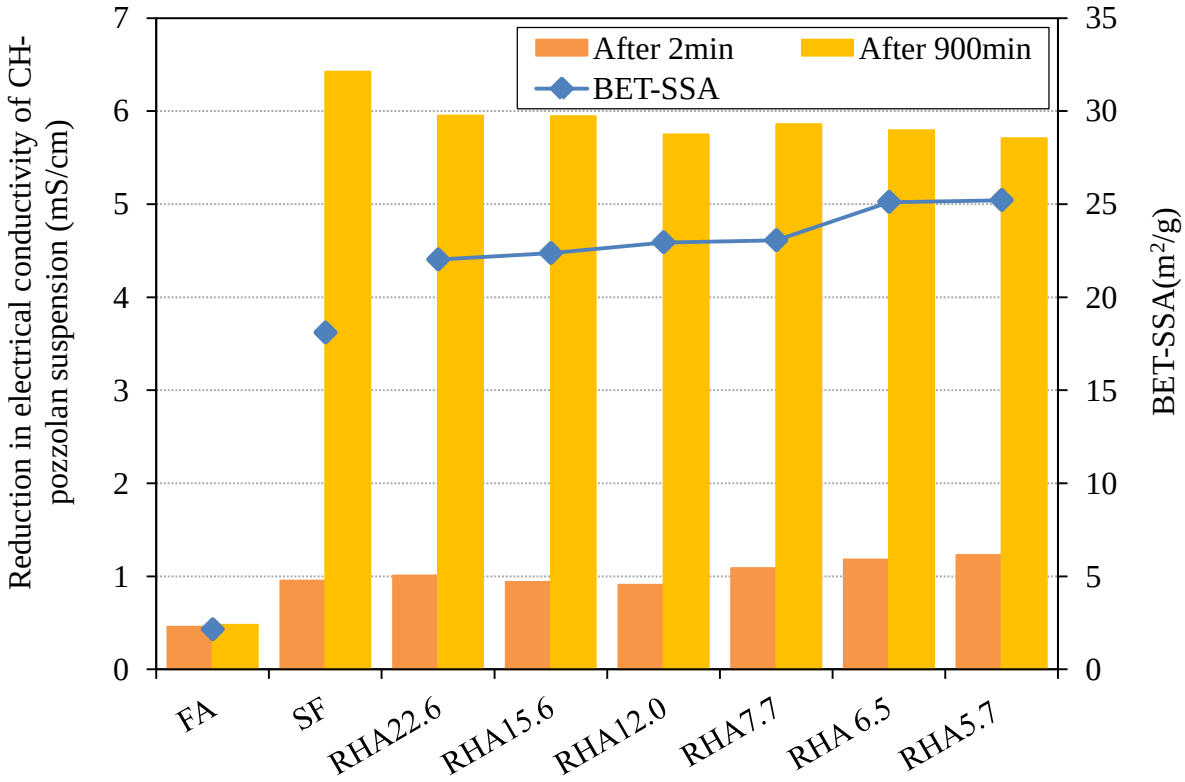

Fig. 4.20 Reduction in electrical conductivity of CH-pozzolan suspension after 2 and 900 min

4.5. Discussion

The investigated RHA in this study is a porous material including macro pores (>50 nm) and meso pores (2-50 nm) confirmed by SEM images and results of BJH method test (Fig. 4.6). Following the pore classification in the characterization of porous material [190, 191], this RHA is a kind of macro-mesoporous material. Moreover, it possesses a very high amorphous silica content (Fig. 3.1 and Table 3.1). Therefore, this RHA can be defined as a macro-mesoporous amorphous siliceous material.

As normal, grinding induces the smaller MPS of RHA (Fig. 4.2). In general, decreasing MPS reduced the total pore volume, and average pore size in RHA particles, but increased the BET-SSA of RHA (Fig. 4.2, Fig. 4.7 and Table 4.1). It is very important to note that the BET-SSA and total pore volume measured by, respectively, the BET and BJH methods are mainly affected by open pore structure of material [170]. The reduction in the total pore volume and average pore size is due to the collapse of most macropores during grinding (Fig. 4.6). Therefore, most pores in the investigated RHA might be open pores, and almost no new pores are formed during grinding. It is proposed that the BET-SSA of RHA is governed by the particle size reduction, the new open pore formation, and open pore collapse [16]. Thus, it can be concluded that an enlargement of the external surface on the RHA particles due to the reduction in MPS of RHA mainly gives the increase in BET-SSA of the RHA over grinding

time. On the other hand, this result reflected the important role of the pore size distribution in influencing other characteristics of RHA. The BET-SSA of RHA is contributed by internal surface areas (surface in the pores inside RHA particles) and external surface areas (surface on RHA particles). More correctly, external BET-SSA of RHA in this study, therefore, increases during grinding. This means that the finer RHA has more external SSA than the coarser one. The variation in external SSA of RHA will dramatically influence the water adsorption and pozzolanic reaction process of RHA, as discussed following.

There exist the dense and porous surfaces (Fig. 4.8). The dense surface is smooth and inert with pozzolanic reaction (Fig. 4.14). Combining the result on mineral composition of RHA by QXRD (Section 3.1 and Fig. 3.1) and the result obtained from pozzolanic reaction (Fig. 4.14). It can be concluded that the dense surface might be formed by quartz converted from amorphous silica during the combustion of rice husk, as mentioned elsewhere [6]. James and Rao concluded that increasing temperature decreases the BET-SSA of RHA, possibly due to crystallite growth [6, 192]. As can be seen in Fig. 4.8, the dense surface formed, i.e. quartz crystallized surface, encloses pores on the surface of RHA particle. Therefore, the decrease in BET-SSA due to the high combustion temperature can be explained by the formation of the crystallized silica cover, i.e. quartz in this study, enclosing the pores on the surface of RHA particles.

In general, the water demand and water adsorption of RHA are higher than those of SF and FA. The water demand depends on the MPS and pore volume in RHA particles, i.e. increases with the coarser RHA and the larger pore volume (Fig. 4.9), whereas water adsorption depends on the BET-SSA of RHA, i.e. increases with the larger BET-SSA (Fig. 4.10). The effect of BET-SSA on water adsorption of RHA was also obtained in the investigation [16]. This means that the result of the water adsorption only indicates the water layers adsorbed on the surface in open pores (internal surface) and on the surface of RHA particles (external surface). On the other hand, the water demand determined by the Puntke method reflects not only the water filled into the pores in RHA particles but also the packing density of the granular mixture. Therefore, water demand will more practically reflect the effect of RHA on the water demand and properties of RHA blended cementitious material.

The pozzolanic reactivity of RHA and other SCMs was evaluated by the variation in electrical conductivity of the saturated CH solution after pozzolan addition. It is borne in mind that the electrical conductivity is a function of the concentration of cations, mainly Ca ions, and Na ions, K ions, etc., dissolved from the pozzolans. In order to eliminate the effect of the cations beyond Ca ions on the variation in the electrical conductivity value measured in CH-pozzolan suspension, electrical conductivity of water-pozzlan suspension was determined. Finally, reactivity of RHA and other SCMs was evaluated by the electrical conductivity value of CH-pozzolan suspension subtracting the value of water-pozzolan suspension. According to the classification of the original method [143], the change of the value of the electrical conductivity 2 min after pozzolan addition is used to evaluate the pozzolanic reactivity. Indeed, the results of the present study figured out that the reduction in the electrical conductivity continued up to 900 minutes (Fig. 4.11, Fig. 4.13, and Fig. 4.20). Thus, the reduction in the electrical conductivity up to 900 minutes should be used to evaluate and compare the reactivity of RHA and SF in this study. After 900 min, the reduction in electrical conductivity of CH-FA

suspension is very low, and significantly lower than those of CH-RHA and CH-SF suspensions (Fig. 4.20). Furthermore, by means of SEM imaging, no C-S-H phases were observed on the surface of FA particles. Therefore, pozzolanic reactivity of FA could not evaluated by this method.

The electrical conductivity values of CH-pozzolan suspension after 2 min are strongly influenced by the BET-SSA and adsorptive capacity of the pozzolan. This result is consistent with the result of the literature analysis in Section 2.3.3 (Fig. 2.15). However, the process of pozzolanic reaction, thereafter, is changed and appears to depend on type and MPS of pozzolan (Fig. 4.11 and Fig. 4.20). It is assumed that the pozzolanic reaction, i.e. the dissolution-precipitation process, is governed by pH value of CH-pozzolan suspension, the surface area of pozzolan [6, 13, 16] and the difference from supersaturated to equilibrium concentration indicating the driving force for precipitation [193, 194]. The alkali content, i.e. K_2O and Na_2O, of RHA is significantly higher than that of SF (Table 3.1), also indicated by the higher electrical conductivity of water-RHA suspension (Fig. 4.12). Thus, pH value of CH-RHA suspension is higher than that of CH-SF suspension. The high pH value increases the dissolution of Si, and then promotes the dissolution-precipitation process [195]. Furthermore, the BET-SSA of RHA is larger than that of SF (Table 3.2 and Fig. 4.10) and hence increases the dissolution of Si into the solution, because the binding or release of protons at Si-OH surface groups is strongly dependent on the exposure surface [196]. However, the driving force for precipitation in CH-SF suspension is stronger than that in CH-RHA suspension, thus the amount of reaction product generated during the pozzolanic reaction of SF might dominate that of RHA in CH solution [16, 193, 194]. Hence, the larger SSA and the higher alkali content make dissolution and precipitation processes in the CH-RHA suspension higher than that in the CH-SF suspension in the initial 120 min, in the case of RHA5.7. However, the total pozzolanic reactivity of SF in saturated calcium solution is higher than that of RHA regardless of the particle size, possibly due to the stronger precipitation in CH-SF suspension.

For RHA, with the same silica content and the same alkali content, the different fineness and hence the different SSA of RHA makes the dissolution-precipitation process of RHA in CH solution different, indicated by the changes in electrical conductivity over time. The electrical conductivity reduction of CH-RHA5.7 suspension was greater than that of CH-RHA22.6 suspension in the initial period of 263 min. Afterwards, the electrical conductivity reduction of CH-RHA22.6 suspension was greater than that of CH-RHA5.7 suspension, indicating the total reactivity of RHA22.6 is higher than that of RHA5.7 in CH solution. RHA5.7 has larger SSA, i.e. the larger external SSA, than RHA22.6 (Fig. 4.2). That induces the higher alkali content dissolved in the suspension (Fig. 4.12), the higher extent of pozzolanic reaction of RHA5.7 and thus the greater thickness of hydrated layer, i.e. C-S-H layer, formed on the surface of the particles resulting in the reduction in the diffusion of water, Ca ion and Si ion through this layer. This mechanism is proposed to be similar to the higher hydration rate of smaller size C_3S/cement particles [101, 197, 198]. Since small particles are being used up rapidly, the transition time from the nucleation and growth to the diffusion controls the process. Besides, the coarse RHA22.6 has larger pore volume in its particles, hence the higher Ca ions might be adsorbed into the pores over time, resulting in the pozzolanic reaction in the pores, the so-called ''internal pozzolanic reaction''. That might be one more reason for the higher pozzolanic

reactivity of RHA22.6. This result is in agreement with the CH consumption of RHA5.7, RHA22.6 and SF in binder paste of mortar, as mentioned in Section 7.

4.6. Concluding remarks

Based on the results obtained in this section, some following conclusions can be drawn:

- The RHA in this study is a macro-mesoporous amorphous siliceous material. The pore size distribution is the key physical property of RHA influencing pore volume, BET-SSA, followed by the water demand and the pozzolanic reactivity of RHA.
- BET-SSA of RHA derives from the internal surface area in pores and the external surface area on the surface of RHA particles. During grinding, most macro-pores collapse and the external SSA of RHA increases.
- Ground RHA particles have dense and porous surfaces. The porous surface displays reactive properties, whereas the dense surface is inert regarding pozzolanic reaction. The dense surface might be formed by quartz converted from amorphous silica during the combustion of rice husk.
- The water demand of RHA increases with the larger pore volume of coarser particles, whereas the water adsorption of RHA increases with the larger SSA of finer particles. The water demand and water adsorption of RHA are higher than those of SF and FA, respectively.
- Foil-like pozzolanic reaction products, like C-S-H phases, are observed on the surface of RHA/SF particles after 4 hours in the CH-RHA and CH-SF suspensions. The variation in electrical conductivity of CH-pozzolan suspension is strongly affected by the dissolved alkali components, SSA, MPS of the pozzolans. The reduction in the electrical conductivity continued up to 900 min. Therefore, the reduction in the electrical conductivity of CH-pozzolan subtracting the electrical conductivity value of water-pozzolan suspension up to 900 min should be used to evaluate and compare the reactivity of RHA and SF in this study. Where the reduction in the electrical conductivity reflects the reduction in Ca ion due to pozzolanic reaction.
- The reduction in electrical conductivity of CH-FA suspension after 900 min is very low, and significantly lower than those of CH-RHA and CH-SF suspensions, and no C-S-H phases were observed on the surface of FA particles. Therefore, pozzolanic reactivity of FA could not evaluated by the variation in electrical conductivity.
- The variation in electrical conductivity indicates that the pozzolanic reaction of RHA might occur earlier, however the total reactivity of SF is higher than that of RHA.
- The reduction in electrical conductivity of CH-RHA5.7 suspension is higher than that of CH-RHA22.6 suspension after 263 min. This indicates the pozzolanic reactivity of RHA5.7 is higher in the early period. The total pozzolanic reactivity of RHA22.6, however, is higher than that of RHA5.7 possibly due to the higher adsorption of Ca ion into pores inducing ''internal pozzolanic reaction''.

5. Mix-design for Self-Compacting High Performance Concrete incorporating various SCMs

5.1. General

In this study, a new mix design method for SCHPC containing various SCMs was developed on the basis of the basic requirements for ordinary concrete proportions regulated in DIN EN 206-1 and DIN 1045-2 [78, 199]. The proposed method aims to design mixture proportions of SCHPC with adequate self-compactability, very high compressive strength, and good durability. Also taken into consideration were the type, content, physical properties and reactivity of SCMs as main factors determining the self-compactibility and compressive strength of the concrete. In this section, the proposed mix-design method will be summarized, the detailed content of which can be found elsewhere [200].

5.2. Reactivity of supplementary cementitious materials

All kinds of SCMs, i.e. nearly inert, pozzolanic and latent hydraulic, have been used to produce SCHPC. For example, LSP is nearly inert, SF, RHA, metakaolin and low calcium class F-FA (according to ASTM C618) are pozzolanic, and GGBFS and high calcium class C-FA (according to ASTM C618) are both latent hydraulic and pozzolanic SCMs [1, 5, 24]. Each kind of SCMs has different effects on the properties of both fresh and hardened concrete. In terms of compressive strength, effect of SCMs is indicated by activity index (k). The k value of SCMs depends on the type and content used. According to [149], the accelerated pozzolanic strength activity of SF is the percentage ratio of average compressive strength of SF cement mortar (10 wt.% SF - 90 wt.% cement) to average compressive strength of reference cement mortar after 7 days cured at 65 ^{o}C. The pozzolanic activity of RHA has been evaluated by this standard [149], the result has shown that RHA has k value higher than 1 and similar to that of SF [12]. Indeed, concrete with the replacement of cement by up to 20 wt.% RHA has higher 28-day compressive strength than that of control concrete with only cement as binder and similar to that of concrete containing SF [1, 6, 9]. FA is considered a pozzolanic SCM. However its reactivity is not comparable with that of RHA and SF. The use of high volume FA in concrete can reduce strength and strength development rate at an early age because of the low degree of reaction between $Ca(OH)_2$ and FA [41-45]. Compressive strength decreases sharply when FA partially replaces Portland cement at levels of more than 40 wt.%. As a result, FA content is restricted to 40 wt.% for most applications [35]. The content and pozzolanic activity index of FA and SF are regulated in [199] [78]. LSP is considered a nearly inert SCM, incorporating LSP with cement does not take part in hydration of cement nor does it contribute significantly to the compressive strength of SCC/SCHPC [37, 38]. In Table 5.1, k values of some common SCMs are shown. In which the k value of RHA is proposed by the author. Herein, the k values are regularly counted for the limited contents. The higher content of SCMs can be applied, however the k values of each SCM will be changed and depends on the extra contents used. Further research needs to be conducted to regulate the k value of each SCM for its extra contents.

Table 5.1 Pozzolanic activity index of SCMs regulated in DIN EN 206-1 and DIN 1045-2 and proposed by the author

SCM	LSP	FA	SF	RHA*
Content (wt.%)	-	0-33	0-11	0-20
k value	0	0.4	1.0	1.0

* proposed by the author

5.3. Procedure of the proposed mix design method

The proposed mix design method considers SCHPC to consist of two phases: aggregate and paste. The paste content is determined on the basis of the minimum voids in the compacted aggregate blend. The adequate self-compactability is mainly governed by paste volume, type, content of SCMs, SP dosage while w/b ratio and reactivity of SCMs are mainly taken into account to achieve the required compressive strength. The procedure of proposed method for proportioning SCHPC containing various SCMs is illustrated in Fig. 5.1 and follows the basic steps below.

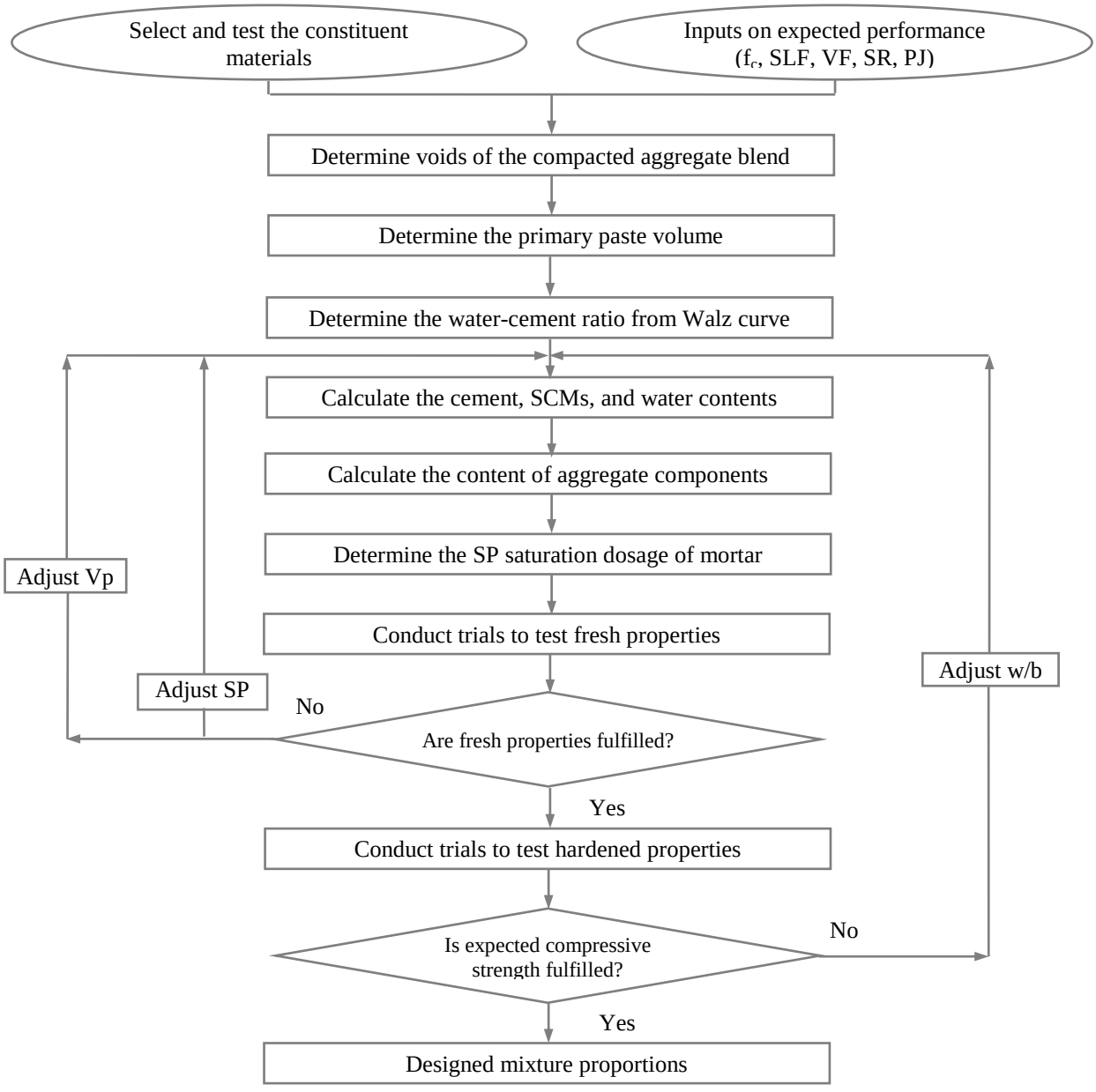

Fig. 5.1 Procedure of mix design method for proportioning SCHPC

Step 1: Determine the void volume of compacted aggregate blend

The ratio of aggregate components are computed on the basis of the Funk and Dinger (q = 0.25) theory [24, 201]. The optimum ratio gives the particle size distribution of aggregate following the ideal curve with the minimum deviation. With the determined ratio of the aggregate components, the bulk density of compacted aggregate blend is determined by experiment. And then the minimum void volume of the compacted aggregate blend can be calculated.

Step 2: Determine the minimum paste volume

The paste volume in SCHPC is significantly larger than that in ordinary concrete. It is required to fill the void volume between aggregate particles, and make sufficient lubricating layers on the surface of aggregate particles. Therefore, the minimum paste volume will be a total of void volume in compacted aggregate blend and excess paste volume making the lubricating layers on surface of aggregate particles. The coefficient related to the shape and the angularity (S-A) of aggregate is taken into account to calculate the excess paste volume, as proposed elsewhere [50].

Step 3: Determine the water-binder ratio

Based on the required compressive strength, as regulated in DIN EN 206-1 and DIN 1045-2, the equivalent w/c ratio is determined from the relation between compressive strength and w/c ratio, i.e. Walz curve [202] (Fig. 5.2). When the type and the content of SCMs replacing cement are known, the w/b ratio can be calculated. The w/b ratio of HPC is generally in range of 0.25-0.4 [6, 203], while the w/b ratio of SCC ranges from 0.26 to 0.48 [33]. Therefore, the suitable w/b ratio for SCHPC should be from 0.25 to 0.4.

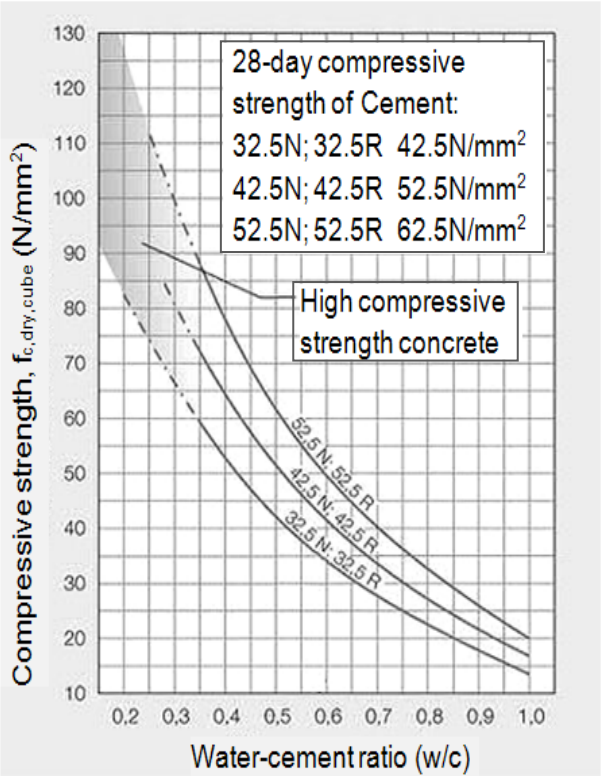

Fig. 5.2 Relation between compressive strength and w/c ratio, Walz curve [202]

Step 4: Determine cement, SCMs, and water contents

Based on the absolute volume of the constituent materials, the known paste volume, w/b ratio, and the cement content replaced by each SCM, the following are determined: the cement, SCM and water contents.

Step 5: Determine aggregate contents

Based on the known paste volume and the ratio of aggregate components, the content of aggregate blend and then the content of the individual aggregate components are obtained.

Step 6: Determine the dosage of Superplasticizer

The primary dosage of SP for SCHPC can be obtained from the SSD of mortar formulated from the SCHPC. As mentioned in Section 3.2.2, the SP saturation dosage (SSD) is determined by testing the mini-cone slump flow of mortar. The SSD is a SP dosage beyond which the mini-

slump flow no longer increases or with the SSD, mortar can reach a maximum mini-slump flow [1].

Step 7: Adjust the water content

The water adsorption of aggregates and the water contribution of SP should be counted as a proportion of the mixing water content. So the adjusted water content can be determined.

Step 8: Trial mixture and adjustments

A trial mixture is prepared using the mixture proportions calculated above, and then the key fresh properties such as filling ability, passing ability, segregation resistance, and plastic viscosity are determined. If the requirements of fresh properties (Table 2. 1) are not fulfilled, the SP dosage should be firstly adjusted. For example, when the filling ability and passing ability are low, increase the SP dosage and vice versa. Adjust the paste volume when the filling ability and passing ability cannot be achieved by adjusting SP dosage. Increase in paste volume leads to greater filling and passing abilities for a given SP dosage [1]. When the key fresh properties cannot be controlled by adjusting SP dosage and paste volume as well, adjust SCMs content considering their effect on these properties. The effect of some SCMs on fresh properties of SCHPC proposed by the author and other authors [50] is presented in Table 5.2. After the key fresh properties are satisfied, cubic specimens of 150x150x150 mm^3 for 28-day compressive strength are cast without vibration and compaction. If the 28-day compressive strength is too low, decrease the w/b ratio and vice versa.

Table 5.2 Effect of SCMs on self-compacting properties of SCHPC proposed by the author and other authors [50]

SCMs	Slump flow	Viscosity	Filling ability	Passing ability	Segregation resistance
LSP* (low wt.%)	⬆	⬇	⬆	⬆	⬇
LSP* (high wt.%)	⬇	⬆	⬇	⬇	⬆
FA	⬆	⬇	⬆	⬆	⬇ ⬆
GGBFS	⬇ ⬆	⬇ ⬆	⬇ ⬆	⬇ ⬆	⬇ ⬆
SF (low wt.%)	⬇ ⬆	⬇	⬆	⬆	⬇ ⬆
SF (high wt.%)	⬇	⬆	⬇ ⬆	⬇	⬇ ⬆
RHA**	⬇	⬆	⬇	⬇	⬆

* Previous works show that the presence of limestone powder within certain content increases the flowability, but the larger content results in higher viscosity and flow time of mortar and SCC [34, 204, 205].

** RHA is used as viscosity agent in SCC, the increase in RHA content decreases the slump flow, passing ability, but simultaneously increases the viscosity and hence segregation resistance [1, 10].

5.4. Validation of the proposed method

To validate the proposed method, eight SCHPC mixtures containing ternary binders proportioned with cement and two different SCMs, such as RHA, LSP, FA, and SF, were designed to fulfill slump flow class SLF2, viscosity class VF2, passing ability class PJ2, segregation resistance class SR2 (Table 2.1) and compressive strength classes of C60/75, C70/85, C80/95 as regulated in DIN EN 206-1 and DIN 1045-2. The air content was set at 2%

for non-air entrained concrete. The mixture proportions are shown in Table 5.3. The mixture types were designated on the basis of w/b ratio, type and percentage of SCM replacing cement by weight. For instance, in the **''30LSP20R10''** mixture, 30 wt.% cement content was replaced by 20 wt.% LSP, and 10 wt.% RHA, and the w/b ratio was 0.30 by weight.

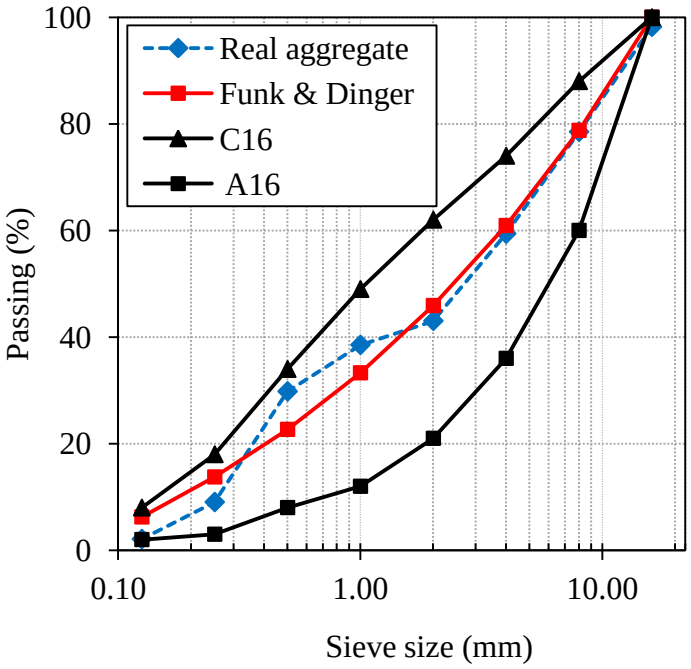

Fig. 5.3 Aggregate grading ranges for SCHPC

The materials used in this study were Portland cement (CEM I 52.5 R), LSP, FA, SF, RHA, natural sand (0-2mm), and crushed basalt stone (2-5 mm, 5-8 mm, 8-11 mm, 11-16 mm). RHA was used with two different mean particle sizes of 5.7 µm and 7.7 µm. The first type was used in mixtures with w/b ratio of 0.26 and the second type was used in the mixtures with w/b ratio of 0.30 and 0.34. The physical properties and the chemical composition of cement and SCMs are summarized in Table 3.1 and Table 3.2. The physical properties of aggregate are presented in Table 3.2. The ideal grading curve of the Funk and Dinger theory with q=0.25, Dmax=16 mm and Dmin=0.63 mm; the grading curve of aggregate used in this study and the required range of aggregate grading for ordinary concrete (A16 and C16) complying with DIN EN 206-1 and DIN 1045-2 are shown in Fig. 5.3. In addition, a polycarboxylate based superplasticizer with density of 1.08 g/cm^3 and 40 wt.% solid content was used.

5.5. Results and discussion

Self-compactability of SCHPC

The experimental results of self-compactability of fresh concrete are presented in Table 5.4. The slump flow of the SCHPCs ranged from 730 to 780 mm, without signs of bleeding and segregation. The V-funnel flow times and T_{500} values were in range of 9.2 - 19.7 s and 2.9 - 6.7 s, respectively. The J-ring step height is equal 10 mm in most cases. The sieve segregation index ranged from 4.7 to 13.6 wt.%. This indicates that the SCHPCs have excellent filling ability, good plastic viscosity, adequate passing ability and good segregation resistance. All of the SCHPC mixtures meet the requirements of slump flow SLF2, viscosity VF2, passing ability PJ2, segregation resistance SR2.

It is well known that the self-compactability of SCHPCs is governed by paste composition and SP content, when the paste volume and aggregate volume are fixed. All trial batches of concretes were made with the SSD of their corresponding mortars. Generally, the demand of SP for adequate self-compacting properties of SCHPC was similar to SSD of the corresponding mortar, as shown in Fig. 5. 4 and in Table 5.3. Mixtures proportioned with w/b ratio of 0.26 satisfied the requirements of self-compactability with the SSD of the corresponding mortars.

For mixtures proportioned with w/b ratio of 0.30 and 0.34, SP dosages for the requirements of self-compactability were slightly adjusted compared with SSD of the corresponding mortars. For instance, ''34LSP20R10'' mixture made with SSD had a slump flow of 650 mm, T_{500} value of 2.75 s, and sieve segregation index of 3.8 wt.%, however the J-ring step height was 20 mm significantly higher than the standardized value of 10 mm (Table 2. 1). Thereafter, SP dosage was increased from the SSD of 0.8 to 0.9 wt.%, all requirements for self-compactability were fulfilled (Table 5.4). The results of properties of fresh SCHPC show that the mixtures incorporating LSP need a much higher SP dosage than the mixtures incorporating FA to meet the required self-compactability (Table 5.4). It can be explained that LSP has angular particles with a rough surface, and smaller size and hence has a larger specific surface area. Whereas FA has larger spherical particles and, therefore, a lower SSA (Table 3.2). As a result, the incorporation of LSP into the mixtures leads to an increase in viscosity of paste and hence a decrease in slump flow of concrete. Therefore to reach the required flowing ability, a higher SP dosage must be used in the mixture containing LSP, compared to the mixture containing FA.

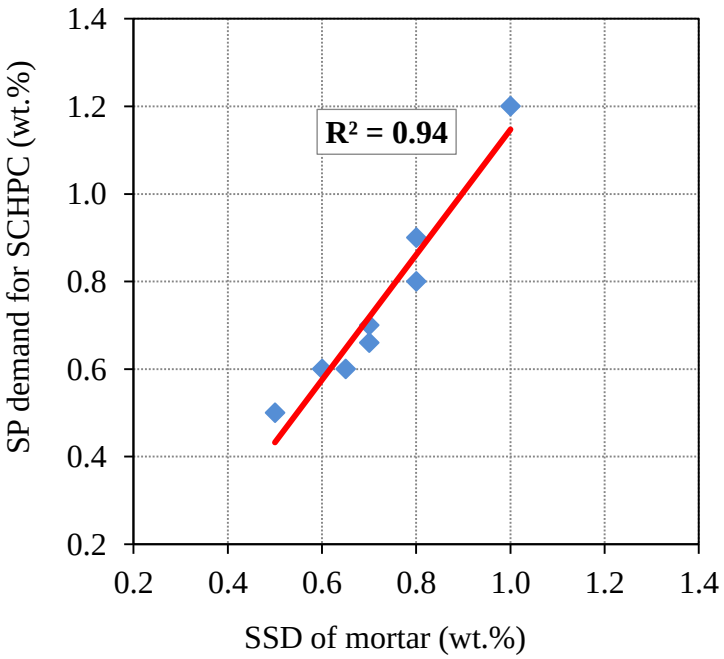

Fig. 5. 4 SP demand for SCHPC vs. SSD of mortar formulated from the SCHPC

Table 5.3 Mixture proportions of SCHPC designed by the proposed method

Mixtures	w/c_{eq}	w/b	Water (kg/m^3)	Cement (kg/m^3)	LSP (kg/m^3)	FA (kg/m^3)	SF (kg/m^3)	RHA (kg/m^3)	Sand (kg/m^3)	Basalt stone (kg/m^3)	SP/SSD[a] (%)	SP[b] (%)
34LSP20R10	0.42	0.34	182	374	107	0	0	53	790	968	113	0.9
34FA20R10	0.38	0.34	178	366	0	104	0	52	790	968	100	0.5
34FA20R15	0.38	0.34	176	336	0	104	0	78	790	968	100	0.6
34FA20R20	0.38	0.34	175	308	0	103	0	103	790	968	94	0.66
30LSP20R10	0.38	0.30	168	397	113	0	0	57	790	968	120	1.2
30FA20R10	0.34	0.30	170	388	0	111	0	55	790	968	92	0.6
26FA20R10	0.29	0.26	155	413	0	118	0	59	790	968	100	0.8
26FA20SF10	0.29	0.26	155	413	0	118	59	0	790	968	100	0.7

[a] Percentage ratio of SP demand for concrete to SSD of mortar; [b]SP demand for concrete

Table 5.4 Test results of self-compactability and compressive strength of SCHPC designed by the proposed method

Mixtures	Slump flow (mm)	T_{500} (sec)	V-funnel (sec)	J-ring step height (mm)	Sieve segregation (%)	Air (%)	Compressive strength (MPa)			Designed strength class
							3days	7days	28days	
34LSP20R10	770	2.9	10.2	10	12.7	1.9	46.3	65.4	93.6	C55/67
34FA20R10	780	2.9	10.5	10	12.5	1.4	52.7	71.0	97.1	C60/75
34FA20R15	770	3.3	12.5	10	10.5	1.3	48.8	71.4	100.6	C60/75
34FA20R20	760	3.7	16.4	10	8.3	1.4	42.2	68.8	102.3	C60/75
30LSP20R10	730	4.8	11.0	10	8.3	2.7	52.1	71.5	98.9	C60/75
30FA20R10	770	3.3	18.5	10	11.0	1.1	63.2	78.0	104.5	C70/85
26FA20R10	760	6.7	19.7	9.5	4.7	1.0	67.5	89.6	123.2	C80/95
26FA20SF10	770	4.0	9.2	10	13.6	2.5	72.5	87.4	118.3	C80/95

Compressive strength of SCHPC

In Fig. 5.5 and Table 5.4, compressive strength of SCHPC is presented. It can be seen that the 28-day compressive strengths of all SCHPC mixtures reached over 90 MPa and meet the designed compressive strength classes. The compressive strength of the mixture containing RHA was similar to that of the mixture containing SF, irrespective of age. As mentioned in Section 2, RHA is a highly reactive SCM, and comparable with SF. This result is also consistent with the reported studies [1, 6, 9]. The compressive strength of the mixture containing FA is slightly higher than that of the mixture containing LSP, regardless of age. LSP is considered as a nearly inert SCM, whereas FA is a pozzolanic SCM with a k value of 0.40. Consequently, pozzolanic activity of FA might contribute the higher compressive strength of the mixture containing FA. These results indicate that application of pozzolanic activity index (k) and the relation between compressive strength and w/c ratio for normal concrete (Walz curve) can be suitable for predicting the compressive strength of SCHPC.

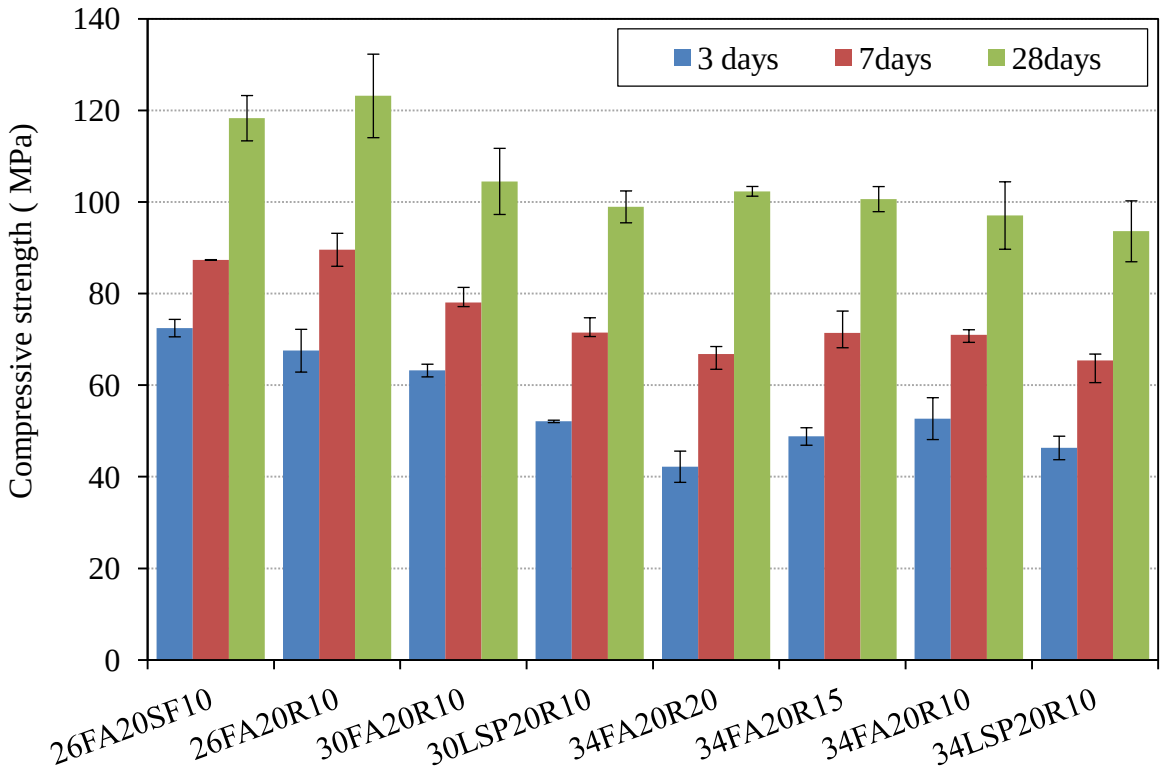

Fig. 5.5 Compressive strength of SCHPC investigated

Durability of SCHPC

All SCHPC mixtures not only meet the requirements of self-compactability and compressive strength but also fulfill the requirements of durability with respect to exposure classes. In the standards DIN EN 206-1 and DIN 1045-2, the durability design is defined by the exposure classes (X), each class determines the limit values for the type of cement, cement content, w/c ratio, air content and compressive strength class. It can be seen from Table 5.3 and Table 5.4 that the designed mixtures have the w/c equivalent ratios from 0.29 to 0.42, the cement content from 308 to 413 kg/m^3 and compressive strength class from C55/67 to C80/95 which satisfy the most restrictive values for w/c of 0.45, cement content of 270 kg/m^3, and compressive strength class of C35/45 required by all exposure classes. Therefore, all SCHPC mixtures fulfill the

durability requirements with respect to the exposure classes XC1, XC2, XC3, XC4 (corrosion induced by carbonation); XD1, XD2, XD3, XS1, XS2, XS3 (corrosion induced by chlorides); XF1, XF2, XF3 (freeze/thaw attack); XA1, XA2, XA3 (chemical attack); and XM1, XM2, (mechanical attack). In summary, it can be said that with a compressive strength in range of 90-130 MPa, the SCHPCs can be expected to have good durability similar to that of high performance and ultra high performance concrete [1, 6, 9, 206].

5.6. Concluding remarks

The aim of this work was to develop a new mix design method for proportioning SCHPC with adequate self-compactability, very high compressive strength, and good durability and to take into consideration the effect of SCMs. From the experimental results, the following conclusions can be drawn:

- A new method for proportioning SCHPC was developed on the basis of the requirements for ordinary concrete proportions regulated in DIN EN 206-1 and DIN 1045-2. The proposed method considers the combination of various SCMs to achieve the adequate self-compactability, high compressive strength in the range of over 90 MPa, and good durability. A proper compressive strength level as in ordinary concrete can be obtained for a particular W/B ratio, a given content and type of MA.
- The procedure of the proposed method for SCC/SCHPC is similar to that of ordinary concrete, so is as simple for mix design of SCC/SCHPC and for practical applications. The packing theory of Funk and Dinger with an exponent q = 0.25 was adopted to determine the grading of aggregate. The primary paste volume for filling ability was computed from the void content of compacted aggregate. The superplasticizer dosage for the concrete was set on the basis of the superplasticizer saturation dosage of the corresponding mortar. w/b ratio was determined on the basis of the required compressive strength.
- The pozzolanic reactivity index of SCMs, i.e. LSP, FA, RHA, and SF, can be accepted to predict the expected compressive strength in mix-design for SCHPC. In range of 0-20 wt.% cement replacement, RHA is very effective in improving compressive strength of SCHPC with the pozzolanic activity index of 1, which is the first time applied, and similar to that of SF.
- It is possible to use common supplementary cementitious materials (LSP, FA) in combination with RHA to produce SCHPC with adequate self-compactability, very high compressive strength and good durability.
- The combination of 10 wt.% RHA and 20 wt.% FA is more beneficial to SP demand and compressive strength of SCHPC than that of 10 wt.% RHA and 20 wt.% LSP.
- 10 wt.% RHA is a very good substitute for 10 wt.% SF in terms of self-compactability and compressive strength. Furthermore, the utilization of RHA is beneficial to the economy of SCHPC and environment.

6. Rheological behaviour and properties of fresh mortar and SCHPC

6.1. Mixture proportions

6.1.1. Mixture proportions of SCHPC

Based on the proposed method, the SCHPC mixtures were designed with a w/b of 0.26, a paste volume of 38.5 vol.% (including air content of 2 vol.%), a fine aggregate volume of 30.4 vol.%, and a coarse aggregate volume of 31.1 vol.%. The cement content was replaced with SCMs, i.e. FA, RHA, and SF by weight, but the paste volume was kept constant [200]. The SSDs of mortars formulated from the SCHPCs were determined, and then the maximum SSD was used in this study. Mixture proportions of SCHPCs are shown in Table 6.1, in which designation of the mixtures are explained previously, for instance, in the ''26FA20R10'' mixture, 30 wt.% cement content was replaced by 20 wt.% FA, and 10 wt.% RHA, and w/b ratio was 0.26 by weight. RHA5.7 was used in this study.

Table 6.1 Mixture proportions of SCHPC

Mixtures	w/b	Water (kg/m^3)	Cement (kg/m^3)	FA (kg/m^3)	RHA (kg/m^3)	SF (kg/m^3)	Sand (kg/m^3)	Basalt stone (kg/m^3)	SP (%)
26FA0R0	0.26	163	625	0	0	0	790	968	1
26FA20R0	0.26	156	481	120	0	0	790	968	1
26FA20R5	0.26	155	447	119	30	0	790	968	1
26FA20R10	0.26	153	413	118	59	0	790	968	1
26FA20R15	0.26	152	380	117	88	0	790	968	1
26FA20R20	0.26	151	347	116	116	0	790	968	1
26FA20SF10	0.26	153	413	118	0	59	790	968	1

6.1.2. Mixture proportions of mortar

The mortars were formulated from the corresponding SCHPCs. The proportions of sand, cement, RHA, SF, FA and water of mortars were identical to those of the corresponding concretes. The mortar mixture proportions used in this study are presented in Table 6.2.

Table 6.2 Mixture proportions of mortar

Mixtures	w/b ratio	Paste (vol.%)	Sand (vol.%)	RHA (wt.%)	SF (wt.%)	MPS of RHA (μm)
REF	0.26-0.30	56	44	0	0	-
10-20%SF	0.26-0.30	56	44	0	10-20	-
10-30%RHA	0.26-0.30	56	44	10-30	0	5.7 - 22.6

6.2. Properties of fresh SCHPC

6.2.1. Filling ability and passing ability

In Fig. 6.1, the effect of FA and RHA on the filling ability and passing ability of SCHPC is shown. Filling ability was evaluated by slump flow, (increasing slump flow indicates a higher filling ability). Passing ability was evaluated by J-ring step height, (increasing J-ring step height indicates a poorer passing ability). It can be seen that the incorporation of 20 wt.% FA increased filling ability compared to the reference sample. The increase in RHA content led to a decrease in filling and passing abilities, whereas the incorporation of SF increased the filling ability and passing ability of SCHPC dramatically.

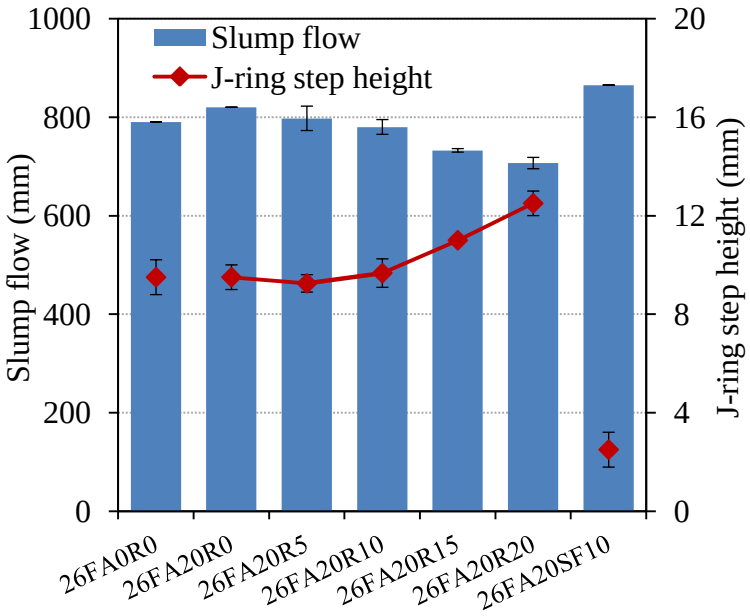

Fig. 6.1 Effect of FA and RHA on the filling ability and passing ability of SCHPC

6.2.2. Plastic viscosity and segregation resistance

The effect of FA and RHA on plastic viscosity and segregation resistance is shown in Fig. 6.2, where plastic viscosity and segregation resistance are evaluated by V-funnel time and sieve segregation index, respectively. Increasing V-funnel time and sieve segregation index indicates the higher plastic viscosity and the lower segregation resistance, respectively. It is clear that the cement replacement by 20 wt.% FA decreased plastic viscosity and segregation resistance. Obviously, the higher the RHA content, the higher the plastic viscosity and the segregation resistance of SCHPC containing 20 wt.% FA are. Whereas the combination of SF and FA dramatically decreased plastic viscosity and thus segregation resistance of SCHPC.

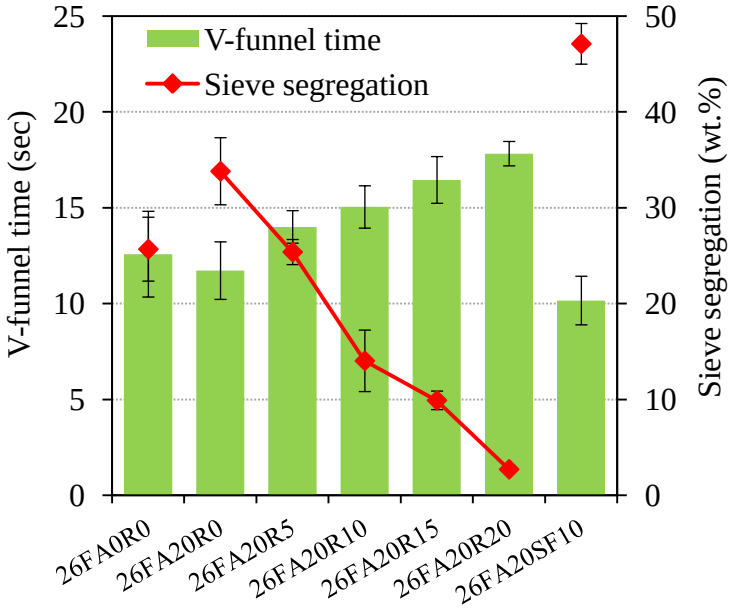

Fig. 6.2 Effect of FA and RHA on plastic viscosity and segregation resistance

6.2.3. Air content and unit weight

The air content and unit weight of SCHPC are presented in Fig. 6.3. The unit weight of SCHPC decreased with the level of the cement replacement by FA and RHA or SF, because the density

of RHA, FA and SF is lower than that of cement (Table 3.2). The air content in the fresh concrete was lower than 2 % that is suitable for non–air entrained concrete as designed. It can be found that ''26FA20R15'' and ''26FA20R20'' mixtures had the air content of 1.3 %, higher than mixtures containing less RHA or no RHA. It might be due to the higher plastic viscosity of the mixture containing a higher RHA content (Fig. 6.1).

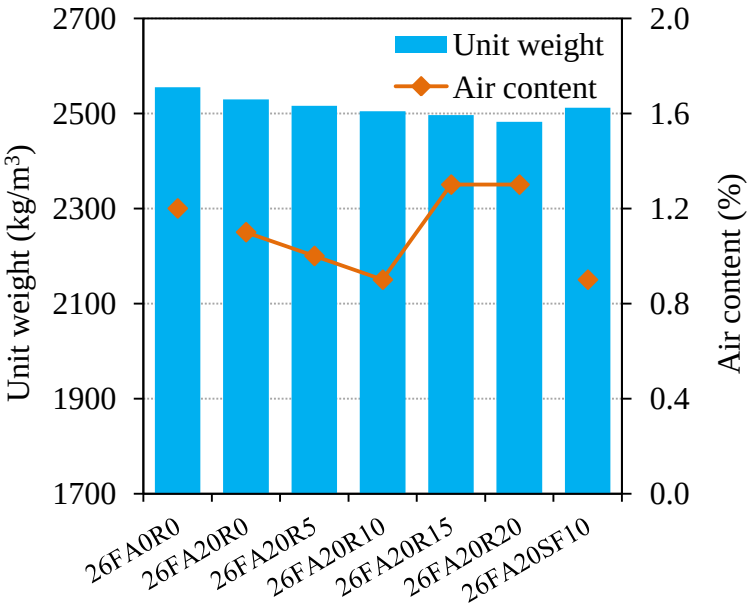

Fig. 6.3 Air content and unit weight of SCHPC

6.2.4. Discussion

The self-compactability of fresh SCC/SCHPC is dependent on characteristics of aggregate, the paste volume, the paste composition [24, 50]. In this study, the aggregates and the paste volumes were kept constant. The paste composition, therefore, is the main factor influencing filling ability, passing ability, plastic viscosity and segregation resistance of SCHPC. The replacement of cement by FA increased filling ability and passing ability, however, it decreased plastic viscosity and thus segregation resistance. FA with spherical shape and coarser particles decreases water demand due to the decrease in surface area (Fig. 4.9 and Table 3.2), induces ball-bearing effect and hence increases the slump flow and decreases V-funnel time when w/b is kept constant. These results agree with the conclusions of other studies [41-43, 205]. The filling ability, in terms of slump flow, is correlated to passing ability. Therefore, increasing filling ability yields good passing ability. However, due to the lower plastic viscosity, the resistance of the mixture containing 20 wt.% FA to segregation was very poor with a sieve segregation index of over 30 wt.% (Fig. 6.2).

The incorporation of RHA into the mixture containing 20 wt.% FA decreased filling ability and passing ability, and increased the plastic viscosity and segregation resistance simultaneously (Fig. 6.1 and Fig. 6.2). The effect was stronger with the higher RHA content. For a given coarse aggregate particle size, segregation resistance or static stability of SCC/SCHPC depends on the difference between the relative densities of aggregate and matrix, yield stress and viscosity of the mixture [1]. Increasing the RHA content decreased the density of the binder (cement+RHA) paste due to the lower density of RHA (Fig. 6.3). Thus, the increase in plastic viscosity is the main reason for the improvement of segregation resistance. RHA is a macro-meso porous material with a very large SSA, with a higher water demand and adsorption compared to cement. The replacement of cement by RHA leads to a reduction in free water, and hence an increase in plastic viscosity of paste, a decrease in slump flow and increase in V-funnel time of concrete. The filling ability and passing ability was poorer with higher RHA content. Therefore, it is very important to note that the self-compactability of SCHPC can be controlled by the content of RHA. In this study, the cement replacement by 20 wt.% FA and 10 wt.% RHA

appears optimal. Moreover, the increase of SP content from 0.8 % to 1.0 % slightly influences the self-compactabilty of ''26FA20R10'' mixture (Table 5.3, Table 5.4, Fig. 6.1 and Fig. 6.2), thus it can be said that the robustness of SCHPC containing RHA is very high with respect to the variation of SP.

The opposite situation was obtained when SF was admixed. The incorporation of SF strongly increased filling ability and passing ability (Fig. 6.1), and dramatically decreased the segregation resistance with sieve segregation index of over 45 wt.% (Fig. 6.2). Despite the very high water demand of SF compared to cement, SF particles are ultra fine and spherical. This increases the packing density of granular mixture, induces the ball-bearing effect, and thus improves the filling and passing abilities while decreasing the plastic viscosity [207]. With a very high SP dosage, the very poor segregation resistance of the mixture containing SF might be due to not only the lower plastic viscosity, and the lower density of the SF blended cement paste, but also the different SP adsorption and compatibility compared to that of the mixture containing RHA. The effect of RHA and SF on rheological properties (plastic viscosity and yield stress) will be investigated in detail in the following Section.

6.2.5. Concluding remarks

- The replacement of cement by 20 wt.% FA results in higher filling ability, lower plastic viscosity and hence lower segregation resistance of SCHPC when w/b ratio and paste volume of concrete are kept constant.
- The combination of 10 wt.% SF and 20 wt.% FA dramatically increases the filling ability and the passing ability, simultaneously decreasing the segregation resistance of SCHPC.
- The self-compacting properties of SCHPC can be controlled by the incorporation of RHA. The presence of RHA decreases filling ability, and increases plastic viscosity and hence segregation resistance of SCHPC, depending on the RHA content used. RHA can be used as a viscosity modifying agent.
- The self-compacting properties of SCHPC containing RHA are slightly affected by the variation in SP content. Therefore, the robustness of SCHPC containing RHA is very high with respect to the variation of SP.
- The combination of RHA and FA improves self-compactability of SCHPC, where FA improves filling ability and RHA controls segregation resistance. With RHA5.7, the combination of 20 wt.% FA and 10 wt.% RHA has the synergistic effect on self-compactability of SCHPC.

6.3. Properties and rheological behaviour of fresh mortar formulated from SCHPC

6.3.1. Superplasticizer saturation dosage of mortar

The SSD of mortar determined by means of the mini-cone slump flow is shown in Fig. 6.4. It can be seen that beyond the SSD, the mini-cone slump flow and T_{250} time did not change significantly.

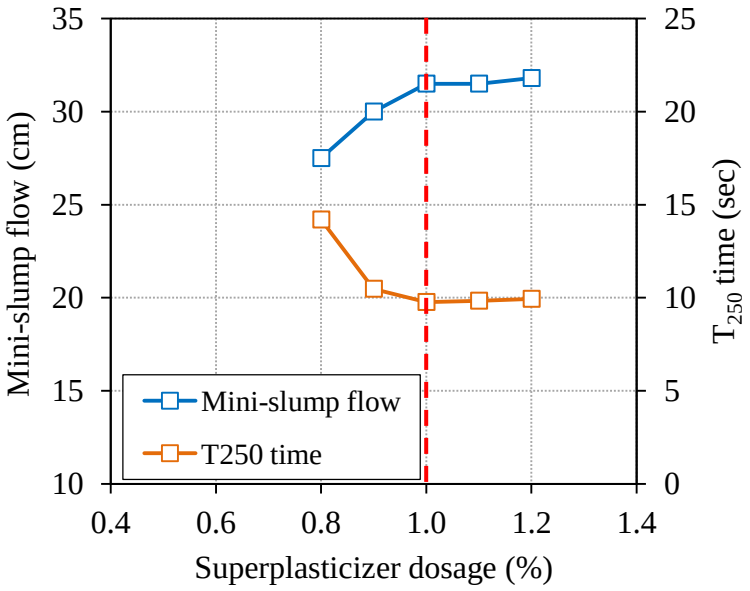

Fig. 6.4 SSD of mortar containing 20 % RHA7.7 determined by min-cone slump flow at w/b of 0.30

Effect of MPS of RHA on SSD

Fig. 6.5 shows the SSD of mortar containing RHA with different MPSs at w/b ratios of 0.26 and 0.30. In this study, cement was placed by 10 wt.% RHA. It can be seen that increasing MPS of RHA resulted in a higher SSD of mortar. At w/b ratio of 0.26, the SSD of reference sample was similar to that of mortar containing RHA5.7. Generally, the lower the w/b ratio, the higher the SSD.

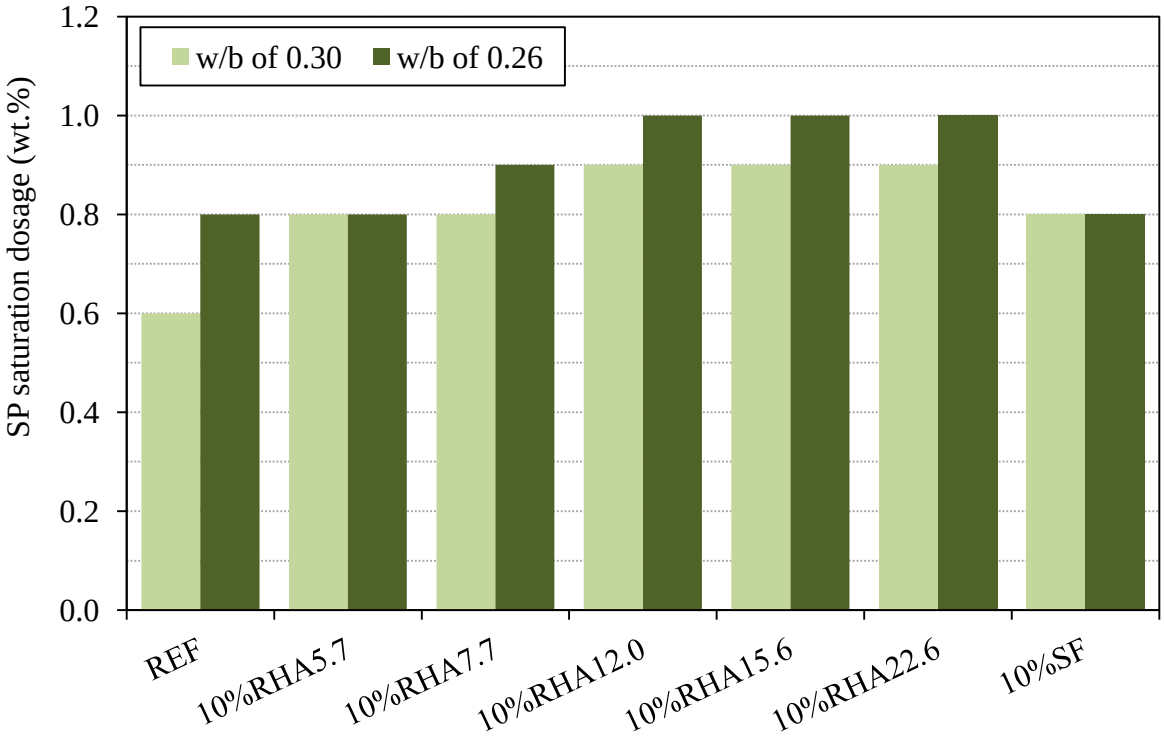

Fig. 6.5 Effect of MPS of RHA on saturation superplasticizer dosage of mortar

Effect of RHA content on SSD of mortar

It is clear that the higher the cement replacement by RHA7.7 at w/b ratio of 0.30, the higher the SSD of mortar (Fig. 6.7). Similar results were obtained when cement was placed by RHA5.7 or SF at w/b of 0.26 (Fig. 6.6). The effect of RHA was stronger at the lower w/b of 0.26.

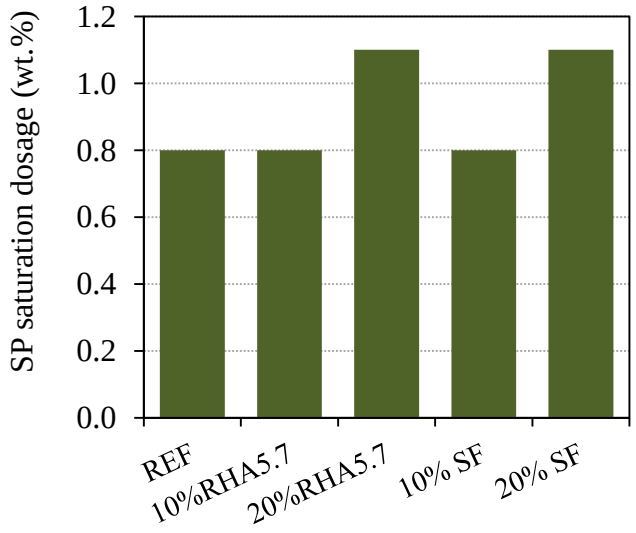

Fig. 6.6 Effect of RHA5.7/ SF content on SSD (w/b of 0.26)

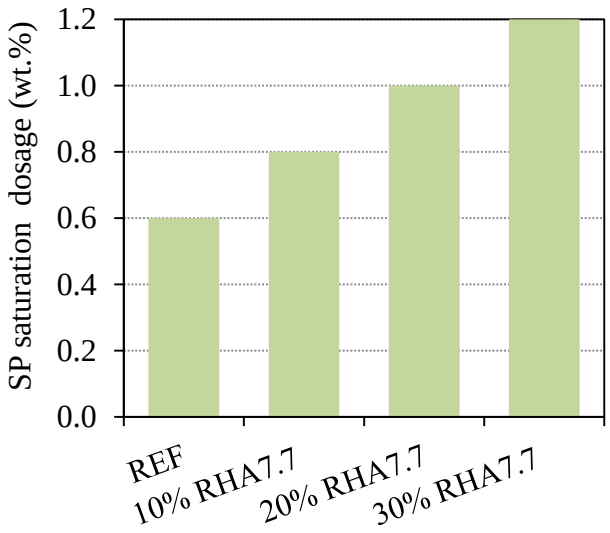

Fig. 6.7 Effect of RHA7.7 content on SSD (w/b of 0.30)

The SSDs determined will be used to investigate the effect of RHA and other SCMs on rheological properties of mortar as follows.

6.3.2. Superplasticizer adsorption of paste formulated from mortar

Fig. 6.8 shows the SP adsorption of paste formulated from mortar made with the maximum SSD of 0.9 wt.% (Fig. 6.5). It is obvious that the incorporation of RHA/SF increased the SP adsorption. BET-SSA of RHA/SF is much larger than that of cement, 10 wt.% RHA/SF incorporation increased BET-SSA of binder, resulting in an increase in SP absorbed surface. With respect to RHA, decreasing MPS increases BET-SSA, i.e. external SSA, hence increased SP adsorption. The sample containing SF had higher SP adsorption than the sample containing RHA. It can be explained by the fact that BET-SSA of RHA in total is higher however the external SSA of RHA might be lower than that of SF.

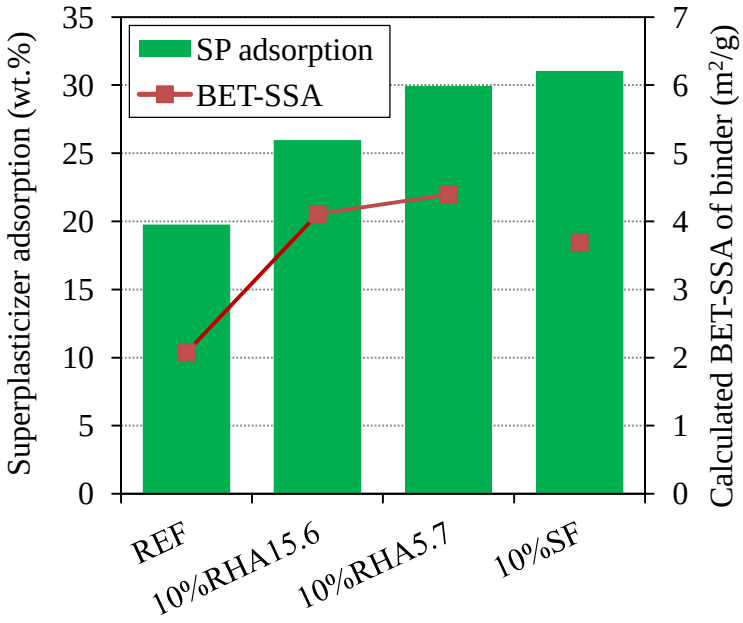

Fig. 6.8 Superplasticizer adsorption of paste formulated from mortar, at w/b of 0.30

6.3.3. Flowing ability and plastic viscosity of mortar

Effect of MPS of RHA on flowing ability and plastic viscosity

In Fig. 6.9, the effect of MPS of RHA on the mini-slump flow and mini-V-funnel time is shown. Obviously, the mixture containing the coarser RHA had lower mini-slump flow and higher mini-V-funnel time than those of the reference sample. It is very important to note that

due to the increase in MPS, the mini-slump flow decreased slightly, whereas the mini-V-funnel time increased dramatically. That means increasing MPS of RHA mainly increased the plastic viscosity of mortar. The effect was stronger at the lower w/b ratio of 0.26.

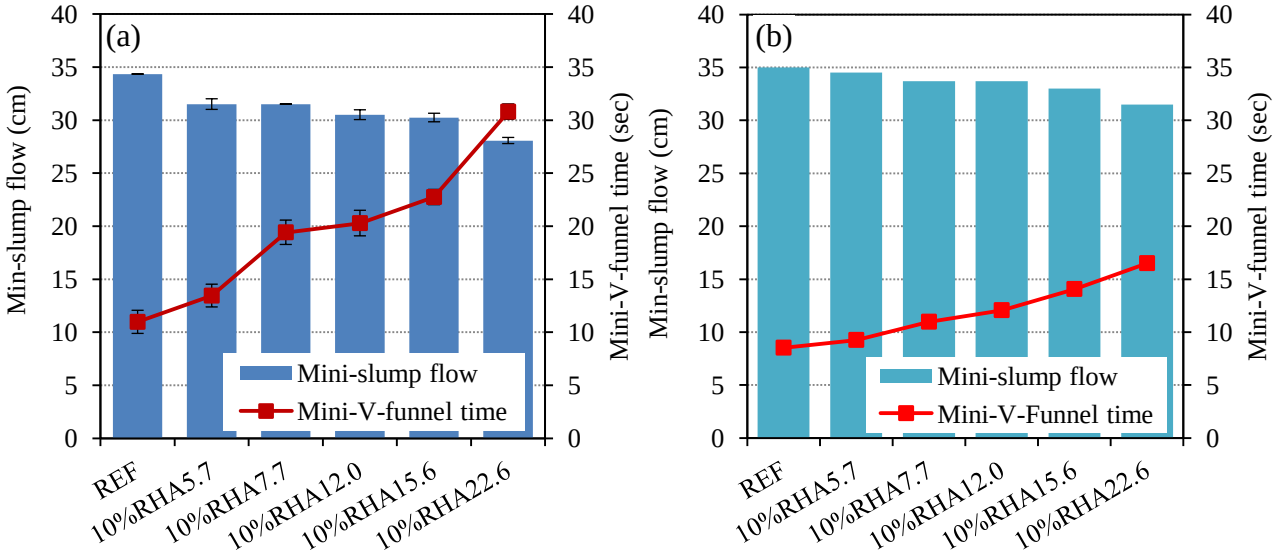

Fig. 6.9 Effect of RHA MPS on mini-slump flow and mini-V-funnel time, at w/b of 0.26 (a) and at w/b of 0.30 (b)

Effect of RHA content on flowing ability and plastic viscosity

The effect of RHA5.7/SF content at w/b of 0.26 and RHA7.7 content at w/b of 0.30 on mini-slump flow and flow time is presented in Fig. 6.10 and Fig. 6.11, respectively. The incorporation of RHA/SF decreased the mini-slump flow and increased the mini-V-funnel time of mortar at w/b of 0.30 and T_{250} time at w/b of 0.26. This effect was stronger when the higher RHA/SF content was used, where the increase in T_{250} time due to the higher content of RHA5.7 was much greater than that due to the higher content of SF. Moreover, it is clearly observed that increasing RHA content decreased mini-slump flow slightly, but increased T_{250} time (Fig. 6.10) and mini-V-funnel time (Fig. 6.11) significantly. These results correspond to the slump flow and V-funnel time of SCHPC above (Fig. 6.1 and Fig. 6.2).

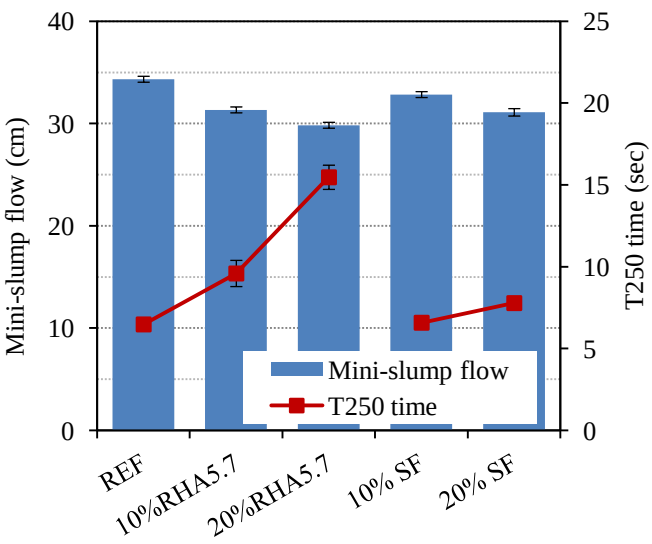

Fig. 6.10 Effect of RHA/SF content on mini-slump flow and T_{250} time (w/b of 0.26)

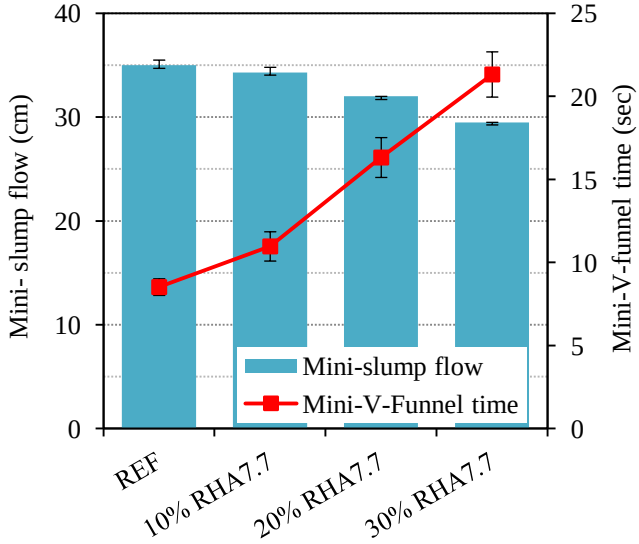

Fig. 6.11 Effect of RHA content on mini-slump flow and mini-V-funnel time (w/b of 0.30)

6.3.4. Workability retention of mortar

Effect of MPS of RHA on workability retention

Mini-slump flow and mini-V-funnel time of mortar containing various types of RHA 15, 30 and 60 min after water addition are shown in Fig. 6.12. It can be clearly seen that the mini-slump flow loss and mini-V-funnel increased over time. The mini-slump flow loss and the increase in mini-V-funnel time of the sample containing RHA were significantly higher than those of the reference sample. The coarser the MPS of RHA, the larger the mini-slump flow loss and the mini-V-funnel time. The effect was stronger 60 min after the addition of water.

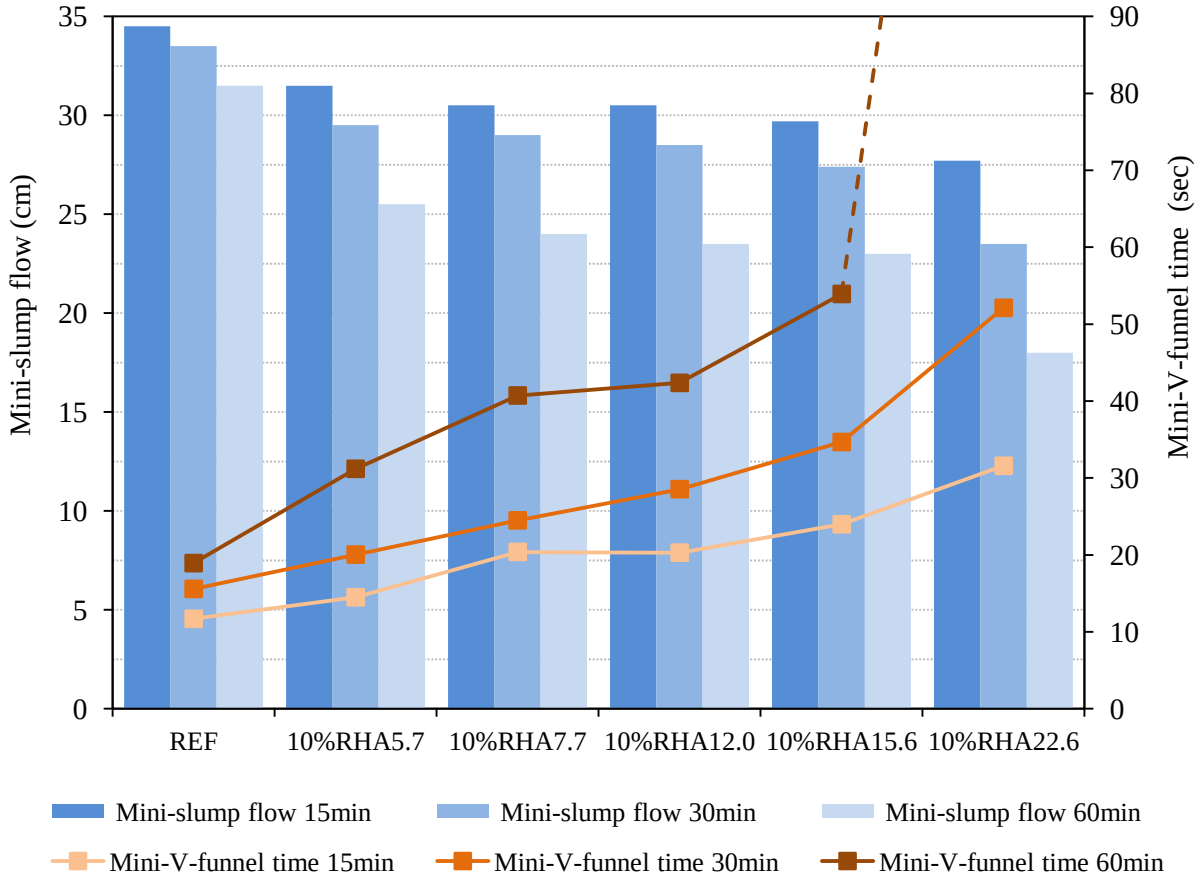

Fig. 6.12 Effect of RHA MPS on workability retention of mortar (w/b of 0.26)

Effect of RHA content on workability retention

In Fig. 6.13, the effect of RHA5.7/SF content on mini-slump flow and T_{250} time 15, 30, 60 min after water addition is presented. Increasing RHA5.7/SF content increased T_{250} time, and decreased mini-slump flow at all ages. This effect was more pronounced at the late age of 60 min. After 60 min, the mini-slump flow loss of samples containing RHA was much higher than that of the sample containing SF. Moreover, the increase in T_{250} time of the samples containing RHA was significantly higher than that of the sample containing SF, particularly with 20 wt.% RHA and at the age of 60 min. That indicates that the plastic viscosity of RHA containing samples increased dramatically over time, especially with higher RHA content.

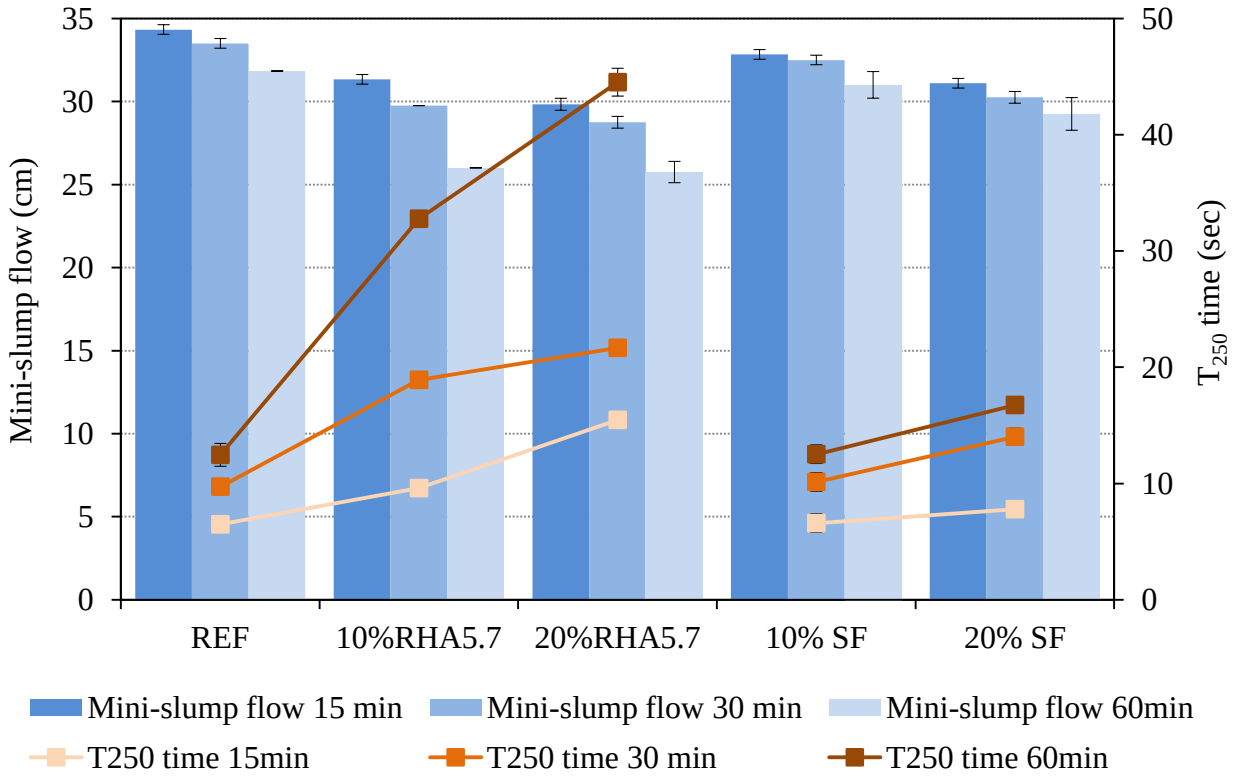

Fig. 6.13 Effect of RHA5.7 SF content on mini-slump flow and T_{250} time over time (w/b of 0.26)

The relation between mini-V-funnel time and T_{250} time is shown in Fig. 6.14. The T_{250} time is closely related to mini-V-funnel time with linear regression of 0.97. Therefore, T_{250} can be used to evaluate the plastic viscosity of mortar.

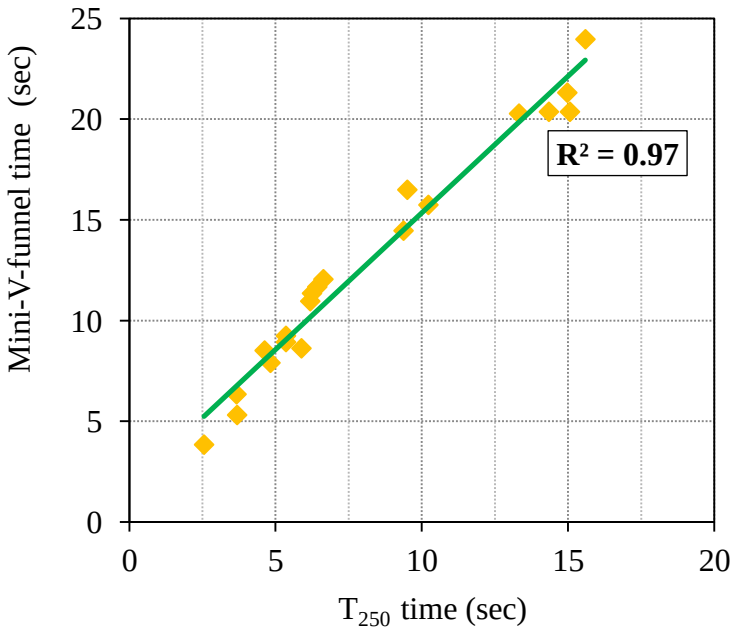

Fig. 6.14 Relation between mini-V-funnel and T_{250} time

6.3.5. Rheological behaviour of mortar

Flow curves obtained from all measurements expressed linearity with rotational velocity lower than 1 rpm, but non-linearity with the higher ones. The examples are shown in Fig. 6.15. Therefore, The Bingham model was applied for the measurements with rotational velocities below 1 rpm to determined yield stress and plastic viscosity. Meanwhile the modified Bingham model was applied with higher rotation velocities to evaluate shear-thickening behaviour. The results are presented below.

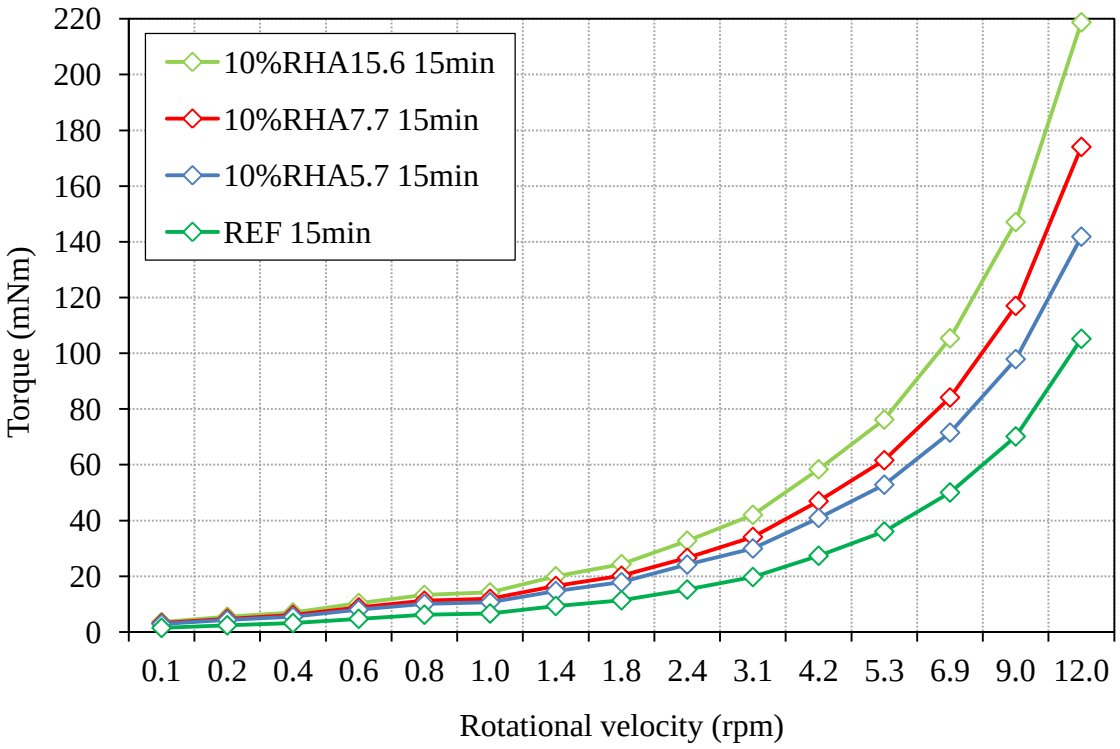

Fig. 6.15 Flow curves for mortar containing RHA with different MPSs 15 min after water addition

Yield stress and plastic viscosity of mortar in accordance with Bingham model

The Bingham relations of rheological measurements and the Bingham parameters are shown in Fig. 6.16 and Table 6.3, respectively. It can be seen that the experimental data fit well with Bingham model with the linear regression of 0.99.

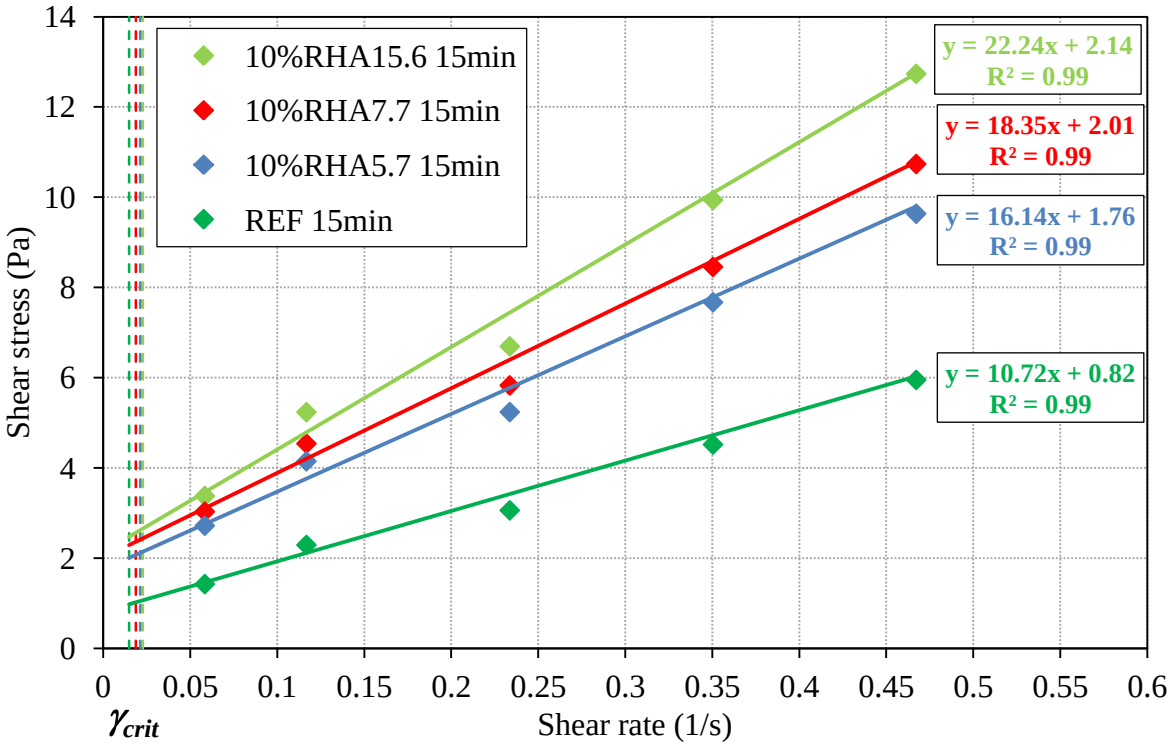

Fig. 6.16 Determine yield stress and viscosity of mortar in accordance with Bingham model, the dot lines indicate the critical shear rates (γ_{crit}), at w/b of 0.26

The results show that the incorporation of RHA/SF increased the yield stress and viscosity of mortar. The effect depends on the RHA/SF content and the MPS of RHA. Increasing MPS of RHA increased the yield stress and viscosity of mortar, particularly at the late age of 60 min (Fig. 6.17 and Fig. 6.19). This result is correspondent with the mini-slump flow and mini-V-funnel time, mentioned above (Fig. 6.12). It is very important to note that the mini-slump flow and mini-slump flow loss of the RHA7.7 containing sample were similar to those of the RHA5.7 containing sample (Fig. 6.12), however the yield stress and the plastic viscosity of the RHA7.7 containing sample were considerably higher than those of the RHA5.7 containing sample, especially at the age of 60 min (Fig. 6.19).

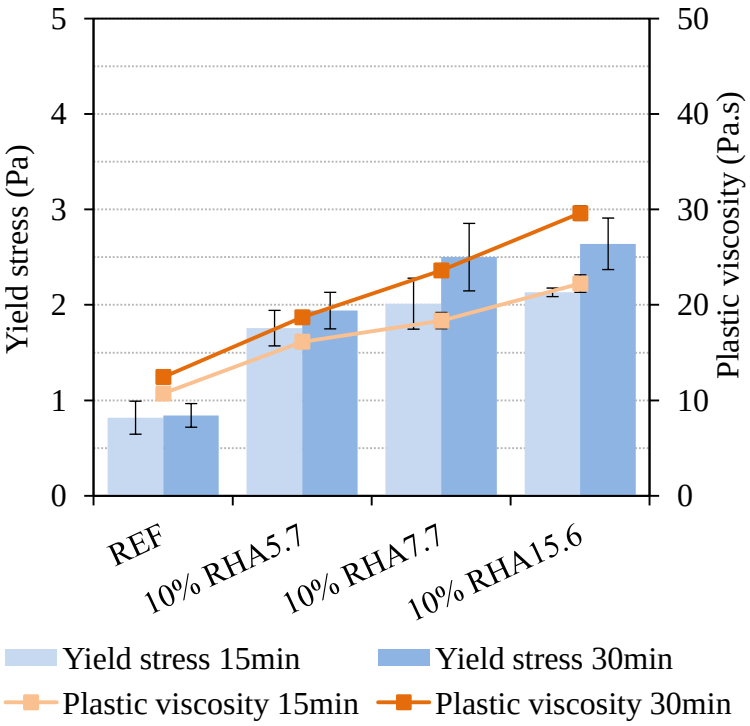

Fig. 6.17 Effect of RHA MPS on yield stress and viscosity of mortar, w/b of 0.26, 15 min and 30 min after water addition

In Fig. 6.18 and Table 6.3, it is obvious that the higher the RHA5.7/SF content, the higher the yield stress and plastic viscosity. The samples containing RHA had higher yield stress and viscosity than those of the SF containing samples and the reference sample (Fig. 6.17). Increasing level of yield stress and viscosity due to the higher RHA content was comparably higher than that due to the higher SF content (Fig. 6.18). It can be found that the effect of RHA content on the plastic viscosity increased and yield stress was stronger at the later age of 30 min (Fig. 6.18). These results are closely associated with the mini-slump flow and the T_{250} time (Fig. 6.13). Combining Fig. 6.18 and 6.13 shows that the increase in RHA5.7 content decreased mini-SLF slightly, but increased theyield stress and viscosity significantly, particularly at the later age.

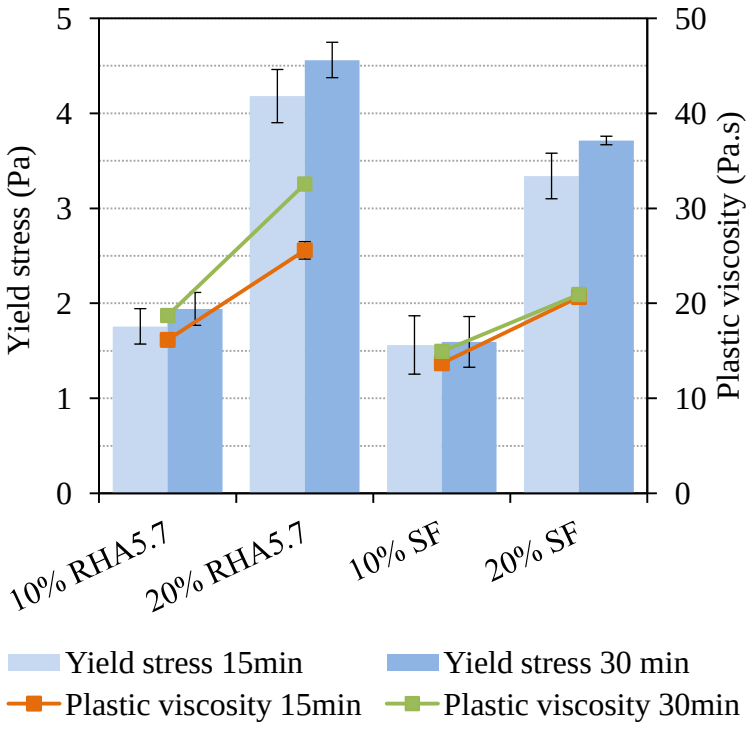

Fig. 6.18 Effect of RHA5.7 or SF content on yield stress and viscosity of mortar, w/b of 0.26, 15 min and 30 min after water addition

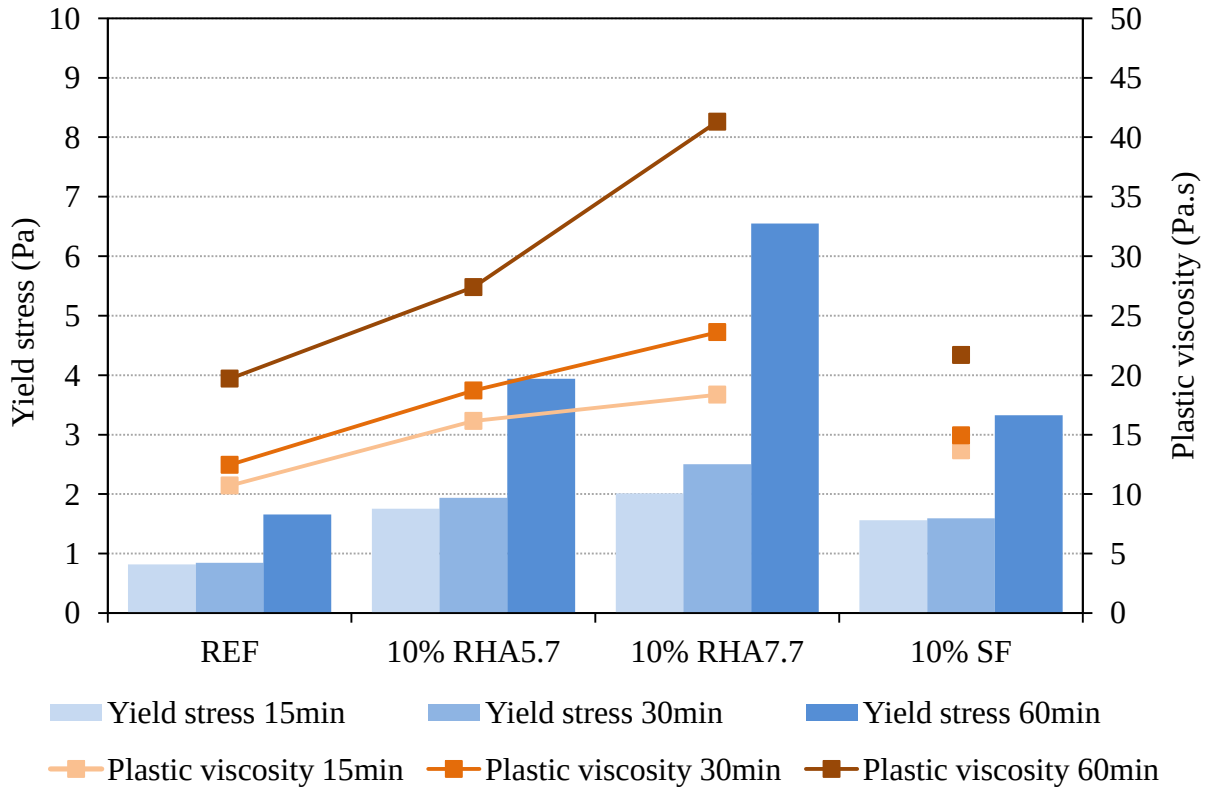

Fig. 6.19 Effect of RHA MPS on yield stress and viscosity of mortar over time

Table 6.3 Results of rheological measurements in accordance with Bingham model

Mixtures (w/b of 0.26)	15 min			30 min			60 min		
	τ_{01}	μ_1	γ_{crit}	τ_{01}	μ_1	γ_{crit}	τ_{01}	μ_1	γ_{crit}
REF	0.82	10.72	0.015	0.84	12.50	0.013	1.66	19.70	0.016
10% RHA5.7	1.76	16.14	0.021	1.94	18.70	0.020	3.90	27.39	0.028
20% RHA5.7	4.18	24.91	0.033	4.56	30.89	0.028	-	-	-
10% RHA7.7	2.01	18.35	0.021	2.50	23.61	0.021	9.07	41.30	0.043
10% RHA15.6	2.14	22.24	0.020	2.64	29.09	0.018	-	-	-
10%SF	1.56	13.67	0.023	1.59	14.93	0.022	3.14	21.07	0.029
20%SF	3.34	20.38	0.036	3.71	20.92	0.028	-	-	-

Shear-thickening behaviour of mortar in accordance with the modified Bingham model

The flow curves for mortars containing RHA/SF and the reference mortar 15 and 60 min after water addition are provided from Fig. 6.20 to Fig. 6.24 and Table 6.4. The shear-thickening behaviour ($c/\mu > 0$) was obtained from all samples regardless of binder composition. Together with the variation in plastic viscosity and yield stress, the shear-thickening degree of mortars, particularly the mortars containing RHA, was considerably changed over the time. Compared to the reference sample, the incorporation of RHA decreased the shear-thickening degree. 15 min after the water addition, increasing MPS of RHA led to a greater shear-thickening degree (higher c/μ value), as can be seen in Fig. 6.20. However, the situation was completely reversed at the age of 60 min, in respect of RHA5.7 and RHA7.7 (Fig. 6.22).

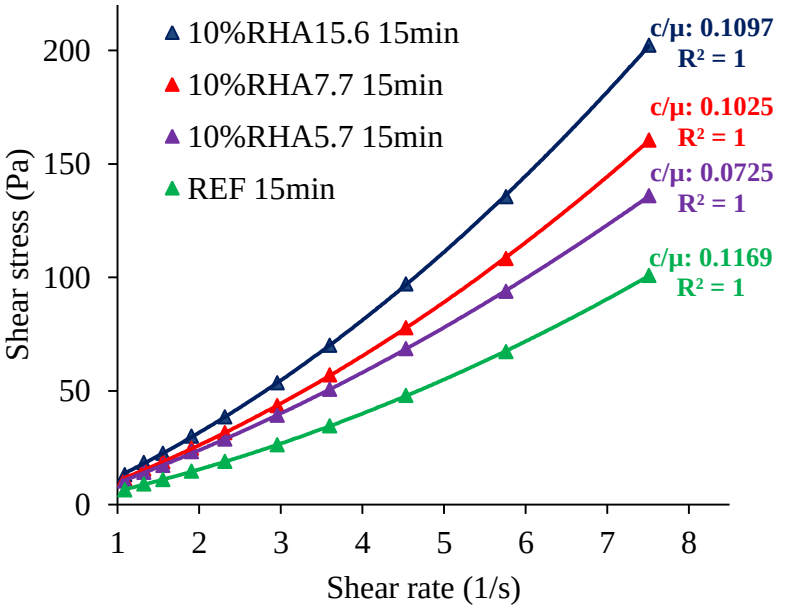

Fig. 6.20 Effect of MPS of RHA on shear thickening behaviour of mortar (w/b of 0.26, 15 min after water addition)

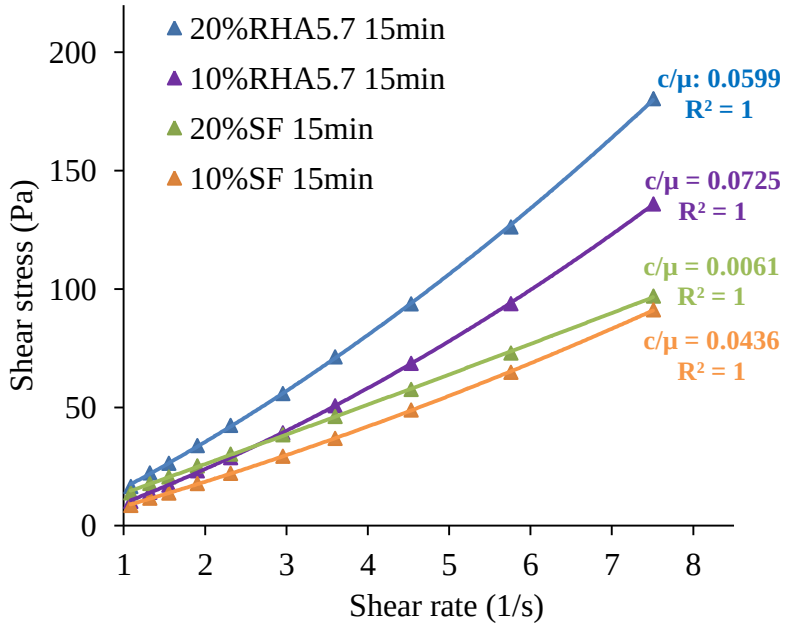

Fig. 6.21 Effect of RHA/SF content on shear thickening behaviour of mortar (w/b of 0.26, 15 min after water addition)

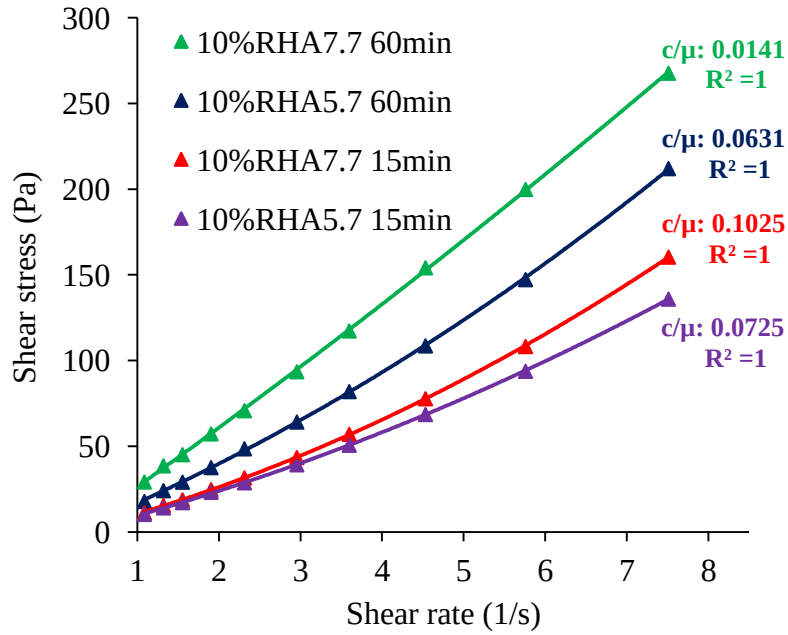

Fig. 6.22 Effect of MPS of RHA on shear thickening behaviour of mortar (w/b of 0.26, 15 and 60 min after water addition

In Fig. 6.21, the effect of RHA5.7/SF content on shear-thickening behaviour is shown. Increasing RHA/SF content resulted in lower shear-thickening degree or greater shear-thinning degree. This effect of SF was much stronger than that of RHA5.7. The flow curve for mortar containing SF expressed linearity (c/μ ≈ 0), especially with 20 wt.% SF.

The shear-thickening behaviour of mortars containing RHA5.7/SF at 15 and 60 min is presented in Fig. 6.23. 60 min after water addition, the mortars appeared less shear-thickening. The effect of RHA5.7 is similar to that of SF. Comparing with SF, the effect of RHA7.7 on reduction in shear-thickening degree was much stronger (Fig. 6.22 and Fig. 6.23).

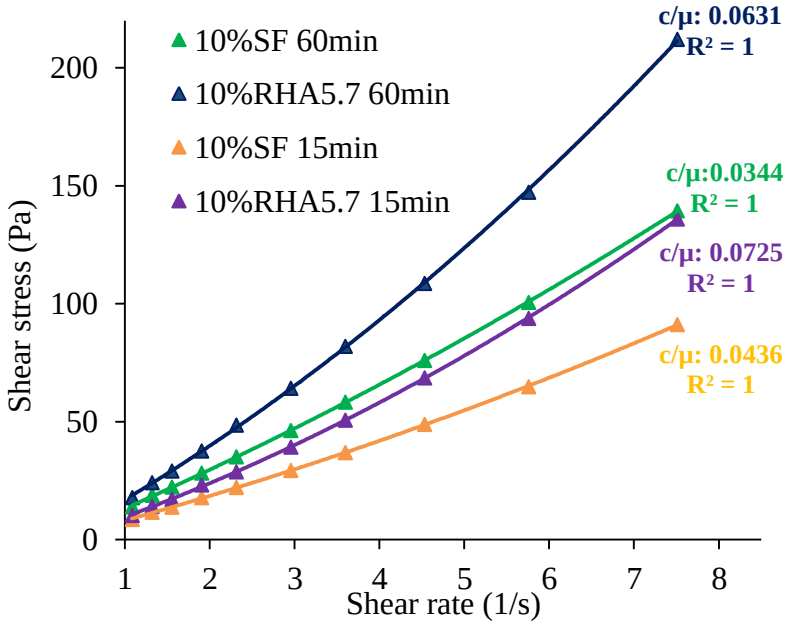

Fig. 6.23 *Shear thickening behaviour of mixture containing RHA in comparison with mixture containing SF (w/b of 0.26, 15 and 60 min after water addition)*

The shear-thickening behaviour of RHA5.7 containing sample and the reference sample at 15 min and 60 min is seen in Fig. 6.24. The reduction in shear thickening degree of the sample containing RHA5.7 appeared less than that of the reference sample. The c/μ ratios of RHA5.7 and the reference samples decreased from 0.0725 and 0.1169 to 0.0631 and 0.0768 respectively. The reduction in shear-thickening degree of RHA7.7 containing sample was considerably stronger than that of the reference sample, i.e. the c/μ ratio of RHA7.7 containing sample declined from 0.1025 to 0.0141 (Table 6.4).

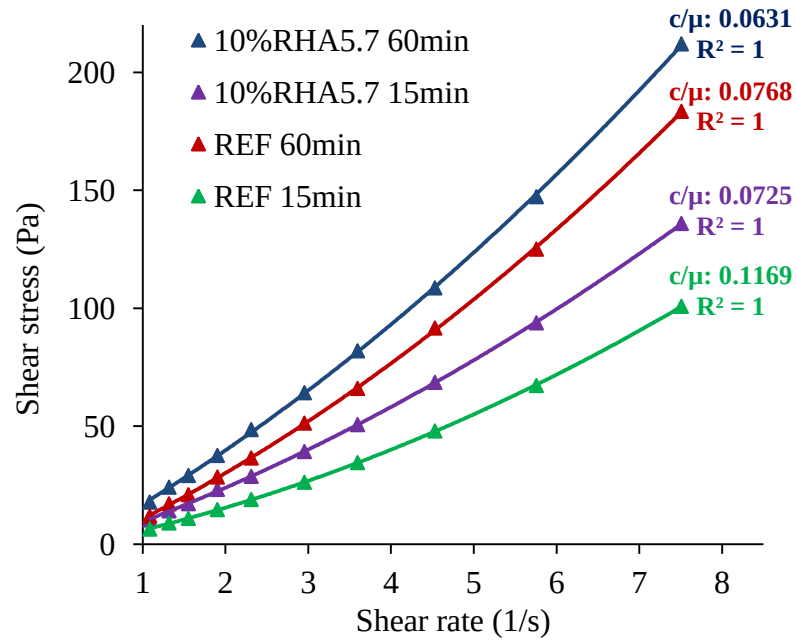

Fig. 6.24 Shear thickening behaviour of mixture containing RHA in comparison with reference mixture (w/b of 0.26, 15 and 60 min after water addition)

Table 6.4 Results of rheological measurements in accordance with modified Bingham model

Mixtures (w/b of 0.26)	15 min				60 min			
	τ_{02}	c	μ_2	c/μ	τ_{02}	c	μ_2	c/μ
REF	1.8005	0.9065	7.7513	0.1169	2.0407	1.2902	16.797	0.0768
10% RHA5.7	3.0576	0.9065	12.549	0.0725	6.4906	1.2788	20.278	0.0631
20% RHA5.7	6.9772	1.0408	17.383	0.0599	-	-	-	-
10% RHA7.7	3.6477	1.3323	12.998	0.1025	9.3328	0.473	33.637	0.0141
10% RHA15.6	3.7708	1.7538	15.982	0.1097	-	-	-	-
10%SF	3.2399	0.418	9.5901	0.0436	5.4108	0.5289	15.383	0.0344
20%SF	7.6094	0.0739	12.174	0.0061	-	-	-	-

6.3.6. Discussion

From the results shown above, it can be said that the rheological behaviour, i.e. yield stress, plastic viscosity, shear-thicken/thinning response and the resulting properties of fresh mortar were significantly affected by the incorporation of RHA. The effect of RHA on rheological properties strongly depends on the MPS and content of RHA used, and this effect changed significantly over the time of hydration.

Generally, the incorporation of RHA increases SSD (Fig. 6.5, Fig. 6.6 and Fig. 6.7), SP adsorption (Fig. 6.8), yield stress, and plastic viscosity (Fig. 6.17, Fig. 6.19 and Table 6.3), hence decreases the resulting mini-slump flow and increases the resulting mini-V-funnel time of mortar (Fig. 6.9). This effect is more pronounced, when a larger MPS and a higher content of RHA are used. A similar effect was obtained when SF was admixed. However, the effect of SF is much lower than that of RHA, particularly when the higher amount and the coarser RHA are used. This means that SF containing mortar has lower SSD, lower yield stress, and plastic viscosity compared to RHA containing sample (Fig. 6.18 and Table 6.3). Similar to SF, RHA has a very high SSA and its particles are chemically highly reactive and may have an affinity for multi-layer adsorption of SP molecules [208]. Using RHA/SF as replacements for cement leads to an increase in SSA of the binder (cement+RHA/SF) thus to an increase in the SP adsorbed surface (Fig. 6.8) and to a decrease in free water compared to the mortar made without RHA/SF. As a result, the mortar incorporating RHA/SF has the higher SSD, the higher SP adsorption, the higher yield stress, and the plastic viscosity and the lower mini-slump flow.

The time-dependent properties of mortar containing RHA are significantly different from those of the reference and SF containing samples. 60 min after the water addition, the RHA containing samples lost much more mini-slump flow and had significantly higher plastic viscosity than the reference and SF containing samples (Fig. 6.13 and Fig. 6.19). For the RHA containing samples, the increase in plastic viscosity is more significant than the mini-slump flow loss. It is generally known that workability retention of fresh concrete is mainly affected by the depletion of the free water in fresh concrete. The free water from a concrete mixture is removed by hydration reactions, by adsorption on the surfaces of hydration products, by the water adsorption in the case of dry aggregate [209-212]. The results in Section 4 show that RHA used in this study is a macro-mesoporous material. RHA will absorb a certain amount of

water. For example, with 10 wt.% cement replacement by RHA22.6, the amount of water needed to fully fill the pore volume in RHA22.6 particles is about 10.4 liter/m^3 mortar and about 4.7 wt.% mixing water. That results in the decrease in free water and hence the decrease in mini-slump flow and the increase in plastic viscosity. At very low w/b ratio of 0.26, the free water in the paste is very low, and hence the water adsorption into the pores of RHA particles might progress in a certain period of time. That might be the main reason for the larger mini-slump flow loss and the significantly higher plastic viscosity of RHA containing mortar 60 min after water addition, especially with coarser RHA and higher content of RHA used. Furthermore, the water adsorption of RHA particles over time induces suction force, which may compose clusters. The formation of the clusters will jam the flow of the particles or increase the inter-particular bonds, as in the clustering theory [213-216], thus might also result in the higher plastic viscosity of RHA blended paste in mortar.

Flow curves of all rheological measurements show that mortar formulated from SCHPC is a shear-thickening material (Fig. 6.20-Fig. 6.24). The shear-thickening degree decreased over time and depends on the MPS of RHA and the content of RHA/SF. The incorporation of RHA/SF leads to the lower mini-slump flow of mortar (Fig. 6.13), which is possibly attributed to the lower shear-thickening degree of RHA/SF containing samples, as mentioned elsewhere [91].

For RHA containing samples, 15 min after the water addition, the coarser the MPS of RHA, the higher the degree of shear-thickening is. As seen in Fig. 4.7 and Table 4.1, the coarse RHA (RHA15.6 and RHA7.7) has larger pore volume than the fine one (RHA5.7). Therefore, incorporating the coarse RHA will lower the free water and also increase the particle size of the granular mixtures of paste in mortar. That might result in a greater shear-thickening degree of mortar of the coarse RHA containing samples compared to that of RHA5.7 containing sample. Increasing content of RHA5.7, which has a smaller grain size than cement (7.07µm), decreases shear-thickening response possibly due to better poly-dispersion [217] and better packing density of granular mixtures. 60 min after the water addition, however, the increase in MPS of RHA decreased the shear-thickening degree of mortar. This can be assumed to the higher mini-slump flow loss of RHA7.7 containing sample. The specific reason for this phenomenon is still unknown.

Different from RHA, SF particles are much finer, spherical and dense, hence SF with ''ball bearing effect'' and lower water demand will increase the mini-slump flow and decrease viscosity and degree of shear-thickening. Moreover, with ultra-fine particles, the incorporation of SF will make poly-dispersion and the packing density of granular mixtures better. Therefore, increasing SF content led to significantly lower degree of shear-thickening (Fig. 6.21).

The results obtained show that the reduction in shear-thickening degree of RHA containing sample, such as RHA7.7, was stronger than reference and SF containing samples respectively (Fig. 6.22, Fig. 6.24 and Table 6.4). The explanation can be based on the higher mini-slump flow loss of RHA7.7 containing sample. It can be hypothesized that the pores in RHA particles might be saturated by water after 60min. This results in lower suction force, and hence weaker inter-particular bind.

6.3.7. Concluding remarks

- The incorporation of RHA increases the SP adsorption of paste and the SP saturation dosage of mortar. Increasing MPS and content of RHA increases the SP saturation dosage of mortar, whereas increasing MPS of RHA decreases SP adsorption of paste. The lower the w/b ratio, the higher the SP saturation dosage of mortar.
- The incorporation of RHA decreases the mini-slump flow, and increases the yield stress and plastic viscosity. This effect is much stronger than that of SF, especially when the coarser RHA and the higher content of RHA are used.
- The increase in MPS and content of RHA predominantly increases plastic viscosity rather than decreases the mini-slump flow of mortar. Therefore, the flowing ability of mortar or SCHPC is slightly affected, while the plastic viscosity and hence segregation resistance of SCHPC can be controlled by the MPS and the content of RHA used.
- 60 min after water addition, mini-slump flow loss and the increase in plastic viscosity of mortar containing RHA is significantly higher than those of reference sample and SF containing sample, possibly due to the progress of water adsorption of RHA.
- 60 min after water addition, the increase in MPS and content of RHA predominantly increases plastic viscosity rather than decreases the mini-slump flow of mortar. It can be explained by the formation of cluster due to the water suction force of RHA.
- Mortar formulated from SCHPC is a shear-thickening material. The degree of shear-thickening declines over time. The incorporation of RHA/SF causes a decline in degree of shear-thickening possibly due to the reduction in mini-slump flow.
- 15 min after water addition, the increase in MPS of RHA leads to the higher shear-thickening degree possibly due to the formation of cluster of RHA particles and the increase in particle size of the granular mixtures. After 60 min, however, the increase in MPS of RHA causes a decrease in the degree of shear-thickening. This can be ascribed to higher mini-slump flow loss, and the weaker inter-particular bind due to the water saturation of RHA particles.
- From 15 to 60 min water addition, the reduction in shear-thickening degree of RHA7.7 containing mortar is greater than those of the reference sample and SF containing sample respectively.
- The increase in RHA5.7/SF content decreases the shear-thickening degree of mortar, where the effect of SF is much stronger than that of RHA5.7. It is attributed to the better poly-dispersion.

7. Hydration and microstructure development of mortar formulated from SCHPC

7.1. Mixture proportions of mortar

To investigate the hydration, microstructure development and the resulting compressive strength (in Section 8) of mortar formulated from SCHPC, ordinary Portland cement, undensified SF, RHA5.7, RHA7.7, RHA12.0, RHA15.6, RHA22.6, and natural sand with a maximum size of 2 mm were used. The mixture proportions of mortar are presented in Section 6.1. 10-30 wt.% cement content was replaced by RHA or SF at w/b of 0.26 and 0.30. The workability of the mortars is presented in Section 6.3.

The hydration and microstructure development of the blended cement paste in mortar were investigated on a reference sample and samples containing 10 wt.% SF, RHA5.7, and RHA22.6 at w/b of 0.26. The results in Section 4 show that the RHA in this study is a macro-mesoporous material, and the pore size distribution is the most important physical property of RHA. The decrease in MPS leads to the reduction in macro pores and the increase in external SSA of RHA. The pore structure of RHA has the strong effect on the rheological properties of mortar and SCHPC, as presented in Section 6. With the same silica content, RHA5.7 and RHA22.6 have a big difference in pore structure, i.e. pore size distribution. It is expected that the variation in pore structure of RHA will strongly influence the hydration and microstructure development of the blended cement. The effect of the pore structure on hydration and microstructure of the blended cement paste can be evaluated by the difference in the hydration and microstructure of samples containing RHA5.7 and RHA22.6.

7.2. Hydration investigations

7.2.1. Degree of cement hydration by quantitative X-ray diffraction

Based on the unhydrated clinker minerals (C_3S, C_2S, C_3A, C_4AF) at 3, 7, 14, 28 and 91 days the degree of cement hydration was determined. The percentage of the unhydrated clinker minerals and the corresponding degree of cement hydration in the paste of mortar are shown in Fig. 7.1 and Fig. 7.2 respectively. It is clearly obtained that the incorporation of RHA/SF increased the degree of cement hydration in the blended cement paste of mortar compared to the reference sample, irrespective of age, except the sample containing RHA22.6 at 3 days. Interestingly, the hydration of cement in the SF/RHA

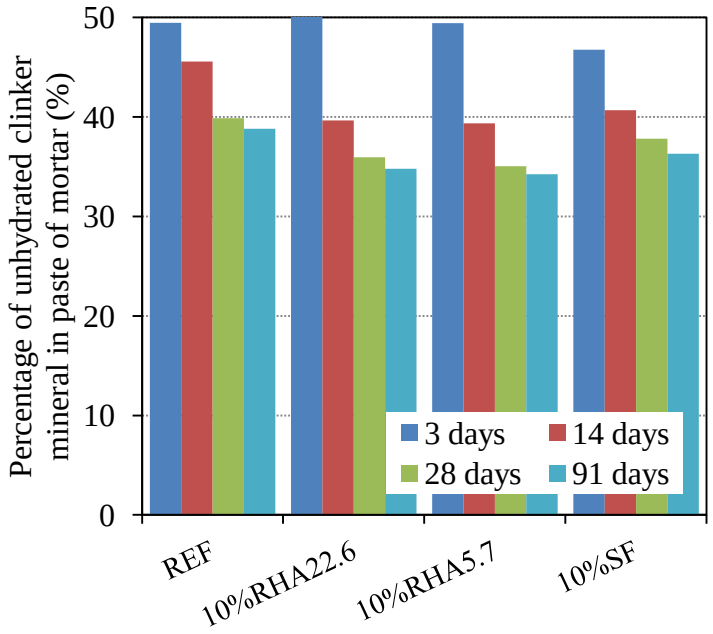

Fig. 7.1 Percentage of unhydrated klinker minerals in paste of mortar

blended paste changed over time depending on the SSA and pore structure of RHA. After 3 days, the cement hydration in the SF blended cement paste dominated those in the RHA 5.7 and RHA22.6 blended cement paste respectively. It might be closely related to the SSA of SF and RHA (Table 3.2, Table 4.1 and Fig. 4.2) resulting in the higher nucleation site effect on the hydration of cement. The situation reverted at the later ages. The cement in the RHA blended paste hydrated much more than that in SF blended paste, especially at 28 and 91 days. The effect of RHA on the hydration of cement depended on its particle size, i.e. SSA and pore size distribution in RHA particles. The sample containing RHA5.7 had a higher degree of cement hydration at 3 days than that of the sample containing RHA22.6, however, similar to that of the sample containing RHA22.6 at 14, 28 and 91 days. That indicates the coarse RHA22.6 promoted the hydration of cement more than the fine RHA5.7 at the later ages (from 3 to 91days).

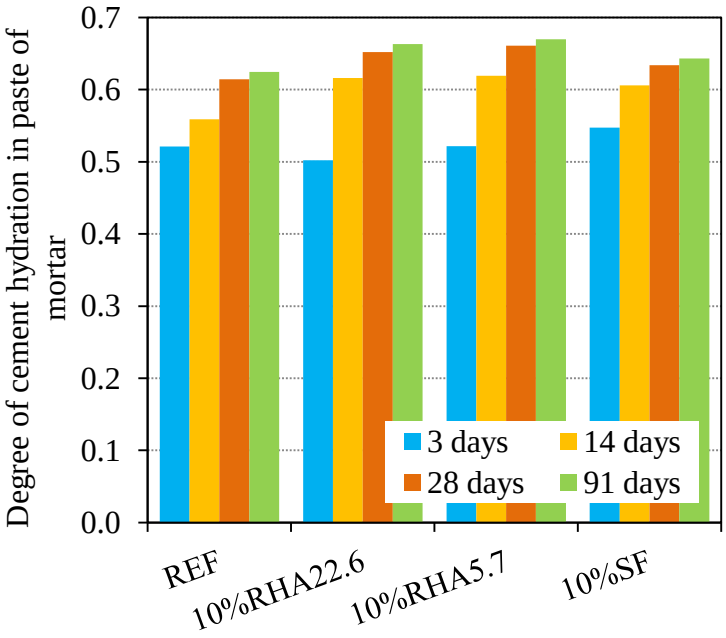

Fig. 7.2 Degree of cement hydration in paste of mortar by QXRD

7.2.2. Degree of cement hydration by BSE-imaging analysis

The degree of cement hydration was also determined by BSE-imaging analysis. Based on the BSE images, the unhydrated cement areas in the paste of mortar were determined by means of grey levels of phases in the cement matrix. The percentage of unhydrated cement and the corresponding degree of cement hydration in paste of mortar at 28 and 91 days are shown in Fig. 7.3 and Fig. 7.4 respectively. The degree of cement hydration determined by BSE-imaging analysis was similar to that determined by QXRD (Fig. 7.2 and Fig. 7.4). Therefore, the determination of the degree of cement hydration by BSE imaging analysis can be acceptable.

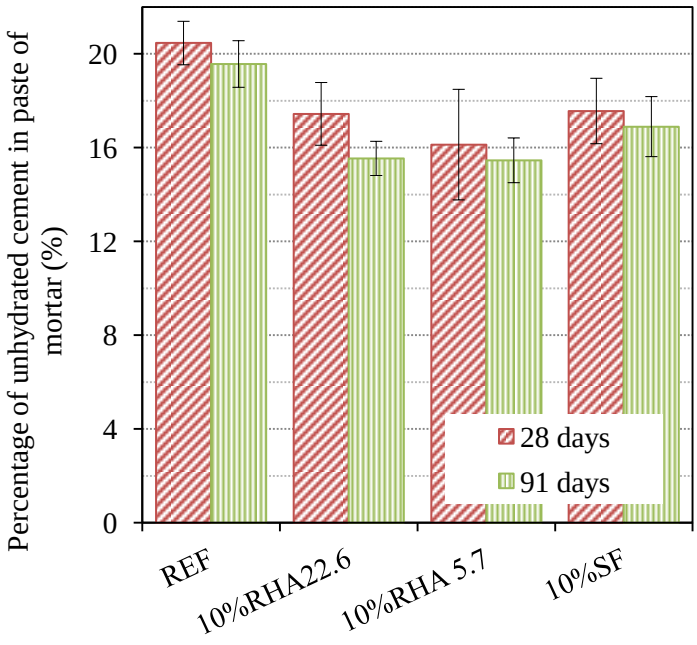

Fig. 7.3 The percentage of undydrated cement in paste of mortar

7.2.3. The hydration of C_3S and C_2S in the blended cement paste of mortar

As analyzed above, the cement hydrated over time, however the hydration of each clinker mineral varied depending on SCMs used. The obtained results of the unhydrated clinker minerals shown that in all samples, C_3A is not detected. It indicates that C_3A hydrated completely after 3 days. The C_3S, C_2S and C_4AF hydrated over time with different rates. The degree of C_3S hydration in cement paste is shown in Fig. 7.5. It is clearly found that the incorporation of RHA/SF dramatically increased the hydration of C_3S. After 14 days, the degree of C_3S hydration of the sample containing RHA/SF was significantly higher than that of the reference sample. The hydration rate of C_3S in RHA/SF blended cement paste was much higher than that of the reference sample especially from 3 to 14 days. And the hydration rate of C_3S in all samples kept constant after 28 days.

The hydration of C_2S over time is displayed in Fig. 7.6. It is clear that degree of C_2S in the reference sample was higher than that of RHA/SF containing samples. Combining Fig. 7.5 and Fig. 7.6 indicates that when C_3S hydrated faster, the hydration of C_2S might slow down in RHA/SF containing samples. And both the degree of C_2S and C_3S hydration in the RHA blended cement paste were higher than those in the SF blended

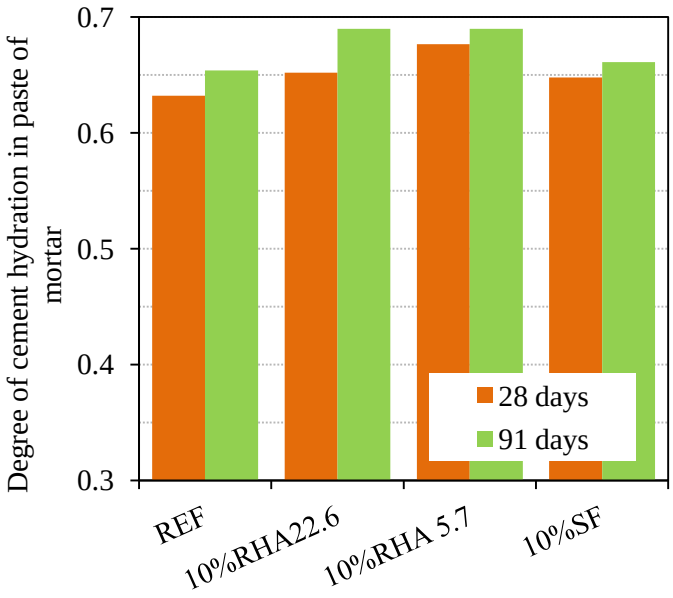

Fig. 7.4 The degree of cement hydration in paste of mortar by BSE-imaging analysis

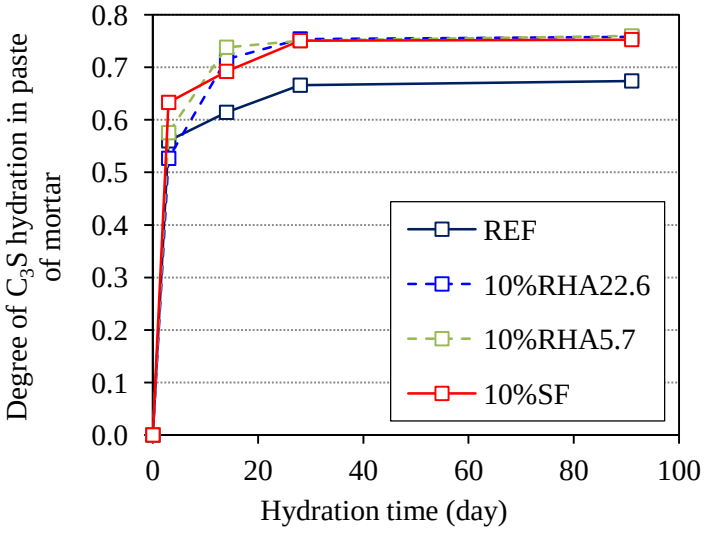

Fig. 7.5 Hydration of C_3S in paste of mortar over the time

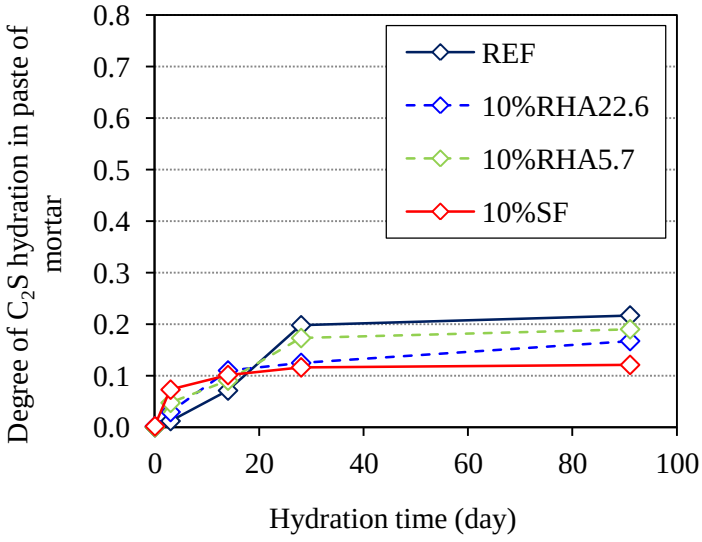

Fig. 7.6 Hydration of C_2S in paste of mortar over the time

cement paste. With these results, it can be said that the incorporation of RHA/SF increased the degree of cement hydration, i.e. C_3S hydration. And the higher degree of cement hydration in the RHA blended cement paste compared to that in the SF blended cement paste was due to the higher degree of C_3S and C_2S hydration.

7.2.4. Calcium hydroxide content in the blended cement paste of mortar

The CH content of mortar samples over time is shown in Fig. 7.7. It can be found that the CH content of the control sample increased with ages. The incorporation of RHA/SF reduced the CH content at late ages, e.g. 91days, where the effect of SF was greater than that of RHA5.7 and RHA22.6, respectively. However, the effect of RHA5.7 dominated those of SF and RHA22.6 at earlier ages (3 and 28 days). This result is closely related to the result of the pozzolanic reactivity presented above. The pozzolanic reaction of the fine RHA5.7 might occur faster and earlier, and hence the CH consumption of the fine RHA exceeds those of RHA22.6 and SF at early ages (3 and 28 days). By contrast, at 91days, the CH consumption of SF and RHA22.6 due to the pozzolanic reaction was greater than that of RHA5.7 in the blended cement paste, as seen in Fig. 7.7.

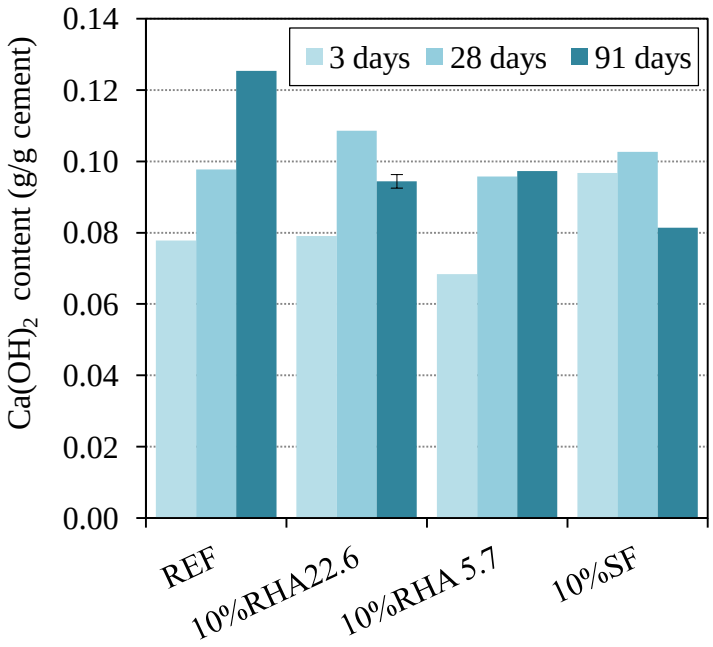

Fig. 7.7 The calcium hydroxide content in the blended paste of mortar over time

7.2.5. Pozzolanic reaction of RHA in the blended cement paste of mortar

Hydrated RHA particles in the blended cement matrix are shown in Fig. 7.9a and Fig. 7.10-Fig. 7.12. The RHA particles were embedded into the matrix after 28 days. The chemical composition of phases formed in the RHA blended cement matrix were analyzed by EDX-phase mapping (Fig. 7.9b). As expected, the C-S-H phases were formed surrounding the RHA particles due to the pozzolanic reaction after 28 days. The chemical composition and X-ray spectra for outer C-S-H phases formed outside RHA particles are presented in Table 7.1 and Fig. 7. 8b,d. With average values of SiO_2 and CaO contents, the Ca/Si molar ratio calculated was about 1.28. These low Ca/Si C-S-H phases are described as ''tobermorite-like'' C-S-H compared to the high Ca/Si C-S-H ''jennite-like'' (Ca/Si~1.7) generated from Portland cement. The low Ca/Si C-S-H trapped significant amounts of Cations, i.e. aluminium, magnesium, potassium, sodium ions.

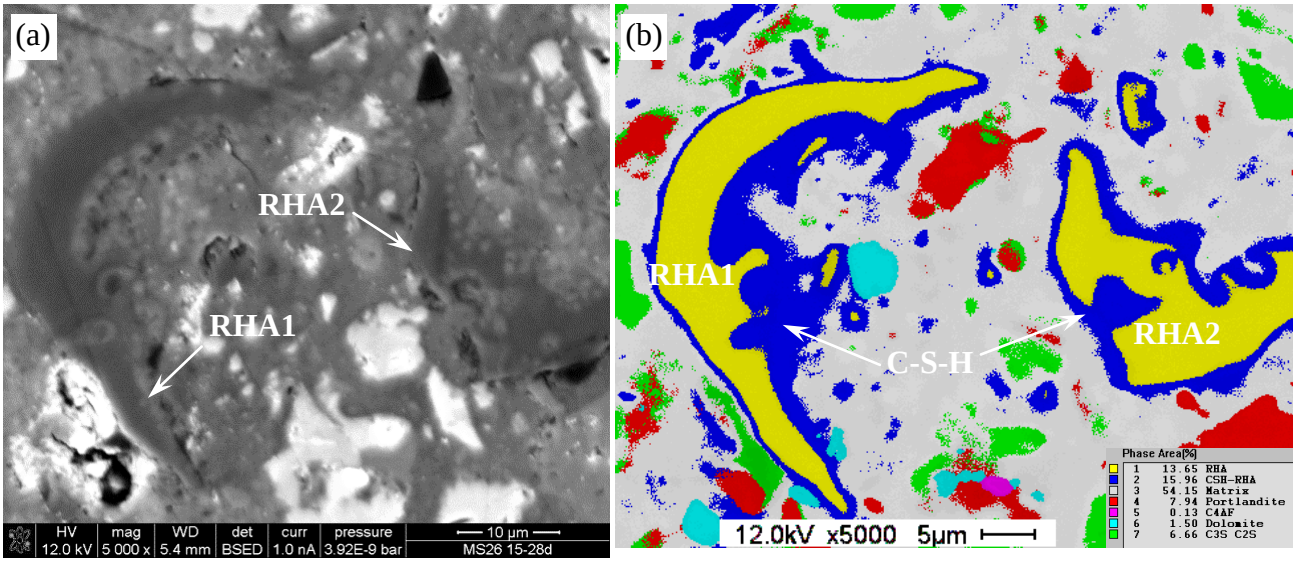

Fig. 7.9 BSE-SEM image (a) and EDX-phases mapping (b) of RHA22.6 blended cement matrix at w/b of 0.26 after 28 days hydration. RHA in yellow, RHA-hydrate rim in blue, portlandite in red, C_2S-C_3S in green, C_4AF in pink, and matrix in white

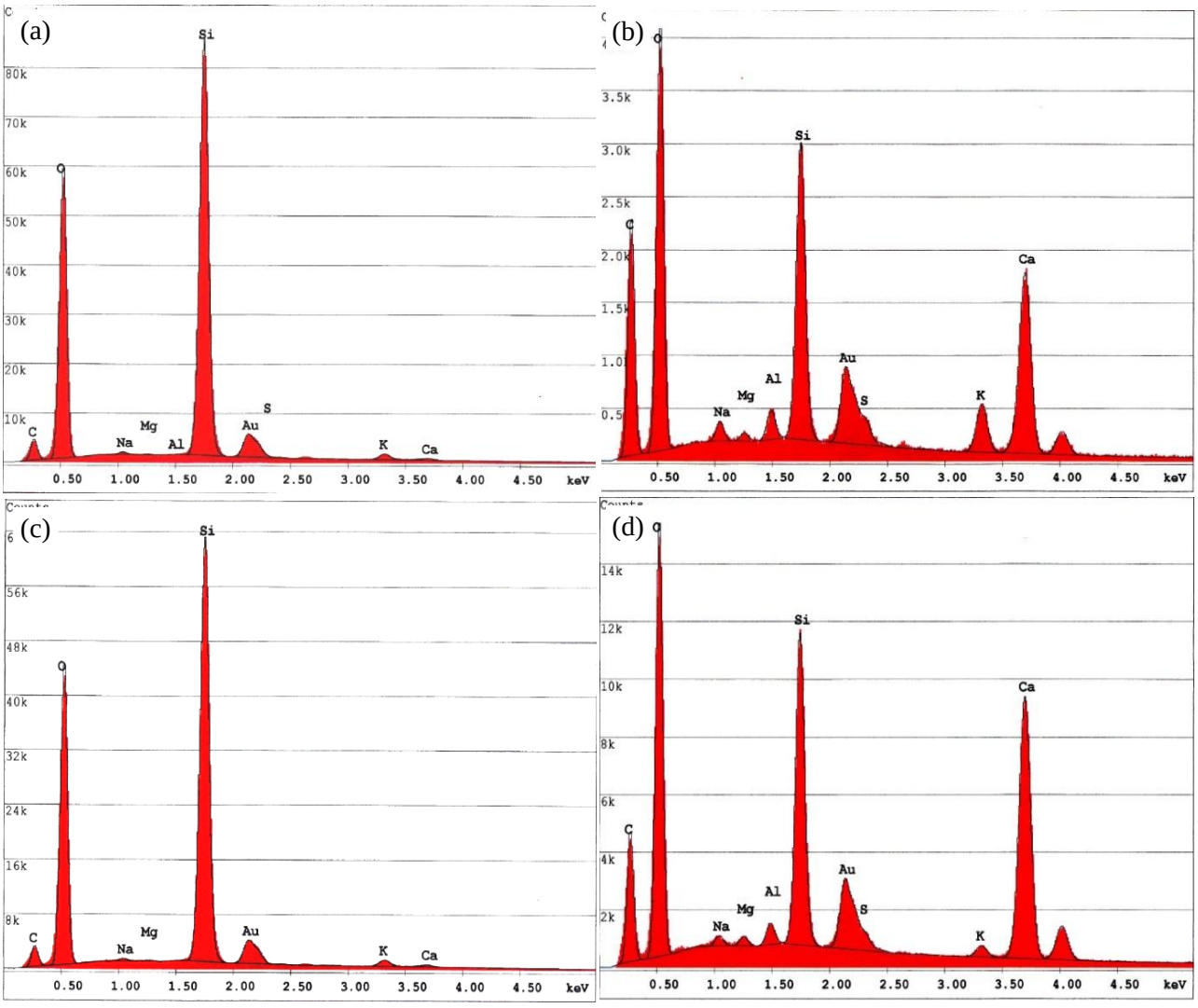

Fig. 7. 8 X-ray spectra for hydrated RHA particles: remnants of RHA particles (a, c) and hydrate rim of RHA particles (b, d), i.e. C-S-H phases, showing in Fig. 7.9b

Table 7.1 Chemical composition (wt.%) of RHA hydrate-rim quantified by EDX-mapping in Fig. 7.9b

Oxides	SiO_2	CaO	Na_2O	K_2O	Al_2O_3	MgO	Ca/Si	(Na+K)/Si
Hydrate RHA1	41.25	41.81	1.95	8.29	3.82	0.76	1.09	0.35
Hydrate RHA2	39.15	54.26	0.95	1.73	2.5	0.88	1.49	0.1
Mean value	40.2	48.03	1.45	5.01	3.16	0.82	1.28	0.23

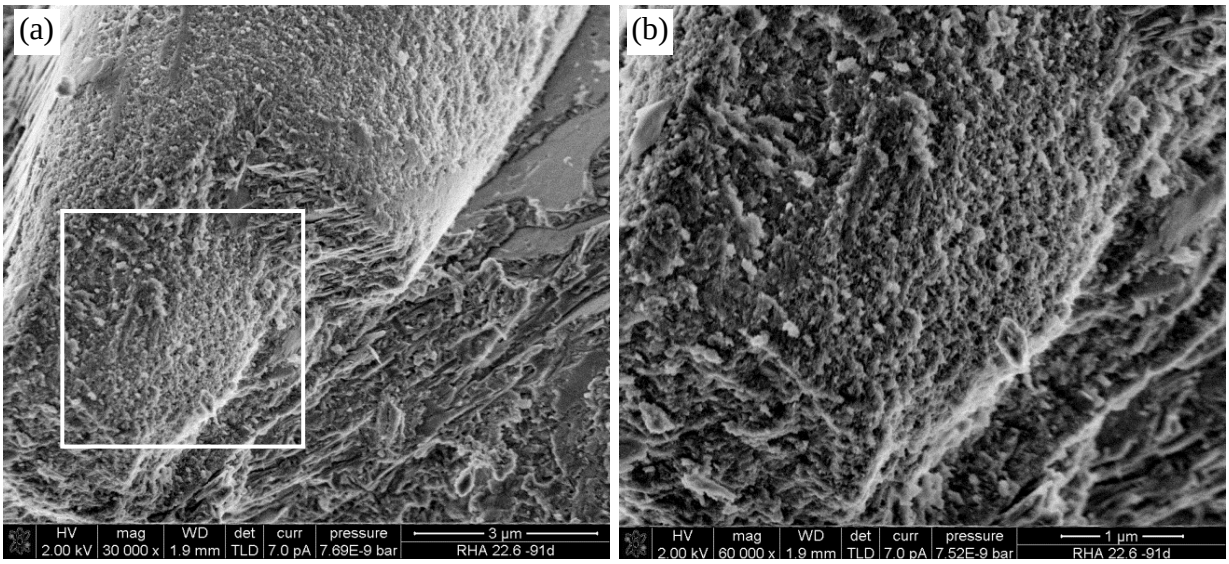

Fig. 7.10 Hydrated RHA particle in the blended cement matrix after 91 days (a) and dissolution surface of the hydrated RHA particle (b)

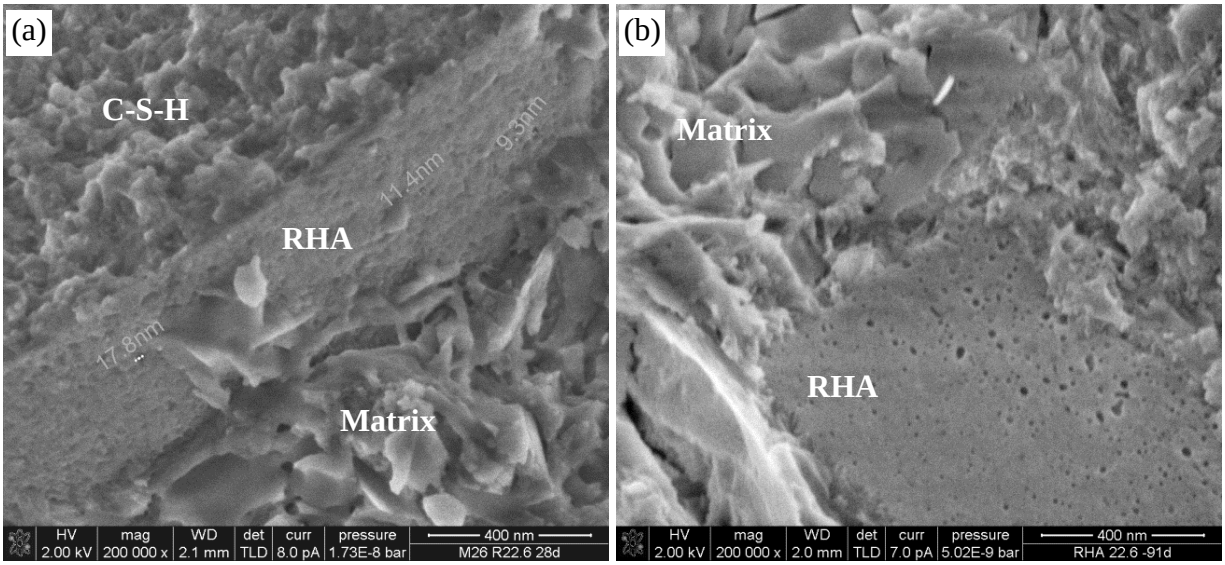

Fig. 7.11 Pozzolanic hydration products,i.e C-S-H phases, formed on the surface of RHA particle after 28 days (a) and pozzolanic hydrates formed partially filled in pores of RHA particle at 28 days (a) and at 91 days(b)

In Fig. 7.11a and Fig. 7.12 a, the pore structure of hydrated RHA particle is shown. The RHA particles were embedded into the bulk cement matrix. The pores in RHA particles were partially filled by the hydration products, i.e. C-S-H phases. By combining BSE-SEM image (Fig. 7.12) and EDX-mapping image (Fig. 7.12 b), it can be found that calcium ions from the cement matrix

penetrated into the pores of the RHA particle. This indicates that the pozzolanic reaction, i.e. ‘‘internal pozzolanic reaction’’ would occur in the pores. And the pozzolanic reaction products, i.e. C-S-H phases, precipitated on the surfaces in the pores. The pores would be filled by the reaction products over time.

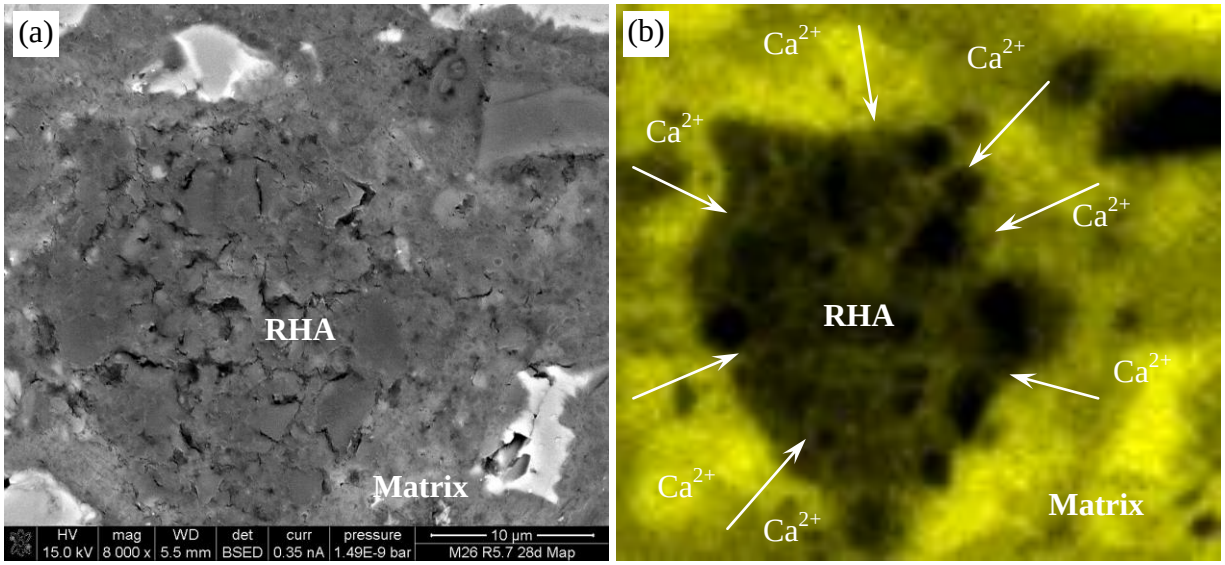

Fig. 7.12 BSE-SEM image of RHA particle in the blended cement matrix (a), The distribution of Ca inside and outside RHA particle by EDX-Ca-mapping (b) at w/b of 0.26 after 28 days hydration

7.3. Microstructural investigations

7.3.1. Microstructural analysis by imaging

The BSE images of the reference sample and samples containing SF, RHA5.7 and RHA22.6 are shown in Fig. 7.13. It is clear to find the common microstructural features, i.e. the remnant cement cores, fully hydrated cement particles (normally small ones), pores, hollow shells (Halley grains), and very thin and unclear Interface transition zone (ITZ) between sand particles and the bulk cement matrix. It can be qualitatively observed that the microstructure of SF containing sample is denser and finer than those of RHA5.7, RHA22.6 containing samples and the reference sample. The matrix of the sample with SF contains smaller and fewer pores than those of RHA5.7, RHA22.6 containing samples and the reference sample. The qualitative observation closely corresponds to the porosities determined by MIP (Fig. 7.18 and Table 7.2). Moreover, the pores in the SF blended matrix appear to be distributed more homogenously. This can be associated with the distribution of SF particles (Fig. 7.15a and Fig. 7.16b) whose pozzolanic hydrates fill capillary pores. The ITZ between sand surface and blended cement matrix in all samples is thin and unclear, especially ITZ of SF containing sample. The ITZ of SF containing sample determined by the variation in grey level also reflected a similar result (Fig. 7.14). In this study, the hollow shells were only observed in the sample containing RHA22.6 even at the late age of 91 days, as marked by solid white arrows in Fig. 7.13d.

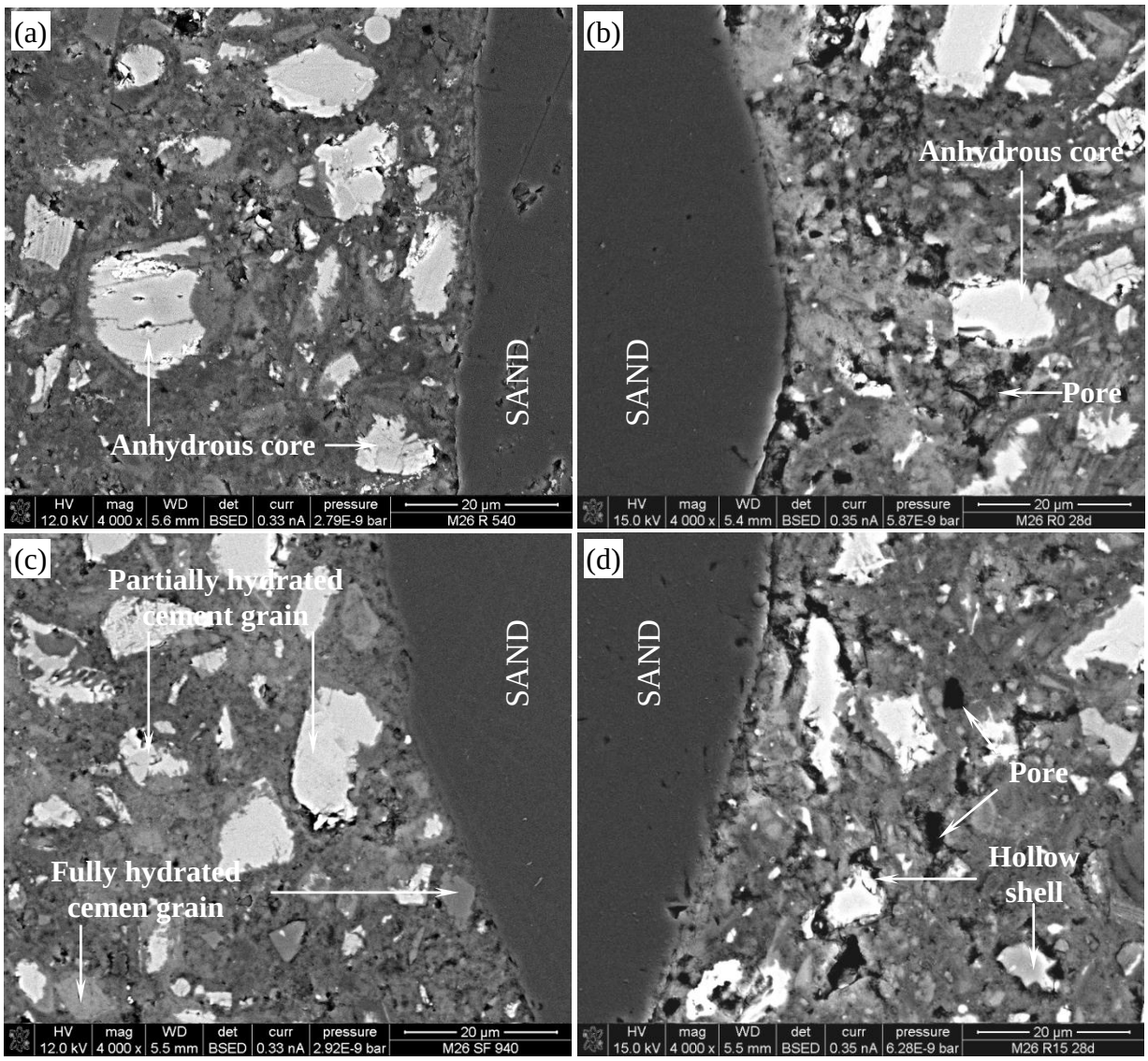

Fig. 7.13 The BSE images of the reference sample (b), and samples containing 10 wt.% SF(c), RHA5.7(a) and RHA22.6(d) at 28 days, w/b ratio of 0.26

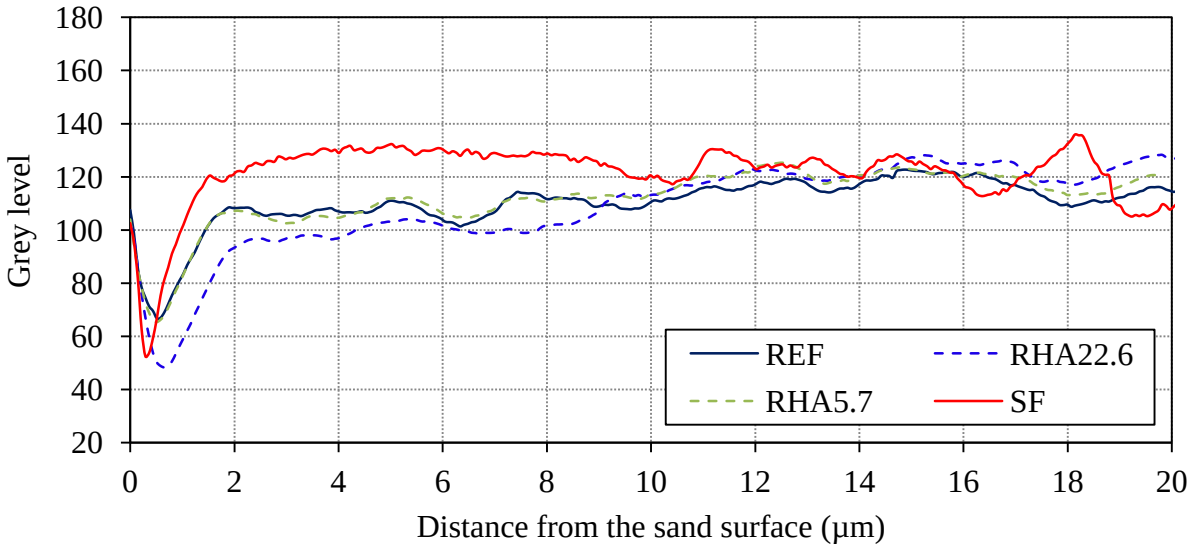

Fig. 7.14 The thickness of ITZ of mortar samples by analysing the variation in the grey level, at 91 days, w/b ratio of 0.26

The distributions of RHA/SF particles (in light blue) in the blended cement matrix are shown by BSE-EDX mapping images (Fig. 7.15). More SF particles than RHA particles can be found, and SF particles were distributed much better than RHA particles in a certain area of the blended cement matrix.

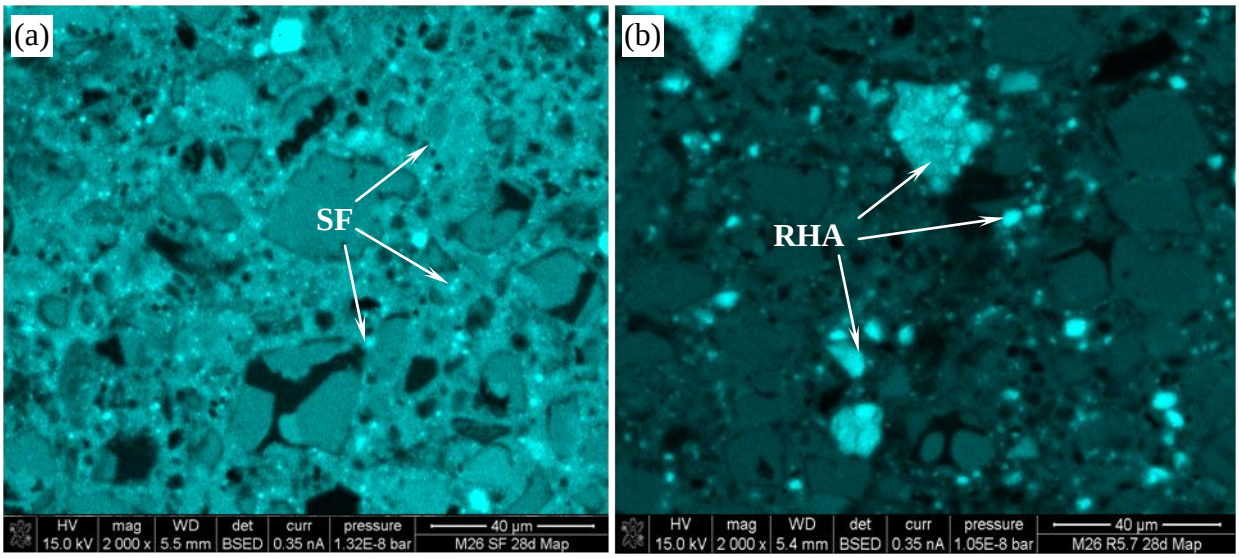

Fig. 7.15 EDX-Si-mapping, the distribution of SF (a) or RHA particles (b) (in light blue) in the blended cement matrix, at w/b of 0.26 after 28 days hydration.

7.3.2. Distribution of calcium, alkali and silicon in the blended cement matrix of mortar

The distributions of calcium in yellow, alkali (mainly potassium) in red, and silicon (indicating RHA/SF particle) in blue in the blended cement matrices of SF and RHA5.7 containing samples are shown in Fig. 7.16 and Fig. 7.17, respectively. Combining Fig. 7.15a and Fig. 7.16b indicates that the ultra fine SF particles were well-dispersed in the blended cement matrix. This results in the well-dispersed silicon and alkali, and hence the pH value would be homogenous, and pozzolanic reaction would occur homogenously in the SF blended cement matrix.

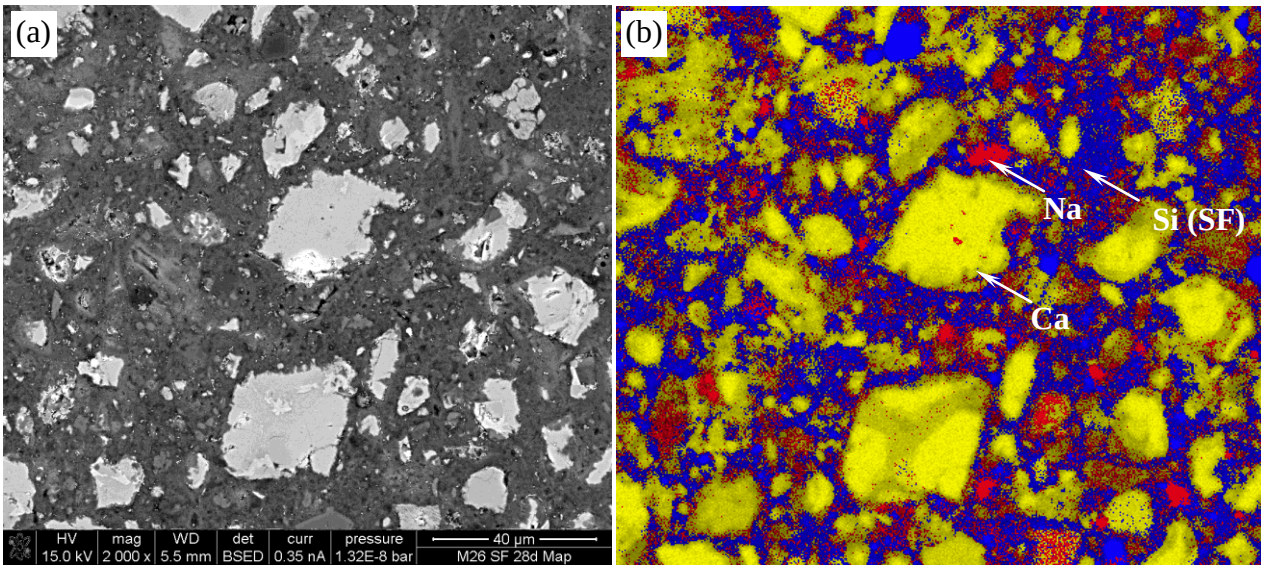

Fig. 7.16 BSE-SEM image of SF blended cement matrix at w/b of 0.26 after 28 days hydration(a) and EDX mapping showing K in red, Si in blue, and Ca in yellow (b)

RHA particles with large difference in the individual particle sizes, however, were not well-dispersed in the matrix (Fig. 7.15b and Fig. 7.17b). This results in the heterogeneity and high concentration of silicon and alkali next to the RHA particles and inside the RHA particles, i.e. in pores, and hence heterogeneity of pH value and the pozzolanic reaction in the RHA blended matrix. The coarser the RHA particle, the higher the concentration of silicon and alkali is. The high concentration of alkali might lead to the concern of alkali silica reaction.

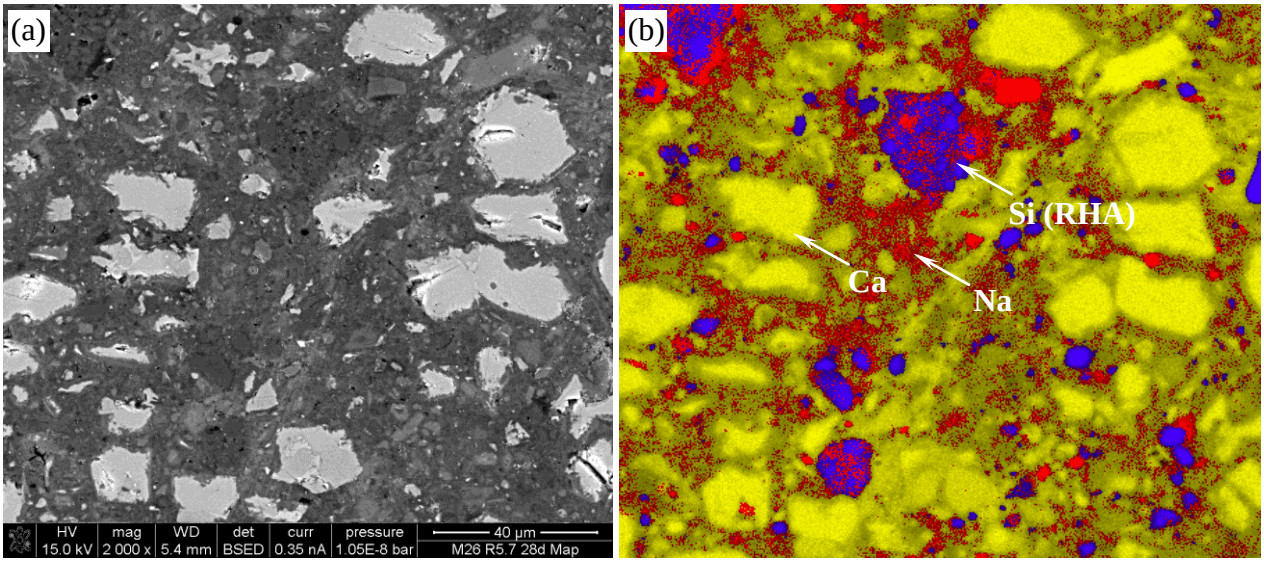

Fig. 7.17 BSE-SEM image of RHA5.7 blended cement matrix at w/b of 0.26 after 28 days hydration(a) and EDX mapping showing K in red, Si in blue, and Ca in yellow (b)

7.3.3. Pore structure in the blended cement matrix of mortar

In Table 7.2 and Fig. 7.18 the capillary porosity and pore size distribution of mortar samples measured by MIP at 3, 28 and 91days are presented. It can be clearly observed that the first peak indicating ''critical pore diameters'' [148, 178] of the differential curve of all samples was lower than 0.014 µm even after 3 days. Towards later ages the peaks move toward the left, indicating the critical pore diameters is refined over time. The inclusion of RHA refined the pore structure and reduced the pore volume as well. The pore-refining effect increased in the following order – coarse RHA < fine RHA < SF. The critical pore diameter of SF containing sample significantly decreased from 0.014µm at 3 days to 0.004 µm at 91days compared to that of RHA 5.7 containing sample from 0.014 to 0.006 µm respectively. Particularly, from 28 to 91 days the capillary porosity of SF containing sample dramatically decreased from 7.62 to 2.13 %. This pore refinement was closely related to the pozzolanic reactivity indicated by CH consumption (Fig. 7.7).

Table 7.2 Capillary porosity (%) of mortar samples at 3, 28 and 91 days

Ages	REF	10% RHA22.6	10% RHA5.7	10% SF
3 days	12.06	11.90	11.51	10.77
28 days	8.85	7.81	6.69	7.62
91 days	7.69	7.35	5.53	2.13

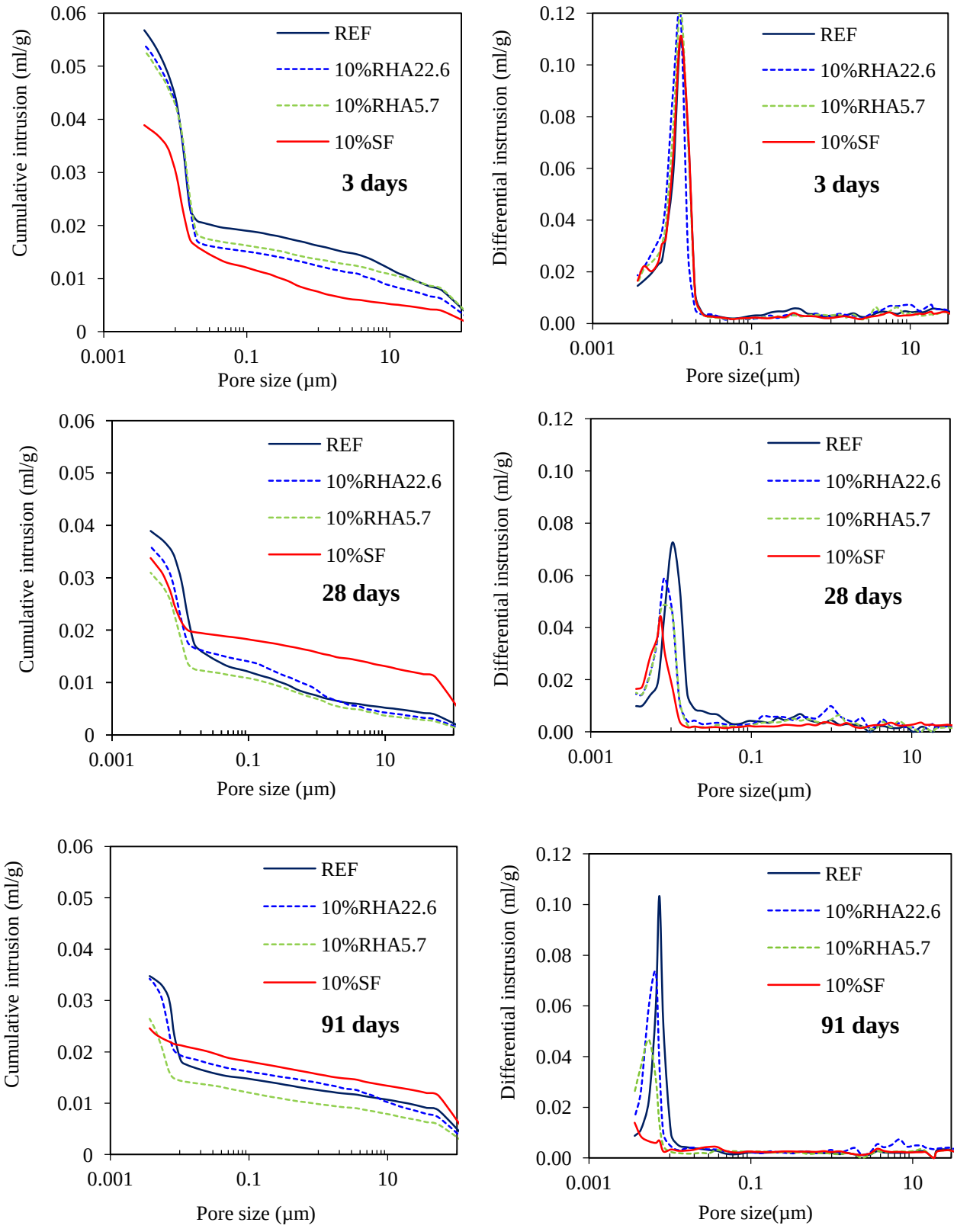

Fig. 7.18 Pore size distribution in the blended cement matrix of mortar containing 10 wt.% RHA/SF at 3, 28 and 91 days

7.4. Discussion

It is clearly evident that the incorporation of RHA/SF significantly increased the degree of cement hydration, i.e. increased the degree of C_3S hydration, in the blended cement paste of mortar regardless of age (Fig. 7.2 and Fig. 7.4). Whereas the effect of SF dominated at early age of 3 days, the effect of RHA was stronger than that of SF particularly at the later ages, e.g. 28 and 91days. The degree of C_2S and C_3S hydration in the RHA blended cement paste was higher than that in the SF blended cement paste (Fig. 7.5 and Fig. 7.6). Additionally, the process of cement hydration in the RHA blended cement paste of mortar was dramatically influenced by the MPS of RHA, i.e. the high hydration rate at 3 days with RHA5.7 and from 3 to 91 days with RHA22.6.

The accelerating effects are mainly attributable to the fact that the cement replacement by 10 wt.% RHA/SF with very large SSA provides more nucleation site for precipitation of cement hydrates and thus accelerates cement hydration, i.e. C_3S, similar to the case of fine limestone powder [102, 218, 219]. The nucleation site effect might be the main cause of the acceleration of cement hydration, i.e. C_3S, before 3 days, and hence the degree of cement hydration increases with the larger external SSA of SCMs, i.e. SF (Fig. 7.2 and Fig. 7.5). Furthermore, the significant difference between RHA and SF is that SF is a dense material, whereas RHA is a porous material. The pore structure, i.e. pore size and pore volume, play an important role in the effect of RHA on the properties of cementitious materials due to the mixing water absorbed in its pores. At early ages, the amount of water absorbed might reduce the dilution effect on cement hydration in the RHA blended cement matrix, especially with the coarse RHA22.6 with larger pore volume. At late ages, Nguyen [148] proposed that this amount of water absorbed into the pores of RHA is released from the pores, when the relative humidity in paste reduces because of cement hydration, and therefore keeps the hydration of cement continuous. Besides, the higher alkali content of RHA than that of SF will increase the pH value of the RHA blended cement paste, and thus accelerate the hydration of cement and pozzolanic reaction of RHA as discussed below. The effect of alkali content of RHA on pozzolanic reaction of RHA in the CH solution has been discussed previously. That could also explain the higher degree of cement hydration in the RHA blended cement paste compared to that in the SF blended cement paste.

In spite of the lower external SSA and thus lower nucleation site effect, the coarse RHA22.6 with the larger pore volume will absorb a higher amount of mixing water, and thus its internal curing effect might be stronger than that of the fine RHA5.7. Therefore, the degree of cement hydration in the coarse RHA22.6 blended cement paste could reach that in the fine RHA5.7 blended cement paste after 91 days (Fig. 7.2 and Fig. 7.4), and might be higher at later ages.

The presence of RHA/SF in cement paste not only accelerates the cement hydration but also refine the microstructure by pozzolanic reaction products. In this study, the pozzolanic reactivity of RHA and SF was evaluated not only by the reduction in the electrical conductivity of CH-pozzolan suspensions, as discussed above, but also by the CH content in binder paste of the mortar samples. The process of pozzolanic reaction of pozzolan in binder paste is correspondent with that in saturated $Ca(OH)_2$ solutions. The fine RHA5.7 with larger SSA, i.e. external SSA, had higher pozzolanic reactivity up to 28 days, indicated by the lower CH content compared to the coarse RHA22.6 and SF. However, the CH content in the fine RHA5.7 blended

paste was significantly higher than that in the coarse RHA22.6 blended paste and the SF blended paste at 91 days, but was still lower than that in the reference sample (Fig. 7.7). This indicates that from 28 to 91 days the pozzolanic reaction of the fine RHA still occurred but to lesser extent than the coarse RHA22.6 and SF. In total, the CH contents after 91 days ascended from in the SF blended paste to in the coarse RHA22.6 blended paste and then in the fine RHA5.7 blended paste. This order is similar to the order of the electrical conductivity in the pozzolan-CH suspensions (Fig. 4.11 and Fig. 4.13). One more time, it confirms that the pozzolanic reactivity of SF is higher than that of RHA, and the coarse RHA22.6 has a higher reactivity than the fine RHA5.7 in both the CH solution and cement system.

Over time, the cement hydration proceeds and the pozzolanic reaction takes place afterwards. The hydrated products of the cement hydration and the pozzolanic reaction fills in the capillary pores, which not only decreases the pore volume, but also changes large pores into small ones, as can be seen in Table 7.2 and Fig. 7.18. It is clearly obtained that the refinement of pore structure is strongly correlated to the pozzolanic reactivity. The pore volume in the fine RHA5.7 blended paste is reduced more than in the SF blended paste in period of time from 3 to 28 days due to the higher pozzolanic reactivity of the fine RHA5.7. Whereas the pozzolanic reactivity of SF is significantly higher than that of the fine RHA5.7 from 28 to 91 days. That results in the remarkable decrease in pore volume in the SF blended cement matrix.

In case of the coarse RHA22.6, its pozzlanic reactivity is higher than that of the fine RHA5.7 after 28 days, indicated by the larger CH consumption (Fig. 7.7). However, capillary porosity of the RHA22.6 blended cement matrix was much higher than that of the RHA5.7 blended cement matrix (Table 7.2 and Fig. 7.18). It is very important to note that the pozzolanic reaction takes place outside and inside the RHA particles indicated by EDX phase-mapping, EDX Ca-mapping and BSE-images (Fig. 7.9, Fig. 7.11 and Fig. 7.12). The coarse RHA22.6 has the larger pore volume and more macropores than the fine RHA5.7 (Table 4.1 and Fig. 4.7). Therefore, the internal pozzolanic reactivity of RHA22.6 is higher than that of RHA5.7. The internal pozzolanic reaction products might precipitate in pores inside RHA particles and have no effect on the pore refinement of the cement matrix surrounding RHA particles.

Based on the experimental results in this study and the analyses above, the mechanism for the successive pozzolanic reactions of RHA is proposed as illustrated in Fig. 7.19 following:

- OH ions from the pore solution attack Si-O-Si bonds, dissolving amorphous silica from the external surface of RHA particles into the aqueous solution, and a certain amount of water is absorbed into the pores of RHA particles. Ca and OH ions in pore solution react with silica to create low Ca/Si C-S-H hydrates which then precipitate on the surfaces of RHA particles and take up an amount of foreign ions, e.g. sodium, potassium, and aluminium.
- Over time, the pozzolanic reaction occurs not only on the external surfaces but also in the pores of RHA particles possibly due to the diffusion of Ca ions from the cement matrix into the pores of RHA particles. The products formed by the internal pozzolanic reaction fill up the pores inside the RHA particles first. A main part of the internal pozzolanic reaction products consolidates the pore structures of RHA particles, and is not effective in refining the pore structure of the RHA blended cement matrix. Therefore, the pore structure of the coarse RHA blended matrix is higher than that of the

fine RHA blended cement matrix, while its pozzolanic reactivity is still higher than that of the fine RHA.

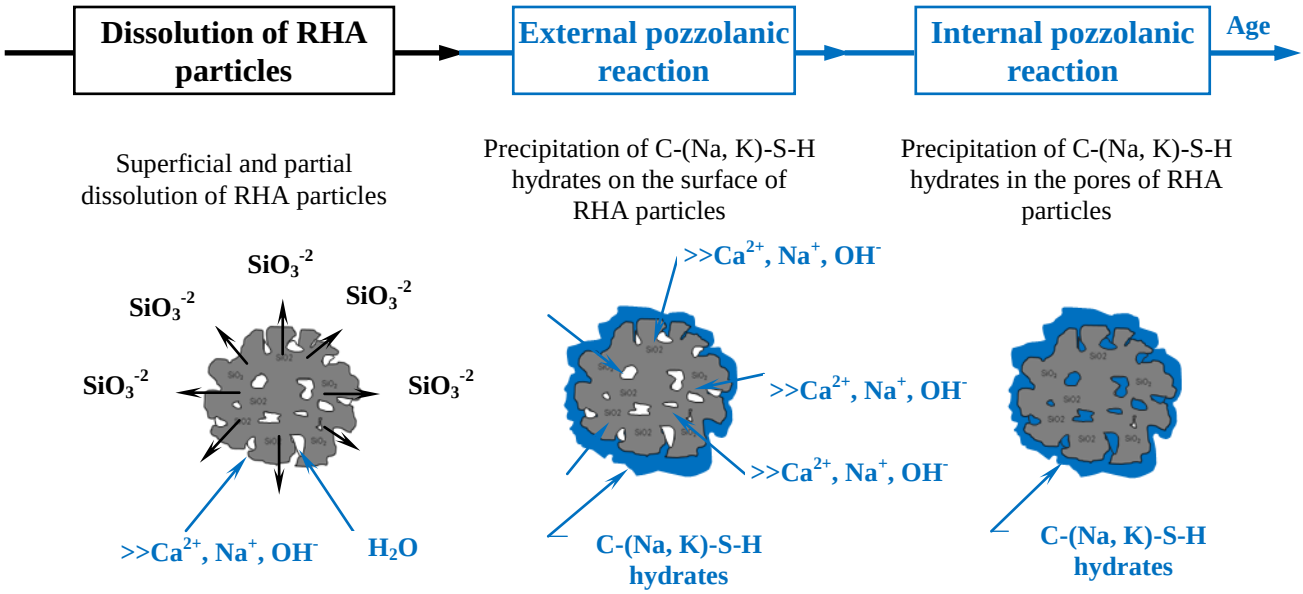

Fig. 7.19 Schematic representation of the mechanism for successive pozzolanic reactions of RHA particles

7.5. Concluding remarks

- The incorporation of RHA/SF increases the degree of cement hydration in mortar. SF is more effective at the early ages (3 days), possibly due to the better nucleation site effect, whereas RHA, especially the coarse RHA22.6, dominates at the late age (28, 91 days) possibly due to the higher internal water curing effect.
- The incorporation of RHA/SF changes the hydration process of the clinker minerals, i.e. C_3S, C_2S. The hydration degree of C_3S in the RHA/SF blended cement matrix is higher than in the reference sample. The incorporation of RHA/SF increases the C_3S hydration rate from 3 to 14 days. The degree of C_3S and C_2S hydration in the RHA blended cement paste is higher than that in the SF blended cement paste. From 28 to 91 days, the degree of cement hydration in the RHA22.6 blended cement paste increased mainly due to the increase in C_2S hydration.
- The pozzolanic reactivity of the fine RHA5.7 is higher at the early ages and lower at the late ages compared to the coarse RHA22.6 and SF respectively, not only in the saturated CH solution but also in the blended cement paste of mortar.
- Pozzolanic reaction takes place outside RHA particles, so called ''external pozzolanic reaction'', and in the pores inside RHA particles, so called ''internal pozzolanic reaction''. Where the external pozzolanic reaction products refine the pore structure of cement matrix, and the internal pozzolanic reaction products consolidate the pore structure of RHA particles. The external pozzolanic reaction products have a low Ca/Si ratio of about 1.28 and take up amount of foreign ions, i.e. aluminium, potassium, sodium ions. The fine RHA5.7 is more effective in pore refinement than the coarse RHA22.6 due to its higher ''external pozzolanic reactivity''. This effect of RHA is not comparable with SF especially at the late ages.

- In the blended cement matrix, SF disperses better than RHA due to its ultra fine particles, resulting in the better dispersion of silicon, potassium and the occurrence of pozzolanic reaction. Therefore, not only pore volume and pore size is lower but also the pores disperse more homogeneously in the SF blended cement matrix than those in the RHA blended cement matrix. The concentration of silicon and potassium is higher in the pores and near RHA particles and it is proportional to the particle size of RHA.

8. Compressive strength of mortar formulated from SCHPC

8.1. Effect of mean particle size of RHA on compressive strength

The development of compressive strength of mortar formulated from SCHPC at w/b of 0.26 is displayed in Fig. 8.1. It can be seen that compressive strength of mortar containing the fine RHA was higher than that of the sample containing coarse one regardless of age. At late ages, i.e. 28 and 91days, the RHA7.7 containing sample had similar compressive strength to that of the RHA5.7 containing sample. Therefore, it can be said that the coarser RHA has a stronger effect on compressive strength than the fine one at late ages, e.g. 91days. This result of compressive strength fits well with the result of the pozzolanic reactivity of RHA analyzed previously. Compressive strength of the fine RHA5.7 containing sample was comparable with that of SF containing sample only before 28 days. At 91days, compressive strength of SF containing sample was significantly higher than that of the RHA containing sample and the control sample. The result is closely related to the 91-day pozzolanic reactivity of SF indicated by the consumption of CH above.

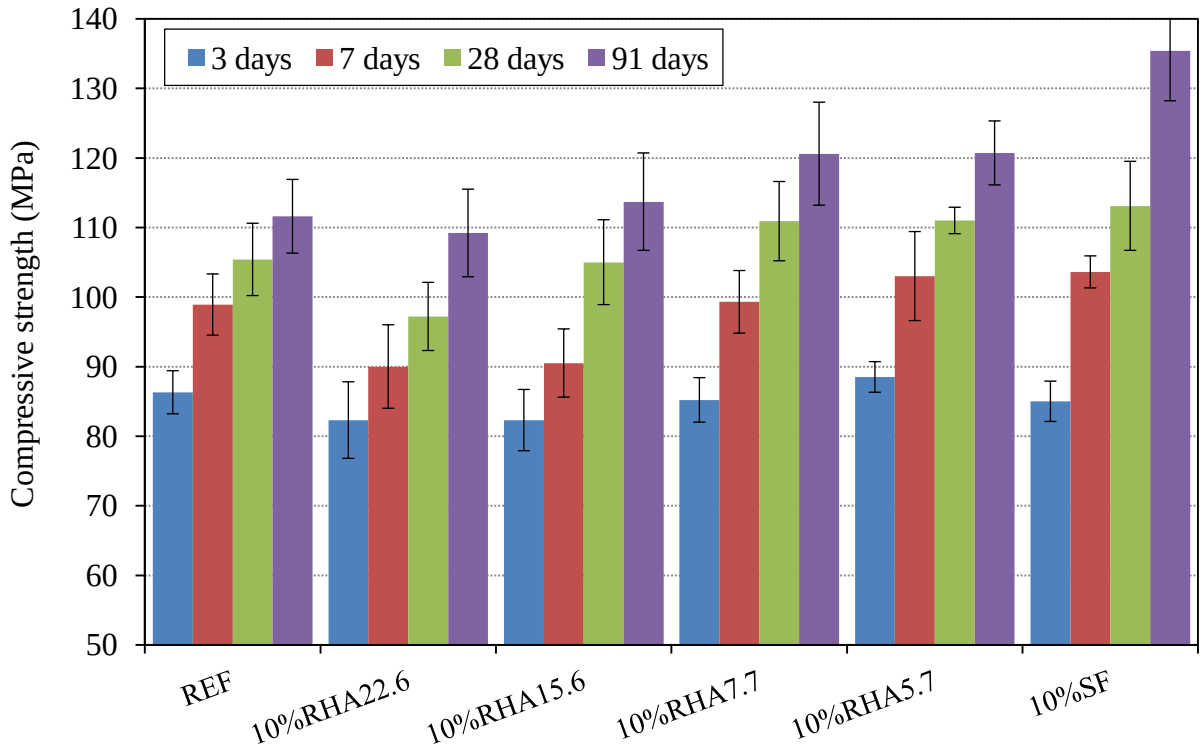

Fig. 8.1 Effect of MPS of RHA on compressive strength, in comparison with SF, at w/b of 0.26

In Fig. 8.2, the effect of MPS of RHA on compressive strength of mortar at w/b of 0.30 is shown. The results obatained indicate that the effect of MPS of RHA on compressive strength at w/b of 0.30 is different from that of MPS of RHA on compressive strength at w/b of 0.26. The compressive strength of RHA containing sample tends to be highest with the coarser MPS at early ages, i.e. RHA15.6 at 3 days, and RHA7.7 at 7 days, and highest with the finer MPS at late ages, i.e. RHA7.7 at 28 days, RHA5.7 at 91 days. Whereas the compressive strength of mortar at w/b of 0.26 reach highest value with RHA5.7 regardless of age. Moreover, the compressive strength of mortar containing RHA at w/b of 0.30 was lower than that of the

referrence sample at 3 days, and higher than that of the referrence sample at later ages. Whereas the compressive strength of mortar containing RHA5.7 at w/b of 0.26 was hihger than that of the referrence sample at all ages. A similar result was obtained when comparing the compressive strength of sample containing RHA with that of the sample containing SF at both w/b of 0.26 and 0.30.

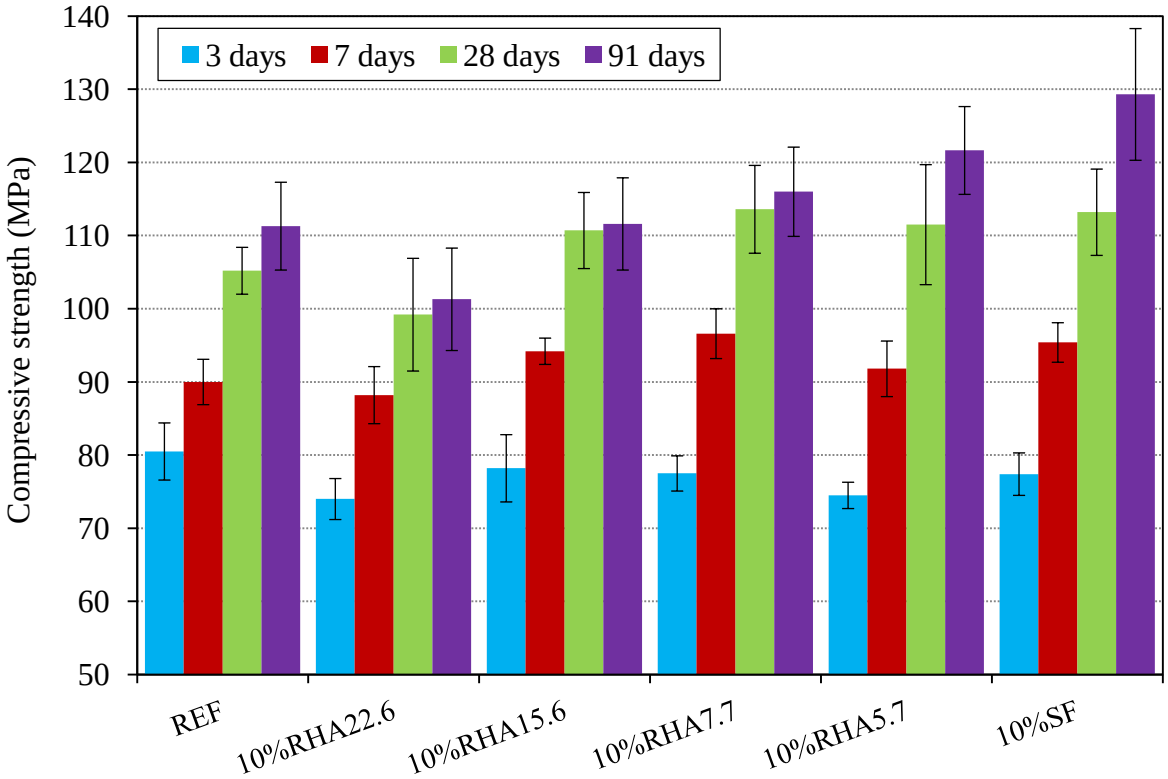

Fig. 8.2 Effect of MPS of RHA on compressive strength, in comparison with SF, at w/b of 0.30

8.2. Effect RHA content on compressive strength

The effect of RHA7.7 content on compressive strength of mortar at w/b of 0.30 is shown in Fig. 8.3. It is obvious that at early ages, such as 3, 7 and 28 days, the higher the RHA7.7 content the lower the compressive strength. However, the compressive strength at 91 days of sample containing 10 wt.% RHA was lower than those of samples containing 20 wt.% and 30 wt.% RHA, where the highest compressive strength at 91 days was obtained from the 20 wt.% RHA containing sample. Therefore, it can be said that, the higher content of RHA is

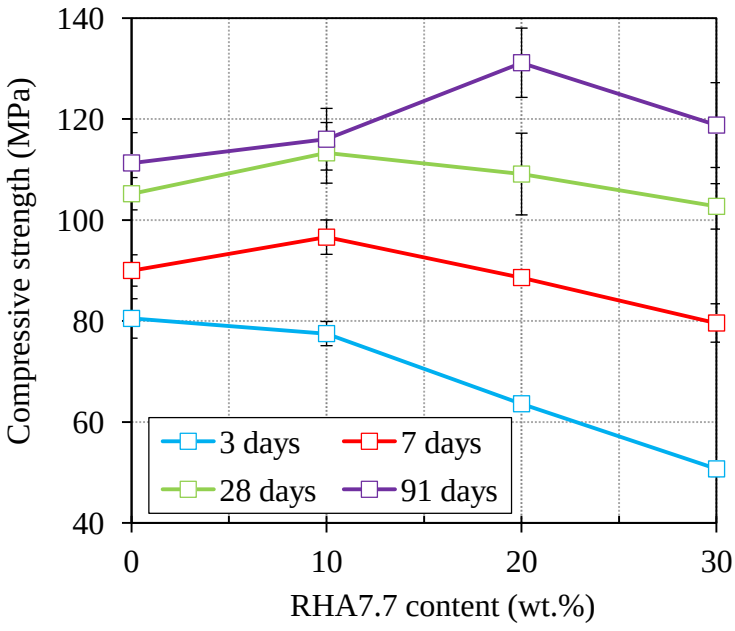

Fig. 8.3 Effect of RHA7.7 content on compressive of SCHPM, at w/b ratio of 0.30

more effective in compressive strength at later ages, such as 91, 360 days. Compared to the reference sample, 3-day compressive strength of sample containg RHA is lower. However, after 28 days the compressive strength of sample containing RHA was similar, or higher than that of the reference sample, regardless of the content used.

8.3. Discussion

Compressive strength of the RHA containing samples at w/b of 0.26 increased with a smaller particle size of RHA. Compared to the reference sample, generally the RHA containing samples had higher compressive strength at 91 days regardless of the fineness of RHA, where samples containing the fine RHA (5.7 μm and 7.7 μm) had higher compressive strength regardless of age. The compressive strength of the SF containing sample was similar to that of the samples containing the fine RHA (5.7 μm and 7.7 μm) before 28 days and significantly higher at 91 days (Fig. 8.1). It can be found that the development of compressive strength of mortar is correlated to the time-dependent pozzolanic reactivity of RHA or SF, the cement hydration process and the microstructure development. That can be explained as follows:

The incorporation of the porous RHA increases the degree of cement hydration at 91 days (Fig. 7.2), possibly mainly due to the internal water curing effect. Furthermore, the pozzolanic reaction of RHA indicated by the CH consumption (Fig. 7.7) occurs to the great extent at this age inducing a significant pore refinement (Table 7.1 and Fig. 7.18) as discussed above. This results in an increase in the compressive strength of mortar samples containing RHA compared to that of the reference sample at late ages. This result is consistent with the compressive strength at late ages of HPC [1, 6] and ultra high performance concrete containing RHA [13, 16].

As discussed above, the fineness of RHA dramatically influences its pore structure, SSA and hence the pozzolanic reaction process and the cement hydration process in the blended cement paste, thus results in a difference in the development of the compressive strength of mortar. The compressive strength of the fine RHA5.7 containing sample was higher than that of the sample containing the coarse RHA22.6, at all ages. Even when the degree of cement hydration in the coarse RHA22.6 blended cement of mortar sample is similar to that in the fine RHA5.7 blended cement of mortar sample (Fig. 7.2) and the pozzolanic reactivity of the coarse RHA22.6 is significantly higher than that of the fine RHA after 91 days, indicated by the larger CH consumption (Fig. 7.7). Despite the higher pozzolanic reactivity of the coarse RHA22.6 from 28 to 91 days, it is not effective in the refinement of the pore structure in the cement matrix (Fig. 7.18 and Table 7.2). As analyzed above, the SSA of RHA is contributed by internal and external surface areas. The pozzolanic reaction takes place on both surface areas succesively. The hydrated products, i.e. C-S-H phases, generated from the ''external pozzolanic reaction'' refine the pore structure of the cement matrix surounding RHA particles meanwhile the whole or a main part of products of ''internal pozzolanic reaction'' consolidates the pore structure of RHA particles. Grinding collapses the pores, thus reducing pore volume and the internal surface areas. Consequently, the coarse RHA22.6 has higher pozzolanic reactivity than the fine RHA5.7 possibly due to the higher internal pozzolanic reactivity. Additionally, the coarse RHA decreases the packing density of granular mixture [13, 157] and the porous RHA particles themselves are the weak points in the blended cement matrix (Fig. 7.15b and Fig. 7.12). So this

affects the compressive strength. One more point is that the nucleation site effect of the fine RHA with larger external SSA might be higher than that of the coarse one. In this study, the RHA5.7 and RHA7.7 were more effective in the compressive strength (Fig. 8.1 and Fig. 8.2) possibly due to their higher external pozzolanic reactivity, better filler effect, and better nucleation site effect than those of the coarse RHA.

In the present study, RHA was not comparable with SF to increase compressive strength of mortar at the late age of 91 days. With extremely fine particles, SF is much better than RHA to yield the higher packing density of the granular mixture [13], that is one of the main reasons for the better self-compacting property (higher slump flow and lower plastic viscosity, Fig. 6.13). One more point should be noticed that the pozzolanic reaction of SF might occur later, however the reactivity in total is higher than that of RHA after 91days (Fig. 4.11 and Fig. 7.7). Similar results were also obtained in other studies [13, 16]. These points support the compressive strength domination of SF containing sample. One more time see Fig. 8.1. Interestingly, the fine RHA was slightly more beneficial to improve compressive strength at 3 days than SF. That can be explained by the higher reactivity of RHA after 3 days (Fig. 7.7), and the reduction of effective w/b ratio in the RHA blended paste due to water adsorption of RHA [16, 148]. These effects of RHA might dominate the nucleation site effect of SF at 3 days. This phenomenon has not been analysed and fully explained so far.

The experimental results (Fig. 8.1 and Fig. 8.2) show that the positive effect of the finer MPS of RHA on the compressive strength of mortar is obtained at w/b ratio of 0.26 regardless of age and at w/b of 0.30 at the late age. The development of compressive strength of mortar incorporating RHA with various MPS can be explained by the air voids content, packing density of granular mixture, the reduction in w/b of the bulk cement paste and pozzolanic reactivity of RHA as follows:

It is well known that air voids content is a negative factor on compressive strength [220]. When the MPS of RHA reduces, the RHA containing mortar has lower SSD and lower viscosity as discussed above. Therefore, less entrained and entrapped air voids are kept in the mixture during mixing and casting. With higher external pozzolanic reactivity, the fine RHA, i.e. RHA5.7, is more effective in refining pore structure in the matrix than the coarse ones (Fig. 7.7 and Table 7.2). Furthermore, the fine RHA improves the packing density of granular mixture because of its filler effect. RHA particles might be the weakest point in the matrix especially at the late age because of their pore structure. The negative effect of RHA is more significant with the coarser particles. However, the amount of water absorbed by RHA particles is higher when the MPS increases causing a reduction in effective w/b ratio of RHA containing mortar, a positive factor on compressive strength especially at early age. It can be suggested that the positive effect of the finer MPS of RHA might be dominant at the low w/b ratio, and at the late age resulting in the higher compressive strength of finer RHA containing sample compared to the coarser RHA containing sample and the reference sample.

8.4. Concluding remarks

- At w/b of 0.26, the incorporation of RHA5.7/SF increases the compressive strength of mortar. The effect is stronger at the late ages, i.e. 28 and 91 days.

- At w/b of 0.26, decreasing MPS of RHA increases the compressive strength of mortar at all ages. The fine RHA (5.7µm and 7.7 µm) are more effective regarding compressive strength than the coarse ones (15.6 and 22.6 µm) due to the higher external pozzolanic reactivity, the better filler effect, and the better nucleation site effect of the fine RHA.
- At w/b of 0.30, the incorporation of RHA/SF decreases the compressive strength at 3days, however increases the compressive strength after 7 days.
- At w/b of 0.30, compressive strength obtained is higher at early ages with the coarse RHA and at late ages with the fine RHA.
- At both w/b of 0.26 and 0.30, compressive strength of mortar containing the fine RHA is comparable with, but lower than that of the sample containing SF before 28 days and at 91 days respectively.
- At w/b of 0.30, the incorporation of 10 wt.% RHA7.7 decreases the compressive strength of mortar at 3 days, however, increases the compressive strength of mortar after 7 days.
- At w/b of 0.30, the increase in RHA7.7 content decreases the compressive strength before 28 days. However, the compressive strength of the sample containing 20-30 wt.% RHA7.7 is higher than that of the sample containing 10 wt.% RHA7.7 at 91 days.

9. Alkali silica reactivity of rice husk ash in paste and mortar formulated from SCHPC

9.1. Mixture proportions

Mortars were formulated from the corresponding SCHPCs. The SCHPC mixtures were designed on the basis of the absolute volume of the constituent materials with a w/b ratio of 0.30, a paste volume of 38.5 vol.% (including air content of 2 vol.%), a fine aggregate volume of 30.4 vol.%, and a coarse aggregate volume of 31.1 vol.%. Cement was replaced with RHA, and SF by weight, but the paste volume was kept constant [200]. The proportions of sand, cement, RHA/ SF and water of the mortars were the same as in the corresponding concretes. For all mixtures, superplasticizer saturation dosages were used. The natural sand was replaced by greywacke and basalt by volume. Greywacke and basalt with maximum particle size of 4 mm were used as a reactive aggregate and a non-reactive aggregate respectively. The mixture proportions and mini-slump flow of mortars are shown in Table 9.1. Furthermore, paste bars having dimension of 10 x10x 60 mm^3 were produced. The testing procedure for mortar bars was applied for the paste bars. The mixture proportions of paste formulated from SCHPCs are presented in Table 9.2.

Table 9.1 Mixture proportions of mortar used in this study

Mixtures	w/b ratio	Sand (vol.%)	SF (wt.%)	RHA (wt.%)	SP (wt.%)	MPS of RHA (μm)	Mini-slump flow (cm)	
							Greywacke	Basalt
REF	0.30	44	0	0	0.5	-	34.5	30.5
20%SF	0.30	44	20	0	1.0	-	33.0	30.5
10%RHA5.7	0.30	44	0	10	0.8	5.7	33.5	-
20%RHA5.7	0.30	44	0	20	1.0	5.7	32.0	31.0
30%RHA5.7	0.30	44	0	30	1.2	5.7	29.5	-
20%RHA7.7	0.30	44	0	20	1.0	7.7	32.0	-
20%RHA15.6	0.30	44	0	20	1.0	15.6	30.0	30.0

Table 9.2 Mixture proportions of paste used in this study

Mixtures	w/b ratio	Cement (wt.%)	RHA (wt.%)	SP (wt.%)	MPS of RHA (μm)
REF	0.30	100	0	0.4	-
20%RHA5.7	0.30	80	20	0.5	5.7
20%RHA7.7	0.30	80	20	0.5	7.7
20%RHA15.6	0.30	80	20	0.5	15.6
20%RHA22.6	0.30	80	20	0.5	22.6

9.2. Alkali silica reaction in mortar containing RHA

9.2.1. Effect of RHA mean particle size

Expansion of mortar bars produced with alkali-reactive greywacke aggregate is shown in Fig. 9.1. According to ASTM C 1260 [187] and German ASR standard [165], expansion level of mortar bar after 14 days in NaOH 1M at 80 ^{o}C lower than 0.10 % seems innocuous, and higher than 0.20 % is indicative of potentially deleterious ASR. The expansion of all samples after 14 days immersion was lower than the threshold (0.10 %). The SF containing sample had lowest expansion level, i.e. no expansion, whereas the expansion of the reference sample was highest nearly to 0.10 %. For the samples containing RHA, the expansion increased when the coarser RHA particle was used. Surprisingly, 28-day expansions of the reference sample and the sample containing RHA15.6 increased dramatically to 0.27 % and 0.46 % respectively. The 28-day expansion of the other samples was still below the standard limit. Furthermore, visible cracks appeared on the surface and along the edges of the mortar bars containing RHA7.7 and RHA15.6 (Fig. 9.2d, e). The width of the cracks increased with coarser RHA, particularly two of three samples containing RHA15.6 were broken, as seen in Fig. 9.2e, f. Whereas there is no cracks on the surface of the SF containing sample and the reference sample irrespective of its excessive expansion (Fig. 9.2a, b). In order to understand more on expansive behaviour of the mortar bars containing RHA, the bars containing RHA7.7, RHA5.7 and SF were immersed in NaOH 1 M at 80 ^{o}C up to 56 days.

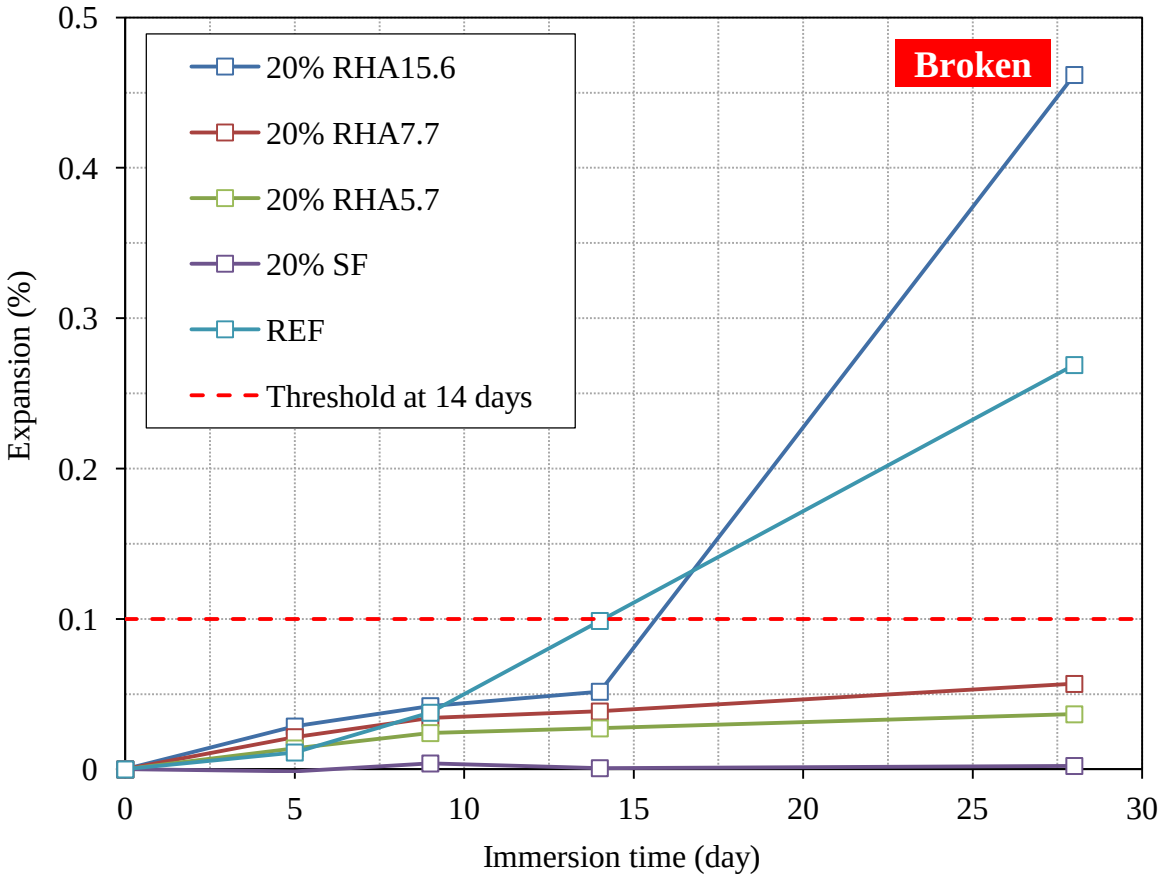

Fig. 9.1 Effect of RHA mean particle size on the expansion of mortar containing reactive Greywacke in the NaOH solution at 80 ^{o}C, after 28 days

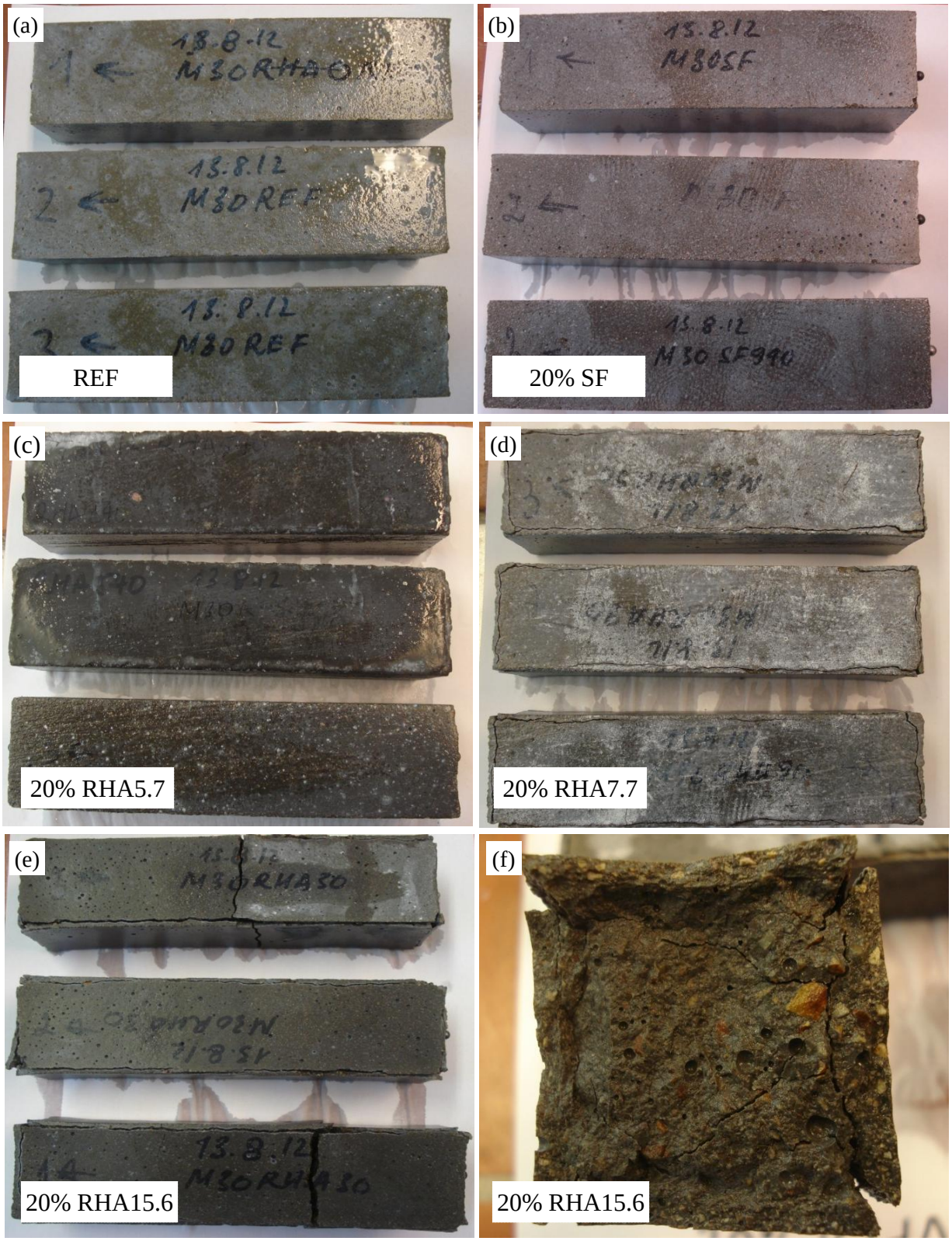

Fig. 9.2 Reference sample (a), samples containing 20 wt.% SF (b), containing 20 wt.% RHA5.7 (c), containing 20 wt.% RHA7.7 (d), containing 20 wt.% RHA15.6 (e), and the broken cross-section of the sample containing 20 wt.% RHA15.6 (f), containing greywacke, in the NaOH 1 M at 80 ^{o}C, after 28 days

The expansion of mortar bars containing RHA/SF after 56 days of immersion is shown in Fig. 9.3. As expected, the samples containing RHA shown great expansion exceeding the limit of 0.10 %, whereas the expansion of the sample containing SF was lower, and far below the level of 0.10 %. A dramatic increase in the expansion and then the disruption of sample containing RHA7.7 was observed (Fig. 9.4). Based on the results of the expansion of the sample containing RHA15.6 after 28 days and the sample containing RHA7.7 after 56 days, it can be expected that the same result will be obtained with the sample containing RHA5.7 at later ages.

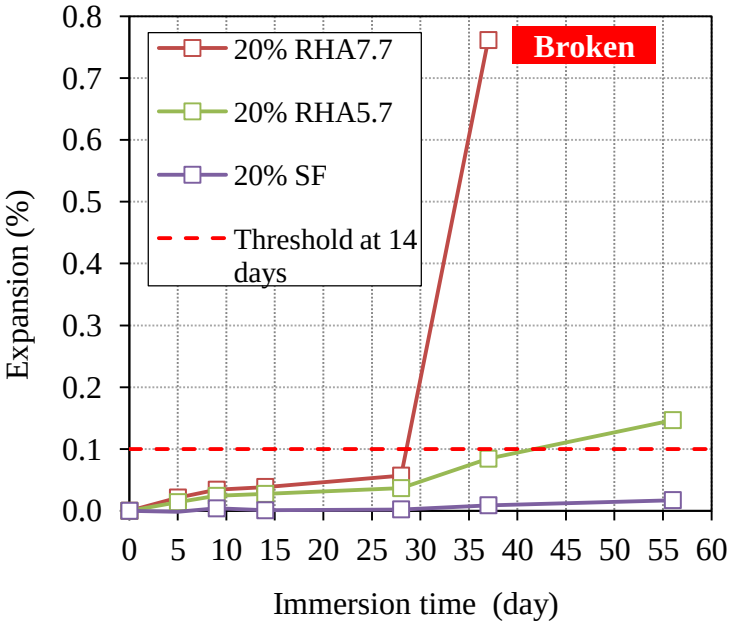

Fig. 9.3 Effect of RHA mean particle size on the expansion of mortar containing greywacke aggregate in the NaOH 1M at 80 ^{o}C, after 56 days

Fig. 9.6 shows the expansion of mortar bars containing non-reactive basalt aggregate and different types of RHA after 28 days of immersion in NaOH. The magnitude of the expansion of these mortar bars was significantly lower than that of the bars containing reactive greywacke aggregate. The expansion level of all samples was lower than 0.10 % after 14 and 28 days. Different from the reference sample containing reactive greywacke aggregate, the reference sample containing non-reactive basalt aggregate had lower expansion than the samples containing non-reactive basalt aggregate and RHA. The sample containing the coarse RHA15.6 had larger expansion than the samples containing the fine RHA5.7 and SF. This indicates that the incorporation of RHA increased the expansion of the mortar bars in NaOH 1M at 80 ^{o}C. Although the expansion level of mortar bars containing RHA15.6 was far below the prescribed limit, the longitudinal cracks appeared along the length of the mortar bars (Fig. 9.5).

Fig. 9.4 Disruption of the sample containing greywacke and 20 wt.% RHA7.7 in NaOH 1M at 80 ^{o}C after 56 days

Fig. 9.5 Sample containing 20 wt.% RHA15.6 and basalt aggregate in the NaOH 1M at 80 °C, after 28 days

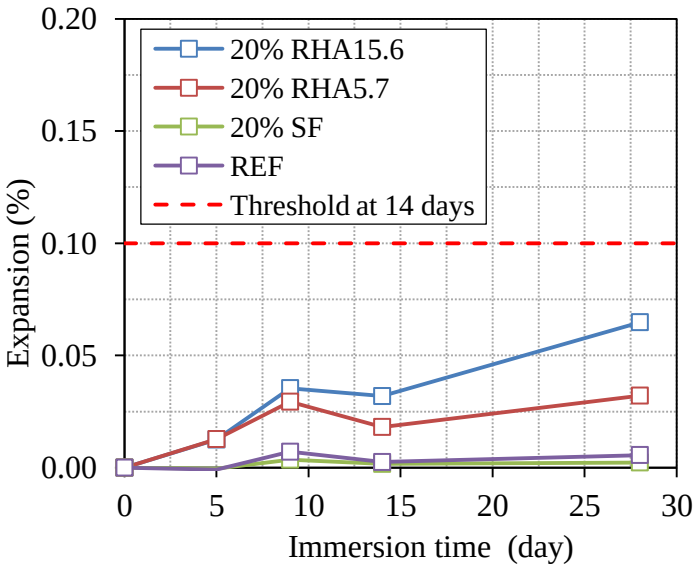

Fig. 9.6 Effect of RHA mean particle size on the expansion of mortar containing basalt aggregate in the NaOH 1M at 80 °C, after 28 days

In Fig. 9.7, the expansion of the RHA15.6 containing samples made with greywacke or basalt aggregate after 28 days of immersion in NaOH 1 M or water at 80 °C is displayed. The mortar bars containing reactive greywacke aggregate shown greater expansion than the mortar bars containing non-reactive basalt aggregate immersed in NaOH 1 M and in water respectively. The difference between the expansion level of the sample containing greywacke and the sample containing basalt immersed in NaOH indicates the effect of greywacke on the expansion due to ASR. Meanwhile, the difference between the samples containing basalt immersed in NaOH and in water indicates the effect of RHA on the expansion due to ASR.

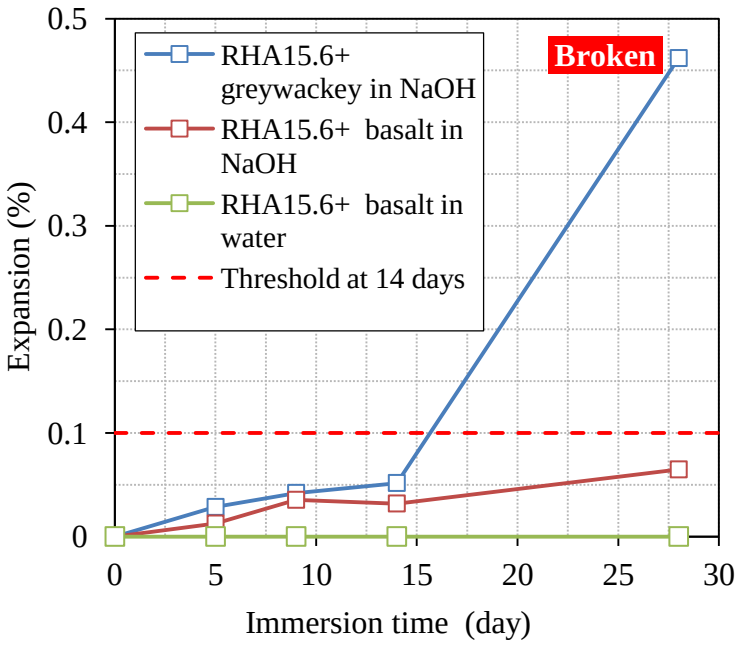

Fig. 9.7 Expansion of mortar containing 20 wt.% RHA15.6 under different testing conditions

9.2.2. Effect of RHA content

The results shown in Fig. 9.1 and Fig. 9.3 indicate that the expansion of the sample containing RHA5.7 is lower than that of the reference sample and the samples containing the coarser ones, i.e. RHA7.7 and RHA15.6. Therefore, the effect of RHA5.7 content on the expansion of mortar bar was evaluated. Expansion results for the mortar bars containing reactive greywacke and different RHA5.7 contents are shown in Fig. 9.8. The expansion of mortar bars containing

RHA5.7 was lower than that of the reference sample at 14 days and 28 days. After 14 days, the mortar bar containing RHA5.7 had expansion levels lower than the threshold of 0.10 %. It can be seen that increasing RHA5.7 content decreased the expansion of the mortar bars. The visual inspection after the accelerated tests also indicates no visible cracks on the surface and along the edges of the mortar bars containing RHA5.7 (Fig. 9.2c and Fig. 9.9). It indicates that RHA5.7 can help to mitigate ASR in mortar containing greywacke, especially with high content.

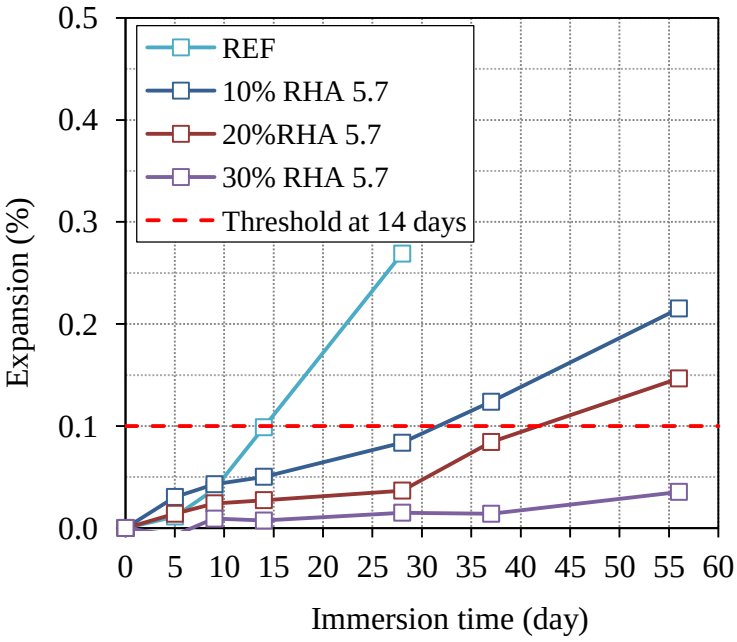

Fig. 9.8 Effect of RHA5.7 content on expansion of sample containing greywacke in the NaOH solution at 80 °C, after 28 days

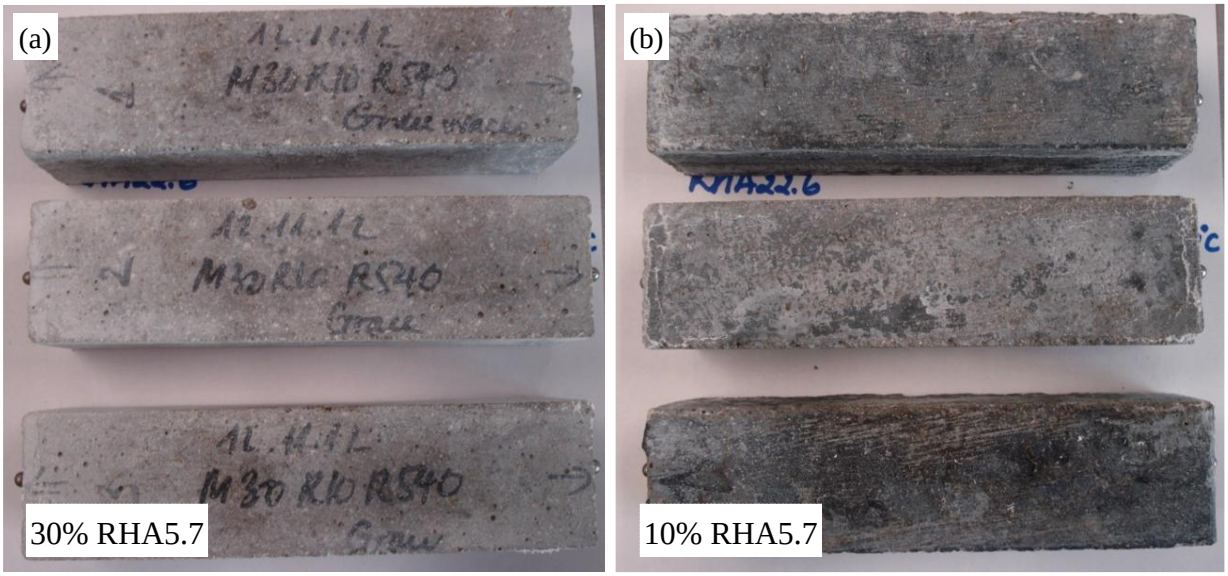

Fig. 9.9 Sample containing Greywacke aggregate and 10 wt.% RHA5.7 (a), 30 wt.% RHA5.7 (b) in the NaOH 1M at 80 °C, after 56 days.

9.2.3. SEM and EDX analyses

The reference sample containing reactive greywacke aggregate and the sample containing reactive greywacke aggregate and RHA15.6 were analyzed by BSE-SEM imaging and BSE-EDX. Common features of deterioration by ASR were obtained in the reference sample and the RHA15.6 containing sample. The greywacke aggregate cracked substantially. Cracks also radiated from the aggregate into the matrix (Fig. 9.10f and Fig. 9.11f). Pores were partially filled by ASR products (Fig. 9.10a and Fig. 9.11a). The cracks and ASR gels were also observed in the matrix (Fig. 9.10c and Fig. 9.11c). The observations are consistent with the large expansion of these two mortar bars presented above.

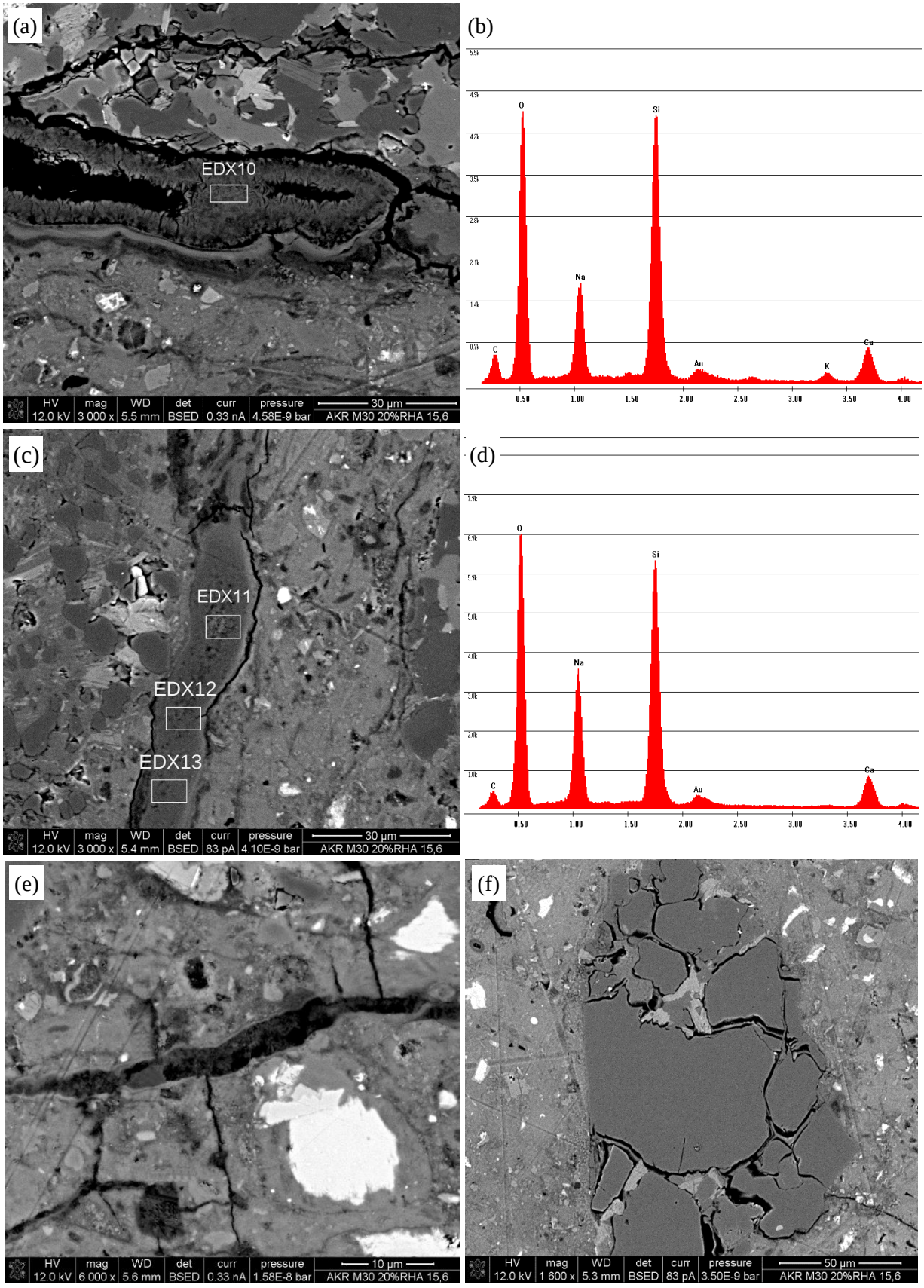

Fig. 9.10 BSE-SEM images of ASR gels formed in pores in the sample containing greywacke and 20 wt.% RHA15.6 in the NaOH 1M at 80 ^{o}C, after 28 days (a, c), X-ray spectra for the ASR gels (b, d), and cracks in the cement matrix (e) and in greywacke aggregate particle (f)

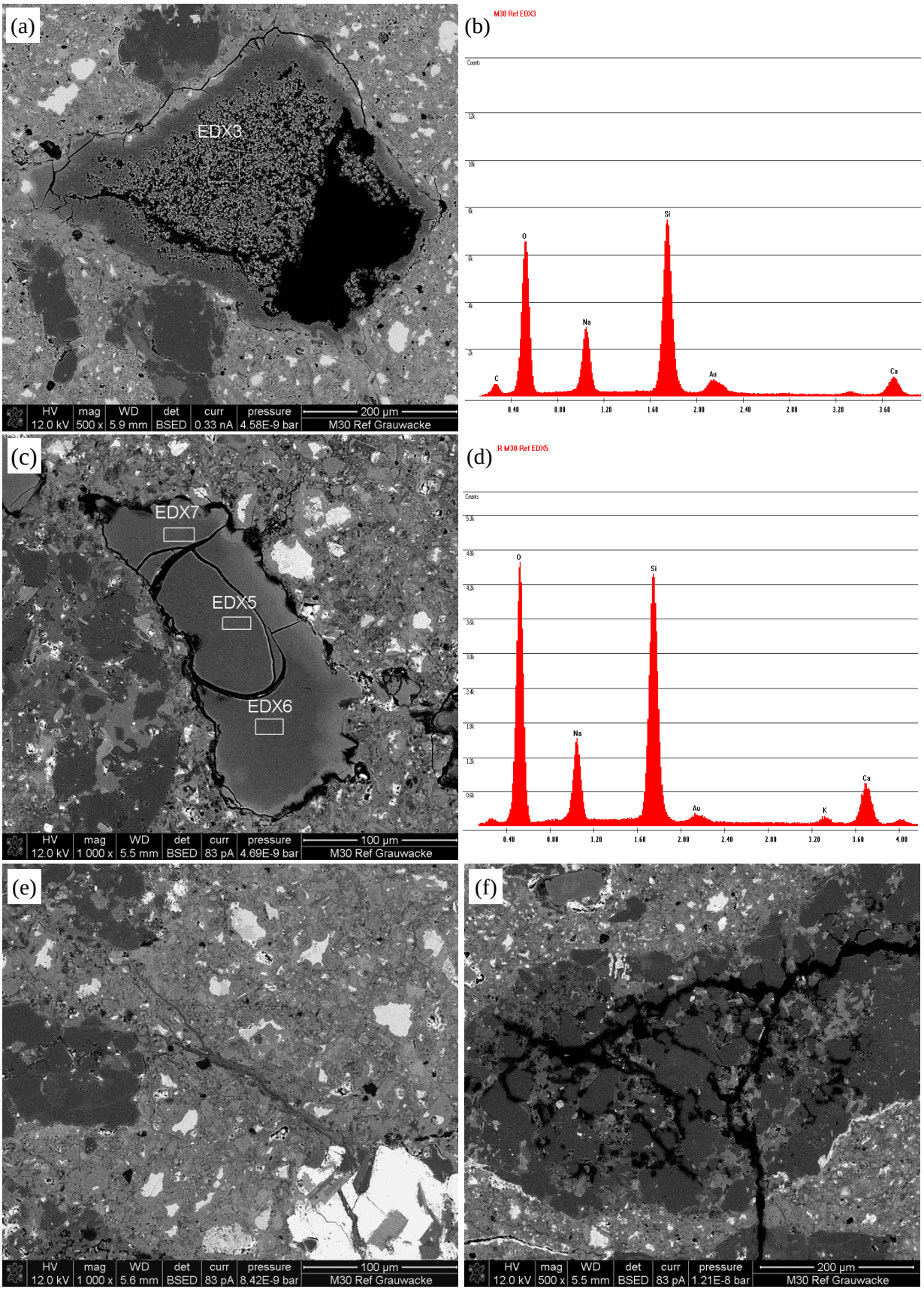

Fig. 9.11 BSE-SEM images of ASR gels formed in the pores in the reference sample containing greywacke in the NaOH 1M at 80 ^{o}C, after 28 days (a, b), X-ray spectra for the ASR gels (c, d), gel flow in the cement matrix (e) and cracks in greywacke aggregate particle (f)

The quantitative analysis of the chemical composition of the ASR products was obtained by using EDX on BSE polished specimens. The spectra for ASR products formed in the sample containing RHA15.6 and the reference sample after 28 days immersion in NaOH 1M are displayed in Fig. 9.10b, d and Fig. 9.11b, d. The oxide composition of ASR products is summarized in Table 9.3 and Table 9.4. It can be found that chemical composition of ASR products, i.e. CaO and Na_2O, changed depending on the location of the products formed. The ASR products formed in pores seem to have higher (Na+K)/Ca ratio than that deposited in matrix and vice versa. The chemical composition of ASR products formed in the reference sample containing greywacke is in the potentially deleterious area of ASR gels proposed by Mansfeld [221], points in green as illustrated in Fig. 9.30. Meanwhile the ASR gels formed in sample containing RHA15.6 are displayed in yellow points.

Table 9.3 Oxide composition (wt.%) by EDX analysis of ASR products formed in the sample containing RHA15.6 in NaOH 1M, at 80 ^oC after 28 days

ASR products filled in pores						
Oxides	SiO_2	CaO	Na_2O	K_2O	Ca/Si	(Na+K)/Si
EDX8	65.35	7.54	25.35	1.76	0.12	0.79
EDX10	66.55	14.91	15.58	2.97	0.24	0.51
Mean value	64.66	12.13	20.66	1.56	0.18	0.65
ASR products deposited in matrix						
EDX11	64.04	14.16	21.8	0	0.24	0.66
EDX12	63.24	18.21	18.55	0	0.31	0.59
EDX13	65.23	15.41	19.36	0	0.25	0.57
Mean value	64.17	15.93	19.90	0.00	0.27	0.61

Table 9.4 Oxide composition (wt.%) by EDX analysis of ASR products formed in the reference sample in NaOH 1M, at 80 ^oC after 28 days

ASR products filled in pores						
Oxides	SiO2	CaO	Na_2O	K_2O	Ca/Si	(Na+K)/Si
EDX2	74.96	4.82	17.76	2.46	0.07	0.50
EDX3	69.53	12.27	16.71	1.49	0.19	0.49
EDX8	67.03	3.48	27.14	2.34	0.06	0.49
Mean value	70.51	6.86	20.54	2.1	0.10	0.50
ASR products deposited in matrix						
EDX5	65.59	18.21	13.73	2.47	0.30	0.45
EDX6	64.45	19.81	13.33	2.4	0.33	0.45
EDX7	63.74	22.74	11.48	2.04	0.38	0.39
Mean value	64.59	20.25	12.85	2.3	0.34	0.43

9.3. Alkali silica reaction of RHA in paste

9.3.1. Alkali silica reaction in paste containing RHA

Pastes formulated from the corresponding SCHPCs were prepared. The paste bars with dimension of 10x10x60 mm^3 were immersed in NaOH 1 M at 20, 40 and 80 ^oC and were examined to observe visible cracking over time. Fig. 9.12 shows the state of the paste bars immersed in NaOH 1 M at 80 ^oC. After 2 days, visible cracks appeared on the paste bars containing RHA22.6 and RHA15.6. After 28 days, the paste bars containing RHA were broken, irrespective of MPS of RHA, whereas no visible cracks were observed on the reference sample (100 % cement). This indicates the incorporation of RHA induced ASR in the pastes, and the deterioration of RHA blended cement paste due to ASR depended on the MPS of RHA.

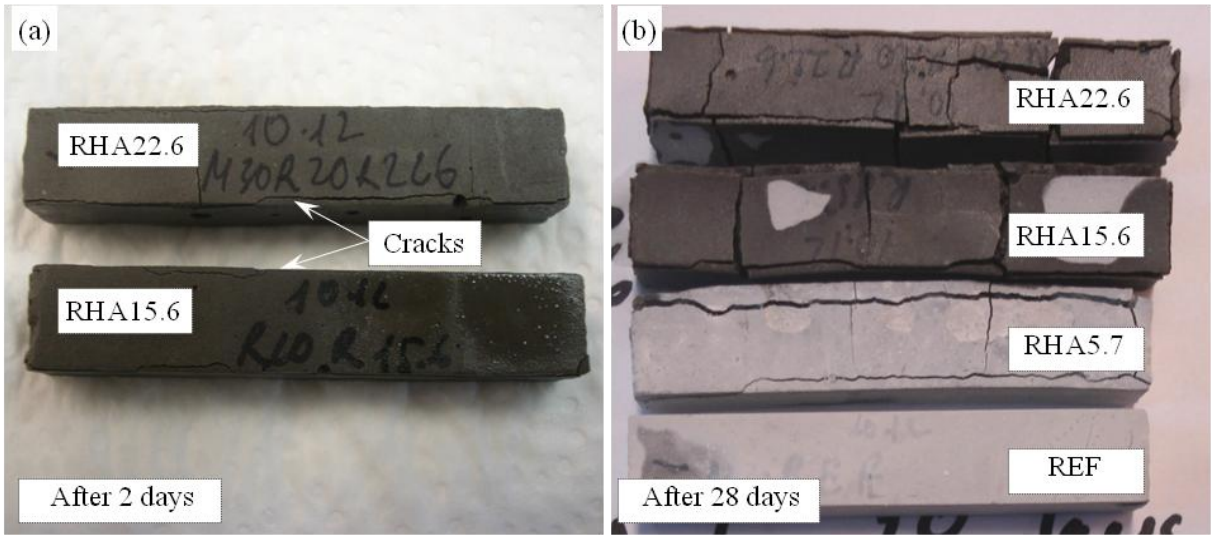

Fig. 9.12 Paste sample in NaOH 1M at 80 ^oC: RHA22.6/RHA15.6 - sample with visible cracks on the surface after 2 days (a) and RHA- sample with disruption after 28 days (b)

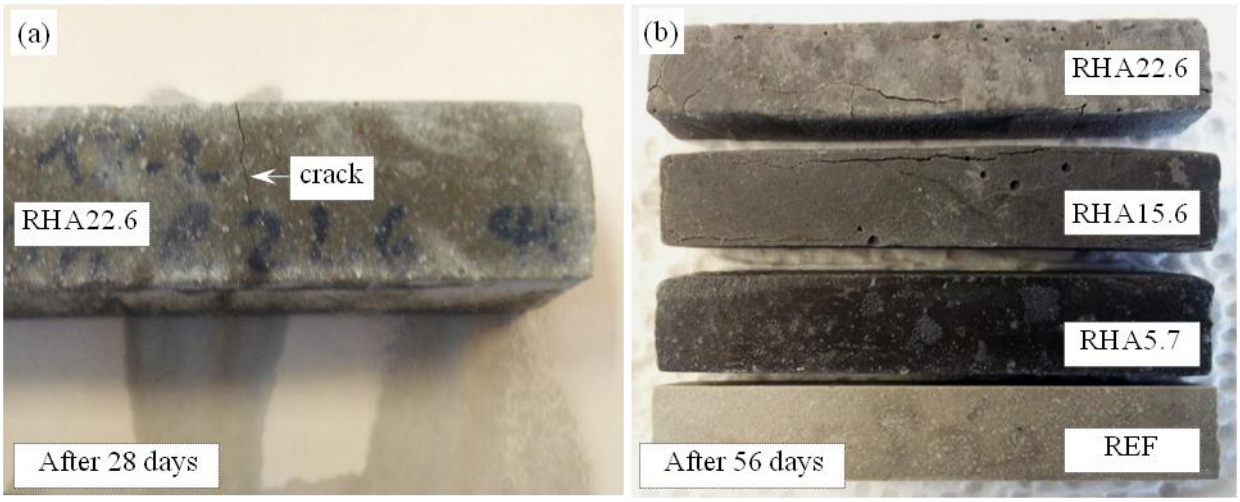

Fig. 9.13 Paste sample in NaOH 1M at 40 ^oC: RHA22.6- sample with visible cracks on the surface after 28 days (a), and RHA22.6/RHA15.6 - sample with disruption after 56 days (b)

In Fig. 9.13, the reference paste sample and the paste samples containing RHA stored in NaOH 1 M at 40 ^{o}C are shown. The first visible cracks on these samples containing RHA22.6/RHA15.6 were obtained after 28 days (Fig. 9.13a), and the disruption of these samples were obtained after 56 days (Fig. 9.13b). This indicates that ASR occurred in the samples containing RHA at 40 ^{o}C later than at 80 ^{o}C.

After 9 months, visible cracks were also detected on the paste bars containing RHA22.6 immersed in NaOH 1 M at 20 ^{o}C (Fig. 9.14a). Fig. 9.14b shows the disruption of the bar containing RHA22.6 and the visible cracks on the surface of the bar containing RHA15.6 after 16 months. This result confirms that the paste sample containing RHA was affected by ASR even at normal temperature, however considerably later than at the higher temperatures. It is very important to note that visible cracks have not been observed on the bar containing RHA5.7. It indicates that there is no concern about ASR with RHA5.7 in cement paste at 20 ^{o}C.

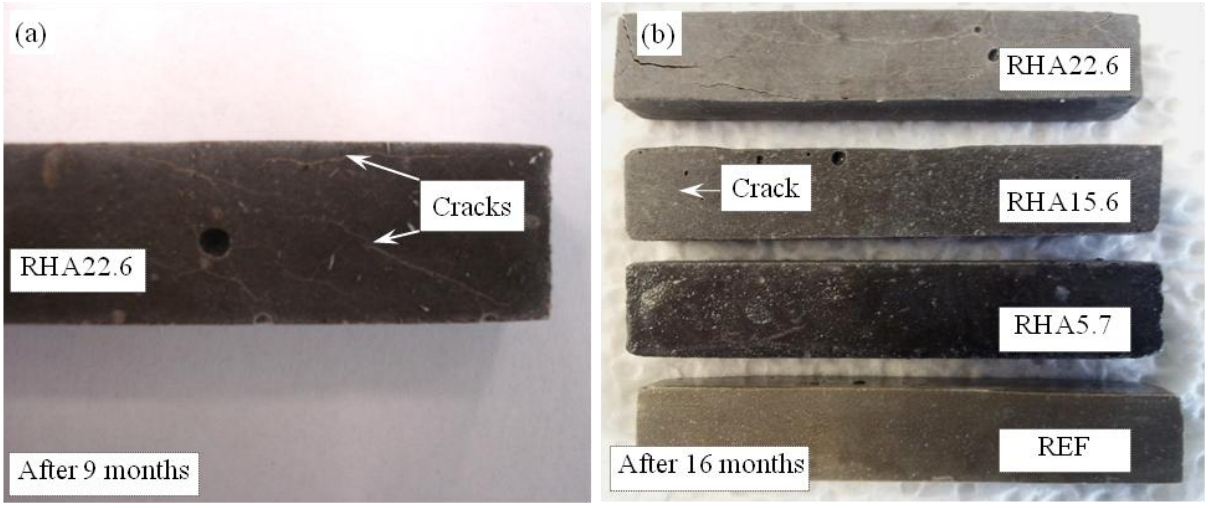

Fig. 9.14 Paste sample in NaOH 1M at 20 ^{o}C: RHA22.6 - sample with visible cracks on the surface after 9 months (a) and disruption after 16 months (b), and RHA15.6-sample with visible cracks on the surface after 16 months (b)

Fig. 9.15 shows BSE and EDX mapping images of paste sample containing 20 wt.% RHA15.6 after 2 days in NaOH 1M at 80 ^{o}C. It can be observed that the ingress of Na ions (indicated in red) from the solution into the matrix led to the corrsion of the sample. The corrosion depth of Na ions after 2 days is about 1.2 mm. The larger depth will be obtained at the later ages, i.e 5, 28 days and consistent with visible cracks observed on the surface of these samples (Fig. 9.12). Furthermore, the EDX mapping image (Fig. 9.15a) displays Na in red, Si in blue, and Ca in yellow where the distribution of Si can be attributed to the distribution of RHA particles in the matrix. Surprisingly, in the Na-affected matrix area, Na mainly distributed together with Si (RHA particles). The pores in the RHA particles may accommodate Na ion, resulting in ASR inside the RHA particles. This problem will be clarified in the next section.

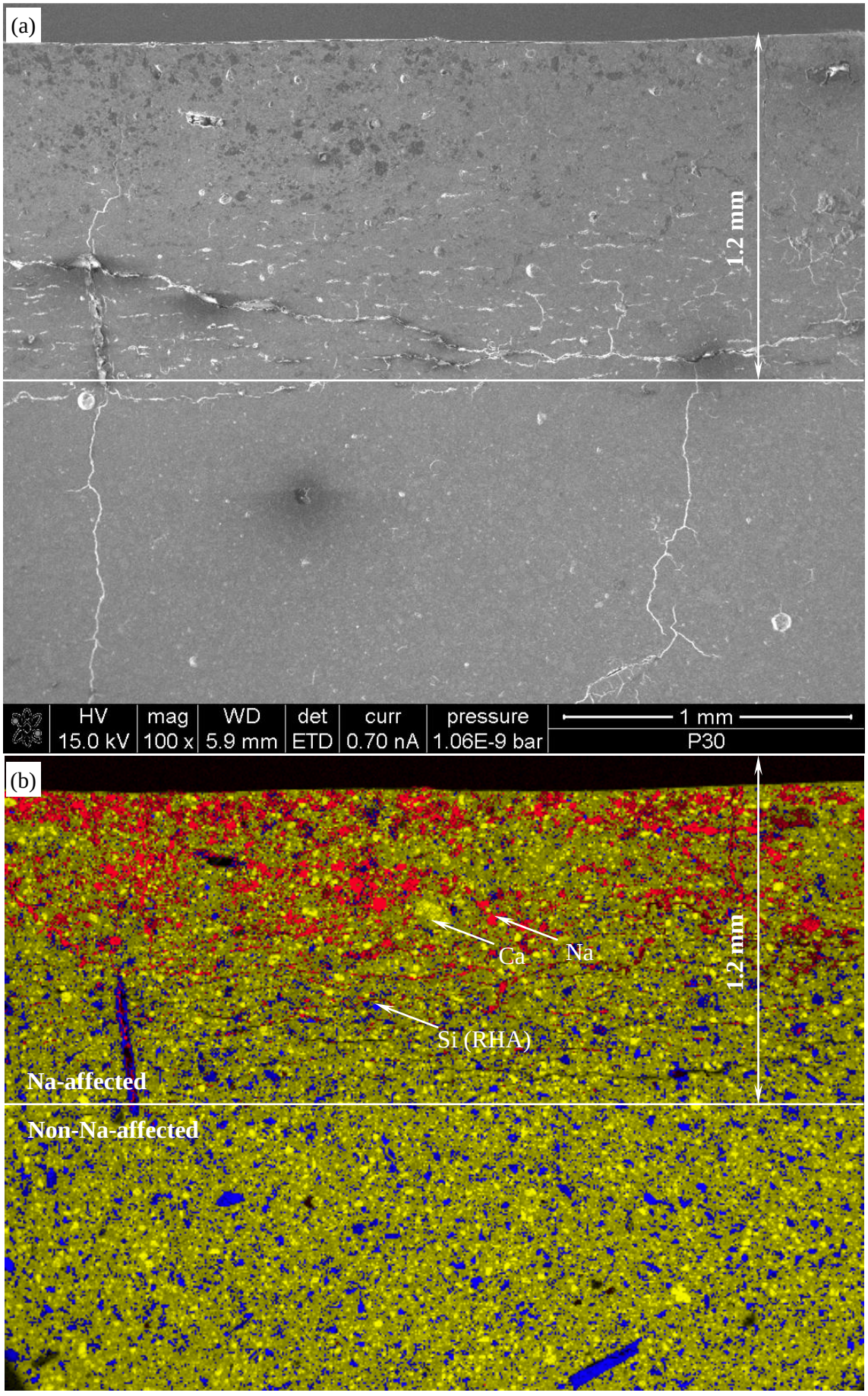

Fig. 9.15 Deterioration of paste sample containing 20 wt.% RHA15.6 in NaOH 1M at 80 ^{o}C, after 2 days: BSE image with corrosion depth (a) and EDX mapping image showing Na in red, Si in blue, and Ca in yellow (b)

Consistent with the deterioration of the paste sample containing RHA, ASR products and cracks were observed by ESEM imaging in pores and in the matrix (Fig. 9.16 and Fig. 9.17). The chemical composition of ASR products were quantified by ESEM-EDX and shown in Table 9.5 and Table 9.6. It can be seen that the chemical composition of ASR products after 2 days of immersion in NaOH contains Si, Ca, and Na. After 5 days, K and Al might be taken up into ASR products (Table 9.6).

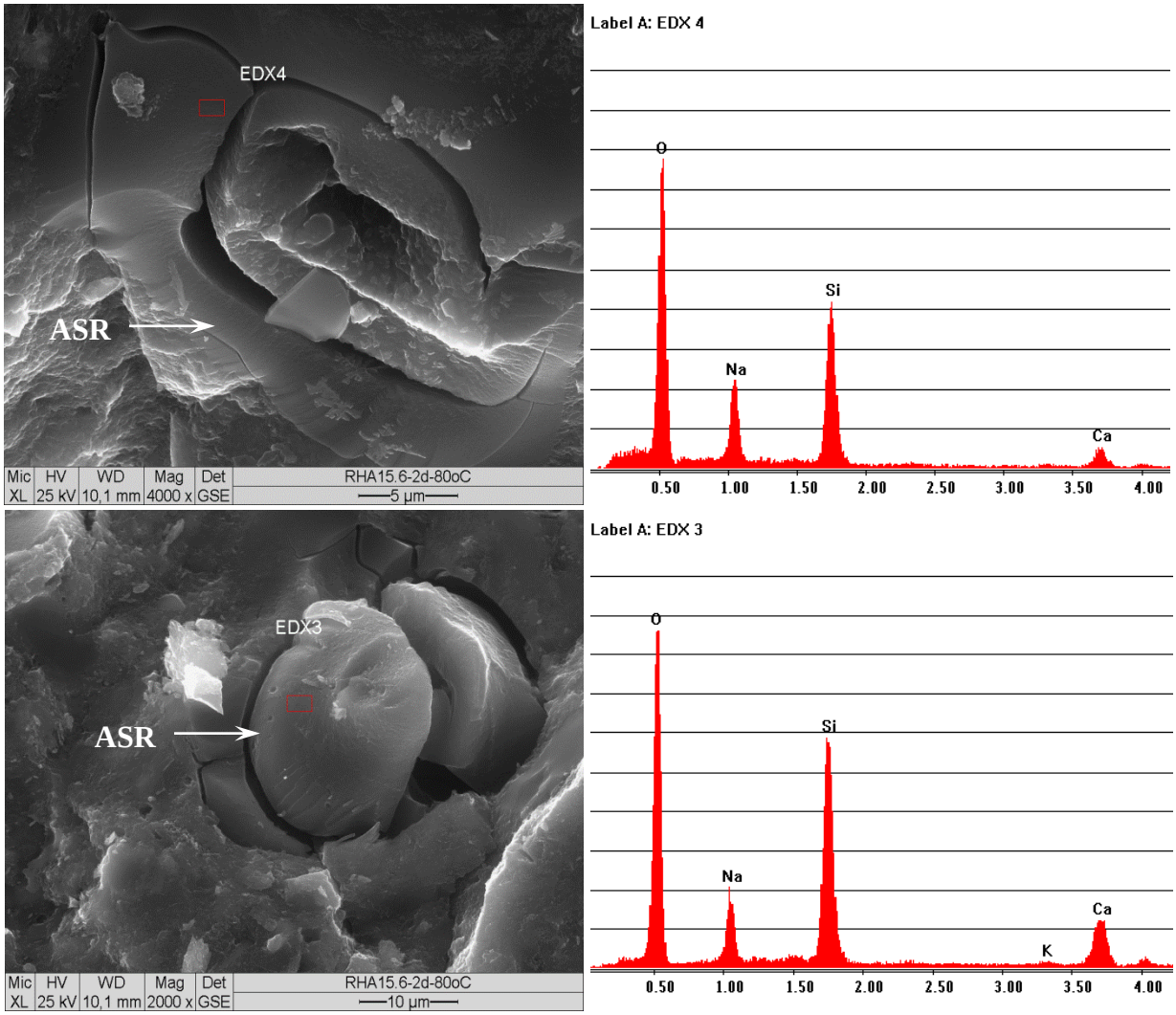

Fig. 9.16 ESEM images showing ASR products formed in pores in the matrix in the paste sample containing RHA15.6 in NaOH 1M at 80 ^{o}C after 2 days

Table 9.5 Oxide composition (wt.%) by ESEM-EDX analysis of ASR products formed in the paste sample containing RHA15.6 in NaOH 1M, at 80 ^{o}C after 2 days

Oxides	SiO_2	CaO	Na_2O	K_2O	Ca/Si	(Na+K)/Si
EDX1	63.5	24.7	11.8	0	0.42	0.36
EDX2	62.2	26.5	11.4	0	0.46	0.35
EDX3	58.7	36.2	5.2	0	0.66	0.17
EDX4	67.4	13.3	19.4	0	0.21	0.56
EDX5	59.3	30.4	10.3	0	0.55	0.34
Mean value	62.2	26.2	11.6	0	0.46	0.36

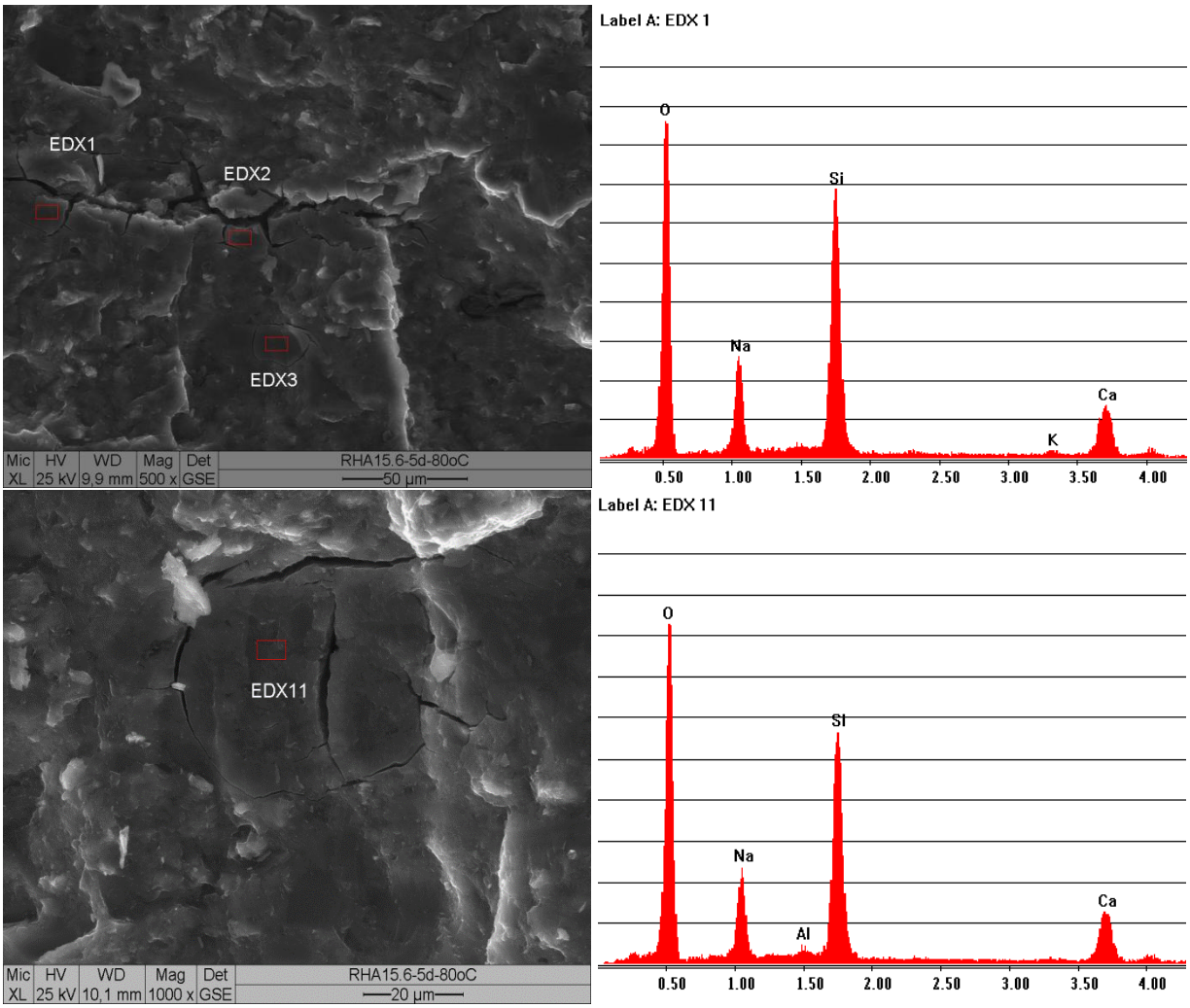

Fig. 9.17 ESEM images showing ASR products deposited in the matrix in the paste sample containing RHA15.6 in NaOH 1M at 80^{o}C after 5 days

Table 9.6 Oxide composition (wt.%) by ESEM-EDX analysis of ASR products formed in the paste sample containing RHA15.6 in NaOH 1M, at 80^{o}C after 5 days

Oxides	SiO_2	CaO	Na_2O	K_2O	Al_2O_3	Ca/Si	(Na+K)/Si
EDX1	62.21	22.62	13.48	1.69	0	0.39	0.45
EDX2	61.98	23.37	13.52	1.13	0	0.40	0.45
EDX3	63.23	24.12	11.04	1.62	0	0.41	0.37
EDX5	65.02	22.03	12.94	0	0	0.36	0.39
EDX6	61.06	28.74	10.21	0	0	0.50	0.32
EDX 11	60.35	23.59	13.50	0	2.56	0.42	0.43
Mean value	62.31	24.08	12.45	0.74	0.43	0.41	0.40

9.3.2. SEM and EDX analyses

NanoSEM and EDX mapping images of hydrated RHA particles in non-Na-affected and Na-affected matrix areas (Fig. 9.15) in the paste sample after 1 day in mould, 1 day in water at 80 ^{o}C and 2 days in NaOH 1 M at 80 ^{o}C are shown in Fig. 9.18, Fig. 9.20 and Fig. 9.21. It can be seen that the coarse RHA particle, i.e. about more than 20µm, in Na-affected area cracked substantially, and cracks radiated from RHA particles to the matrix, can also be seen in Fig. 9.23a and Fig. 9.24b. Interestingly, there is no evidence of cracks with the fine RHA particles, i.e. finer than about 5µm (Fig. 9.25). Whereas the hydrated RHA particles in non-Na-affected area embedded into the matrix, irrespective of MPS of RHA (Fig. 9.18).

EDX-phase mapping shows that C-S-H phases, in blue, were formed by pozzolanic reaction surrounding the RHA particles (Fig. 9.18b and Fig. 9.20b). The pozzolanic reaction rim was also obtained with the hydrated RHA particles in cement paste of mortar after 28 days hydration at 20 ^{o}C (Fig. 7.9b). The X-ray spectra and chemical composition for the C-S-H phases are presented in Fig. 9.19, Fig. 9.22a, Fig. 9.23c Fig. 9.24c, Table 9.7 Table 9.8 and Table 9.9, respectively. The Ca/Si molar ratio of these C-S-H phases is about 0.74 (in non-Na-affected area) and 1.10 (in Na-affected area). Both of them are described as ''tobermorite-like'' C-S-H, as mentioned in Section 7. The C-S-H phases formed by RHA in Na-affected area not only had the higher Ca/Si ratio but also higher Na_2O content. It indicates that these C-S-H phases have uptaken an amount of Na ions migrated from the solution into the matrix. The content of calcium oxide clearly dominates that of alkali oxide, i.e. Ca/Si ratio is much higher than (Na+K)/Si, the hydrates can be called calcium-alkali-silicate hydrates: C-(Na, K)-S-H

Furthermore, EDX-phase mapping shows that ASR products, in red, were formed inside the RHA particles in Na-affected area (Fig. 9.20b). ASR products formed inside the small and the large RHA particles. The large RHA particles cracked substantially. The X-ray spectra and chemical composition of the ASR products formed inside the large RHA particles are shown in Fig. 9.22b and Table 9.8 respectively. The (Na+K)/Si ratio of the ASR products is much higher than Ca/Si ratio, contrary to those of C-S-H products above. EDX spectra taken from the interior of RHA particles (EDX14-Fig. 9.23a, d and EDX16-Fig. 9.24a, d) shows similar results. This is also indicative of the faster and higher penetration of sodium ions compared to calcium ions, as mentioned elsewhere [222]. Alkali silica reaction of RHA might take place faster than its pozzolanic reaction. The oxide composition of these hydrates are shown in Table 9.10 and lie inside the area of swelling ASR gels proposed by Mansfeld [19, 221]. These hydrates can be called alkali-calcium silicate hydrates: Na, K-(C)-S-H.

Table 9.7 Chemical composition (wt.%) of hydrated RHA particles in non-Na-affected matrix area quantified by EDX-mapping (Fig. 9.18b)

Oxides	SiO_2	CaO	Na_2O	K_2O	Al_2O_3	Ca/Si	(Na+K)/Si
Unhydrated RHA	97.5	0	0.30	2.2	0	-	-
C-S-H- RHA1	54.47	38.36	0.69	3.26	3.22	0.75	0.10
C-S-H- RHA2	56.38	37.71	0.77	3.29	1.86	0.72	0.10
Mean value	55.43	38.04	0.73	3.28	2.54	0.74	0.10

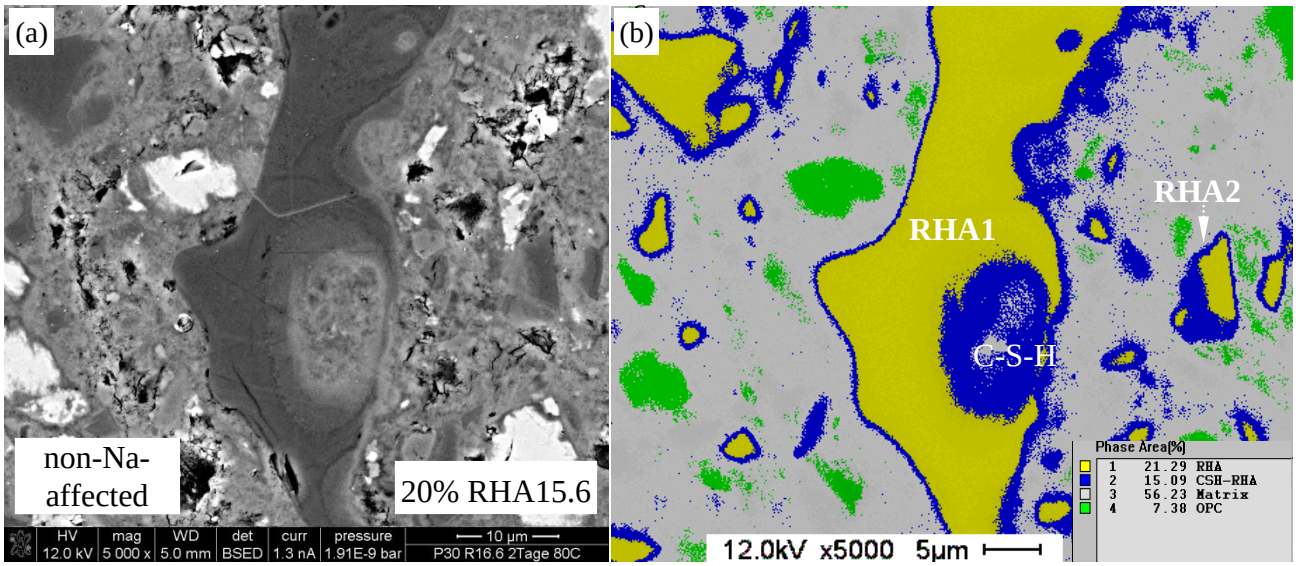

Fig. 9.18 BSE-SEM (a) and EDX-phase mapping (b) images of hydrated RHA particles in non-Na-affected matrix area in paste sample containing 20 wt.% RHA15.6 at w/b of 0.30 after 4 days hydration. RHA in yellow, RHA-hydrate rim in blue, OPC in green, and matrix in white

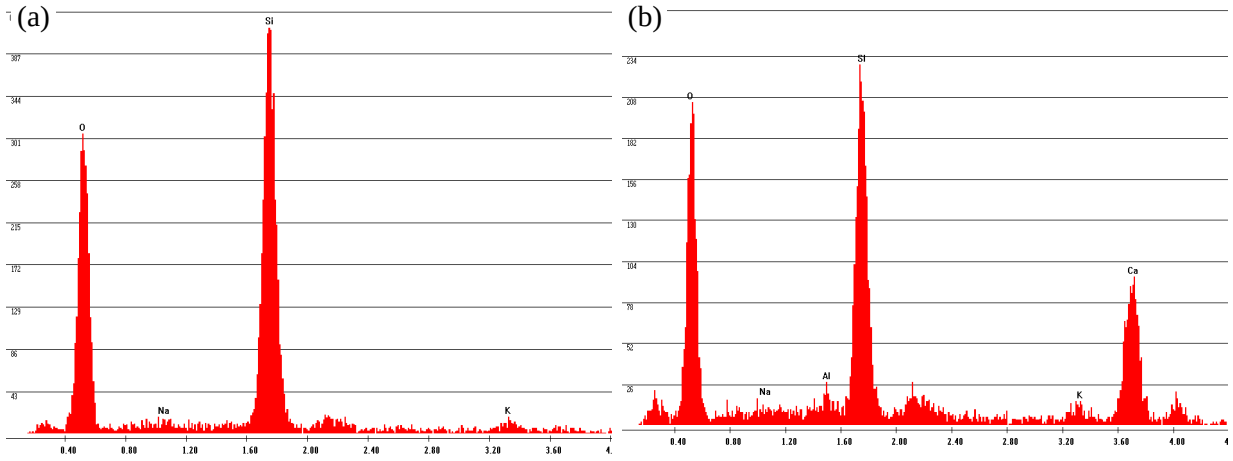

Fig. 9.19 X-ray spectra for hydrated RHA particles: remnants of RHA particles (a) and hydrate rim of RHA particles (b), i.e. C-S-H phases, showing in Fig. 9.18b

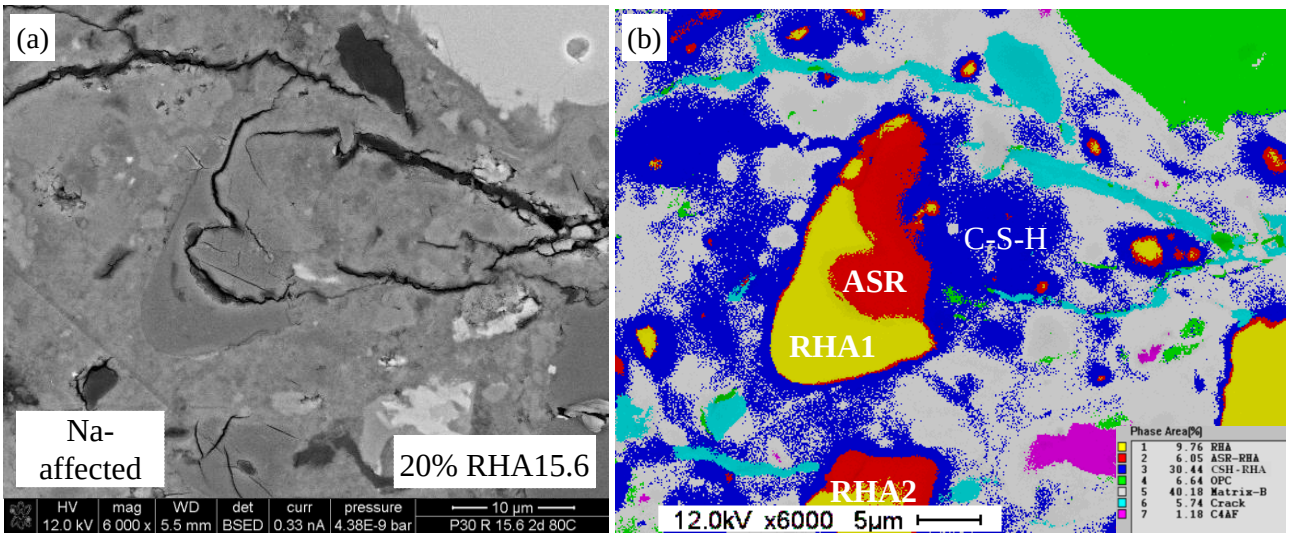

Fig. 9.20 BSE-SEM (a) and EDX-phase mapping (b) images of hydrated RHA particles in Na-affected matrix area in paste sample containing 20 wt.% RHA15.6 at w/b of 0.30 after 4 days hydration (2 days in NaOH 1M). RHA in yellow, RHA-hydrate rim in blue, and ASR in red

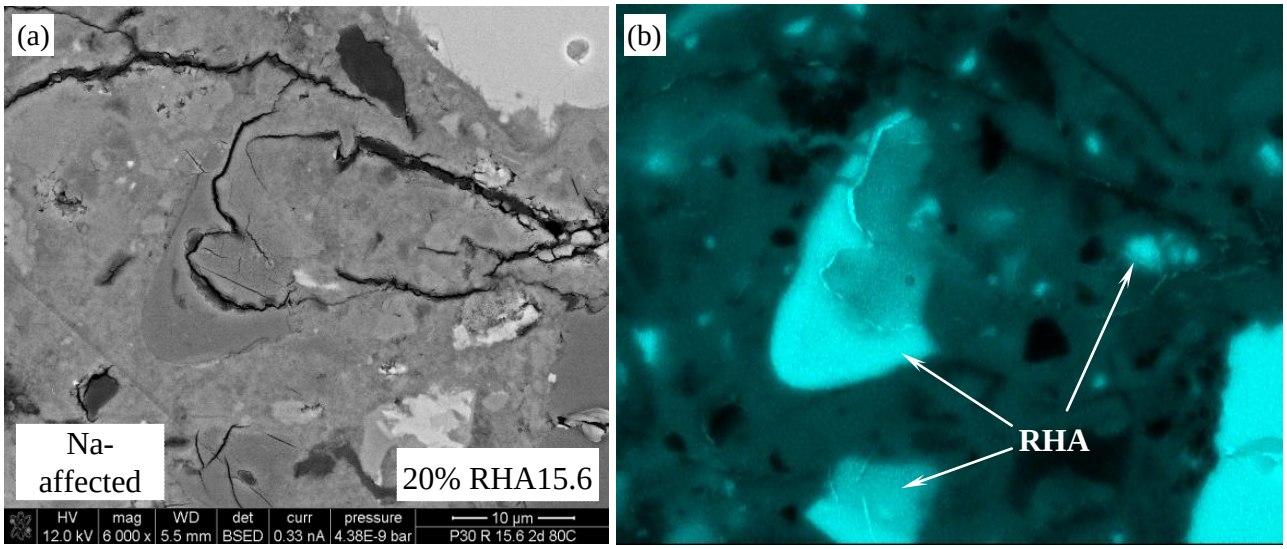

Fig. 9.21 BSE-SEM (a) and EDX-Si-mapping (b) images of hydrated RHA particles in Na-affected matrix area in paste sample containing 20 wt.% RHA15.6 at w/b of 0.30 after 4 days hydration (2 days in NaOH 1M). RHA particles in slight blue

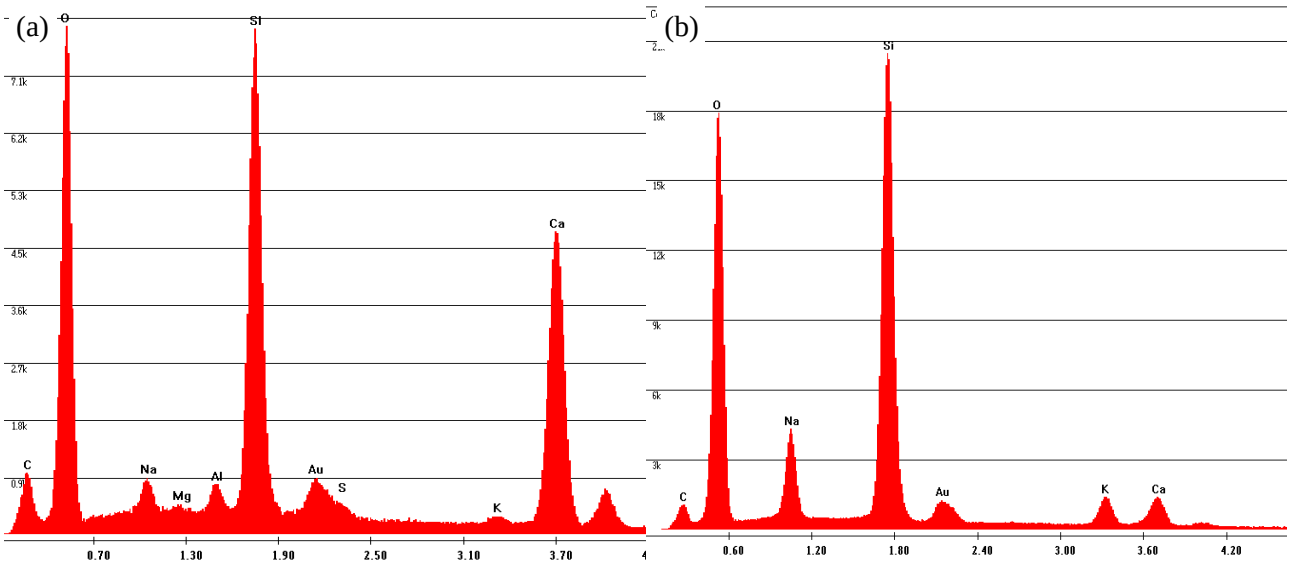

Fig. 9.22 X-ray spectra for hydrated RHA particles: pozzolanic hydrate-rim of RHA particles, i.e. C-(Na, K)-S-H phases (a) ASR products, i.e. (Na, K)-C-S-H phases (b) showing in Fig. 9.20b

Table 9.8 Chemical composition (wt.%) of hydrated RHA particles in Na-affected matrix area quantified by EDX-mapping in Fig. 9.20b

Oxides	SiO_2	CaO	Na_2O	K_2O	Al_2O_3	Ca/Si	(Na+K)/Si
Unhydrated RHA	98.0	0.8	-	1.1	-	-	-
C-S-H-RHA	46.47	47.93	2.39	1.04	2.18	1.10	0.13
ASR-RHA1	76.7	7.9	9.4	6.0	-	0.11	0.34
ASR-RHA2	79.28	7.20	7.04	6.46	-	0.10	0.28
Mean value	78.0	7.55	8.22	6.46	-	0.11	0.31

Fig. 9.23a,b and Fig. 9.24a,b show SEM images of ASR affected RHA and agglomerated SF particles. The agglomerated SF particles (about 100-200 µm) [18, 223, 224] is much larger than RHA particles (about 20-30 µm). Furthermore, ASR occurs outside the agglomerated SF particles, whereas it can be observed inside the RHA particles. The mechanism and the process of ASR of RHA might therefore differ from those of the agglomerated SF particles due to the pore structure of RHA.

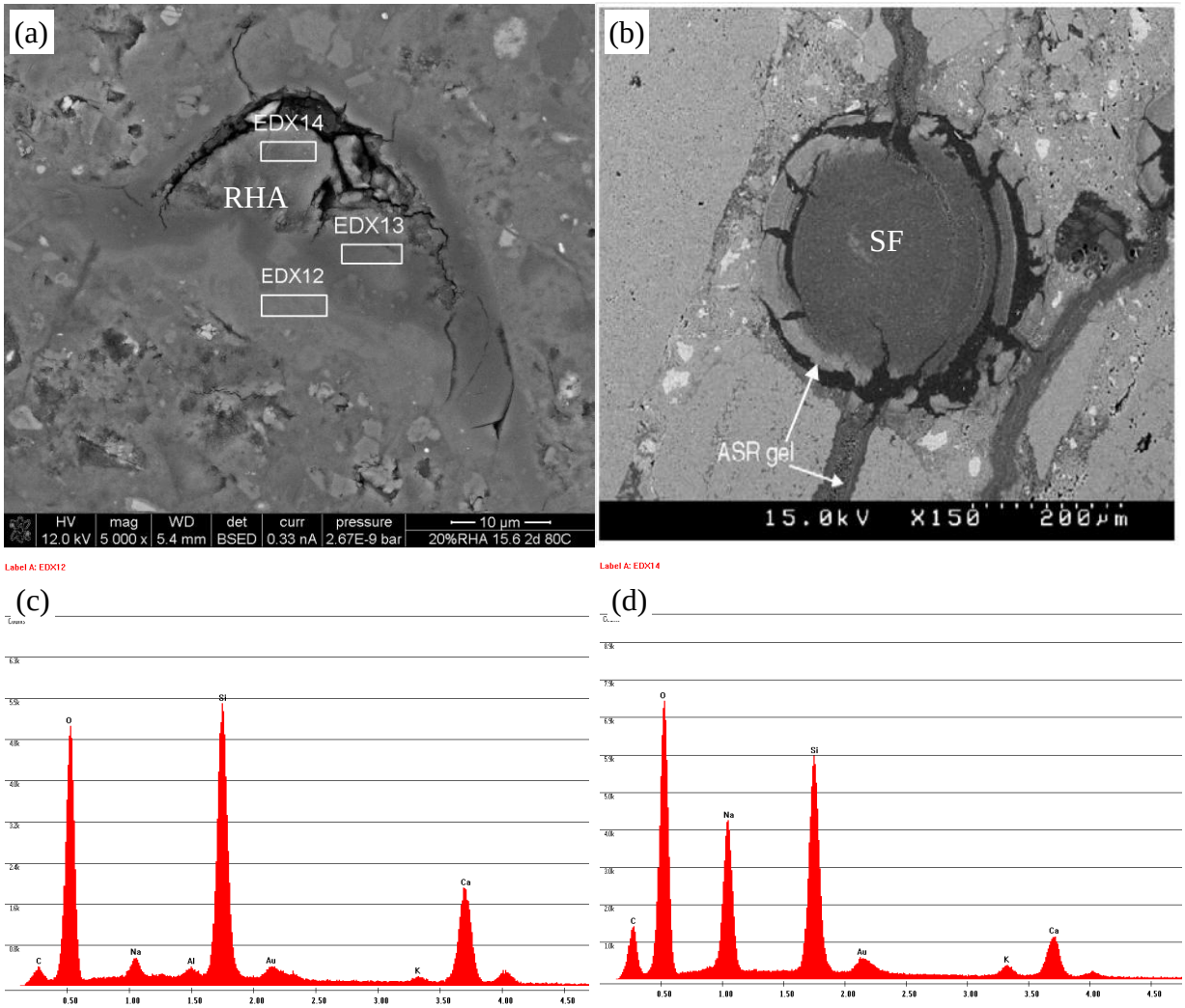

Fig. 9.23 Comparing ASR gels formed by agglomerated SF particles and by RHA particles. The agglomerated SF particles are much larger than RHA particles. ASR gels formed surrounding the agglomerated SF particles (b), however inside the RHA particle (a), EDX12 (c) and EDX14 (d)

Table 9.9 Oxide composition (wt.%) of pozzolanic-like reaction hydrates formed surrounding the RHA particles

Oxides	SiO_2	CaO	Na_2O	K_2O	Al_2O_3	Ca/Si	(Na+K)/Si
EDX12	58.01	35.77	2.86	1.44	0.09	0.66	0.13
EDX15	49.70	43.35	4.57	1.15	1.23	0.93	0.21
EDX17	49.09	37.98	10.87	1.29	2.06	0.83	0.46
EDX3	52.19	40.49	5.33	0.57	0.68	0.83	0.21
Mean value	52.25	39.40	5.91	1.11	1.01	0.81	0.25

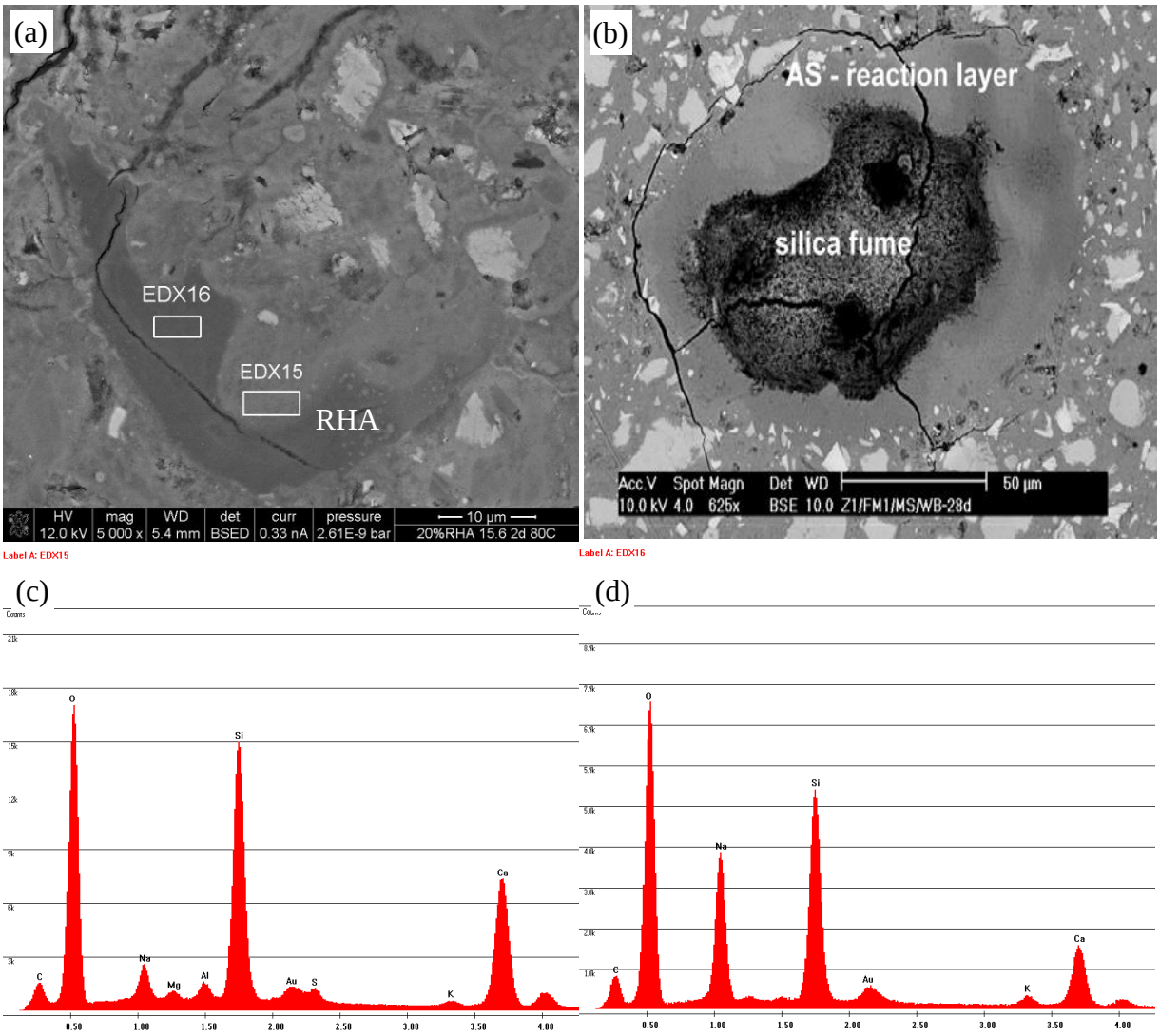

Fig. 9.24 Comparing ASR gels formed by agglomerated SF particles and by RHA particles. The agglomerated SF particles are much larger than RHA particles. ASR gels formed surrounding the agglomerated SF particles (b), however inside the RHA particle (a), EDX15 (c) and EDX16 (d)

Table 9.10 Oxide composition (wt.%) of ASR-like hydrates formed inside the cracked large RHA particles

Oxides	SiO_2	CaO	Na_2O	K_2O	Ca/Si	(Na+K)/Si
EDX9	66.55	13.54	18.78	1.14	0.22	0.57
EDX10	63.23	8.61	27.46	0.69	0.15	0.85
EDX13	56.4	21.67	18.79	3.14	0.41	0.72
EDX14	55.22	17.78	23.73	3.28	0.34	0.91
EDX16	50.81	24.39	22.15	2.65	0.51	0.91
Mean value	58.44	17.2	22.18	2.18	0.32	0.78

In Fig. 9.25 a, b, the fine RHA particle (about 5µm) and the coarse RHA particle (about 20µm) in Na-affected area are shown. The coarse RHA particle cracked substantially, whereas the fine one was still dense and stable, as mentioned above. Elementary analyses by EDX indicate that

chemical composition of hydrates outside and inside the fine RHA particle is similar, as seen in Fig. 9.25c, d and Table 9.11. The Na_2O content of the inner hydrates was still higher than that of outer hydrates. Both of them might be C-S-H phases containing alkali which are not expansive or the inner hydrates are a kind of ASR products with a high ratio of Ca/Si. Whereas the chemical composition of the outer hydrates of the coarse RHA particles was much different from that of the inner hydrates Fig. 9.23 (c, d). The hydrates outside the coarse RHA are a kind of C-S-H phase containing alkali, and the hydrates inside the coarse RHA is a kind of ASR containing calcium which are expansive.

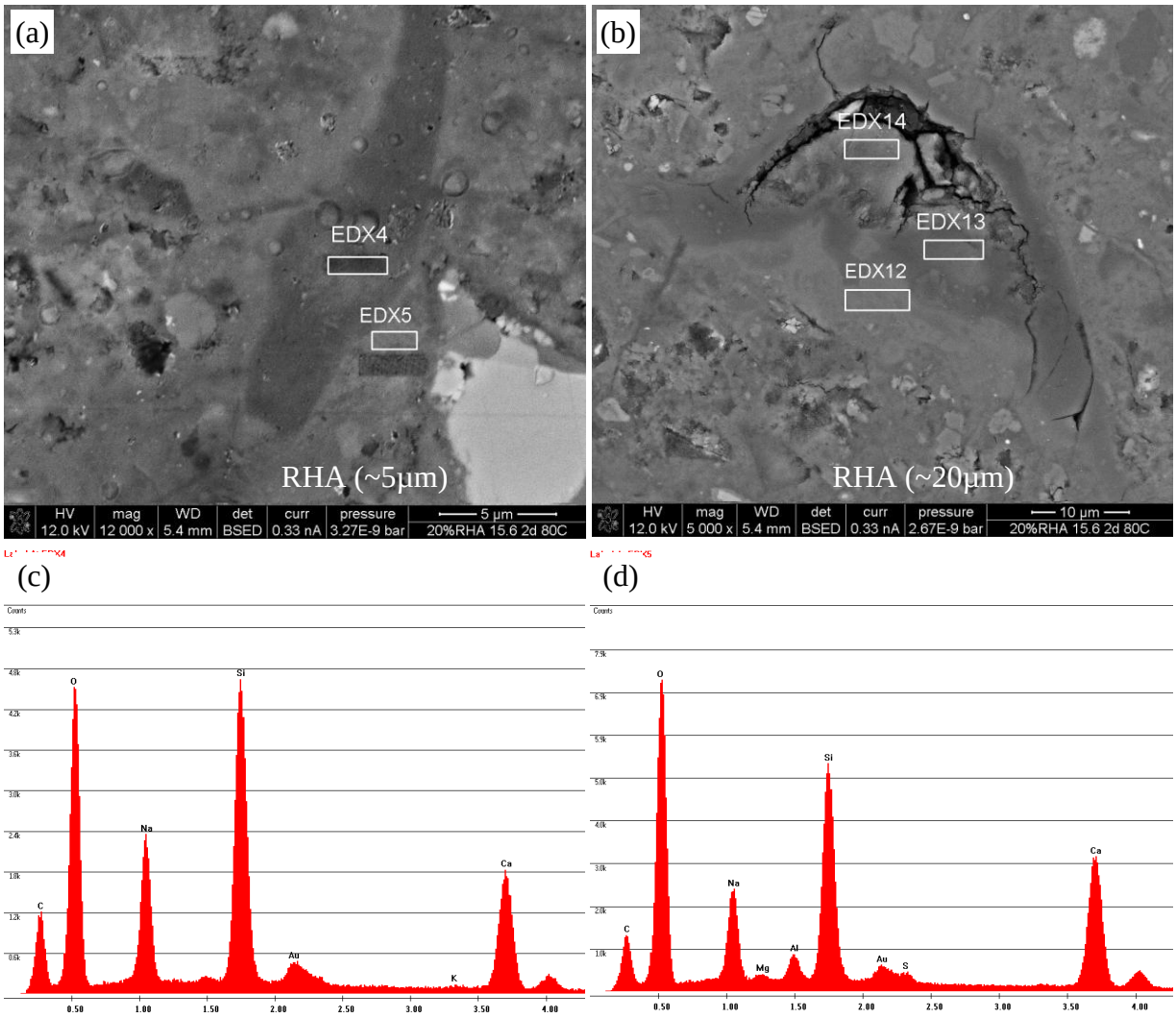

Fig. 9.25 The hydrated RHA particle, about 5µm (a), about 20µm (b), and spectra for hydrates formed inside (EDX4, c) and outside (EDX5, d) the fine hydrated RHA particle after 2 days immersion in NaOH at 80 °C

Table 9.11 Oxide composition of ASR-like hydrate formed inside the non-cracked fine RHA particles

Oxides	SiO_2	CaO	Na_2O	K_2O	Al_2O_3	Ca/Si	(Na+K)/Si
EDX2	55.2	30.9	11.3	2.6	0	0.6	0.5
EDX4	50.5	33.4	15.6	0.57	0	0.7	0.6
Mean value	52.9	32.2	13.5	1.6	0	0.7	0.5
EDX5	42.0	44.0	12.0	0.0	2.1	1.12	0.55

9.4. Characterization of ASR products formed by RHA

To characterize the ASR products formed by RHA, RHA15.6 was dry mixed with $Ca(OH)_2$ powder in 1 min, and then NaOH 1 M was added and mixed in 3 min to obtain homogeneous slurry. Afterward, the slurry was the subdivided and cast in polyethylene bottles and stored at 20, and 80 ^oC. The slurry composition contains 68 wt.% SiO_2 (from RHA), about 13 wt.% alkali oxide (Na_2O from NaOH, and K_2O from RHA) and 19 wt.% CaO (from $Ca(OH)_2$). The slurry composition was selected on the basis of the oxide composition of ASR products formed by RHA analysed in the previous section and the batch composition proposed by Hou, X., L.[225] for production of ASR gels from Opal, solid $Ca(OH)_2$ and NaOH 1 M. The samples stored at 20 and 80 ^oC were dried at room temperature after 1 day and 4 days respectively. The visual inspection after the test indicates that the volume of slurry increased significantly, e.g. the initial volume of slurry is about 50 % the volume of bottle, after 1 day the volume of slurry stored at 80 ^oC was bout 70-80 % the volume of bottle. The solid products were examined by optical microscopy and SEM-EDX. The morphology of ASR products obtained by optical microscopy and ESEM imaging is shown in Fig. 9.26 and Fig. 9.27 respectively, and qualitative composition of these hydrates are shown in Fig. 9.28 and Table 9.12. The mean value of the ASR products lie in the swelling area of ASR gels proposed by Mansfeld [221]. It is obvious that the (Na+K)/Si ratio of the hydrates is much higher than Ca/Si ratio.

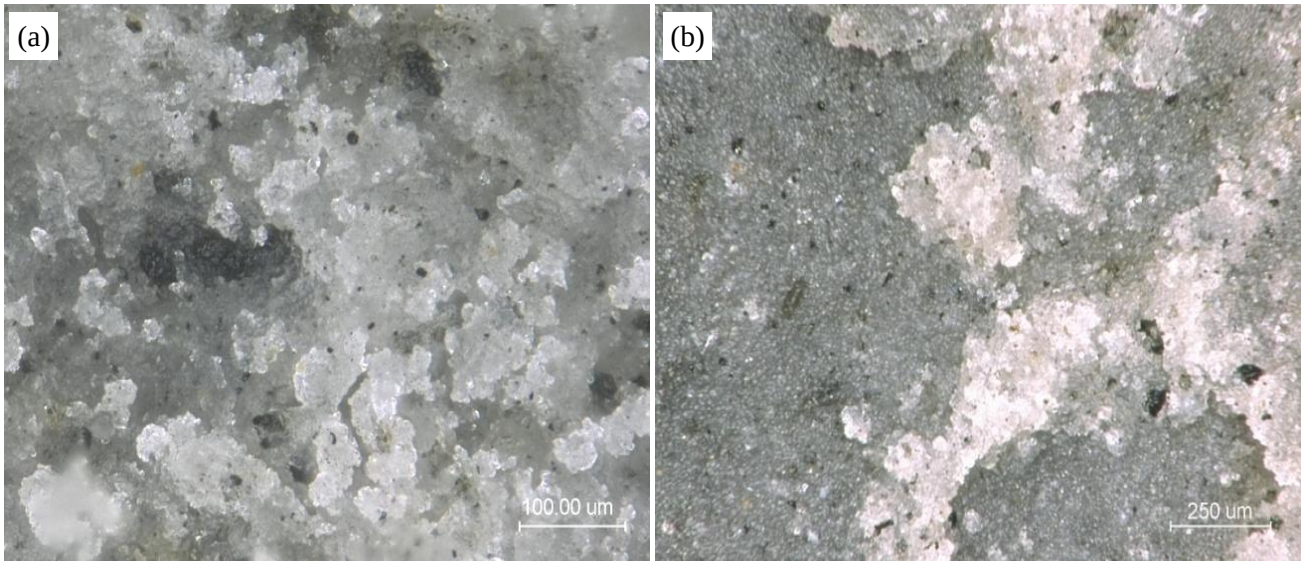

Fig. 9.26 Optical microscopy images of ASR products formed in mixture of RHA, NaOH and $Ca(OH)_2$ at 80 ^oC after 1 day (a) and at 20 ^oC after 4 days (b)

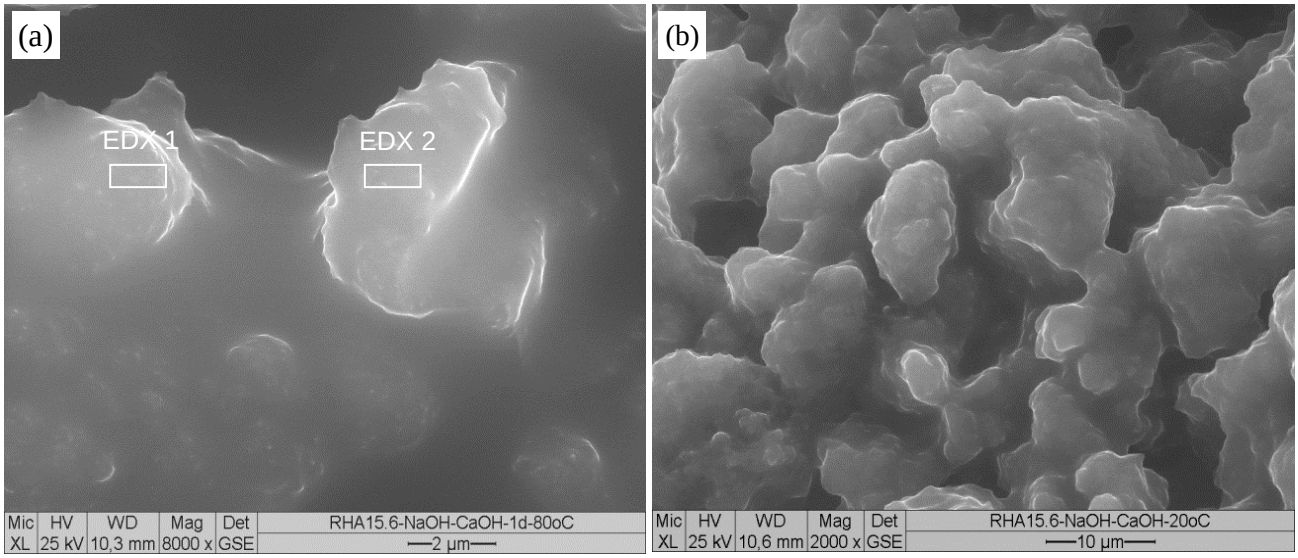

Fig. 9.27 ESEM images of ASR products of ASR products formed in mixture of RHA, NaOH and $Ca(OH)_2$ at 80 ^oC after 1 day (a) and at 20 ^oC after 4 days (b)

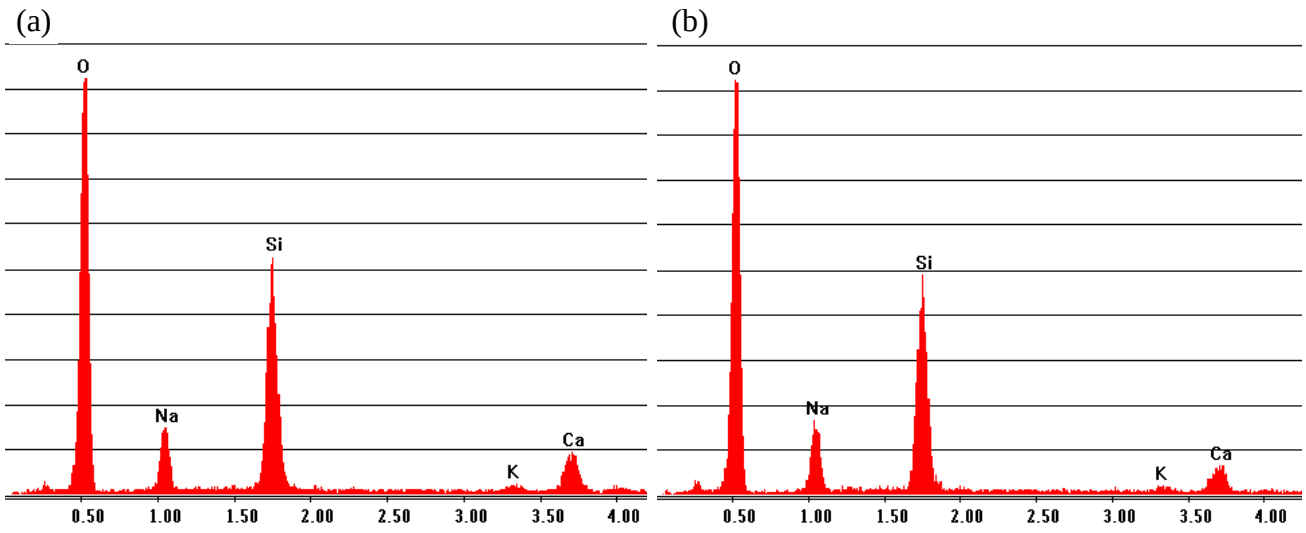

Fig. 9.28 X-ray spectra for ASR products formed in mixture of RHA, NaOH and Ca(OH)2 at 80 ^oC after 1 day (a) and at 20 ^oC after 4 days (b)

Table 9.12 Chemical composition (wt.%) by EDX analysis of ASR products formed in mixture of RHA, NaOH and $Ca(OH)_2$ at 80 ^oC after 1 day

Oxides	SiO_2	CaO	Na_2O	K_2O	Ca/Si	(Na+K)/Si
EDX1	69.1	15.4	13.2	2.4	0.24	0.41
EDX2	68.1	7.7	22.9	1.4	0.12	0.68
Mean value	68.60	11.55	18.05	1.90	0.18	0.55

9.5. Discussion

Experimental results show that the behaviour of RHA with ASR under the accelerated test is strongly dependent on its MPS, and content of RHA used. Temperature is a very important factor influencing the process of ASR of RHA. The resistance of mortar formulated from SCHPC is strongly affected by reactive aggregate used.

9.5.1. The resistance of mortar formulated from SCHPC to ASR

The resistance of mortars formulated from SCHPC with w/b of 0.30 to ASR was evaluated by the accelerated test in accordance with the American standard [187] and the German standard [165]. According to these methods, at 16 days after casting and 14 days in NaOH 1M at 80 ^{o}C, expansions of mortar bars lower than 0.10 % are indicative of being innocuous, and higher than 0.20 % are indicative of potentially deleterious ASR. It is very important to note that mortar used in these standards is made with w/b of 0.47. The 25x25x285 mm^3 sized mortar bars are used in American standard [187], whereas the size of mortar bars in the German standard [165] is 40x40x160 mm^3. The ingress level of Na ion into the matrix increases with the reduction in the cross sectional area of mortar bars [16] and the higher w/b ratio of mortar which increases the porosity of the matrix. The ingress level of Na ion mainly affects the variation in the length of mortar bars which indicates the deterioration of mortar in the ASR test. Therefore, the expansion threshold of these standards should be used as a reference.

In this study, the mortars were made with reactive greywacke aggregate and non-reactive basalt aggregate. For the mortars containing greywacke, the expansion of all investigated mortar bars was lower than the limit at 14 days, where the expansion of the reference sample containing reactive greywacke aggregate is at the highest level, near to 0.10 % (Fig. 9.1), and increasing MPS of RHA increased the expansion of mortar bars. Based on the expansion criteria, it can be concluded that the mortar formulated from SCHPC is innocuous with ASR damage. However, it should be concerned that although the mortar bars containing the coarse RHA, i.e. RHA7.7 and RHA15.6, had an expansion level lower than the reference sample, visible cracks existed on the surface and along the edges of these samples containing the coarse RHA Fig. 9.2d, e. Moreover, the mortar bars containing RHA15.6, and RHA7.7 were disrupted after 28 days and 56 days immersion in NaOH 1M at 80 ^{o}C respectively, and the expansion of the sample containing RHA5.7 dramatically increased to over the threshold of 0.10 % after 56 days in NaOH 1M (Fig. 9.3). The situation obtained from the sample containing SF was absolutely different. The expansion of mortar bars containing SF was lower than that of the mortar containing RHA and far below the threshold even up to 56 days immersion in NaOH 1 M (Fig. 9.3). This indicates that mortar containing SF is durable regarding ASR damage. And, SF is much more effective in mitigating ASR in mortar and SCHPC than RHA, even when the amorphous silica content of RHA is similar to that of SF (Table 3.1). The larger particle size and pore structure of RHA might induce this difference. These factors will be analyzed in detail in next sections. The positive effect of SF on ASR is also obtained from the other studies [21, 23, 163, 226]. The pozzolanic SCMs, such as FA and SF, refine pore structure of cement matrix, hence reduce the diffusivity of alkali ions into the concrete. The pozzolanic reaction of these SCMs produces C-S-H with low Ca/Si ratio which has negative charge. The negatively charged C-S-H takes up cations, especially alkali ions. That is the mechanism by which the pozzolanic SCMs mitigate or eliminate ASR reaction [21, 22, 227]. Experimental results presented in previous section indicate that SF has higher pozzolanic reactivity than RHA and the porosity of the mortar containing SF is lower than that of the mortar containing RHA (Table

7.2 and Fig. 7.18). For RHA, the pozzolanic reaction takes place firstly on the surface of RHA particle and then inside the pore of the RHA particles. The fine RHA particle (RHA5.7) with larger SSA, i.e. larger external SSA, has higher external pozzolanic reactivity than the coarse ones (RHA15.6, RHA22.6), as analysed in Section 7.2.5, thus the RHA5.7 refines pore structure of mortar better than the coarse RHA22.6 (Table 7.2 and Fig. 7.18). That can explain for the expansive behaviour of mortar bars containing SF, RHA5.7, RHA7.7 and RHA15.6 mentioned above.

The increase in RHA5.7 content resulted in the decrease in the expansion level of mortar bars (Fig. 9.8) could also be explained by the refinement of pore structure of the matrix and the reduction in alkali concentration in pore solution due to the uptake of alkali by the low Ca/Si-C-S-H. Similar results of effect of RHA content on ASR has been obtained when RHA with MPS of 4 µm and 8µm was used [7, 163].

For mortars made with non-reactive basalt aggregate, it can be seen in Fig. 9.6 that all reference sample and sample containing RHA had expansion level lower than 0.10 % at 14 days and 28 days as well. These results indicate that all mortars containing basalt are not deleterious regarding ASR. However, it is very important to note that the reference sample containing non-reactive basalt aggregate has lower expansion than the sample containing RHA, and the bars containing RHA15.6 still cracked substantially along the edges (Fig. 9.5). The cracking was also observed along the edges of 10x40x160 mm^3 and 40x40x160 mm^3 sized UHPC bars containing RHA with MPS of 7.41 µm [16]. This phenomenon implies that the incorporation of RHA exacerbate, rather than prevent ASR damage in mortar formulated from SCHPC, especially with coarse RHA particles.

9.5.2. Paradoxical effect of RHA on ASR

To avoid the effect of aggregate on ASR, and to evaluate the effect of RHA on ASR, the paste formulated from SCHPC was produced. The 10x10x60 mm^3 sized paste bars were exposed in NaOH 1 M at 20, 40, and 80 ^oC, similar to the testing procedure in the accelerated test used on mortar bars. By visual inspection, the paste bars containing RHA22.6 and RHA15.6 exhibited visible cracking after 2 days (at 80 ^oC), after 28 days (at 40 ^oC) and after about 9 months (at 20 ^oC). Visible cracking only appeared on the paste bars containing RHA5.7 only at 80 ^oC after 28 days (Fig. 9.12-Fig. 9.14). Interestingly, corresponding to the lower expansion of reference mortar bars containing basalt, there was no evidence of cracking on the reference paste bars regardless of curing temperatures, i.e. 20, 40 and 80 ^oC. ESEM images and ESEM-EDX shown a lot ASR products filled in the pores and deposited in the matrix of the paste bar containing RHA (Fig. 9.16 and Fig. 9.17). Apparently, RHA constitutes rather than prevent ASR deterioration. RHA particles indeed act as micro-reactive aggregates and react with alkali hydroxide to generate the expansive ASR products. Therefore, it can be concluded that RHA has paradoxical effect on ASR in the presence of high alkali concentration, especially with the coarse MPS of RHA and at high temperature, i.e. 80 ^oC. The paradoxical effect on ASR has also been obtained with the agglomerated SF (Fig. 9.23 and Fig. 9.24) [18, 23, 223, 224] and

coarse glass cullet [228]. However, the negative effect on ASR is obtained only when the MPS of SF is in range of 40 to 100 µm and larger, and the MPS of the glass cullet is larger than 1 mm. Whereas herein MPS of RHA is in the range of 5.7 to 22.6 µm. With this range of MPS or larger, FA, especially low-calcium FA, is effective in mitigating ASR in mortar and concrete containing reactive aggregate, even when the alkali content of FA is similar or higher than that of RHA [20, 22, 227, 229, 230]. As concluded in Section 4., RHA is a porous amorphous siliceous material. The SSA of RHA derives from the surface and mainly from the pore structure inside the RHA particles. The pore structure of RHA makes its behaviour, such as pozzolanic activity, in cementitious materials different from the common SCMs, e.g. FA, SF, as analyzed in Section 7. Furthermore, it is very important to note that the nature of amorphous silica of RHA is termed opaline silica [231, 232] which is one of the most reactive forms of silica in metastale group containing opal, tridymite, cristobalite, and silica glass: intermediate glass (52-66% SiO_2), acid glass (more than 66% SiO_2). Aggregate containing opal typically reacts more rapidly, and aggregate containing more than 5 wt.% opal is considered potentially reactive [19, 225, 233].

9.5.3. Mechanism for successive pozzolanic and alkali silica reactions of RHA

Based on the crack patterns and the elemental analyses on the affected RHA particles in the deteriorated paste as described in Section 9.3.2 and the reference to the mechanism for ASR deterioration of coarse glass cullet [228] and reactive aggregate [222], the hypothesis on the successive reactions of RHA particles was given, as illustrated in Fig. 9.29. Depending on MPS of RHA, different types of hydrates could be obtained. According to elemental analyses, it seems that only one type of hydrate, i.e. C-S-H- like pozzolanic product containing alkalis, were formed inside and surrounding the fine RHA particles. Whereas the coarse RHA led to formation of two types of hydrates. The C-(Na, K)-S-H–like pozzolanic hydrates were formed surrounding the RHA particles resulting in the pozzolanic reaction ring around the RHA particles, as indicated in blue in Fig. 9.18b and Fig. 9.20b. The chemical composition of this type of hydrate is presented in Table 7.1, Table 9.7, Table 9.8 and Table 9.9, and X-ray spectra can be seen in Fig. 7. 8b, d, Fig. 9.19b, Fig. 9.22a, Fig. 9.23c (EDX12), and Fig. 9.24c (EDX15). The pozzolanic reaction rim acts as a semi-permeable membrane which allows Ca, Na, and OH ions migrate from the matrix into RHA particles. The penetration of these ions led to the production of the second type of hydrate, i.e. Na, K-(C)-S-H-like ASR products whose compositions are shown in Table 9.8 and Table 9.10, and X-ray spectra are shown in Fig. 9.22b, Fig. 9.23d (EDX14), and Fig. 9.24d (EDX16). The chronology of the reactions for RHA particles could be the following:

- Amorphous silica from the external surface of RHA particles attacked by OH ions dissolves into the aqueous solution, and a certain amount of water is absorbed into the pores of RHA particles. Ca and OH ions in pore solution react with silica to produce C-(Na, K)-S-H hydrates which then precipiate on the surfaces of RHA particles and could take up an amount of Na, K, and Al ions. That results in the formation of the pozzolanic reaction rim, and RHA particles are partially or completely tightly packed inside the rim.

- The reaction rim will become thicker over time. It acts as a semi-permeable membrane which allows the penetration of Na, K, Ca and OH ions but not allow leakage of ASR gels generated after the formation of the pozzolanic reaction rim.
- Na, K, Ca and OH ions penetrate into RHA particles. Na, K ions penetrates much faster than Ca ions [20, 234], hence ASR occurs earlier. The alkalis react with silica and produce ASR gels which react with Ca ions, adsorb water in the pores of RHA particles and expand [235]. The resultant expansive ASR hydrates accumulated inside RHA particle are responsible for the cracking of RHA particles and the surrounding cement matrix.

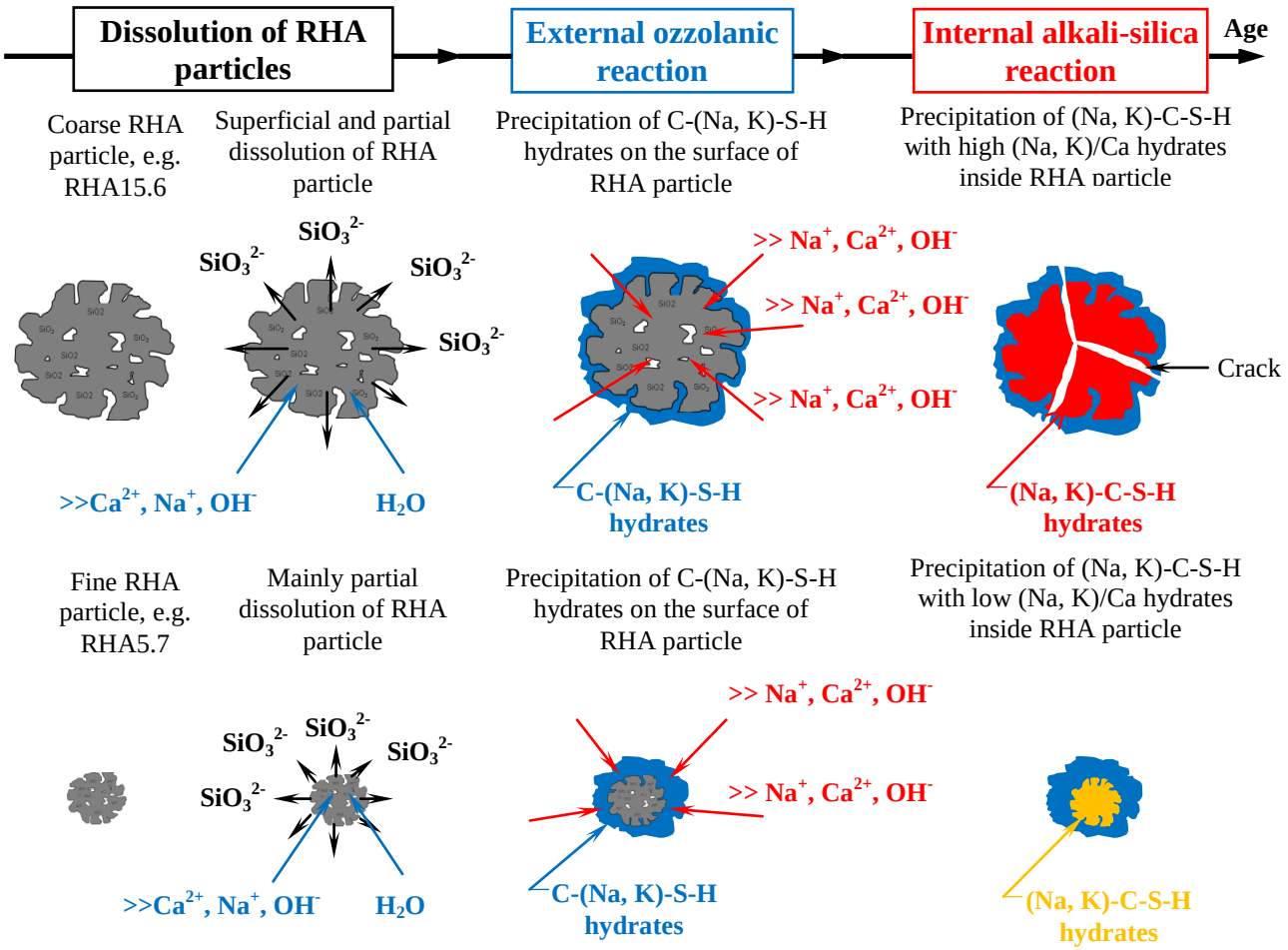

Fig. 9.29 Schematic representation of the mechanism for successive pozzolanic and alkali silica reactions of RHA particles

9.5.4. Pozzolanic reaction and ASR products of RHA

The chemical composition of pozzolanic reaction and ASR products in this study were analysed by EDX spectroscopy methods using a scanning electron microscope. It is generally known that in the range of some cubic microns, the excitation volumes analysed may contain phases other than C-(Na, K)-S-H and Na, K-(C)-S-H phases. The obtained spectra illustrated the presence of silicon, calcium, sodium, potassium, and minor other metal elements, i.e. aluminium, magnesium. This is indicative of the purification of the C-(Na, K)-S-H and Na, K-(C)-S-H phases analysed.

The NanoSEM and ESEM imaging and EDX-SEM analyses described above provide evidence of the formation of ASR products in pores, in the matrix (Fig. 9.16 and Fig. 9.17), and inside

the RHA particles (Fig. 9.20, Fig. 9.23 and Fig. 9.24) in the RHA blended cement paste. It is very interesting to note that pozzolanic and alkali silica reactions of RHA take place successively from the exterior to the interior of RHA particles, as presented in the previous section. The chemical composition of pozzolanic reaction hydrate can be seen in Table 7.1, Table 9.7, Table 9.8 and Table 9.9, and X-ray spectra can be seen in Fig. 7. 8b, d, Fig. 9.19b, Fig. 9.22a, Fig. 9.23c (EDX15), and Fig. 9.24c (EDX12). The oxide composition of this kind of C-(Na, K)-S-H phase is displayed in the blue point in the ternary phases diagram (Fig. 9.30). The chemical composition of ASR hydrate can be seen in Table 9.8, Table 9.10 and Table 9.11, and X-ray spectra can be seen (Fig. 9.22b, Fig. 9.23a, d (EDX14), and Fig. 9.24a, d (EDX16)). The oxide composition of these ASR products shown in red points, and lie in the brown area (Fig. 9.30). It can be found out that Ca/Si ratio and (Na+K)/Si ratio of the pozzolanic reaction products is much higher and lower than those of ASR products respectively. Similar results have also been obtained in other studies [223, 228, 236]. Additionally, the disolved silica in micropores in the cement matrix may react with Na and OH ions to generate ASR products without potassium (Fig. 9.16 and Table 9.5). The oxide compositions of this ASR products are displayed in ping points, most of them lie in the swelling area of ASR products proposed by Mansfeld (Fig. 9.30).

It is very clear that the calcium appears to be the main component of ASR products. The ratio of calcium to alkali oxides plays a very important role in the expansive behaviour of ASR products. The ASR products formed inside the non-cracked fine RHA particles (Fig. 9.25) had a higher Ca/(Na+K) ratio than the ASR products formed inside the cracked coarse RHA particles (Table 9.8, Table 9.10, and Table 9.11). It can be explained that the fine RHA particles contain less pore volume, and the pozzolanic reaction rim formed on their surface is thicker than that of the coarse RHA particles. Therefore, the concentration of Na ions penetrating inside the fine RHA particles is lower. This indicates that the ASR products with the higher Ca/(Na+K) ratio is non-expansive and vice versa. Prezzi, et al. has also shown that the higher the ratio of calcium to alkali, the less expansive the ASR products are [223, 236]. The role of calcium to alkali ratio on expansion of ASR products is still controversial. There might be the optimum ratio of calcium to alkali to give the expansion of ASR products formed by RHA. The (Na/K)-C-S-H with the high Ca/(Na+K) ratio shown in black point is outside the swelling area (Fig. 9.30).

The synthetic ASR products made by RHA, $Ca(OH)_2$ and NaOH 1M illustrated in violet points lie in the swelling area as well (Fig. 9.30). Although the initial content of CaO is much higher than that of Na_2O+K_2O, the ASR products had content of Na_2O+K_2O higher than that of CaO. This is indicative of higher reaction rate and extent of alkali-silica reaction of RHA with NaOH. The process of the reaction can be explained as following. The reaction between alkali hydroxide with silica occurs early, and produce alkali silica gels which then take up calcium, water and expand [19]. The rates of ASR and pozzolanic reaction of RHA need to be further investigated.

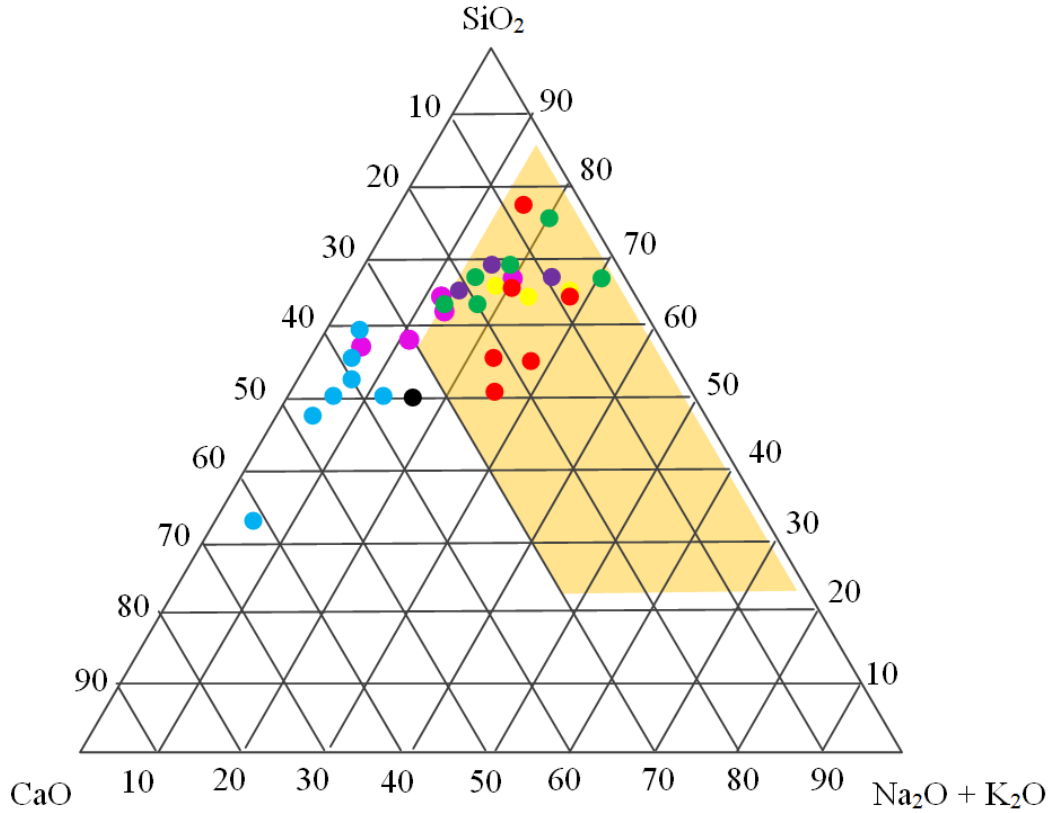

Fig. 9.30 Ternary phase diagram (SiO_2-CaO-Na_2O/K_2O) for pozzolanic reaction and ASR products formed by RHA. Swelling area of ASR products in brown, pozzolanic reacton in blue point, and ASR products: ASR products formed in pores in pink points, ASR products formed inside RHA particles: red point

9.6. Concluding remarks

Based on the experimental investigation into the resistance of mortar formulated from SCHPC containing reactive or non-reactive aggregates, and alkali silica reaction of RHA in paste, some conclusions can be drawn.

- In accordance with threshold of ASTM C 1260 and German alkali guidelines, the mortar formulated from SCHPC containing reactive greywacke aggregate can be durable regarding ASR, only when SF and RHA5.7 are used
- The increase in MPS of RHA increases the expansion of mortar containing reactive greywacke and basalt due to ASR. The mortar bars containing RHA15.6 are disrupted when reactive greywacke is used, and crack substantially when non-reactive basalt is used.
- The increase in RHA5.7 content decreases the expansion of mortar containing reactive greywacke aggregate due to ASR. This indicates the positive effect of RHA5.7 on mitigating ASR in mortar formulated SCHPC.
- SF is significantly more effective than RHA in mitigating ASR in mortar formulated from SCHPC containing reactive greywacke aggregate.
- RHA has paradoxical effect on ASR of paste formulated from SCHPC in the presence of the high alkali concentration, especially with the coarse MPS of RHA and at the high temperature. RHA constitutes rather than prevent ASR deterioration. RHA particles indeed

act as micro-reactive aggregates and react with alkali hydroxide to generate the expansive ASR products even when MPS of RHA is in the range of 5.7-22.6 µm.

- The alkali silica reactivity of RHA depends on the MPS of RHA and the temperature. Increasing MPS of RHA and temperature increases the alkali silica reactivity of RHA.
- In cement paste, the pozzolanic reaction and ASR of RHA take place successively from the exterior to interior of RHA particles. The mechanism for the successive reactions of RHA as following:
  - Amorphous silica from the external surface of RHA particles attacked by OH ions dissolves into the pore solution, and a certain amount of water is absorbed into the pores of RHA particles. Ca and OH ions in pore solution react with silica to produce C-(Na, K)-S-H hydrates which then precipiate on the surfaces of RHA particles and take up amount of sodium, potassium, and aluminium ions. That results in formation of the pozzolanic-like reaction rim, and RHA particles are partially or completely tightly packed inside the rim.
  - The pozzolanic reaction rim will be thicker over time. It acts as a semi-permeable membrane which allows the penetration of Na, K, Ca and OH ions but does not allow leakage of ASR gels generated after the formation of the reaction rim.
  - Na, K, Ca and OH ions penetrate into RHA particles. Na, K ions penetrate much faster than Ca ions. Hence ASR reaction occurs earlier. The alkalis react with silica and produce ASR gels which react with Ca ions, adsorb water in the pores of RHA particles and expand. When the expansive pressure exceeds the tollerance of RHA surrouded by the pozzolanic reaction rim and the cement matrix, the RHA particles and the surrounding cement matrix will crack.
- The oxide composition of C-S-H as pozzolanic products of RHA contain an amount of sodium and potassium: C-(Na, K)-S-H, whereas the ASR products of RHA contain an amount of calcium: Na, K-(C)-S-H. Where the Ca/(Na+K) of pozzolanic products is much higher than that of ASR products and vice versa.
- To mitigate ASR of RHA in cementitous materials, RHA should be ground into very fine particle sizes. With which its pore structure collapses and external pozzonalic reactivity increases hence more alkali content is absorbed by pozzolanic low Ca/Si C-S-H phases and pore structure of cement matrix is more refined.

10. Conclusions and Further Research

10.1. Conclusions

The RHA in this study is a macro-mesoporous amorphous siliceous material which possesses a very high amorphous silica content comparable with that of SF, and porous structure with macro and mesopores inside its particles. The pore size distribution is the key physical property of RHA influencing pore volume, specific surface area (BET-SSA), then the water demand and the pozzolanic reactivity of RHA. The SSA of RHA derives from the internal surface area in pores and the external surface area on the surface of particles. During grinding, most macro-pores collapse and hence the internal SSA of RHA decreases, whereas the external SSA of RHA increases. Increasing grinding time decreases the mean particle size (MPS) of RHA, pore volume in RHA particles, water demand of RHA, but slightly increases the BET-SSA of RHA.

By means of the variation in electrical conductivity of CH-pozzolan suspension, the pozzolanic reactivity of SF and RHA with different MPS was investigated. The foil-like C-S-H as the pozzolanic reaction products can be observed on the porous surface of RHA and the surface of SF particles after 4 hours of hydration in the CH-RHA suspension at 40 °C. The pozzolanic reaction of RHA might occur earlier, however total pozzolanic reactivity of SF is higher than that of RHA. The pozzolanic reactivity of RHA with MPS of 22.6µm (RHA22.6) is higher than that of RHA with MPS of 5.7µm (RHA5.7) possibly due to the higher adsorption of Ca ions into pores of RHA particles inducing ''internal pozzolanic reaction''. The reduction in the electrical conductivity of CH-pozzolan subtracting the electrical conductivity value of water-pozzolan suspension up to 900 min is proposed to evaluate and compare the pozzolanic reactivity of RHA with different MPS to that of SF in this study.

A new method for proportioning SCHPC was developed on the basis of the requirements for ordinary concrete proportions regulated in DIN EN 206-1 and DIN 1045-2. The proposed method considers the combination of various SCMs to achieve adequate self-compactability, high compressive strength of over 90 MPa, and good durability. The superplasticizer demand of SCHPC is closely related to the superplasticizer saturation dosage (SSD) of mortar formulated from the corresponding SCHPC. The pozzolanic reactivity indexes of SCMs, i.e. Limestone powder (LSP), fly ash (FA), RHA, and SF, were used to predict the expected compressive strength. In range of 0-20 wt.% cement replacement, RHA is very effective in improving compressive strength of SCHPC with the pozzolanic reactivity index of 1 which is the first time applied, the same as that of SF.

The replacement of cement by 20 wt.% FA results in higher filling ability, lower plastic viscosity and hence lower segregation resistance of SCHPC when w/b ratio and paste volume of concrete are kept constant. The combination of 10 wt.% SF and 20 wt.% FA dramatically increases the filling ability and the passing ability, simultaneously decreasing the segregation resistance of SCHPC. The self-compacting properties of SCHPC can be controlled by the incorporation of RHA. The presence of RHA decreases filling ability, and increases plastic viscosity and hence segregation resistance of SCHPC, depending on the RHA content used. RHA can be used as a viscosity modifying agent. The self-compacting properties of SCHPC containing RHA are slightly affected by the variation in SP content. Therefore, the robustness of SCHPC containing RHA is very high with respect to the variation of SP.

The incorporation of RHA increases SP adsorption of paste and the SP saturation dosage of mortar. Increasing MPS and content of RHA increases the SP saturation dosage of mortar, whereas increasing MPS of RHA decreases SP adsorption of paste. The lower the w/b ratio, the higher the SP saturation dosage of mortar. The incorporation of RHA decreases mini-slump flow, and increases yield stress and plastic viscosity. This effect is much stronger than that of SF, especially when the coarser RHA and the higher content of RHA are used. The increase in MPS and content of RHA predominantly increases plastic viscosity rather than decreases the mini-slump flow of mortar. Therefore, the flowing ability of mortar or SCHPC is slightly affected, while the plastic viscosity and hence segregation resistance of SCHPC can be controlled by the MPS and the content of RHA used.

60 min after water addition, mini-slump flow loss and the increase in plastic viscosity of mortar containing RHA is significantly higher than those of the reference sample and the SF containing sample, possibly due to the progress of water adsorption of RHA. After 60 min, the increase in MPS and content of RHA predominantly increases plastic viscosity rather than decreases the mini-slump flow of mortar.

Mortar formulated from SCHPC is a shear-thickening material. The shear-thickening degree declines over time. The incorporation of RHA/SF decreases the shear-thickening degree of mortar. 15 min after water addition, the increase in MPS of RHA leads to the higher shear-thickening degree. After 60 min, however, the increase in MPS of RHA decreases the shear-thickening degree. From 15 to 60 min after water addition, the reduction in shear-thickening degree of RHA7.7 containing mortar is greater than those of the reference sample and the SF containing sample respectively. The increase in RHA5.7/SF content decreases the shear-thickening degree of mortar. Where the effect of SF is much stronger than that of RHA5.7. It is attributed by the better poly-dispersion.

The incorporation of RHA/SF increases the degree of cement hydration in mortar. SF is more effective at early ages (3 days), possibly due to the better nucleation site effect, whereas RHA, particularly the coarse RHA22.6, dominates at the later ages (28, 91 days) possibly due to the higher internal water curing effect.

The incorporation of RHA/SF changes the hydration process of the clinker minerals, i.e. C_3S, C_2S. The hydration degree of C_3S in the RHA/SF blended cement matrix is higher than that in the reference sample. The incorporation of RHA/SF increases the C_3S hydration rate from 3 to 14 days. The degree of C_3S and C_2S hydration in the RHA blended cement paste is higher than that in the SF blended cement paste. From 28 to 91 days, the degree of cement hydration in the RHA22.6 blended cement paste increased mainly due to the increase in C_2S hydration.

With the same amorphous silica, the difference in MPS of RHA, resulting in the difference in pore structure of RHA, results in the different pozzolanic reaction process, pozzolanic reactivity of RHA and the effect of pozzolanic reaction on the pore refinement of the cement matrix. Pozzolanic reaction of RHA takes place on the surface (external pozzolanic reaction), and in the pores inside RHA particles (internal pozzolanic reaction). Where the external pozzolanic reaction products refine the pore structure of cement matrix, and the internal pozzolanic reaction products consolidate the pore structure of RHA particles. The external pozzolanic reaction products has low Ca/Si ratio of about 1.28 and take up amount of foreign ions, i.e.

aluminium, potassium, sodium ions. The fine RHA5.7 is more effective in pore refinement than the coarse RHA22.6 due to its higher external pozzolanic reactivity. This effect of RHA is not comparable with SF, especially at late ages.

In the blended cement matrix, SF disperses better than RHA due to its ultra fine particles resulting in the better dispersion of silicon, potassium and the occurrence of pozzolanic reaction. Therefore, not only pore volume and pore size is lower but also the pores disperse more homogeneously in the SF blended cement matrix than those in the RHA blended cement matrix. The concentration of silicon and potassium is higher in the pores and near RHA particles and it is proportional to the particle size of RHA.

The incorporation of RHA/SF increases the compressive strength of mortar formulated from SCHPC especially at the ages (28, 91 days). At w/b of 0.26, compressive strength of mortar reach the highest value with RHA with MPS of 5.7 μm. whereas, at w/b of 0.30, compressive strength obtained is higher at early ages with the coarse RHA (15.6 and 22.6 μm) and at late ages with the fine RHA (5.7 and 7.7 μm). At w/b of 0.30, the increase in RHA7.7 content decreases the compressive strength before 28 days. However, the compressive strength of the sample containing 20 wt.% RHA7.7 is higher than that of the sample containing 10 wt.% RHA7.7 at 91 days.

The mortar formulated from SCHPC containing reactive greywacke aggregate is safe from ASR only when SF and RHA5.7 are used. The increase in MPS of RHA increases the expansion of mortar containing reactive greywacke aggregate and non-reactive basalt aggregate due to ASR. The increase in RHA5.7 content decreases the expansion of mortar containing reactive greywacke aggregate due to ASR. This indicates the positive effect of RHA5.7 on mitigating ASR in mortar. SF is significantly more effective than RHA in mitigating ASR in mortar containing reactive greywacke aggregate.

RHA has paradoxical effect on ASR of paste formulated from SCHPC in the presence of the high alkali concentration. RHA constitutes rather than prevent ASR deterioration. RHA particles indeed act as micro-reactive aggregates and react with alkali hydroxide to generate the expansive ASR products even when MPS of RHA is in the range of 5.7-22.6 μm. Increasing MPS of RHA and temperature increases the alkali silica reactivity of RHA.

In cement paste, the pozzolanic reaction and ASR of RHA take place successively from the exterior to interior of RHA particles. The mechanism for the successive reactions of RHA has been proposed.

The oxide composition of C-S-H as pozzolanic products of RHA containing an amount of sodium and potassium: C-(Na, K)-S-H. The ASR products of RHA contain an amount of calcium: Na, K-(C)-S-H. Where the Ca/(Na+K) ratio of pozzolanic products is much higher than that of ASR products and vice versa.

To mitigate ASR of RHA in cementitous materials, RHA should be ground into very fine particle sizes. With which its pore structure collapses and external pozzonalic reactivity increases hence more alkali content is absorbed by pozzolanic low Ca/Si C-S-H and pore structure of cement matrix is more refined.

10.2. Further research

The results in this thesis indicate that there exist several gaps of knowledge on using RHA in concrete in general, and in SCHPC in particular. Some topics can be figured out as follows:

SCHPC has adequate self-compactability and very high compressive strength. How high is compressive strength of SCHPC when self-compactability is still satisfied?

The addtion of RHA results in the significant increase in plastic viscosity, and the slight decrease in mini-slump flow of mortar. What is the mechanism for the effect of RHA on rheological properties of SCHPC?

Increasing shear rate increases viscosity of mortar containing RHA, and the viscosity of mortar containing RHA increases dramatically over time. How is the thixotropy and rheopecty of SCHPC containing RHA?

BET-SSA of RHA is larger than that of SF. BET-SSA of RHA derives from the surface and the pores inside RHA particles. What is the difference in the nucleation site effect of RHA and SF on the cement hydration. And has surface in pores of RHA particles the nucleation site effect on the cement hydration?

What is the nature of ASR of RHA? The effect of silica nature of RHA on the alkali silica reactivity of RHA?

Chemical composition of ASR products formed by RHA containing certain amount of calcium, aluminium. What is the effect of calcium and aluminium content on the expansion of ASR products?

In the blended cement matrix, pozzolanic reaction rim formed surrounding RHA particles, over hydration time, Ca, Na, K ions penetrating into the pores of RHA particles react with silica to generate ASR products containing amount of calcium, and pozzolanic reaction products containing amount of alkali. What is the difference between pozzolanic reaction and ASR of RHA?

References

1. Safiuddin, M., Development of self-consolidating high performance concrete incorporating rice husk ash. 2008, University of Waterloo, Canada. p. 326.
2. EFNARC, Guidelines for Viscosity Modifying Admixtures for concrete. 2006: p. 12.
3. Gesoglu, M., E. Güneyisi, and E. Özbay, Properties of self-compacting concretes made with binary, ternary, and quaternary cementitious blends of fly ash, blast furnace slag, and silica fume. contruction and building materials, 2009. 23(5): p. 1847-1854.
4. Åžahmaran, M., Ö.s. Yaman, and M. Tokyay, Transport and mechanical properties of self consolidating concrete with high volume fly ash. Cement and Concrete Composites, 2009. 31(2): p. 99-106.
5. Mehta, P.K. Rice husk ash - a unique supplementary cementing material. in Advances in concrete technology. 1994. Center for mineral and Energy Technology, Ottawa.
6. Bui, D.D., Rice Husk Ash as a mineral admixture for high performance concrete. 2001, Delft University: The Netherlands. p. 122.
7. Rodriguez de Sensale, G., Effect of rice-husk ash on durability of cementitious materials. Cement and Concrete Composites, 2010. 32(9): p. 718-725.
8. Chao-Lung, H., B.L. Anh-Tuan, and C. Chun-Tsun, Effect of rice husk ash on the strength and durability characteristics of concrete. Construction and Building Materials, 2011. 25(9): p. 3768-3772.
9. Nguyen, V.T., Ye, G., Breugel, K.V., Fraaij, A.L.A., Bui, D.D., The study of using rice husk ash to produce ultra high performance concrete. Construction and Building Materials, 2011. 25(4): p. 2030-2035.
10. Memon, S.A., Shaikh, M.A., Akbar, H., Utilization of rice husk ash as viscosity modifying agent in self-compacting concrete. Construction and building materials, 2011. 25(2): p. 1044-1048.
11. FAO, Rice Market Monitor, 2012, accessed 2012 07 Oct; Available from: http://reliefweb.int/sites/reliefweb.int/files/resources/ap288e.pdf.
12. Van, V.-T.-A., et al., Mesoporous structure and pozzolanic reactivity of rice husk ash in cementitious system. Construction and Building Materials, 2013. 43(0): p. 208-216.
13. Nguyen, V.T., Rice husk ash as a mineral admixture for ultra high performance concrete, in Materials and Environment. 2011, Delft university of technology. p. 140.
14. Lothenbach, B., K. Scrivener, and R.D. Hooton, Supplementary cementitious materials. Cement and Concrete Research, 2011. 41(12): p. 1244-1256.
15. Van, V.T.A., Ludwig, H. M., Study on pozzolanic activity of rice husk ash in cement system, in Workshop on Performance-based Specifications for Concrete. 2011: Leipzig.
16. Van, V.T.A., Characteristics of rice husk ash and application in Ultra-High Performance Concrete, in Finger Institute for Building Materials Science. 2013, Bauhaus-University Weimar: Weimar. p. 143.
17. Duchesne, J. and M.A. Berube, The effectiveness of supplementary cementing materials in suppressing expansion due to ASR: Another look at the reaction mechanisms part 1: Concrete expansion and portlandite depletion. Cement and Concrete Research, 1994. 24(1): p. 73-82.
18. Maas, A.J., J.H. Ideker, and M.C.G. Juenger, Alkali silica reactivity of agglomerated silica fume. Cement and Concrete Research, 2007. 37(2): p. 166-174.
19. Stark, J., Alkali-Kieselsäure-Reaktion, ed. S.d.F.A.F.-I.f. Baustoffkunde. Vol. 3. 2008: F.A. Finger-Institut für Baustoffkunde, Bauhaus-Universität Weimar. p. 139.
20. Xu, G.J.Z., D.F. Watt, and P.P. Hudec, Effectiveness of mineral admixtures in reducing ASR expansion. Cement and Concrete Research, 1995. 25(6): p. 1225-1236.
21. Aquino, W., D.A. Lange, and J. Olek, The influence of metakaolin and silica fume on the chemistry of alkali-silica reaction products. Cement and Concrete Composites, 2001. 23(6): p. 485-493.

22. Thomas, M., The effect of supplementary cementing materials on alkali-silica reaction: A review. Cement and Concrete Research, 2011. 41(12): p. 1224-1231.

23. Diamond, S., Alkali silica reactions-Some paradoxes. Cement and Concrete Composites, 1997. 19(5-6): p. 391-401.

24. De Schutter, G., Bartos, P., Domone, P., Gibbs J., Self-compacting concrete. 2008, Caithness, Scotland, UK: Whittles Publishing. p. 296.

25. Zhu, W. and P.J.M. Bartos, Permeation properties of self-compacting concrete. Cement and Concrete Research, 2003. 33(6): p. 921-926.

26. Okamura, H.O., M.:, Self-compacting concrete. Journal of advanced concrete technology, 2003: p. 5-15.

27. Persson, B., A comparison between mechanical properties of self-compacting concrete and the corresponding properties of normal concrete. Cement and Concrete Research, 2001. 31(2): p. 193-198.

28. Okamura, H., Ozawa, K., Mix design for self-compacting concrete, in Concrete library of JSCE. 25. 1995. p. 107-120.

29. Ma, J., Orgass, M., Dehn, F., Schmidt, D., and Tue, N.V., Comparative investigations on ultra-high performance concrete with and without coarse aggregates, in in Proceedings of the 1st International Symposium on Ultra High Performance Concrete. 2004: Kassel, Germany. p. 205-212.

30. Shindoh, T., and Matsuoka, Y.,, Development of combination-type self-compacting concrete and evaluation test methods. Journal of Advanced Concrete Technology, 2003. 1(1): p. 26-36.

31. Neville, A., Concrete-Neville's Insights and Issues. 2006: Thomas Telford Ltd. p. 320.

32. Neville, A.M., Properties of Concrete, ed. F.a.F. Edition. 1996, New York, USA: John Wiley & Sons, Inc. p. 844.

33. Domone, P.L., Self-compacting concrete: An analysis of 11 years of case studies. Cement and Concrete composites, 2006. 28(2): p. 197–208.

34. Yahia, A., M. Tanimura, and Y. Shimoyama, Rheological properties of highly flowable mortar containing limestone filler-effect of powder content and W/C ratio. Cement and Concrete Research, 2005. 35(3): p. 532-539.

35. Liu, M., Wider Application of Additions in Self-compacting Concrete. 2009, University College London: London. p. 392.

36. Carlsward, J., Emborg, M., Utsi, S., Oberg, P. Effects of constituents on the workability and rheology of self-compacting concrete. in The 3rd International RILEM Symposium on Self-Compacting Concrete. 2003. Bagneux, France: RILEM Publications S.A.R.L.

37. Bosiljkov, V.B., SCC mixes with poorly graded aggregate and high volume of limestone filler. Cement and Concrete Research, 2003. 33(9): p. 1279-1286.

38. Ye, G., et al., Influence of limestone powder used as filler in SCC on hydration and microstructure of cement pastes. Cement and Concrete Composites, 2007. 29(2): p. 94-102.

39. Pera, J., S. Husson, and B. Guilhot, Influence of finely ground limestone on cement hydration. Cement and Concrete Composites, 1999. 21(2): p. 99-105.

40. Zhu, W. and J.C. Gibbs, Use of different limestone and chalk powders in self-compacting concrete. Cement and Concrete Research, 2005. 35(8): p. 1457-1462.

41. Sukumar, B., Nagamani, K., Srinivasa Raghavan, R., Evaluation of strength at early ages of self-compacting concrete with high volume fly ash. Construction and Building Materials, 2008. 22(7): p. 1394-1401.

42. Bouzoubaâ, N., Lachemi, M., Self-compacting concrete incorporating high volumes of class F fly ash: Preliminary results. Cement and Concrete Research, 2001. 31(3): p. 413-420.

43. Khatib, J.M., Performance of self-compacting concrete containing fly ash. construction and building materials, 2008. 22(9): p. 1963-1971.

44. Sonebi, M., Bartos, P. J. M., Filling ability and plastic settlement of self-compacting concrete. Materials and Structures, 2002. 35(8): p. 462-469.

45. Yahia, A., Tanimura, M., Shimabukuro, A., Shimoyama, Y., Effect of rheological parameters on self compactiblity of concrete containing various mineral admixtures, in Proc of the first RILEM international symposium on selfcompacting concrete. 1999: Stockholm. p. 523–535.

46. Siddique, R., Properties of self-compacting concrete containing class F fly ash. Materials & Design, 2011. 32(3): p. 1501-1507.

47. Poon, C.S., S.C. Kou, and L. Lam, Compressive strength, chloride diffusivity and pore structure of high performance metakaolin and silica fume concrete. Construction and Building Materials, 2006. 20(10): p. 858-865.

48. Tafraoui, A., et al., Metakaolin in the formulation of UHPC. Construction and Building Materials, 2009. 23(2): p. 669-674.

49. EFNARC, The european guidelines for self-compacting concrete, specification, production and use. 2005. p. 63.

50. Koehler, E.P., Fowler, D. W., Aggregates in self-consolidating concrete, in ICAR Project 108. 2007, International Center for Aggregates Research, The University of Texas at Austin. p. 362.

51. Hu, C., et al., Validation of BTRHEOM, the new rheometer for soft-to-fluid concrete. Materials and Structures, 1996. 29(10): p. 620-631.

52. Yen, T., et al., Flow behaviour of high strength high-performance concrete. Cement and Concrete Composites, 1999. 21(5-6): p. 413-424.

53. Yamada, K., Takahashi, T., Hanehara, S., Matsuhisa, M., Effects of the chemical structure on the properties of polycarboxylate-type superplasticizer. Cement and Concrete Research, 2000. 30(2): p. 197-207.

54. Golaszewski, J., Szwabowski, J., Influence of superplasticizers on rheological behaviour of fresh cement mortars. Cement and Concrete Research, 2004. 34(2): p. 235-248.

55. Bonen, D. and S.L. Sarkar, The superplasticizer adsorption capacity of cement pastes, pore solution composition, and parameters affecting flow loss. Cement and Concrete Research, 1995. 25(7): p. 1423-1434.

56. Flatt, R.J., sHoust, Y. F., A simplified view on chemical effects perturbing the action of superplasticizers. Cement and Concrete Research, 2001. 31(8): p. 1169-1176.

57. Ozawa, K., Maekawa, K., Okamura, H., Development of high performance concrete. Journal of the Faculty of Engineering, The University of Tokyo XLI(3). 1992a.

58. Aarre, T., Domone, P.L.J., Testing-SCC: Summary report on work package 2: Development of mix designs and material selection. 2004, Dansk Beton Teknik, University College London p. 10.

59. Aarre, T., Domone, P., Reference concretes for evaluation of test methods for SCC, in International RILEM Symposium on Self-Compacting Concrete, O. Wallevik, Nielsson, I. , Editor. 2003, RILEM Publications SARL. p. 495 - 505.

60. EFNARC, Specification and Guidelines for Self-Compacting Concrete. 2002: p. 32.

61. ASTM-C136., Standard test method for sieve analysis of fine and coarse aggregates, in Annual Book of ASTM Standards. 2004.

62. Noguchi, T., Oh, S.G., and Tomosawa, F., Rheological approach to passing ability between reinforcing bars of self-compacting concrete, in Proceedings of the First International RILEM Symposium on Self-compacting Concrete Â.a.P. Skarendahl, Ö. , Editor. 1999, RILEM Publications, Bagneux, France: Stockholm, Sweden. p. 59-71.

63. Xie, Y., et al., Optimum mix parameters of high-strength self-compacting concrete with ultrapulverized fly ash. Cement and Concrete Research, 2002. 32(3): p. 477-480.

64. Kwan, A.K.H., Use of condensed silica fume for making high strength, self-consolidating concrete. Canadian Journal of Civil Engineering, 2000. 27(4): p. 620-627.

65. Tasi, C.T., Li, S., and Hwang, C.L., The effect of aggregate gradation on engineering properties of high performance concrete. Journal of ASTM International, 2006. 3(3): p. 1-12.

66. Su, J.K., Cho, S.W., Yang, C.C., and Huang, R., Effect of sand ratio on the elastic modulus of self-compacting concrete. Journal of Marine Science, 2002. 10(1): p. 8-13.

67. Westerholm, M., Rheology of the Mortar Phase of Concrete with Crushed Aggregate, in Division of Mineral Processing, Department of Chemical Engineering and Geosciences. 2006, Luleå University of Technology, Sweden. p. 94.

68. Hu, J., and Wang, K., Effects of aggregate on flow properties of mortar, in Proceeding of the Mid-Continent Transportation Research Symposium. 2005: Ames, Iowa, Iowa State University. p. 8.

69. Engineers, J.S.o.C., Recommendation for Self - Compacting Concrete. Concrete Engineering Series 31, JSCE, 1999.

70. DIN EN 206-9, Additional Rules for Self-compacting Concrete 2010. p. 29.

71. Saak, A.W., Jennings, H.M, Shah, S.P. , New methodology for designing self-compacting concrete. ACI Materials Journal, 2001. 98: p. 429-439.

72. Su, N., K.-C. Hsu, and H.-W. Chai, A simple mix design method for self-compacting concrete. Cement and Concrete Research, 2001. 31(12): p. 1799-1807.

73. Chowdhury, S.B., P. C.:, New methodology to proportion self-sonsolidating concrete with high-volume fly ash. ACI Materials Journal, 2010. 107(3): p. 222-230.

74. Kheder, G.F.A., R.S.: , New method for proportioning self-compacting conrete based on compressive strength requirements. ACI Materials Journal, 2010. 107(5): p. 490-497.

75. Dinakar, P., K.P. Sethy, and U.C. Sahoo, Design of self-compacting concrete with ground granulated blast furnace slag. Materials & Design, 2013. 43(0): p. 161-169.

76. Spiratos, N., Page, M., Mailvaganam, N., Malhotra, V.M., Jolicoeur, C. , Superplasticizers for Concrete: Fundamentals, Technology, and Practice. 2003, Ottawa, Canada: Supplementary Cementing Materials for Sustainable Development, Incorporated. p. 322.

77. DIN EN 206-1., Specification, performance, production and conformity. 2001: p. 77.

78. DIN 1045-2., Concrete specification, properties, production and conformity- Aplication rules for DIN EN 206-1. 2008. p. 62.

79. KH., K., Workability, testing, and performance of self-consolidating concrete. ACI Materials Journal 1999. 96(3): p. 346-354.

80. Billberg, P., Petersson, O., Westerholm, M., Wustholz, T., Reinhardt, HW., Test methods for passing ability, in Summary report on work package 3.2. 2004. p. 5.

81. RILEM-TC174-SCC., Self-compacting concrete State-of-the-art report of RILEM technical committe 174-SCC, ed. P.O. Skarendahl A, editors. 2000: RILEM Publications S.A.R.L., France. p. 168.

82. Bonen, D. and S.P. Shah, Fresh and hardened properties of self-consolidating concrete. Progress in Structural Engineering and Materials, 2005. 7(1): p. 14-26.

83. Khayat, K.H., Workability, testing, and performance of self-consolidating concrete. ACI Materials Journal 1999. 96(3): p. 346-354.

84. Uchikawa, H., D. Sawaki, and S. Hanehara, Influence of kind and added timing of organic admixture on the composition, structure and property of fresh cement paste. Cement and Concrete Research, 1995. 25(2): p. 353-364.

85. Hanehara, S. and K. Yamada, Interaction between cement and chemical admixture from the point of cement hydration, absorption behaviour of admixture, and paste rheology. Cement and Concrete Research, 1999. 29(8): p. 1159-1165.

86. Felekoglu, B. and H. Sarıkahya, Effect of chemical structure of polycarboxylate-based superplasticizers on workability retention of self-compacting concrete. Construction and Building Materials, 2008. 22(9): p. 1972-1980.

87. Coussot, P., Rheometry of Pastes, Suspensions and Granular Materials. 2005: John Wiley & Sons Inc. p. 292

88. Tattersall, G.H., Banfill, P. F. G. , The rheology of fresh concrete. 1983, London: Pitman. p. 356.

89. Yahia, A. and K.H. Khayat, Analytical models for estimating yield stress of high-performance pseudoplastic grout. Cement and Concrete Research, 2001. 31(5): p. 731-738.

90. Feys, D., Heirman, G., Schutter, G. D., Verhoeven, L. R., Vandewalle, D. V. G.,. Comparison of two concrete rheometers for shear thickening behaviour of SCC. in Proc. of the 5th Int. RILEM Symposium on Self-compacting Concrete. 2007. Ghent

91. Feys, D., Verhoeven, R., Schutter, D., G., Fresh self compacting concrete, a shear thickening material. Cement and Concrete Research, 2008. 38(7): p. 920-929.

92. Quanji, Z., Thixotropic behavior of cement-based materials: effect of clay and cement types, in Civil, Construction, and Environmental Engineering. 2010, Iowa State University: Iowa. p. 144.

93. Wallevik, J., Rheology of Particle Suspensions. 2003, The Norwegian University of Science and Technology: Trondheim, Norway p. 413.

94. Klug, Y., and Holschemacher, K., Comparison of the hardened properties of self compacting and normal vibrated concrete, in 3rd International Symposium on Self-Compacting Concrete, O. Wallevik, Nielsson, I., Editor. 2003, RILEM Publications SARL: Reykjavik, Iceland. p. 596-605.

95. Trägårdh, J. Microstructural features and related properties of self-compacting concrete. in First International RILEM Symposium on Self-Compacting Concrete. 1999. RILEM Publications SARL.

96. Leemann, A., et al., Influence of compaction on the interfacial transition zone and the permeability of concrete. Cement and Concrete Research, 2006. 36(8): p. 1425-1433.

97. De Schutter, G., Au denaert, K., Durability of Self-Compacting Concrete, in Final report of RILEM TC 205-DSC: , G. De Schutter, Au denaert, K., Editor. 2007. p. 185.

98. Locher F.W., R.W., Sprung S., Erstarren von Zement (in German). Zement Kalk Gips, 1976. 29(10): p. 435-442.

99. Mills, R.H., Factors influencing cessation of hydration in water cured cement pastes, Symposium on structure of Portland cement paste and concrete, in Special report 90, Highway Research Board. 1966: Washington. p. 406-424.

100. Escalante-García, J.I. and J.H. Sharp, Effect of temperature on the hydration of the main clinker phases in portland cements: part i, neat cements. Cement and Concrete Research, 1998. 28(9): p. 1245-1257.

101. H.F.Taylor., Chement chemistry. 1997, London: Tomas Helford. p. 480.

102. Lothenbach, B., et al., Influence of limestone on the hydration of Portland cements. Cement and Concrete Research, 2008. 38(6): p. 848-860.

103. Richardson, I.G., Groves, G. W., The incorporation of minor and trace elements into calcium silicate hydrate (C—S—H) gel in hardened cement pastes. Cement and Concrete Research, 1993. 23(1): p. 131-138.

104. Pardal, X., Pochard, Isabelle., Nonat, Andre., Experimental study of Si-Al substitution in calcium-silicate-hydrate (C-S-H) prepared under equilibrium conditions. Cement and Concrete Research, 2009. 39(8): p. 637-643.

105. Hong, S.-Y. and F.P. Glasser, Alkali binding in cement pastes: Part I. The C-S-H phase. Cement and Concrete Research, 1999. 29(12): p. 1893-1903.

106. Hong, S.Y., Glasser, F. P., Alkali sorption by C-S-H and C-A-S-H gels: Part II. Role of alumina. Cement and Concrete Research, 2002. 32(7): p. 1101-1111.

107. Gutteridge, W.A. and J.A. Dalziel, Filler cement: The effect of the secondary component on the hydration of Portland cement: Part I. A fine non-hydraulic filler. Cement and Concrete Research, 1990. 20(5): p. 778-782.

108. Gutteridge, W.A., Dalziel, J. A., Filler cement: The effect of the secondary component on the hydration of Portland cement: Part 2: Fine hydraulic binders. Cement and Concrete Research, 1990. 20(6): p. 853-861.

109. Mehta, P.K., Aïtcin, P.-C., Microstructural basis for selection of materials and mix proportions for high strength concrete, in Second International Symposium on High Strength Concrete. 1990, ACI SP-121, W.T. Hester, ed.: American Concrete Institute, Farmington Hills, Michigan, USA. p. 265-282.

110. Ollivier, J.P., J.C. Maso, and B. Bourdette, Interfacial transition zone in concrete. Advanced Cement Based Materials, 1995. 2(1): p. 30-38.

111. Mehta, P.K. and P.J.M. Monteiro, Concrete : Microstructure, Properties, and Materials: Microstructure, ed. edition. 2005: Publisher: McGraw-Hill Professional. p. 659

112. Attiogbe, E.K., See, H.T., and Daczko, J.A., Engineering properties of self-consolidating concrete, in the First North American Conference on the Design and Use of Self-Consolidating Concrete, J.A.D. S.P. Shah, and J.N. Lingscheit, Editor. 2002, Hanley-Wood, LLC, Illinois, USA. p. 331-336.

113. Schmidt, M., Fehling, E. Ultra-high-performance concrete: research development and application in Europe. in the 7th International Symposium on the Utilization of High-strength/High-performance concrete, 2005. American Concrete Institute, Washington DC, USA.

114. Mehta, P.K., and Monteiro, P.J.M. , Concrete: Structure, Properties and Materials. 1993: Englewood Cliffs, NJ; Prentice Hall. p. 548.

115. Zhu, W., M. Sonebi, and P.J.M. Bartos, Bond and interfacial properties of reinforcement in self-compacting concrete. Materials and Structures, 2004. 37(7): p. 442-448.

116. Alexander, M.G. and B.J. Magee, Durability performance of concrete containing condensed silica fume. Cement and Concrete Research, 1999. 29(6): p. 917-922.

117. Zhu, W., Quinn, J, and Bartos, P.J.M. Transport properties and durability of selfcompacting concretes. in Proceedings of the Second International Symposium on Self-Compacting Concrete. 2001. Tokyo, Japan.

118. Collepardi, M., Thaumasite formation and deterioration in historic buildings. Cement and Concrete Composites, 1999. 21(2): p. 147-154.

119. Hartshorn, S.A., J.H. Sharp, and R.N. Swamy, Thaumasite formation in Portland-limestone cement pastes. Cement and Concrete Research, 1999. 29(8): p. 1331-1340.

120. Hime, W.G. and B. Mather, Sulfate attack, or is it? Cement and Concrete Research, 1999. 29(5): p. 789-791.

121. Barnett, S.J., et al., Study of thaumasite and ettringite phases formed in sulfate/blast furnace slag slurries using XRD full pattern fitting. Cement and Concrete Composites, 2002. 24(3-4): p. 339-346.

122. Beaupre, D., P. Lacombe, and K.H. Khayat, Laboratory investigation of rheological properties and scaling resistance of air entrained self-consolidating concrete. Materials and Structures, 1999. 32(3): p. 235-240.

123. Khayat, K.H., Optimization and performance of the air-entrained self-consolidating concrete. ACI Materials Journal, 2000. 97(5): p. 526-535.

124. Persson, B., Internal frost resistance and salt frost scaling of self-compacting concrete. Cement and Concrete Research, 2003. 33(3): p. 373-379.

125. Makishima, O., Tanaka, H., Itoh, Y., Komada, K., Satoh, F. Evaluation of mechanical properties and durability of super quality concrete. in Proceedings of the 2nd International RILEM Symposium on Self-Compacting Concrete. 2001. Tokyo: COMS Engineering Corporation.

126. Jiang, S., B.-G. Kim, and P.-C. Aitcin, Importance of adequate soluble alkali content to ensure cement/superplasticizer compatibility. Cement and Concrete Research, 1999. 29(1): p. 71-78.

127. Kim, B.-G., Jiang, S., Aïtcin, P.-C. Influence of molecular weight of PNS superplasticizers on the properties of cement pastes containing different alkali contents. in The role of admixtures in high performance concrete. 1999. France: RILEM.

128. Ferraris, C.F., Alkali-Silica Reaction and High Performance Concrete, in NISTIR 5742. 1995, Building and Fire Research Laboratory, National Institute of Standards and Technology: Gaithersburg. p. 24.

129. Lagerblad, B., Träghardh, J. . Alkali-silica reaction in high strength concrete. in International RILEM Workshop on Durability of High Performance Concrete. 1994. RILEM.

130. Nair, D.G., Sustainable-affordable housing for the poor in Kerala. 2006, Delft University of Technology: Delft, the Netherlands. p. 214.

131. Cook, D., Rice husk ash cements: their development and applications. 1984, Vienna: United Nations Industrial development organization.

132. Feng, Q., et al., Reply to the discussion by Ayhan Demirbas of the paper "Study on the pozzolanic properties of rice husk ash by hydrochloric acid pretreatment". Cement and Concrete Research, 2005. 35(5): p. 1018-1019.

133. Chandrasekhar, S., P.N. Pramada, and J. Majeed, Effect of calcination temperature and heating rate on the optical properties and reactivity of rice husk ash. Journal of materials science, 2006. 41(23): p. 7926-7933.

134. Malhotra, V.M., Ramachandran, V.S., Feldman, R.F., Aitcin, P.C., Condensed-Silica Fume in Concrete. 1987, Florida.: CRC Press (Eds), Inc. p. 240.

135. Swamy, R.N., Cement Replacement Materials. Vol. Vol. 3. 1986: Surrey University Press. p. 259.

136. Rizwan, S.A., High performace motars and concretes using secondary raw materials, in Maschinenbau, Verfahrens-und Energietechnik. 2006, Technischen Universität Bergakademie Freiberg: Freiberg. p. 114.

137. Zhang, M.H., Malhotra, V.M. , High performance concrete incorporating rice husk ash as a supplementary cementing material. ACI Materials Journal 1996. 93(6): p. 629-636.

138. Chandrasekhar, S., Satyanarayana, K. G., Pramada, P. N., Raghavan, P. , Review Processing, properties and applications of reactive silica from rice husk—an overview. Journal of materials science, 2003. 38(15): p. 3159 – 3168.

139. Muthadhi, A.A., R. Kothandaraman, S., Rice Husk Ash - Properties and its Uses: A Review. Journal of the Institution of Engineers. India, 2007. 88: p. 50-56.

140. REPORTS, R.T., Final Report Siliceous by-products for use in concrete, in Materials and Structures. 1988, Kluwer Academic Publishers. p. 69-80.

141. Mehta, P.K., Siliceous ashes and hydraulic cements prepared therefrom. 1978.

142. Paya, J., et al., Determination of amorphous silica in rice husk ash by a rapid analytical method. Cement and Concrete Research, 2001. 31(2): p. 227-231.

143. Luxán, M.P., Madruga, F., Saavedra, J. , Rapid evaluation of pozzolanic activity of natural products by conductivity measurement. Cement and Concrete Research, 1989. 19(1): p. 63-68.

144. Sugita, S., Shoya, M., and Tokuda, H. Evaluation of Pozzolanic Activity of Rice Husk Ash. in the 4th CANMET/ACI International Conference on Fly ash, Silica Fume, Slag and Natural Pozzolans in Concrete. 1992. Istanbul, Turkey.

145. Paya, J., et al., Enhanced conductivity measurement techniques for evaluation of fly ash pozzolanic activity. Cement and Concrete Research, 2001. 31(1): p. 41-49.

146. Wansom, S., Janjaturaphan, S., and Sinthupinyo, S., Pozzolanic Activity of Rice Husk Ash:Comparison of Various Electrical Methods. Journal of Metals, Materials and Minerals, 2009. 19(2): p. 1-7.

147. Zhang, M.H., R. Lastra, and V.M. Malhotra, Rice-husk ash paste and concrete: Some aspects of hydration and the microstructure of the interfacial zone between the aggregate and paste. Cement and Concrete Research, 1996. 26(6): p. 963-977.

148. Nguyen, V.T., et al., Hydration and microstructure of ultra high performance concrete incorporating rice husk ash. Cement and Concrete Research, 2011: p. 1104–1111.

149. ASTM-C1240-05., Standard Specification for Silica Fume Used in Cementitious Mixtures, A.S.f.T.a. Materials, Editor. 2005: Philadelphia, USA.

150. El-Dakroury, A. and M.S. Gasser, Rice husk ash (RHA) as cement admixture for immobilization of liquid radioactive waste at different temperatures. Journal of Nuclear Materials, 2008. 381(3): p. 271-277.

151. Ganesan, K., K. Rajagopal, and K. Thangavel, Rice husk ash blended cement: Assessment of optimal level of replacement for strength and permeability properties of concrete. Construction and Building Materials, 2008. 22(8): p. 1675-1683.

152. Habeeb, G.A., Fayyadh, M.M., Rice Husk Ash Concrete: the Effect of RHA Average Particle Size on Mechanical Properties and Drying Shrinkage. Australian Journal of Basic and Applied Sciences, 2009. 3(3): p. 616-1622.
153. Le, H.T., Nguyen, S. T., Ludwig, H-.M., A study on High Performance Sand Concrete containing Rice Husk Ash. International Journal of Concrete Structures and Materials, 2014. 8(4): p. 301-307.
154. Qing-ge, F., et al., Concrete with highly active rice husk ash. Journal of Wuhan University of Technology-Mater. Sci. Ed., 2004. 19(3): p. 74-77.
155. Feng, Q., et al., Study on the pozzolanic properties of rice husk ash by hydrochloric acid pretreatment. Cement and Concrete Research, 2004. 34(3): p. 521-526.
156. Nehdi, M., J. Duquette, and A. El Damatty, Performance of rice husk ash produced using a new technology as a mineral admixture in concrete. Cement and Concrete Research, 2003. 33(8): p. 1203-1210.
157. Bui, D.D., J. Hu, and P. Stroeven, Particle size effect on the strength of rice husk ash blended gap-graded Portland cement concrete. Cement and Concrete Composites, 2005. 27(3): p. 357-366.
158. Sousa Coutinho, J., The combined benefits of CPF and RHA in improving the durability of concrete structures. Cement and Concrete Composites, 2003. 25(1): p. 51-59.
159. Chindaprasirt, P., et al., Sulfate resistance of blended cements containing fly ash and rice husk ash. Construction and Building Materials, 2007. 21(6): p. 1356-1361.
160. Gastaldini, A.L.G., et al., Chloride penetration and carbonation in concrete with rice husk ash and chemical activators. Cement and Concrete Composites, 2007. 29(3): p. 176-180.
161. Salas, A., et al., Comparison of two processes for treating rice husk ash for use in high performance concrete. Cement and Concrete Research, 2009. 39(9): p. 773-778.
162. Sugita, S., et al., The resistance of rice husk ash concrete to carbonation, acid attack and chloride ion penetration. ACI Materials Journal, 1997. 172(12): p. 29–43.
163. Hasparyk, N.P., Monteiro, P.J.M., and Carasek, H., Effect of Silica Fume and Rice Husk Ash on Alkali-Silica Reaction. ACI Materials Journal, 2000. 97(4): p. 486-492.
164. Ramezanianpour, A.A., Zarrabi, K., and Mahdikhani, M. Mitigation of alkali aggregate reaction of concrete incorporation rice husk ash (RHA). in The 13rd ICAAR. 2008. Trondheim.
165. DAfStb-Richtlinie, Vorbeugende Maßnahmen gegen schädigende Alkalireaktion im Beton (Alkali-Richtlinie). 2007: Berlin.
166. Safiuddin, M., J.S. West, and K.A. Soudki, Flowing ability of the mortars formulated from self-compacting concretes incorporating rice husk ash. Construction and building materials, 2011. 25(2): p. 973-978.
167. Sua-iam, G. and N. Makul, Utilization of limestone powder to improve the properties of self-compacting concrete incorporating high volumes of untreated rice husk ash as fine aggregate. Construction and Building Materials, 2013. 38(0): p. 455-464.
168. Nehdi, M., M. Pardhan, and S. Koshowski, Durability of self-consolidating concrete incorporating high-volume replacement composite cements. Cement and Concrete Research, 2004. 34(11): p. 2103-2112.
169. Ahmadi, M.A., Alidoust, O., Sadrinejad, I., Nayeri, M. , Development of Mechanical Properties of Self-Compacting Concrete Contain Rice Husk Ash International Journal of Computer and Information Engineering 2007. 1(4): p. 259-262.
170. Rouquerol, F., Rouquerol, J., and Sing, K., Adsorption by Powders and Porous Solids: Principles, Methodology and Applications. 1998: Academic press. p. 467.
171. Barrett, E.P., L.G. Joyner, and P.P. Halenda, The Determination of Pore Volume and Area Distributions in Porous Substances. I. Computations from Nitrogen Isotherms. Journal of the American Chemical Society, 1951. 73(1): p. 373-380.
172. Puntke W., Wasseranspruch von feinen Kornhauf-werken. beton 52, 2002: p. 242–248.

173. Young, J.F., Humidity control in the laboratory using salt solutions—a review. Journal of Applied Chemistry, 1967. 17(9): p. 241-245.

174. Hernández, F.J.R., Lechado, S. M., Navarro, J. F. V., Experimental study on the influence of two different additives onto the flow behaviour of a fresh cement paste. Advances in Cement Research, 2011. 23(5): p. 255 –263

175. Kraus, M., Einfluss von Leistungs-Ultraschall auf die frühe Zementhydratation, in Fakultät Bauingenieurwesen, F.A. Finger-Institut für Baustoffkunde. 2011, Bauhaus-Universität Weimar: Weimar. p. 136.

176. Vogel, R., Eine Messzelle für Spezialmörtel. 2007.

177. Ostheeren, K., Rheologische Untersuchungen an Basismörteln Selbstverdichtender Betone mit Sanden unterschiedlicher Kornformen, in Aufbereitung von Baustoffen und Wiederverwertung. 2008, Bauhaus-Universität Weimar: Weimar. p. 120.

178. Ye, G., Experimental Study & Numerical Simulation of the development of the Microstructure and Permeability of Cementitious Materials. 2003, Delft University Press. p. 186.

179. Scrivener KL, P.H., Pratt PL, Parrott LJ., Analysis of phases in cement paste using backscattered electron images, methanol adsorption and thermogravimetric analysis. MRS Sympos Proc, 1987. 85: p. 67-76.

180. Kjellsen, K.O., R.J. Detwiler, and O.E. Gjorv, Backscattered electron image analysis of cement paste specimens: Specimen preparation and analytical methods. Cement and Concrete Research, 1991. 21(2-3): p. 388-390.

181. Diamond, S. and M.E. Leeman. Pore Size Distributions in Hardened Cement Paste by Sem Image Analysis. in MRS Online Proceedings Library. 1995.

182. Igarashi, S., M. Kawamura, and A. Watanabe, Analysis of cement pastes and mortars by a combination of backscatter-based SEM image analysis and calculations based on the Powers model. Cement and Concrete Composites, 2004. 26(8): p. 977-985.

183. Vaughan, D., Energy-Dispersive X-Ray Microanalysis: An Introduction. 1999: NORAN Instruments. p. 59.

184. Ramachandran V.S., B.J.J., Handbook of Analytical Techniques in Concrete Science and Technology. 2000, Norwich, New York, U.S.A.: William Andrew. p. 1003.

185. Klimesch, D.S. and A. Ray, Use of the second-derivative differential thermal curve in the evaluation of cement-quartz pastes with metakaolin addition autoclaved at 180°C. Thermochimica Acta, 1997. 307(2): p. 167-176.

186. Ramachandran VS, P.R., Beaudoin JJ, Delgado AH. , Handbook of thermal analysis of construction materials. 2002: Noyes Publications.

187. ASTM-C1260-01, Standard test method for potential alkali reactivity of aggregates (mortar-bar method). 2001, American Society for Testing and Materials: Philadelphia, USA.

188. Armesto, L., et al., Combustion behaviour of rice husk in a bubbling fluidised bed. Biomass and Bioenergy, 2002. 23(3): p. 171-179.

189. Stroeven, P., D.D. Bui, and E. Sabuni, Ash of vegetable waste used for economic production of low to high strength hydraulic binders. Fuel, 1999. 78(2): p. 153-159.

190. IUPAC, Manual of symbols and terminology for physicochemical quantities and units, Commission on Colloid and Surface Chemistry including Catalysis. 2001, Wageningen, The Netherlands.

191. Zdravkov, B., et al., Pore classification in the characterization of porous materials: A perspective. Central European Journal of Chemistry, 2007. 5(2): p. 385-395.

192. James, J., Rao, M. S., Characterization of silica in rice husk ash. The america ceramic society bulletin, 1986. 65(8): p. 1177-1180.

193. De Meer, S., C.J. Spiers, and C.J. Peach, Pressure solution creep in gypsum: Evidence for precipitation reaction control. Physics and Chemistry of the Earth, 1997. 22(1-2): p. 33-37.

194. Koutsoukos, P.G., A.N. Kofina, and D.G. Kanellopoulou, Solubility of Salts in Water: Key Issue for Crystal Growth and Dissolution Processes. Pure and Applied Chemistry, 2007. 79(5): p. 825-850.

195. Suzuki, K., et al., Effect of NaCl or NaOH on the formation of C-S-H. Cement and Concrete Research, 1986. 16(3): p. 333-340.

196. Hiemstra, T., Riemsdijk W, H. V., Multiple activated complex dissolution of metal (hydr)oxides: a thermodynamic approach applied to quartz. Journal of colloid and interface science 1990. 136(1): p. 132-150.

197. S.Garrault, T.B., A. Nonat., Formation of the C-S-H Layer during the Early Hydration of Tricalcium Silicate Grains with Different Sizes. J. Phys. Chem, 2006. 10(1): p. 270-275.

198. Costoya Fernández, M.M., Effect of particle size on the hydration kinetics and microstructural development of tricalcium silicate. 2008, EPFL. p. 234.

199. DIN-EN206-1., Specification, performance, production and conformity. 2001. p. 77.

200. Le, H.T., et al., The mix design for self-compacting high performance concrete containing various mineral admixtures. Materials and Design. 2015, (In press).

201. Brouwers, H.J.H. and H.J. Radix, Self-Compacting Concrete: Theoretical and experimental study. Cement and Concrete Research, 2005. 35(11): p. 2116-2136.

202. Heidelbergcement., Betontechnische Daten. 2009. p. 269.

203. Neville, A., Aitcin, P.C., High performance concrete - an overview. Materials and Structures, 1998. 31: p. 111-117.

204. Surabhi.C.S., M.S., Syam Prakash.V. Influence of Limestone Powder on Properties of Self-Compacting Concrete. in 10th National Conference on Technological Trends (NCTT09). 2009. Trivandrum, Kerala, India

205. Uysal, M. and M. Sumer, Performance of self-compacting concrete containing different mineral admixtures. construction and building materials, 2011. 25(11): p. 4112-4120

206. Aitcin, P.C., The durability characteristics of high performance concrete: a review. Cement and Concrete Composites, 2003. 25(4-5): p. 409-420.

207. Ammar, Y., Shear-thickening behavior of high-performance cement grouts - Influencing mix-design parameters. Cement and Concrete Research, 2011. 41(3): p. 230-235.

208. Nehdi, M., Mindess, S., Aitcin, P. C., Rheology of High-Performance Concrete: Effect of Ultrafine Particles. Cement and Concrete Research, 1998. 28(5): p. 687-697.

209. Mehta, P.K., Monteiro, P.J. , Concrete structure, properties and materials, ed. n. ed. 1993, New Jersey: Prentice-Hall. p. 548.

210. Soroka, I. and D. Ravina, Hot weather concreting with admixtures. Cement and Concrete Composites, 1998. 20(2–3): p. 129-136.

211. Ahmad, I. and S. Azhar, Temperature variation in high slump drilled shaft concrete and its effect on slump loss. Cement and Concrete Research, 2004. 34(2): p. 207-217.

212. Erdoğdu, Ş., Effect of retempering with superplasticizer admixtures on slump loss and compressive strength of concrete subjected to prolonged mixing. Cement and Concrete Research, 2005. 35(5): p. 907-912.

213. Brady, J.F. and G. Bossis, The rheology of concentrated suspensions of spheres in simple shear flow by numerical simulation. Journal of Fluid Mechanics, 1985. 155: p. 105-129.

214. Bossis, G. and J.F. Brady, The rheology of Brownian suspensions. The Journal of Chemical Physics, 1989. 91(3): p. 1866-1874.

215. Cyr, M., C. Legrand, and M. Mouret, Study of the shear thickening effect of superplasticizers on the rheological behaviour of cement pastes containing or not mineral additives. Cement and Concrete Research, 2000. 30(9): p. 1477-1483.

216. Feys, D., R. Verhoeven, and G. De Schutter, Why is fresh self-compacting concrete shear thickening? Cement and Concrete Research, 2009. 39(6): p. 510-523.

217. Barnes, H.A., Shear-Thickening (``Dilatancy'') in Suspensions of Nonaggregating Solid Particles Dispersed in Newtonian Liquids. Journal of Rheology, 1989. 33(2): p. 329-366.

218. Bonavetti, V., et al., Limestone filler cement in low w/c concrete: A rational use of energy. Cement and Concrete Research, 2003. 33(6): p. 865-871.

219. Oey, T., et al., The Filler Effect: The Influence of Filler Content and Surface Area on Cementitious Reaction Rates. Journal of the American Ceramic Society, 2013: p. 1-13.

220. Spiratos, N.P., M.; Mailvaganam, N.; Malhotra, V.M.; Jolicoeur, C. , Superplasticizers for Concrete: Fundamentals, Technology, and Practice. 2003, Ottawa, Canada: Supplementary Cementing Materials for Sustainable Development, Incorporated. p. 322.

221. Mansfeld, T., Das Quellverhalten von Alkalisilikatgelen unter Beachtung ihrer Zusammensetzung. 2008, Bauhaus-Universität Weimar. p. 143.

222. Ichikawa, T. and M. Miura, Modified model of alkali-silica reaction. Cement and Concrete Research, 2007. 37(9): p. 1291-1297.

223. Juenger, M.C.G. and C.P. Ostertag, Alkali–silica reactivity of large silica fume-derived particles. Cement and Concrete Research, 2004. 34(8): p. 1389-1402.

224. Pfeifer, C., J. Stark, and B. Möser, Durability and microstructural development during hydration in ultra-high performance concrete, in Concrete Repair, Rehabilitation and Retrofitting II. 2008, CRC Press. p. 87-88.

225. Hou, X., L.J. Struble, and R.J. Kirkpatrick, Formation of ASR gel and the roles of C-S-H and portlandite. Cement and Concrete Research, 2004. 34(9): p. 1683-1696.

226. Gudmundsson, G. and H. Olafsson, Alkali-silica reactions and silica fume: 20 years of experience in Iceland. Cement and Concrete Research, 1999. 29(8): p. 1289-1297.

227. Monteiro, P.J.M., et al., Influence of mineral admixtures on the alkali-aggregate reaction. Cement and Concrete Research, 1997. 27(12): p. 1899-1909.

228. Idir, R., M. Cyr, and A. Tagnit-Hamou, Pozzolanic properties of fine and coarse color-mixed glass cullet. Cement and Concrete Composites, 2011. 33(1): p. 19-29.

229. Shehata, M.H. and M.D.A. Thomas, The effect of fly ash composition on the expansion of concrete due to alkali–silica reaction. Cement and Concrete Research, 2000. 30(7): p. 1063-1072.

230. Thomas, M., et al., Effect of fly ash on the expansion of concrete due to alkali-silica reaction – Exposure site studies. Cement and Concrete Composites, 2011. 33(3): p. 359-367.

231. Kamiya, K., et al., Comparative Study of Structure of Silica Gels from Different Sources. Journal of Sol-Gel Science and Technology, 2000. 19(1-3): p. 495-499.

232. Chaudhary, D.S. and M.C. Jollands, Characterization of rice hull ash. Journal of Applied Polymer Science, 2004. 93(1): p. 1-8.

233. Farny, J.A., Kosmatka, S. H., Diagnosis and Control of Alkali-Aggregate Reactions in Concrete. 1997: Portland Cement Association. p. 23.

234. Chatterji, S., Chemistry of alkali–silica reaction and testing of aggregates. Cement and Concrete Composites, 2005. 27(7–8): p. 788-795.

235. Dron, R. and F. Brivot, Thermodynamic and kinetic approach to the alkali-silica reaction. Part 2: Experiment. Cement and Concrete Research, 1993. 23(1): p. 93-103.

236. Prezzi, M., Monteiro, P.J.M., Sposito, G. , Alkali-Silica Reaction - Part 1: Use of the Double-Layer Theory to Explain the Behavior of the Reaction Product Gels ACI Journal, 1997. 94(10): p. 10-17.

Erklärung (German Declaration)

Ich erkläre, dass ich die vorliegende Arbeit selbständig und nur unter Verwendung der angegebenen Quellen und Hilfsmittel angefertigt habe.

Weimar, 05.05.2014 Ha Thanh Le

List of Publications

Conferences

1. **Le, H. T.**, Siewert, K., Ludwig, H.-M., Synergistic effects of rice husk ash and fly ash on properties of self-compacting high performance concrete, in Proceedings of Hipermat the 3rd symposium on Ultra high performance concrete and Nanotechnology for High performance construction materials, Kassel, Germany, 2012, pp. 187-195.
2. **Le, H. T.**, Rößler, C., Siewert, K., Ludwig, H.-M., Rice husk ash as a pozzolanic viscosity modifying admixture for self-compacting high performance mortar, in the 18th International Conference on Building materials (Ibausil 18), Weimar, Germany, 2012, pp. 0538-0545.
3. **Le, H. T.**, Siewert, K., Ludwig, H.-M., Rheological behaviour of fresh mortar formulated from self-compacting high performance concrete incorporating RHA, in peer reviewed proceeings of the 1st international RILEM conference on rheology and processing of construction materials, Paris, France, 2013, pp. 131-138.

Journals

4. **Le, H. T.,** Nguyen, S. T., Ludwig, H.-M., A study on high performance fine-grained concrete containing rice husk ash, International Journal of Concrete structures and Materials, 2014. 8(4): p. 301-307.
5. **Le, H. T.,** Müller. M., Siewert, K., Ludwig, H.-M., The mix design for self-compacting high performance concrete containing various mineral admixtures, Materials and Design, (In press).
6. **Le, H. T.,** Kraus, M., Siewert, K., Ludwig, H.-M., Effect of macro-meso porous RHA on rheological properties of mortar formulated from self-compacting high performance concrete, Construction Building Materials, 2015. 80(0): p. 225-235.
7. **Le, H. T.,** Siewert, K., Ludwig, H.-M., Alkali silica reaction in mortar formulated from self-compacting high performance concrete containing rice husk ash, Construction Building Materials, (revised).
8. **Le, H. T.,** Ludwig, H.-M., Effect of rice husk ash and other mineral admixtures on properties of self-compacting high performance concrete, Materials and Design, (under review).

Curriculum Vitae

Name:	Ha Thanh Le (Lê Thanh Hà)
Date of birth:	September 10th, 1981
Place of birth:	Ha Noi, Vietnam
Email:	lehautc@daad-alumni.de
1999 - 2004	Undergraduate thesis of Civil Engineering at Department of Building Materials Technology - National University of Civil Engineering, Hanoi, Vietnam
2004 - 2006	Master of science thesis at Department of Building Materials Technology - National University of Civil Engineering, Hanoi, Vietnam
2005 - present	Lecturer at Section of Building Materials, Institute of Construction Engineering - University of transport and communications, Hanoi, Vietnam
2009 - 2014	Doctoral thesis at F.A. Finger - Institute for Building Materials Science (FIB) - Bauhaus University Weimar, Germany
2014 - 2015	One of three holders of STIBET Graduation Scholarship for international doctoral candidates, Bauhaus University Weimar, Germany
	One of three holders of STIBET Research-Assistantship for international doctoral candidates, Bauhaus University Weimar, Germany
	Research assistant at F.A. Finger - Institute for Building Materials Science, Bauhaus University Weimar, Germany
	Reviewer for *International Journal of Concrete Structures and Materials (SCIE)*
	Reviewer for *Materials Research Innovations (SCI)*

Weimar, 05.05.2014